Department of Precision and Microsystems Engineering

Mode coupling in nanomechanical string resonators

T. Jansen

Report no: 2021.039
Coach: ir. A. Keşkekler
Professors: dr. F. Alijani, dr. R.A. Norte
Specialisation: Dynamics of Micro- and Nanosystems (DMN)
Type of report: MSc. thesis
Date: July 13, 2021

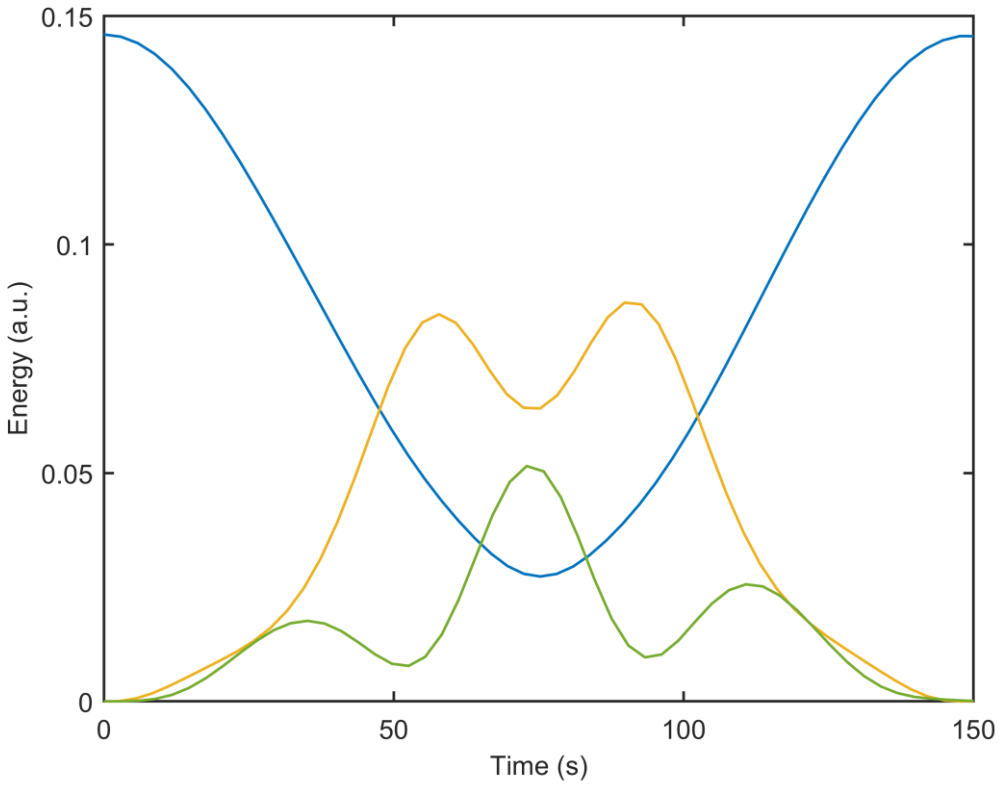

Mode coupling in nanomechanical string resonators

Towards Fermi-Pasta-Ulam-Tsingou mechanics

by

Tim Jansen

to obtain the degree of Master of Science

in

Mechanical Engineering

at the

Faculty of Mechanical, Maritime and Materials Engineering

of the Delft University of Technology,

to be defended publicly on Tuesday July 13, 2021 at 9:30 AM.

Student number:	4370430	
Project duration:	February 6, 2020 - July 13, 2021	
Thesis committee:	Dr. F. Alijani,	Department of Precision and Microsystems Engineering, TU Delft
	Dr. R.A. Norte,	Department of Precision and Microsystems Engineering, TU Delft
	ir. A. Keşkekler,	Department of Precision and Microsystems Engineering, TU Delft
	M. Xu, MSc.	Department of Precision and Microsystems Engineering, TU Delft
	Dr. L. Noel,	Department of Precision and Microsystems Engineering, TU Delft

TU Delft

Bit by bit, I've realized
That's when I need them
That's when I need my father's eyes
My father's eyes
That's when I need my father's eyes,
look into my father's eyes
My father's eyes
Then the jagged edge appears
Through the distant clouds of tears
I'm like a bridge that was washed away
My foundations were made of clay
As my soul slides down to die
How could I lose him?
What did I try?
Bit by bit, I've realized
That he was here with me
And I looked into my father's eyes

Eric Clapton

Preface

Writing this thesis is probably one of the final steps of becoming a third generation engineer - after my grandfather and father. I start to wonder whether it was nature or nurture, the matter of genes versus environment, that has put me on this track. Regardless of the origin, I have certainly enjoyed the past years. In these years, I have been introduced to the diversity of mechanical engineering through various scales of mechanical structures, with dimensions ranging from several hundreds of meters, to structures which are so small that they are barely visible with the naked eye. Regardless, one may draw the analogy of nature versus nature in engineering as well: the behavior of a structure is highly influenced by its design (its genes) and the environment it resides in. This thesis is no exception: it basically studies the behavior of an engineered structure in a certain environment, placing this structure in a different environment may, or may not change its behavior entirely.

The past year has certainly served its fair share of unfortunate events; I could not have reached this point without some people. First, I would like to thank Farbod, Ata and Richard, my supervisors, for sharing their exceptional knowledge on nonlinear dynamics, measurement techniques and resonator design. Your suggestions and remarks have always guided me in the right direction; thanks for that! Additionally, I would like to thank Minxing and Zichao for spending considerable time in the clean room, doing measurements: I really appreciate it. I would also like to extend my gratitude to one of my predecessors, Vincent, who has kindly supplied me with lots of his codes, which significantly sped up my research.

In particular, I would like to thank my parents and my sister for always standing by me and believing that everything would be alright, while you have had a tough time as well. Without your support, I certainly could not have made it this far. I would also like to thank my roommates and friends, who offered to help distract my mind from the challenges I faced, by offering to go out for a bike ride or have a beer: thanks! Lastly, I would like to thank my girlfriend Laura, who has continuously supported me in my journey here. The care, freedom and understanding you gave me certainly helped me get to this point, thank you!

This thesis is the product of over a year's work, but the research is certainly not finished, I hope that all readers may extract useful knowledge from it.

Tim Jansen
Delft, June 2021

Abstract

In the early years of numerical simulation methods, Fermi, Pasta, Ulam and Tsingou (FPUT) discovered that an undamped, weakly nonlinear equation describing the motion of a chain of masses and springs could show complex dynamics. Integration of these equations from an initial displacement in the form of the fundamental mode resulted in significant mode coupling: energy was transferred from the fundamental mode to several other modes, before the energy would return to the initial condition. To date, very little observations of such behavior in mechanical vibrations have been reported. Recent developments in fabrication of high stress Silicon-Nitride (Si_3N_4) string resonators have shown that it is possible to generate resonators with extremely high Q-factors, proving a potential testbed for these mechanics. This research shows, through modal conversion of the FPUT potential, that one may observe significant FPUT behavior in systems with non-integer frequency ratios and certain coupling coefficients. In addition, it is shown that for the default FPUT β-model, the effect of damping is negligible for fundamental mode Q-factors higher than 10,000. Simulations of the experimental frequency response of a high-Q Si_3N_4 string resonator show that the nonlinear dynamics of these resonators may be approximated by an analytical model that does not possess the required frequency ratios and coupling coefficients for FPUT behavior. Another string model, for which no mechanical equivalent has (yet) been found, may potentially show FPUT behavior. Several string-like resonator designs are tested using a numerical tool which can extract the modal coefficients. These resonators are modelled using simplified deformation models, which account only for axial deformation of the structure. The results for various string-like designs show that the eigenfrequencies and nonlinearity may be engineered easily, but these do not generate the required coupling coefficient for FPUT behavior.

Contents

1 Introduction

The document that lies in front of you is a study on the nonlinear dynamics of string resonators. Nonlinear dynamics are inherently present in any structure. However, whether these -often complex- dynamics become visible is largely related to the size of the structure and the environment it resides in.

Let's for example take a guitar string. Gently plucking this string will generate a wave in the string, which will cause vibration at its fundamental frequency. The air surrounding this string will also start to vibrate at this frequency, generating waves. Eventually, these waves will enter the human ear, which the human perceives as a sound or a tone. Once the guitar string is plucked, the tone will slowly fade out as time progresses. The mechanism behind this fading-out is damping, which causes the string to lose the energy that was put into it by plucking the string. Imagine that the fading-out happens on a much longer time-scale: the string will then vibrate at a certain frequency for a very long time, as very little energy is lost in each vibration cycle.
By plucking the string stronger and stronger, one can generate waves that are so strong that the sound generated by the string changes slightly or that it may even cause one of the other strings to vibrate as well. Imagine that we would pluck an undamped string so strongly that some of the other strings on the guitar are excited as well, generating a different sound. Plucking this string strongly will thus excite other strings, which will change the sound guitar produces as this sound will consist of many tones. In dynamics, these tones are often referred to as a "mode": each of these modes has its own tone (frequency) and a corresponding shape of vibration (wavelength). The effect where a string of a guitar is excited through excitation of another string, is caused by a coupling between various strings. However, this coupling is not only present between multiple strings. Excitation of a single string can also cause excitation of multiple modes of this *single* string, which is known as mode coupling. This mode coupling is most significant when a string is plucked strongly, specifically in the regime where the plucking force and the resulting string amplitude no longer follow a linear, but a nonlinear relationship: the nonlinear regime.
Nonlinear dynamics are most easily observed for systems which have very little (or negligible) damping. Experimentally testing structures without any damping is quite an intensive process, as it requires very strict environmental conditions. However, since the emergence of computers in the Fifties of the last century, this has become significantly easier, since these computers can compute solutions to certain sets of equations which represent the dynamics of the studied structures.
Before diving into the exact topic of this research, it is important to first look at some theories on dynamics, as will be done in the next three sections.

1.1. Linear and nonlinear dynamics

Dynamics is the part of physics that is concerned with the response of systems to forces. The response of a system to a force will cause motion of the system. In linear dynamics, the response to an (external) force function F at time t is dependent on three system parameters: mass m, stiffness k and damping coefficient c. This motion may be expressed in an equation; which is commonly referred to as an equation of motion.

For a linear system, this equation of motion is as follows:

$$\ddot{q} + \frac{c}{m}\dot{q} + \frac{k}{m}q = \frac{F(t)}{m}. \tag{1.1}$$

The equation clearly scales linearly with q, $\dot{q}$ and $\ddot{q}$, the amplitude, velocity and acceleration of the motion, respectively. Once a system starts to vibrate, e.g. due to an excitation in the form of a instantaneous force (e.g. by plucking it), it will deform, generating kinetic and potential energies. During the resulting vibration cycle, the kinetic and potential energy will be exchanged continuously. These vibrations, like guitar strings, do not continue infinitely, as some of the energy will be lost in each vibration cycle. At a certain frequency, the response of the system is largest, and the kinetic and potential energies have equal magnitudes [31]. This frequency is commonly referred to as the eigenfrequency and it is a function of the mass and stiffness of the system, according to the following formula:

$$\omega_0 = \sqrt{\frac{k}{m}}. \tag{1.2}$$

In the absence of damping, any excitation would lead to an infinitely sustained motion. Should damping be present in the system (i.e. $c > 0$), some of the energy will dissipate and thus this will (slightly) decrease the eigenfrequency, generating a resonance frequency. The damping coefficient is often written in terms of the resonance frequency and the (dimensionless) Q-factor: $c = \frac{\omega_0}{Q}$. This Q-factor is expressed as the ratio of internal energy versus the dissipated energy of a system [29, 36]. A system that has a clear response at a certain frequency is called a *resonator*. The resonance frequency is often considered to be equal to the eigenfrequency under the assumption that damping is small. Any physical system, e.g. the guitar string, has many of these eigenfrequencies, which each have their own shape, the combination is commonly referred to as modes [19, 31]. Each of the modes of a string may be visualized, as is done in Figure 1.1 for the first three modes of a string. The total response of a string may be a function of multiple modes. In the linear regime, the effects

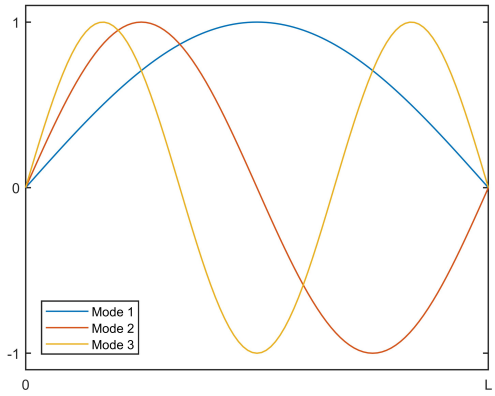

Figure 1.1: The first three mode shapes of a string.

of other modes are usually small. However, as the force is increased, the amplitude increases and the linear equation (Eq. 1.1) can no longer accurately describe the response of the system, as the displacement of the string no longer scales linearly with the applied force. The origin of this behavior may be sought in the fact that any vertical displacement (w in Fig. 1.2) of the string with length L will also cause the string to stretch in the length direction by a factor ΔL. For small (linear) amplitudes ($w \ll L$), this ΔL is negligible. For larger amplitudes, this stretching is no longer negligible and thus a different formulation is required [19]. The effect of this larger displacement is that the structure stretches, which in turn increases the tension in the material. This additional displacement-induced-tension increases the resistance of the structure to displacements in a nonlinear manner, resulting in a stiffness that scales with the cube of the displacement. This type of (geometric) nonlinearity commonly referred to as the Duffing nonlinearity. The following formula describes motion of such a nonlinear resonator for a nonlinear coefficient b and a force of $\bar{F} = \frac{F}{m}$:

$$\ddot{q} + \frac{\omega_0}{Q}\dot{q} + \omega_0^2 q + bq^3 = \bar{F}\cos(\omega_f t). \tag{1.3}$$

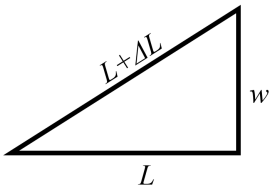

Figure 1.2: String element of length L under a vertical displacement denoted by w. This displacement causes the length to increase from L to $L+\Delta L$.

The example showed that the displacement-induced-tension increases the stiffness. For hardening nonlinearity, b is positive. If the displacement-induced-tension decreases the stiffness (softening), b is negative. The frequency response of such a hardening Duffing resonator is depicted in Figure 1.3. Here, clearly, the

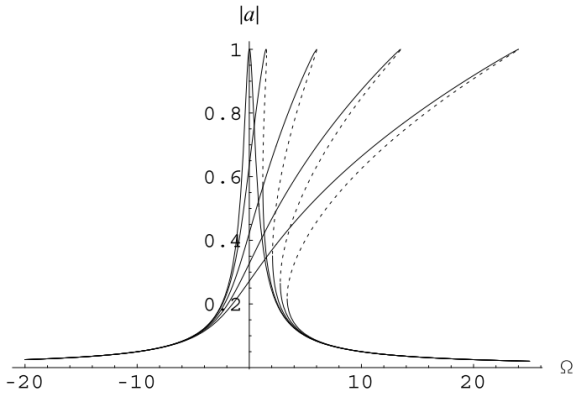

Figure 1.3: The response of a resonator with Duffing nonlinearity. The response is shown for several values of F. The frequency Ω is defined as $\omega_0 - \omega_f$. Source: [19].

frequency of the resonator that is associated to a certain amplitude increases as the drive power is increased, due to the increase in stiffness from the positive (hardening) Duffing coefficient.
The previous examples have considered the vibration of a single mode. In reality, a system has multiple (an infinite number of) modes, which become increasingly important once a system is driven further into the nonlinear regime. The response for two modes (q_1 and q_2) can be expressed using the following formula [19]:

$$\begin{aligned} \ddot{q}_1 + \frac{\omega_1}{Q_1}\dot{q}_1 + \omega_1^2 q_1 + b_{111}^{(1)} q_1^3 + b_{122}^{(1)} q_1 q_2^2 &= \bar{F}_1 \cos(\omega_{f1} t) \\ \ddot{q}_2 + \frac{\omega_2}{Q_2}\dot{q}_2 + \omega_2^2 q_2 + b_{112}^{(2)} q_1^2 q_2 + b_{222}^{(2)} q_2^3 &= \bar{F}_2 \cos(\omega_{f2} t). \end{aligned} \tag{1.4}$$

Both of these equations of motion contain a term that is dependent on the amplitude of both modes, the $b_{122}^{(1)}$- and $b_{112}^{(2)}$-terms. These terms create a *coupling* between modes 1 and 2. This coupling may be induced via various types of forces, but this report is primarily focused on the mechanical coupling between modes. For special conditions of ω_1 and ω_2, this coupling is strongest, resulting in a stronger response of mode 2 through increased driving of mode 1. These special conditions are most significant for cases where $\omega_1 = n\omega_2$ and n is integer. This relation, the *internal resonance* condition, couples the internal modes of the resonator. The effects of this relation may be found by assuming that the modal amplitudes can be written in terms of a trigonometric function, e.g. $q_1 = \cos(\omega_1 t)$ and $q_2 = \cos(\omega_2 t)$. Substituting these modal amplitudes into the nonlinear parts of the first equation of motion gives Eq. 1.5.

$$\bar{F}_{NL.1} = b_{111}^{(1)} \cos^3(\omega_1 t) + b_{122}^{(1)} \cos(\omega_1 t)\cos^2(\omega_2 t) \tag{1.5}$$

Using that $\cos^3(\omega t) = \frac{1}{4}(3\cos(\omega t) + \cos(3\omega t))$ and $\cos(\omega_i t)^2 \cos(\omega_j t) = \frac{1}{4}\left(\cos((2\omega_i - \omega_j)t) + 2\cos(\omega_j t) + \cos((2\omega_i + \omega_j)t)\right)$ will generate the following nonlinear force term:

$$\bar{F}_{NL.1} = b_{111}^{(1)} \frac{1}{4}(3\cos(\omega_1 t) + \cos(3\omega_1 t)) + b_{122}^{(1)} \frac{1}{4}(\cos((2n-1)\omega_1 t) + 2\cos(\omega_1 t) + \cos((2n+1)\omega_1 t)) \tag{1.6}$$

Which shows that the Duffing term ($b^{(1)}_{111}$) excites both ω_1 and a harmonic at $3\omega_1$. The $b^{(1)}_{122}$-term only excites uneven harmonics of the first mode, causing coupling between the modes at these uneven harmonics of the first mode. For example, if $n = 3$, the harmonic of the first mode in the Duffing term will weakly excite the third mode and the coupling terms will also become stronger, generating energy transfer.

1.2. Fermi-Pasta-Ulam-Tsingou behavior

During the period when computers emerged as methods that could "compute" solutions of complicated scientific problems, many researchers began to see their potential in generation of new knowledge. Some of these researchers were Fermi, Pasta, Ulam and Tsingou, who conducted a series of numerical experiments on an undamped chain of N masses (of mass $m = 1$kg) and $N+1$ linear springs (of $k = 1\text{Nm}^{-1}$), to which a small nonlinear perturbation (α or β, Fig. 1.4a) was added, to generate the following equations of motion (EoM) of mass i:

$$\ddot{x}_i = (x_{i+1} + x_{i-1} - 2x_i) + \alpha[(x_{i+1} - x_i)^2 - (x_i - x_{i-1})^2] \tag{1.7}$$

$$\ddot{x}_i = (x_{i+1} + x_{i-1} - 2x_i) + \beta[(x_{i+1} - x_i)^3 - (x_i - x_{i-1})^3], \tag{1.8}$$

where $i = 1, 2, ..., N$. The nonlinear perturbation, quadratic in the degrees of freedom for the α-model and cubic for the β-model, was expected to aid in the rate at which the system would "thermalize" to reach equipartition: the state where all modes of the system have equal energy. However, to their astonishment, they observed that when they would excite the first mode and let the system vibrate freely (ring down) over time, the energy would first transfer to several higher modes (modes 3, 5 and 7 in Fig. 1.4b), before (nearly) all of it returned to the initial condition after 15,000 cycles [11]! Similar to what was previously shown for the

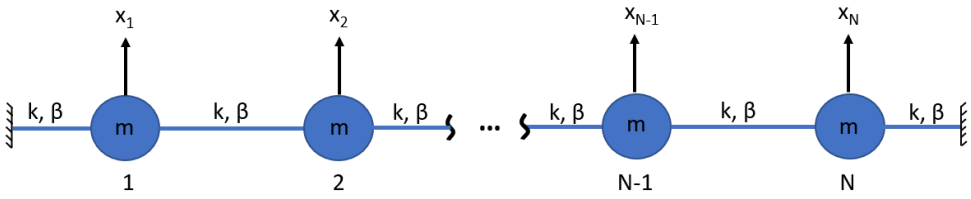

(a)

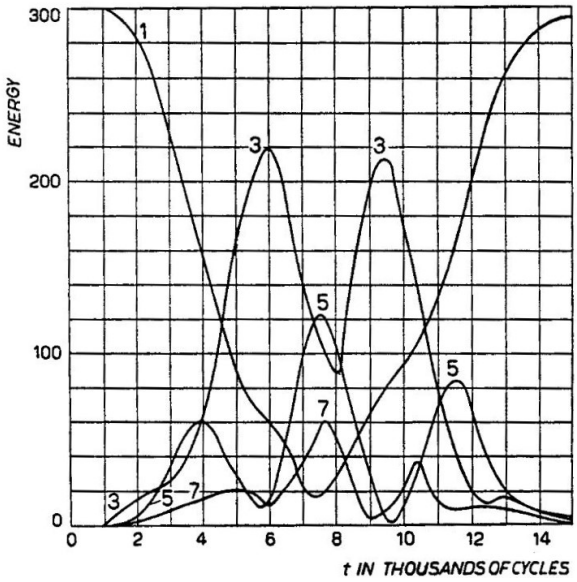

(b)

Figure 1.4: 1.4a a chain of N masses of mass m, connected by $N+1$ springs of linear and nonlinear stiffness of k and β, respectively. A.1a FPUT recurrence for the β-model, for $N = 16$ and $\beta = 8Nm^3$. Source: [11].

vibration of a guitar string, they thus observed that energy was exchanged between the modes (or tones) of the string, before showing recurrent behavior, where the energy returned to the initially excited mode. This phenomenon is referred to as Fermi-Pasta-Ulam-Tstingou (FPUT) recurrence.

Since the publication of these results, many researchers have tried to explain the observed behavior through mathematical and dynamical theories. A prominent explanation is provided by Zabusky and Kruskal, who claim that the behavior may be approximated by the solutions of the Korteweg-de-Vries equation, which generates stable waves which can interact while keeping their form (solitons), resulting in exchange of energy [4].
Later, Chirikov proposed an explanation that deals with chaos [4]. Chaos basically implies that a system is extremely sensitive to the initial conditions; a slight change in these initial conditions may generate significantly different dynamics. Chirikov claimed that the exchange of energy was generated through overlapping nonlinear resonances of several modes of the system [6]. This theory theory of resonance is widely adopted in later studies [12, 28, 33, 34].
Though many theories try to explain this behavior, the number of physical observations is scarce. There are several reports of this behavior in optical waves, but for mechanical vibrations, this is hardly ever observed as is shown in [23, 35]. Recently, Barnard showed that the thermal vibrations of a carbon nanotube (CNT) can show quasi-periodic modulations over time (see Fig. 1.5), which is associated to a change in the resonance frequencies the system [3]. Several modal frequencies appear to have an influence in these changes in frequencies, and numerical simulations show that this is closely related to FPUT-behavior.

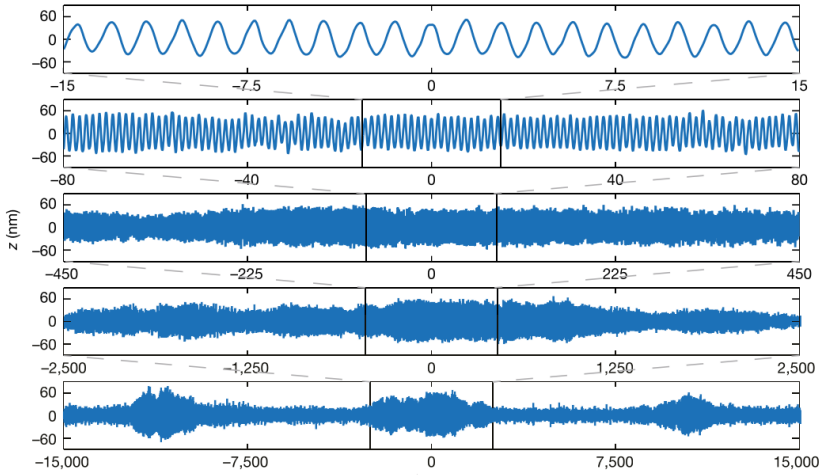

Figure 1.5: Amplitude of the CNT over time, showing quasi-periodic modulations in the amplitude over time. Source: [3].

Other than this work, there are no observations of such behavior in mechanical systems. Midtvedt stated that FPUT behavior will only become visible for systems which have a strong (nonlinear) coupling already for low energies, as well as a long time scale for dissipation to the environment, such that energy can be exchanged among other modes before it is dissipated to the environment [21]. The first topic, the strength of the nonlinearity, is often related to the geometry and/or material of a system, as was shown in the previous section. The second topic, that of low dissipation (i.e. high Q-factors in Eq.'s 1.3 and 1.4), could be achieved by using a material or structure which inherently has small energy dissipation. The next section will show what the most dominant damping mechanisms in string resonators are, as well as means to mitigate this damping.

1.3. High Quality factor Silicon-Nitride string resonators

Recent developments in manufacturing techniques of Silicon-Nitride (Si_3N_4) (nano)resonators have made these very small nanoresonators a promising test-bed system for FPUT behavior [10, 13, 37]. These nanoresonators typically have lengths of around a millimeter and width and thicknesses even smaller than 10% of the thickness of a hair. Si_3N_4 (string) resonators have been shown to exhibit excellent sensing performance: the material is stable, allowing for constant dynamical characteristics and above all, these resonators have been shown to achieve very low dissipation per vibration cycle (high Q-factors) [36, 37].
Many mechanisms appear to dissipate energy, e.g. through intrinsic, medium and clamping loss mechanisms. Placing a resonator in a vacuum will reduce the medium losses, and thus two mechanisms remain: clamping losses and internal (material) losses.
Material losses could result from irreversible motion of the atoms of the material, which results in energy

losses. This type of dissipation mechanism is always present in a system; its magnitude depends on the type of material of the resonator. Clamping losses are related to the shape of the resonator under vibration: near the clamped edges of a string resonator, the string cannot deflect into a perfect mode shape (as is shown in Fig. 1.1), which will cause energy to dissipate into the substrate of the resonator. Several methods have been proposed to reduce this effect. Increasing the internal energy is one of them, as is shown in the following equation.

$$Q_{str} \approx \frac{W_{tension}}{2\pi W_{bending}} Q_{bending} \approx \frac{0.5\sigma A \int_0^L [\frac{\partial}{\partial x} u(x)]^2 dx}{0.5 E I_z \int_0^L [\frac{\partial^2}{\partial x^2} u(x)]^2 dx} Q_{\text{bending}} \tag{1.9}$$

Here, Q_{bending} is the Q-factor that accounts for losses in due to bending of the string in relaxed states [30]. The Q-factor of a string resonator may thus be increased by increasing the numerator of Eq. 1.9 by increasing the pre-stress of the material [36, 37].

Secondly, by using strain engineering techniques [10, 13] one can reduce the clamping loss even further. This method uses local variations in the strain of a resonator that localize a mode shape far away from the clamped edges, as well as local increases in stress that further increase the internal energy, as is displayed in Fig. 1.6.
Internal (material) losses in string resonators could have two origins, volume and surface losses. In strings of

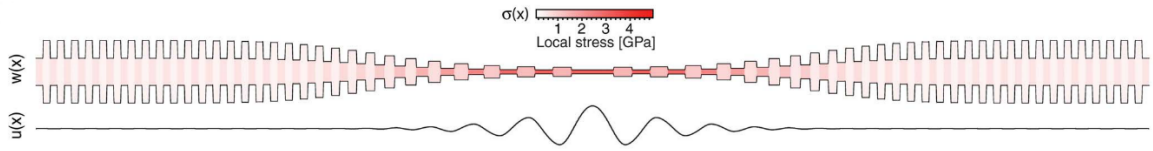

Figure 1.6: A design that reduces clamping losses by localizing the mode shape near the centre of the resonator. Source: [10].

thickness smaller than $400nm$, the surface losses are most significant. The largest surface loss mechanisms are those related to material and manufacturing roughness. Additionally, non-uniform strain fields will result in thermal losses as the resulting non-uniform deformation causes heat production.
Several research groups have shown that high stress string resonators with a constant cross-section may reach Q-factors around 1 million [30, 37]. Further reduction of the losses through strain engineering may increase the Q-factor by another order of magnitude [10, 13]. Furthermore, the wide manufacturing possibilities of these Si_3N_4 materials show that more complex geometries may also be fabricated [27], making this material a possible test-bed for FPUT mechanics.

1.4. Goals of the research

This thesis is focused on dynamics and specifically the nonlinear dynamics of string-like resonators. The goal of this thesis is to determine whether one may possibly observe Fermi-Pasta-Ulam-Tsingou recurrence through mode coupling in string resonators.
To explore this, the following research questions are set-up:

1. What are the requirements of FPUT behavior?
2. Which models may predict the nonlinear dynamics of vertical vibrations in continuous string resonators?
3. Which string resonator designs could (in theory) potentially show FPUT behavior?

The research will first elaborate upon the requirements for Fermi-Pasta-Ulam-Tsingou (FPUT) recurrence. Subsequently, analytical string models are proposed, which show what the origin of the nonlinearity in string resonators is. These analytical string models are subsequently verified using experiments. Finally, the resemblance between the numerical FPUT experiment and string models is analyzed, before showing possible improvements in string resonator designs to improve mode coupling in such resonators. The main findings of this research are elaborated upon in a scientific paper format in Chapter 2. The conclusions, discussions and recommendations of the research may be found in Chapter 3. More detailed information about the FPUT problem, string vibrations and FPUT mechanics in string resonators may be found in Appendices A, B and C. Supplementary material may be found in Appendix D to F.

2

Paper

This chapter will contain the main findings of the research. they are presented in a scientific paper.

Mode coupling in nanomechanical string resonators*

Tim Jansen[a]

[a]Dynamics of Micro and Nano Systems, Department of Precision and Microsystems Engineering, Delft University of Technology, The Netherlands

ARTICLE INFO

Keywords:
Fermi-Pasta-Ulam-Tsingou physics
Silicon Nitride
String Resonators
Mode Coupling
Internal Resonance
Duffing Nonlinearity
FPUT
FPU

ABSTRACT

In the early years of numerical simulation methods, Fermi, Pasta, Ulam and Tsingou (FPUT) discovered that an undamped, weakly nonlinear equation describing the motion of a chain of masses and springs could show complex dynamics. Integration of these equations from an initial displacement in the form of the fundamental mode resulted in significant mode coupling: energy was transferred from the fundamental mode to several other modes, before the energy would return to the initial condition. To date, very little observations of such behavior in mechanical vibrations have been reported. Recent developments in fabrication of high stress Silicon-Nitride (Si_3N_4) string resonators have shown that it is possible to generate resonators with extremely high Q-factors, proving a potential testbed for these mechanics. This research shows, through modal conversion of the FPUT potential, that one may observe significant FPUT behavior in systems with non-integer frequency ratios and certain coupling coefficients. In addition, it is shown that for the default FPUT β-model, the effect of damping is negligible for fundamental mode Q-factors higher than 10,000. Simulations of the experimental frequency response of a high-Q Si_3N_4 string resonator show that the nonlinear dynamics of these resonators may be approximated by an analytical model that does not possess the required frequency ratios and coupling coefficients for FPUT behavior. Another string model, for which no mechanical equivalent has (yet) been found, may potentially show FPUT behavior. Several string-like resonator designs are tested using a numerical tool which can extract the modal coefficients. These resonators are modelled using simplified deformation models, which account only for axial deformation of the structure. The results for various string-like designs show that the eigenfrequencies and nonlinearity may be engineered easily, but these do not generate the required coupling coefficient for FPUT behavior.

1. Introduction

In 1953, during the early years of numerical simulation methods, Fermi, Pasta, Ulam and Tsingou conducted a series of numerical experiments on the thermalization of various nonlinear systems. One of those nonlinear systems was an undamped chain of N masses, connected by $N+1$ springs with a linear stiffness and a weak nonlinear perturbation; quadratic for the α-model and cubic for the β-model. The Equations of Motion (EoMs) for this β-model are as follows [11]:

$$\ddot{x}_i = (x_{i+1} + x_{i-1} - 2x_i) + \beta[(x_{i+1} - x_i)^3 - (x_i - x_{i-1})^3] \quad (1)$$

here $i = 1, 2, ..., N$. The researchers hypothesized that this nonlinear perturbation would cause the energy in the system to thermalize quickly, leading to equipartition of energy. However, to their astonishment, the energy appeared to be distributed among several modes of the system, before returning to the initial condition (Fig. 1). Up to now, many research groups have undertaken efforts to explain this behavior: its origin is sought in nonlinear resonances which are closely linked to chaos theories in nonlinear dynamics [6, 12]. Though many reports of theoretical research on these Fermi-Pasta-Ulam-Tsingou (FPUT) mechanics have been published, reports of experimental observations are scarce. Several reports claim to have observed FPUT behavior in optical waves [23, 35]. However, observations of this behavior in mechanical vibrations are much more scarce. Recently, Barnard linked quasiperiodic behavior in the amplitude of a carbon nanotube to FPUT behavior, but full recurrence is not observed there [3]. The lack of observations in mechanical vibrations may be attributed to effects from damping and (manufacturing) imperfections, which could limit energy transfer [26]. Recent advances in design and manufacturability of high stress Silicon-Nitride (Si_3N_4) resonators may circumvent these limitations. High stress Si_3N_4 nanostrings are shown to have low damping at room temperature and good mechanical stability [37]. In addition, recent research shows that more complicated designs may further increase the Q-factors, through reduction of clamping losses [10, 27]. This report will show which requirements should be satisfied to observe this FPUT behavior in string-like resonator designs. The procedure is as follows: Section 2 will first explore the requirements and limitations of FPUT behavior. Subsequently, two analytical string models will be presented and experimentally verified in Section 3. Section 4 will then show if FPUT behavior may be observed for any of these string models, as well as methods to improve the modal coefficients of some designs. Finally, Section 5 will elaborate upon the conclusions and possible improvements of the research.

2. Fermi-Pasta-Ulam-Tsingou mechanics

The present study is focused on the β-model, as this (cubic) order of nonlinearity is inherently present in string systems (Section 3). Time integration of the EoMs of Eq. 1, and subsequent Fourier transformations generate a formulation for the modal linear energy. This linear energy (consisting of the kinetic and potential energy generated of the system) was assumed to sufficiently represent the total energy, since the nonlinear energy remained small [11]. The

*This paper is part of the authors master thesis of the same name under supervision of dr. F. Alijani, dr. R.A. Norte and ir. A. Keşkekler.

ORCID(s): 0000-0002-4265-3179 (T. Jansen)

FPUT researchers found that for an undamped chain of 16 mass elements ($N = 16$) of mass 1kg, connected to one another with springs with linear stiffness $k = 1\text{Nm}^{-1}$ and nonlinearity $\beta = 8\text{Nm}^{-3}$ (referred to as the "default" FPUT β-model), energy transfer and subsequent energy recurrence may be observed. This section will show that by performing a modal coordinate transformation, one may find the direct relations between the respective modes of the model.

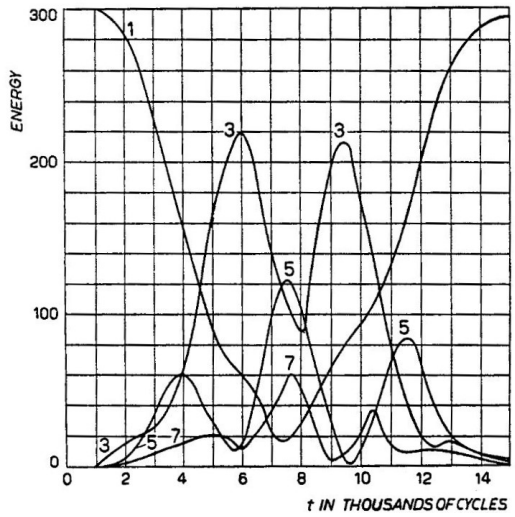

Figure 1: FPUT mechanics for $N = 16$ and $\beta = 8N/m^3$. Adopted from [11].

2.1. FPUT model in modal coordinates

A modal coordinate transformation is quite an intensive process, as the increase of Degrees of Freedom (DoFs) or number of considered modes increases the number of equations and modal interactions. The number of DoFs may not just be chosen randomly. Tuck and Menzel (née Tsingou) have shown that the number of DoFs (N) determines the magnitude of the initial nonlinearity in the EoMs: few DoFs increase the initial nonlinearity, which could show different dynamics [34].

The modal conversion is conducted for the default FPUT β-model. The procedure is as follows: first, the EoMs from Eq. 1 are integrated to find the equations for the kinetic and potential energies (Eq. 2). Subsequently, the modal energy formulations are derived through substitution of Eq. 3 (where subscript u denote max-1 eigenvectors, where $\phi_u) = 1$). The conversion from these max-1 eigenvectors to mass normalized eigenvectors is conducted using the scaling parameter $\alpha = \sqrt{\frac{2}{m_{tot}}}$. Finally, the modal EoMs are found by taking the derivatives of the energies with respect the modal coordinates, generating Eq. 4.

$$T = \sum_{i=1}^{N} \frac{m}{2}\dot{x}_i^2,\ V = \sum_{i=1}^{N+1} \frac{k}{2}(x_i - x_{i-1})^2 + \frac{\beta}{4}(x_i - x_{i-1})^4 \quad (2)$$

$$\mathbf{x} = \mathbf{\Phi}_u^T \mathbf{q}_u = \alpha \mathbf{\Phi}_u^T \mathbf{q}_\mathbf{m} \rightarrow x_i = \alpha \sum_{n=1}^{6} \sin\left(\frac{\pi n i}{N+1}\right) q_k \quad (3)$$

$$\ddot{q}_r + k_r^{(r)} q_r + \sum_{j=1}^{6}\sum_{k=j}^{6}\sum_{l=k}^{6} b_{jkl}^{(r)} q_j q_k q_l = 0,\ r = 1, 2, ..., 6 \quad (4)$$

Table 1
Single-mode modal coefficients for the default FPUT β-model. The variables are normalized with respect to the first mode.

n	(1)	(2)	(3)	(4)	(5)	(6)
$\tilde{k}_n$	1.00	3.97	8.80	15.33	23.34	32.55
$\tilde{\omega}_n$	1.00	1.99	2.97	3.92	4.83	5.71
$\tilde{b}_{nnn}$	1.00	15.73	77.39	236.39	625.60	1059.65

In this modal conversion, it is assumed that the first six modes of the system can represent the dynamics with sufficient accuracy (hence the summation from 1 to 6 in Eq. 3). The linear frequency ratio of the fifth mode which is computed using the above-mentioned method is different to that resulting from a modal analysis: 5.00 versus 4.83 respectively (App. A.2). The former ratio generates little energy transfer, as is shown in Fig. 2, which is a ringdown simulation (using Matlab's ODE45 solver) from an initial excitation of the first mode. The origin of this discrepancy likely originates from the modal conversion. The modal coefficients of the default FPUT model are tabulated in Table 1, the nonlinear modal coupling coefficients may be found in Table A.4.

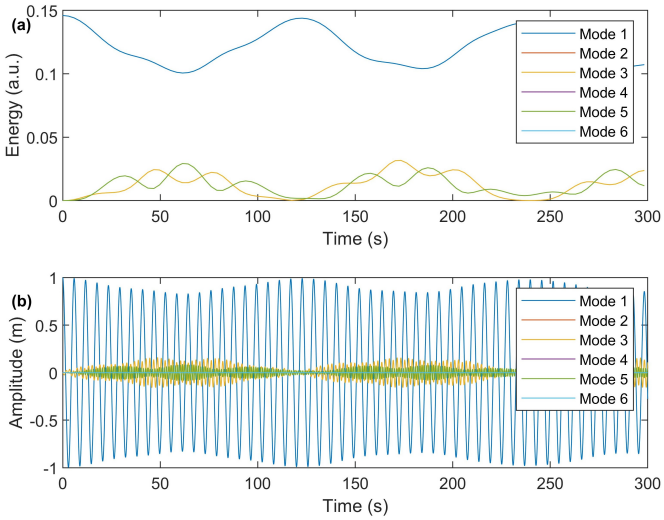

Figure 2: FPUT simulation for $N = 16$ and $\beta = 8\text{Nm}^{-3}$. The linear frequency ratios of the first six modes of $\frac{\omega_0}{\omega_0} = 1.00, 1.99, 2.97, 3.92, 5.00$ and 5.71.

The linear stiffness ratios from the modal analysis ($\tilde{k}_n$) follow the equation:

$$\tilde{k}_n = \frac{\omega_n^2}{\omega_0^2} = 4\sin^2\left(\frac{\pi n}{2(N+1)}\right) / 4\sin^2\left(\frac{\pi}{2(N+1)}\right) \quad (5)$$

which generates non-integer frequency ratios (shown by $\tilde{\omega}_n$ in Table 1), which are slightly lower than the mode number n [33]. Irrational frequency ratios can generate quasiperiodic behavior [24]. This could generate modulation of the amplitude (beatings, where the local minima and maxima vary over time), as is shown in Fig. 3, resulting from a ringdown simulation for initial excitation of the first mode. The energy plot in Fig. 3 is similar to Fig. 1: it shows energy transfer and energy recurrence. The exclusion of higher modes

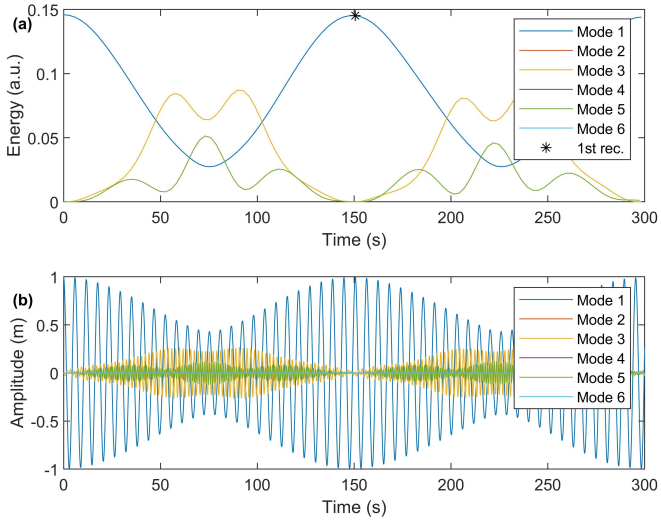

Figure 3: Numerical ring-down simulation for the modal EoMs of the $N = 16$ and $\beta = 8\text{Nm}^{-3}$, from initial excitation of the first mode. **(a)** depicts the linear energy vs. time. **(b)** depicts the modal amplitude vs. time.

Table 2
Modal coupling coefficients for modes 1,3, and 5 of the N = 16 FPUT β-model, normalized with respect to $b^{(1)}_{111}$.

Eq.	(1)	(3)	(5)
$\tilde{b}_{111}$	1	0.99	0
$\tilde{b}_{113}$	2.97	17.59	14.83
$\tilde{b}_{115}$	0	14.83	50.02
$\tilde{b}_{133}$	17.59	0	43.99
$\tilde{b}_{135}$	29.67	87.99	0
$\tilde{b}_{155}$	50.02	0	0
$\tilde{b}_{333}$	0	77.38	0
$\tilde{b}_{335}$	43.99	0	440.05
$\tilde{b}_{355}$	0	440.05	0
$\tilde{b}_{555}$	0	0	625.60

than mode 6 causes some -expected- differences in the energy plots. The modal amplitude plot shows that though the third mode's energy is dominant for some time, its modal amplitude remains smaller than that of the first mode. This implies that while the amplitude of this mode remains small, energy dominance may still occur due to higher linear stiffness of higher modes. Energy transfer is generated by the nonlinear coupling terms of the uneven modes (Table 2), where the nonlinear parts of the EoMs are represented by $b^{(r)}_{jkl}q_jq_kq_l$ of each column (r). These coefficients are derived from a single potential, E_{tot}, which accounts for all possible modal contributions. The energies associated to modes 1 and 3 are represented by many terms, e.g. $E_{1113}(\propto q_1^3q_3)$: $\frac{d}{dq_1}E_{1113} = 3\frac{d}{dq_3}E_{1113}$, and thus ($b^{(1)}_{113} = 3b^{(3)}_{111}$).
Fig. 3 shows that only the uneven modes are excited, as the energy (and amplitude) of the even modes remain zero. The origin of this behavior may be explained through the theory of resonant terms. The first mode's equation for the nonzero nonlinear parts from Table 2 are written in Eq. 6.

$$F^{(1)}_{\text{NL}} = b^{(1)}_{111}q_1^3 + b^{(1)}_{113}q_1^2q_3 + b^{(1)}_{133}q_1q_3^2 + b^{(1)}_{135}q_1q_3q_5 + b^{(1)}_{155}q_1q_5^2 + b^{(1)}_{335}q_3^2q_5. \tag{6}$$

Distinction can be made between three amplitude dependencies, which scale with either one mode (q_j^3), two modes ($q_j^2q_k$) or three modes ($q_jq_kq_l$). Assuming that these modal displacements may be approximated by harmonic solutions of the form $q_n = \cos(n\omega_0 t)$ (where the mode frequencies follow an integer relation with the mode number n) results in the following equation:

$$\begin{aligned} q_jq_kq_l = \frac{1}{4}\big[&\cos((j-k-l)\omega_0 t) + \cos((j+k-l)\omega_0 t) \\ &+ \cos((j-k+l)\omega_0 t) + \cos((j+k+l)\omega_0 t). \end{aligned} \tag{7}$$

Now, any combination of *uneven* j, k and l will yield an uneven pre-factor from the ($j\pm k\pm l$)-terms. This implies that the uneven modes j , k and l will only excite uneven harmonics of ω_0, generating energy transfer between only the uneven modes. The equations of motion for this default FPUT problem may thus be reduced to only those for the uneven modes. The unique feature of FPUT behavior is that under initial static deflection of (only) the first mode, multiple modes are excited. At $t = 0$, $q_{0.1} \neq 0$, $q_{0.3} = 0$ and $q_{0.5} = 0$ will generate the following equations:

$$\ddot{q}_1 + k^{(1)}_1 q_{0.1} + b^{(1)}_{111}q^3_{0.1} = 0,\ \ddot{q}_3 + b^{(3)}_{111}q^3_{0.1} = 0 \text{ and } \ddot{q}_5 = 0. \tag{8}$$

Which shows that the initial excitation of the first mode generates a nonzero term in the EoM of mode 3, which will initiate energy transfer [33]. Without this $b^{(3)}_{111}$-term (the back-coupling term), the energy will only be distributed through excitation of the harmonics of the first mode, which will prevent energy dominance by the third mode (Fig. A.6).

2.2. Limitations of the FPUT problem

The previous subsection has shown that energy recurrence is generated through two variables: the linear frequency ratios and a back-coupling term. To determine if this FPUT behavior may be observed in mechanical resonators, it is important to characterize its limitations first. Possible limitations of the FPUT behavior may be influenced by (1) damping, (2) linear frequency ratios, (3) the nonlinearity of the resonator, and (4) the initial conditions.
The influence of damping on this default FPUT problem is studied first, by tracing the percentage of energy that returns to the first mode during the first recurrence period, for various Q-factors. The Q-factors of the higher modes are assumed to scale with the fundamental mode Q-factor (Q) and the inverse of the mode number n: $Q_n = \frac{Q}{n}$, i.e. if $n = 3$, $Q_3 = \frac{Q}{3}$. The effect of damping is checked by sweeping the first mode's Q between 500 and 1 million (and the Q-factors of the higher modes scale according to the above relation). Using this relation, it was found that for Q-factors larger than 10,000 more than 99.5% of the initial energy returns to the initially excited mode, showing that damping is negligible for those Q-factors (Fig. A.7). Should the damping of the higher modes be (much) higher, then these higher modes will dissipate part of their energy to the environmental bath, reducing the magnitude of the following recurrence peak.
The three remaining parameters are swept altogether, as these are related through the ratio of initial linear versus initial nonlinear forces:

$$r_{\text{NL2L}} = \frac{b^{(1)}_{111}q^3_{0.1}}{k_1q_{0.1}} = \frac{b^{(1)}_{111}}{k_1}q^2_{0.1} \tag{9}$$

For the default FPUT model, this ratio is 21%. The linear stiffness (or frequencies) are swept by varying the stiffness of the higher modes (k_n, where $n = 2, 3, ..., 6$) with respect to the first mode. In this sensitivity study, the stiffness of these modes is swept between 90% and 110% of their original value (as is reported in the first row of Table 1). The nonlinear stiffness is subsequently swept between $\beta = 0$ and 20Nm^{-3} . Finally, the maximum initial amplitude of the first mode ($q_{u_{0.1}} = \alpha q_{0.1}$) is swept between 0.1and 3.25m. Fig. 4 depicts the results of the parameter sweep for the default initial amplitude $q_{u_{0.1}} = 1\text{m}$. The results are presented in terms of the maximum linear energy of the third mode with respect to the fundamental mode ($\max(\frac{E_3(t)-E_1(t)}{E_0})$), which will show if, and by how much the third mode's energy dominates that of the first mode. The figure shows that gener-

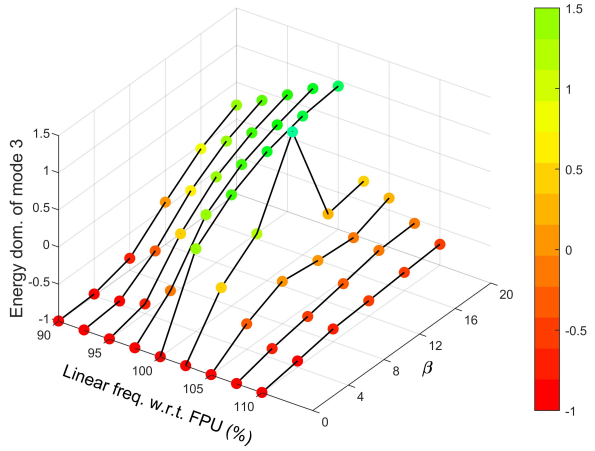

Figure 4: Energy dominance of the third mode w.r.t. the initial energy, for initial excitation of the first mode: $q_{u_{0.1}} = 1m$. The simulations were run with a Q-factor of 100,000.

ally, for low nonlinearity ($\beta = 0\text{Nm}^{-3}$ or 4Nm^{-3}) or increased linear stiffness (percentages $\geq$ 105%), there is little energy dominance. On the other hand, for lower stiffness percentages ($\leq$ 100%) *and* higher nonlinearity ($\beta \geq 8\text{Nm}^{-3}$); there is significant energy dominance. This is a result of the Duffing nonlinearity, which causes frequencies to increase with increasing amplitude (and magnitudes of the nonlinearity). The decreased linear frequencies could thus be compensated through increased nonlinearity. Similar effects may be seen for the fifth mode (App. A.3). Increasing the magnitude of the initial conditions may increase the energy dominance and vice versa. However, the assumption that the nonlinear energy remains small becomes less valid for increased nonlinearity and higher initial amplitudes - these increase the initial nonlinear force ratio from Eq. 9.

Nelson reported a similar result for a tolerance study of the quadratic FPUT α-model [26]. They found that inhomogeneously adding tolerances to both the linear and nonlinear stiffness may promote energy transfer compared to the cases where these tolerances were added to *only* the linear or nonlinear terms. In addition, for higher numbers of elements N, they observed less energy transfer. This is verified here as well, as increasing N will increase the linear frequencies to near-integer values (Eq. 5); in the present study this is observed for percentages larger than 100%.

3. String models

The previous section has shown that FPUT behavior is visible for systems with certain modal coefficients. This section will show what dynamics are visible in pre-stressed string resonators with a constant cross-section, which could be potential test beds for FPUT mechanics. Two models will be analysed: the first model accounts only for vertical string displacements, the second model accounts for both vertical and longitudinal displacements of the string. These models will subsequently be fitted to experimental results, to determine which model shows the best agreement.

3.1. Analytical string models

Analytical models for string vibrations are extensively studied in literature. The analysis in this paper is based on the studies by Anand, Nayfeh and Zhao [2, 24, 38]. Fig. 5 depicts a string and its associated displacement directions. The displacements in x-, y- and z-directions are referred to as longitudinal, transverse and vertical displacements, which are denoted by u, v and w, respectively. It is assumed here that the forces related to bending are negligible, due to the small thickness of the string. The Young's modulus, density

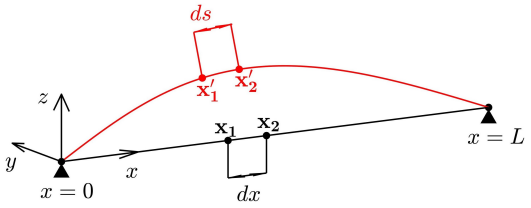

Figure 5: Simply supported string of length L. Shown is an element with length dx. The initial configuration of the string is shown in black; the deformed string is shown in red. The string is pre-loaded in the x-direction with load $T_0 = \sigma_0 A$.

and cross-sectional area are given by E, ρ and A, respectively. The derivatives with respect to x are denoted by a subscript (e.g. u_x). The deformation of element dx to ds may be found using Pythagoras' theorem:

$$ds = \sqrt{(dx+du)^2 + dv^2 + dw^2} = dx\sqrt{(1+u_x)^2 + v_x^2 + w_x^2}. \tag{10}$$

The total tension ($T(x,t) = EA\epsilon_{tot}$) in the string is dependent on the initial strain due to the pre-load $\left(\epsilon_0 = \frac{T_0}{EA}\right)$ and the displacement-induced strain $\left(\frac{ds-dx}{dx}\right)$:

$$T(x,t) = EA(\epsilon_0 + \epsilon) = T_0 + EA\frac{ds-dx}{dx} = T_0 + EA\left[\sqrt{(1+u_x)^2 + v_x^2 + w_x^2} - 1\right]. \tag{11}$$

The tension in each displacement direction is given by the ratio of each displacement with respect to the total displacement ds. The EoMs for all three directions are found by evaluating the following equation, where $m = \rho A$; the linear mass density of the string:

$$u_{tt} = \frac{1}{m}\frac{\partial}{\partial x}[T_x],\ v_{tt} = \frac{1}{m}\frac{\partial}{\partial x}[T_y] \text{ and } w_{tt} = \frac{1}{m}\frac{\partial}{\partial x}[T_z]. \quad (12)$$

The longitudinal and vertical (and transverse) wave speeds may be formulated as $c_0 = \sqrt{\frac{\sigma_0}{\rho}}$ and $c_1 = \sqrt{\frac{E}{\rho}}$, respectively. The initial stress ($\sigma_0 \approx 1$GPa) is much smaller than the Young's modulus ($E \approx 250$GPa) of the material: $c_1^2 - c_0^2 \approx c_1^2$.
Two displacement formulations will be analysed here. The first is based on the assumption that the displacement of the string will consist of vertical displacements only, here $u_x = 0,\ v_x = 0$ and $w_x \neq 0$. This results in the following EoM:

$$w_{tt} = c_0^2 w_{xx} + \frac{3}{2}c_1^2 w_x^2 w_{xx}. \quad (13)$$

The second model is based on the assumption that the vertical displacement cannot occur without stretching the string in the longitudinal direction: $u_x \neq 0,\ v_x = 0$ and $w_x \neq 0$. The EoMs for this displacement formulation are:

$$u_{tt} = c_0^2 u_{xx} + \frac{1}{2}c_1^2\frac{\partial}{\partial x}\left[w_x^2\right] \quad (14a)$$

$$w_{tt} = c_0^2 w_{xx} + c_1^2[u_x w_{xx} + u_{xx} w_x + \frac{3}{2}w_x^2 w_{xx}]. \quad (14b)$$

Eq. 14 is dependent on two displacement directions: u and w. The inertia of the longitudinal vibrations (u_{tt}) will be small for vertical vibrations, where $w >> u$. This allows for formulation of u in terms of w. The EoM for the vertical vibration is thus written as:

$$w_{tt} = c_0^2 w_{xx} + \frac{c_1^2}{2L}\left[\int_0^L w_x^2 dx\right] w_{xx}. \quad (15)$$

This is clearly of a different form than Eq. 13. The EoMs may be converted to modal EoMs, using Galerkin's method. The physical coordinates are first transformed into modal coordinates using the relation between the displacement w and the mode shapes ϕ_{u_n}:

$$w(x,t) = \sum_{n=1}^{N} \phi_{u_n}(x) q_{u_n}(t), \text{ where } \phi_{u_n}(x) = \sin\left(\frac{n\pi x}{L}\right). \quad (16)$$

The linear (in w) parts of Eq.'s 13 and 15 are equal AND generate the following linear stiffness, which is the square of the linear frequencies:

$$k_n = \omega_n^2 = \frac{n^2\pi^2}{L^2}\frac{\sigma_0}{\rho}. \quad (17)$$

The fundamental mode frequency is denoted by $\omega_0 (= \omega_1)$. Galerkin's method uses a weight function ϕ_{u_r}; the mode shape of mode r to determine the influence of mode n onto mode r. For example, for the w-displacement model, this requires solving the following equation:

$$\int_0^L \phi_{u_r}\left(\phi_{u_n} q_{u_n,tt} - c_0^2 \phi_{u_n,xx} q_{u_n} - \frac{3}{2}c_1^2(\phi_{u_n,x})^2 \phi_{u_n,xx} q_{u_n}^3\right) dx = 0. \quad (18)$$

Table 3
Modal coupling coefficients for the first three modes of two displacement models. The coefficients are normalized with respect to $\frac{\pi^2}{4}\frac{E}{\sigma_0}$.

	w-displacement			uw-displacement		
Eq.	**(1)**	**(2)**	**(3)**	**(1)**	**(2)**	**(3)**
$\tilde{b}_{111}$	1.5	0	1.5	1	0	0
$\tilde{b}_{112}$	0	4.5	0	0	4	0
$\tilde{b}_{113}$	4.5	0	27	0	0	9
$\tilde{b}_{122}$	12	0	18	4	0	0
$\tilde{b}_{123}$	0	36	0	0	0	0
$\tilde{b}_{133}$	27	0	0	9	0	0
$\tilde{b}_{222}$	0	24	0	0	16	0
$\tilde{b}_{223}$	18	0	108	0	0	36
$\tilde{b}_{233}$	0	108	0	0	36	0
$\tilde{b}_{333}$	0	0	121.5	0	0	81

where the derivatives with respect to x and t are denoted by the subscripts , x and , t. The free vibrations of a single mode ($n = r$) for the w- and uw-displacement models are given by the following (non-dimensional) equations, respectively:

$$\tilde{q}''_{u_n} + n^2\tilde{q}_{u_n} + \frac{3}{8}\pi^2 n^4 \frac{E}{\sigma_0}\tilde{q}_{u_n}^3 = 0 \quad (19a)$$

$$\tilde{q}''_{u_n} + n^2\tilde{q}_{u_n} + \frac{1}{4}\pi^2 n^4 \frac{E}{\sigma_0}\tilde{q}_{u_n}^3 = 0. \quad (19b)$$

The non-dimensionalisation was conducted using that $\tau = \omega_0 t$ and $q = \tilde{q}L$(App. D.2). These equations show the linear stiffness scales with the mode number n squared. The nonlinear part of equations scales with the ratio of Young's modulus and pre-stress, and the mode number to the power four. The magnitude of the Duffing term for w-displacement model is larger than that of the uw-displacement model. For both models, this strength may be tuned through variance of E, σ_0 and n. Neglecting the displacement in the longitudinal direction hence overestimates the nonlinear stiffness. A similar trend may be observed in the coupling coefficients, as is shown in Table 3, where it is clear that both the coupling coefficients ($\tilde{b}_{jkl}^{(r)}$) as well as the Duffing nonlinearities of the modes ($\tilde{b}_{iii}^{(j)}$) are larger for the w-displacement model. This model contains some nonzero coupling terms, which are zero for the uw-displacement model; e.g. the back-coupling $\tilde{b}_{111}^{(3)}$-term, which is required for FPUT behavior. The origin of this term is in the nonlinear parts of the equations of motion: the w- and uw-displacement models have nonlinear terms of $\frac{3}{2}w_{xx}w_x^2$ and $\frac{w_{xx}}{2L}\int_0^L w_x^2 dx$. A string model for the uvw-displacements is analysed in App. B.1; it shows coupling for degenerate transverse and vertical mode frequencies. This model is however not considered in this paper, as it is assumed here that vibrations remain planar.

3.2. Numerical string models

The modal coupling coefficients may also be found using numerical methods. Muravyov and Rizzi have developed the STiffness Evaluation Procedure (STEP), which can calculate the (nonlinear) modal coefficients from prescription of multiple mode shapes [22]. A former DMN student (V. Bos) has successfully generated software which computes these coefficients using Matlab and COMSOL Multiphysics

[5]. Bos' STEP method showed excellent agreement for the coefficients of the uw-displacement model.

3.3. Verification of experimental results

To verify which analytical model can accurately predict string vibrations, the experimental frequency response of two Si_3N_4 strings was analysed by placing the resonator in a vacuum chamber. Excitation of this resonator was achieved by using a piezo-element; measurements were conducted using a Polytech vibrometer.

Experimental ringdown of the first string resonator (with characteristics $L = 1110\mu$m, $w = 4\mu$m, $t = 92$nm, $E = 250$GPa, $\sigma_0 = 509$MPa and $\rho = 3100$kgm^{-3}) from a weakly nonlinear condition generated a Q-factor of the fundamental mode, which is estimated to be around 200,000 at a pressure of 2.69×10^{-6}mbar (Fig. B.6). The experimental frequency response is subsequently measured for several drive levels, generating multiple frequency response curves. The experimental results show Duffing behavior, where from a certain drive level, the frequency and amplitude cease to increase under an increase of the driving force. This phenomenon is a multi-mode interaction which is known as frequency locking. This phenomenon is often seen in multi-mode nonlinear Duffing systems [17].

These experiments are simulated using AUTO, a numerical bifurcation software, which can trace periodic solutions of nonlinear systems. The w- and uw-displacement models replicate the amplitude-frequency curves very well for Young's moduli of $E = 450$GPa and $E = 675$GPa, respectively (Fig. 6), but these models do not instantly replicate this frequency locking. This frequency locking is however observed for the uw-displacement model if the higher mode frequencies are increased by 0.5% (Fig. 6(a)). This slight shift of the frequency ratios increases the effect of the resonant terms, generating larger amplitudes of the higher (uneven) modes (according to Eq. 6). Conversely, no appropriate frequency shift fraction could be found to replicate the locking behavior for the w-displacement model (Fig. 6(b)). Both displacement models are fitted for high Young's moduli, which indicate that there is a (significant) discrepancy between the experimental and numerical results. The experimental ringdown from a weakly nonlinear initial condition (Fig. B.6) show little energy transfer, which implies that -for this resonator- the uw-displacement model (which also replicates the frequency locking) is expected to most accurately simulate the string's dynamics. Similar results are found for a second experiment, which is conducted on a Si_3N_4 string with characteristics $L = 700\mu$m, $w = 4\mu$m, $t = 344$nm, $\sigma_0 = 850$MPa and a fundamental mode Q-factor of 1.36×10^6 at a pressure of 9.81×10^{-5} mbar (Fig. B.19). The Q-factor of this resonator is about six times higher than that of the 1110μm string, which was found for a lower air pressure. This high Q-factor may result from the significant pre-stress of this 700μm resonator, which increases the stored energy in the resonator. A remarkable result, since the increased thickness (344nm versus 92nm) increases the bending resistance of the resonator, which should -in theory- increase the bending energy loss (App B.4). The experimental results of this specimen reveal small nonlinear Duffing effects: the frequency shifts are small; only 0.2% of the fundamental mode frequency. Some minor frequency locking is observed as well, where the frequencies -instead of lock-

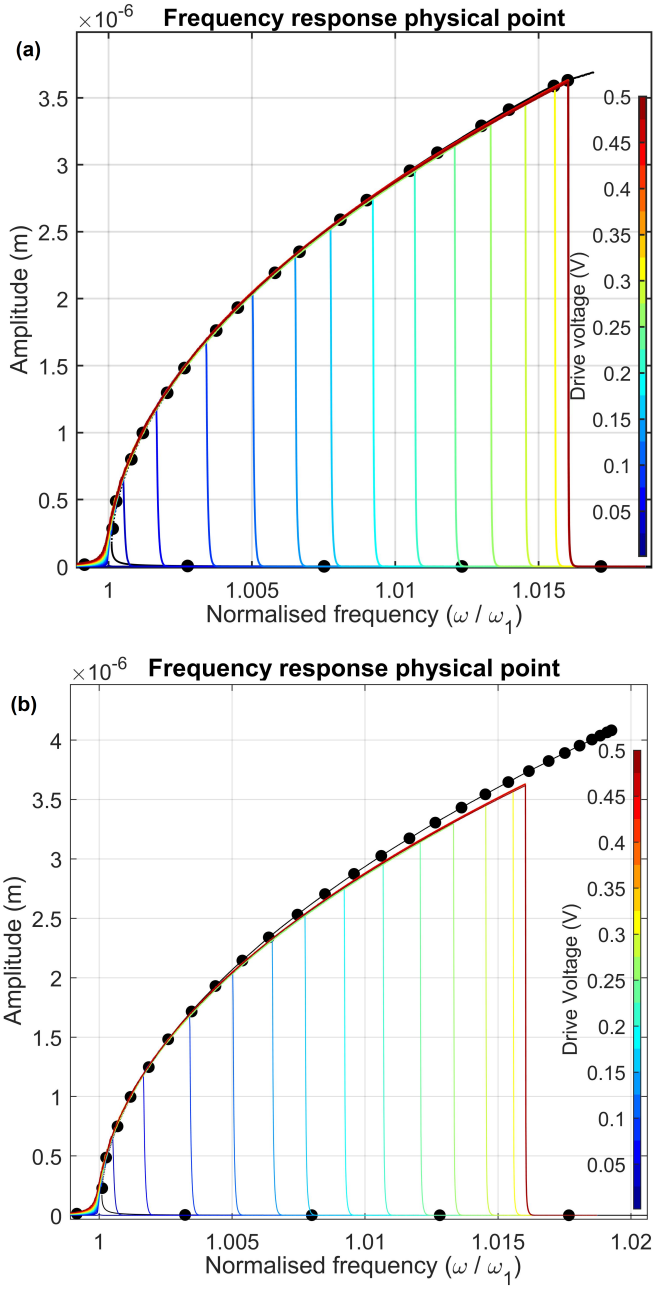

Figure 6: Experimental and simulated frequency response (at 0.36L) of a 1110μm string. The colored lines display experimental results for various drive voltages, showing locking from 0.3V. The black dots depict the simulation results for a driving voltage of 0.32V. The simulation in **(a)** is run for the uw-displacement model, showing locking for a small shift (0.5%) in the higher modes' linear frequencies. The simulation in **(b)** is run for the w-displacement model, which does not generate frequency locking.

increase only by a very small fraction under an increase of driving voltage. The results are fitted for both the w- and uw-displacement models for Young's moduli of 3667GPa and 5500GPa respectively. Neither model shows locking, which could be related to the small nonlinearity: excitation of the first mode in the weakly nonlinear regime will not cause sufficient excitation of the higher modes to cause significant modal interaction to generate frequency locking. This small (relative) nonlinearity could result from the higher pre-stress (Eq. 19). These high Young's moduli required for fitting imply that the discrepancy of the numerical and experimental results becomes more significant for increased thickness and/or pre-stress. The experimental ringdown shows a linear decay of the first mode; this could imply that there is little energy transfer, which is expected for the uw-displacement model. However, it is important to note that this ringdown is conducted from a weakly nonlinear initial condition, where nonlinear effects are small. This, together with the observation that both models fit the Duffing behavior quite accurately, while neither model generates locking, does not generate conclusive results regarding which model is most valid for this 700μm resonator.

4. FPUT mechanics in string resonators

The previous sections have elaborated upon the possible limitations of FPUT behavior and the dynamics of continuous cross-sectional string resonators. This section will show which string models could theoretically display FPUT behavior. Furthermore, some design methods are tested to determine whether they can generate the required coefficients.

4.1. Linear variables

The linear stiffness (and frequencies) of the FPUT problem ratios from Table 1 are -unlike strings- non-integer. Shifting these frequencies in strings may be achieved through a small change in the stiffness of the string. The magnitudes of the linear stiffness of the FPUT model and that of a nanostring are much different, which will be elaborated in a later section.

4.2. Nonlinear variables

The nonlinear variables consist of two parts: the Duffing terms ($b^{(n)}_{nnn}$), which scale with the amplitude of only a single mode, and the modal coupling terms ($b^{(n)}_{jkl}$), which scale with the amplitudes of multiple modes. The ratios of the Duffing terms of both the w- and uw-displacement models are approximately equal to those of the FPUT model: they scale with the frequency ratios of the considered modes. However, Table 3 shows that the magnitude of the nonlinear terms is larger for the w-displacement model than for the uw-displacement model. Furthermore, the former model has more nonzero coupling coefficients, generating a stronger coupling. This stronger coupling is especially related to the nonzero $b^{(3)}_{111}$-term, which is required for FPUT behavior: it generates energy transfer from mode 1 to mode 3 under pure excitation of the first mode. This w-displacement model will therefore be studied next. Theoretically, the uw-displacement model does not generate this initial energy transfer (as this $b^{(3)}_{111}$-term is zero), reducing the likelihood of it displaying FPUT behavior.

Table 4
Variables for the FPUT model and a $L = 1110\mu$m Si_3N_4 string.

	FPUT	w-disp. model
ω_0 [rads^{-1}]	0.19	1.15×10^6
$b^{(1)}_{111}$ [m^{-2}s^{-2}]	8.19×10^{-4}	3.07×10^{33}
α [-]	0.34	1.26×10^6
h [m]	6.45	2.07×10^{-11}

4.3. Initial force ratio

Provided that the frequency ratios are shifted slightly, one could thus set the hypotheses that this w-displacement model can show FPUT behavior. Though the magnitudes of the (non)linear coefficients are different, one could still determine if a system can generate the required initial nonlinear-to-linear force ratio r_{NL2L}. For the default FPUT problem, this ratio was 21%. In non-dimensional terms, this equation writes:

$$\tilde{r}_{\mathrm{NL2L}} = \frac{\tilde{F}_{\mathrm{nonlin}}}{\tilde{F}_{\mathrm{lin}}} = \frac{\tilde{b}^{(1)}_{111}\tilde{q}^3_{0.1}}{\tilde{k}^{(1)}_1\tilde{q}_{0.1}} = \tilde{q}^2_{0.1} = \left(\frac{w_{\max}}{\alpha\Phi_{u.\max}h}\right)^2. \quad (20)$$

Where, $\tilde{b}^{(1)}_{111}/\tilde{k}^{(1)}_1 = 1$ by choosing the space scaling parameter to be $h = \omega_0(b^{(1)}_{111})^{-\frac{1}{2}}$. For equal initial force ratios, it should thus hold that $\tilde{q}_{0.1\mathrm{FPU}} = \tilde{q}_{0.1\mathrm{string}}$. The maximum physical displacement $w_{\max}$ of the 1110μm string resonator may be calculated from these modal amplitudes using the modal coordinate transformation relation (Eq. 3) and the parameters from Table 4:

$$w_{\max.\mathrm{string}} = \tilde{q}_{0.1}\alpha_{\mathrm{string}}h_{\mathrm{string}} = 11.82\mu m. \quad (21)$$

Fig. 7 depicts the numerical ringdown from a static displacement of 11.82μm for the first mode. This simulation is conducted for linear frequency ratios from Table 1, as the integer frequency ratios show less energy transfer (Fig. 2). The linear energy depicts FPUT behavior. However, since the strength of the nonlinear terms has increased significantly, the single-mode energy ($E_n = \frac{1}{2}m^{(n)}_n\dot{q}^2_n + \frac{1}{2}k^{(n)}_n q^2_n + \frac{1}{4}b^{(n)}_{nnn}q^4_n$) is monitored as well; this indicates that the nonlinear energy fraction is still small, probably due to the initially satisfied initial force ratio. The modal amplitudes clearly show the expected beatings, though the modal amplitudes of the higher modes do not exceed the first modes, similar to the original FPUT problem.

Two remarks can be made for the required initial condition. First, the magnitude of the displacement is quite large: it is nearly times larger than the maximum displacement of the experimental results, which could be hard to achieve without breaking the resonator. Secondly, the displacement of these simulations is a static displacement of the first mode. Experimentally creating such a static displacement is not (yet) possible in these nanostructures. To verify whether this may be observed in an experimental set-up, one should apply a more physical initial condition, for example by adding a velocity to the first mode. The results of such dynamic initial conditions are shown in App. C.1, where the first mode is given an

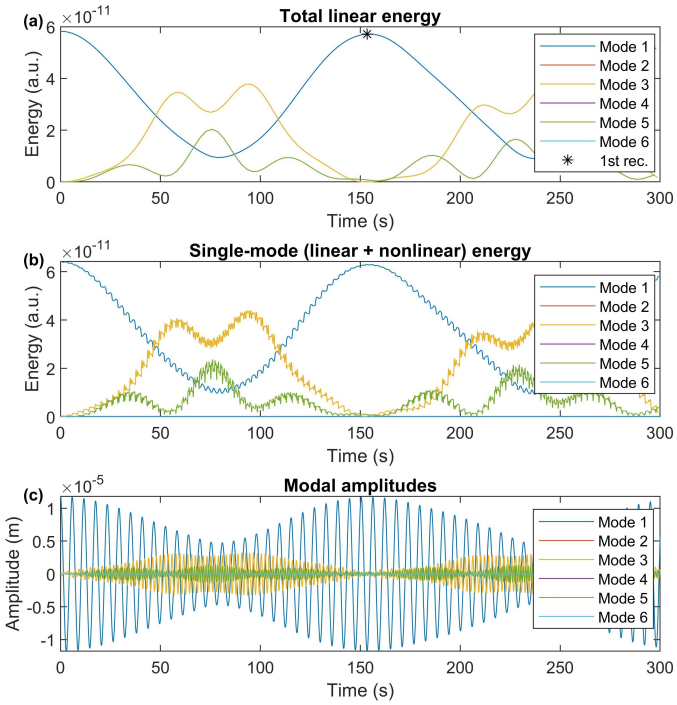

Figure 7: Numerical ringdown from a maximum displacement of 11.82μm of the first mode. **(a)** depicts the linear energy vs. time, **(b)** depicts the single-mode (linear + nonlinear) energy vs. time and **(c)** shows the modal amplitudes vs. time. The simulation was run with a fundamental mode Q-factor of 100,000.

initial velocity and some higher modes are (weakly) excited as well. FPUT-like behavior is still observed for these initial conditions.

4.4. Design for FPUT behavior

Section 3 shows that the modal coupling coefficients are dependent on the displacement formulation for continuous strings. Additionally, in order to see FPUT behavior, one requires non-integer frequency ratios, as well as some coupling coefficients: primarily a nonzero back-coupling to generate initial energy transfer. However, the analytical model that generates such a coupling term (the w-displacement model) cannot fit the experimental results accurately, as it does not generate all observed dynamics. Furthermore, from a continuum mechanics point of view, this model appears to be inaccurate, as a longitudinal displacement is required to allow for vertical displacement of the resonator. This chapter will therefore explore (using the STEP method) some possibilities to generate an improved coupling for string-like resonator models that include longitudinal displacements. The present form of the STEP software only works for truss elements in COMSOL, which account only for axial deformations due to u- and w-displacements. The procedure is as follows: a string design of length L is divided into n truss-elements. The cross-section of each of these elements may be varied, such that the mass and stiffness of the string may be altered locally. The STEP method is subsequently used to find the modal coefficients of the design.

The local variance of the cross-section (and thus the mass and stiffness) will alter the mode shapes and the resonance frequencies of the string. By changing the mode shapes, one should thus also be able to alter the modal coupling coefficients (App. B.7).

Fig. 8 depicts a design which has such an asymmetric mass density. It is found that such a design does not generate new coupling terms. However, it does shift the frequencies and it allows for significant tuning of the nonlinearity, which - compared to continuous strings- significantly increases the relative nonlinearity of the higher modes.

Recent research by Dou and Li shows that the Duffing coefficients of clamped-clamped beams may be tuned in a similar manner [9, 18]. Their method was tested for string resonators (with much smaller thickness to increase the validity of using truss models). It was found that their results cannot be verified by only using truss models (App. C.2), indicating that their improvements likely result from more advanced deformation modelling.

Figure 8: First mode shape of an asymmetrical string-like resonator design with two cross-sectional areas, with a respective ratio of 10.

For string-like resonators, it appears that the local variance of cross-sectional area does generate different relative nonlinearity (especially for the higher modes), but it does not generate new coupling terms. Nonetheless, this does not mean that string-like resonators may never show FPUT behavior. More complicated string designs, or different structures (e.g. the T-design from Dou and Li [9, 18]) could still generate FPUT behavior as this generates a nonzero (quadratic) back-coupling term.

5. Discussion & Conclusion

This paper has shown methods to generate FPUT behavior in string resonators. A coordinate transformation of the β-model from physical to modal coordinates may generate a better understanding of the coupling between the eigenmodes of the system [28, 33]. This transformation showed that FPUT behavior is caused by initial excitation of the third mode through a back-coupling term; a $b^{(3)}_{111}$-term. In addition, an eigenfrequency analysis of the original equations of motion (Eq. 1) has shown that the linear frequencies ratios are non-integer (Eq. 5). A subsequent sensitivity study has shown that FPUT behavior (for the default FPUT problem, where $N = 16$ and $\beta = 8\text{Nm}^{-3}$) is hardly influenced by damping in the high-Q regime, for Q-factors of the first, third and fifth mode larger than 10,000, 3333 and 2000 respectively. This sensitivity study also indicates (in Fig. 4) that a decrease in the magnitude of the frequency ratios may be compensated by increasing the magnitude of the nonlinearity,

which implies that FPUT behavior is not associated to the variables from the original FPUT report only [11]. FPUT behavior may thus be observed for structures with different relative nonlinearities, such as nanostrings, provided that the initial nonlinear to linear force ratio satisfies some ratio.

Two analytical string models were presented: a model that includes only vertical (w) displacements and a model that includes both longitudinal (u) and vertical (w) displacements (Fig. 5). It was found that the former model generates stronger nonlinearity than the latter model. This stronger nonlinearity was present in both a stronger Duffing strength, as well as stronger coupling coefficients and a nonzero back-coupling term (Table 3). The nonlinearity of both models was found to scale with the mode number n and the ratio of Young's modulus and pre-stress ($\frac{E}{\sigma_0}$).

Simulations of experimentally obtained frequency responses on a high-stress Si_3N_4 nanostring of length 1110μm show that the uw-displacement model generates qualitatively the same results. This model shows frequency locking and a proper fits of the Duffing curves (Fig. 6), where the w-displacement model only replicates the Duffing curve. A second experiment on a shorter (though thicker) string resonator shows a small nonlinear effect: the frequency shift is small and frequency locking is minor, which may be explained by the higher pre-stress (lower relative nonlinearity) in the resonator. The w-, as well as the uw-displacement model were fitted onto the Duffing curves, but neither model showed locking behavior. This may be an effect of the small relative nonlinearity, which does not excite the higher modes sufficiently to cause significant modal interaction.

The observation that both displacement models seem to fit both experimental Duffing curve quite well is not peculiar, since both experimental results are dominated by the Duffing nonlinearity of the first mode. However, this does not generate conclusive results that can determine which displacement model is most accurate. Nonetheless, the experimental ringdown of both resonators show a constant decay of the first mode. This works in favor of the uw-displacement model, since the modes are less strongly coupled to the other modes than the w-displacement model. This latter model would -in absence of other nonlinearities- exchange energy directly to the third mode through excitation of the first mode, which would probably show a different decay (including a possible increase of the amplitudes of the higher modes and subsequent increase of the first mode). It is important to note that the experimental ringdown experiments were conducted in the weakly nonlinear regime, where the effect of such nonlinearities is small, which does not have significant mode coupling, generating a linear decay (nonlinear damping then is small as well).

The simulations replicate the strings' qualitative dynamics fairly well: slope fits and (for one resonator) resonator). However, quantitative agreement could be found, as the Young's moduli were significantly higher, varying from 450GPa to 5500GPa: 1.8 and 22 times larger than the default Young's modulus of Si_3N_4. This discrepancy could originate from incorrect conversion of the experimental data, or from the negligence of other significant nonlinearities (e.g. from bending), requiring more advanced modelling of the strings' displacements.

To determine whether any of these analytical string models could show FPUT behavior, their coefficients were compared to the FPUT model, and it was shown numerically that the w-displacement model for the 1110μm nanostring can show FPUT behavior for initial conditions which generate an initial nonlinear to linear force ratio of 21%, for an initial displacement of 11.82μm (nearly thee times that of Fig. 6). A larger nonlinearity of the resonator, which may be achieved by lowering the pre-stress, may decrease the required initial displacement to more "physical" quantities. The frequency ratios of this w-displacement model should be non-integer; integer frequency ratios will generate energy some transfer, but this is not sufficient to generate energy dominance.

Finally, it was shown that the nonlinearity of string resonators may be changed through local variance of the cross-sectional area of the string. The numerical software that was used to find these coefficients is only valid for truss elements, which neglect possibly significant displacement mechanisms, such as bending. It was found that local increase of the cross-section of strings may increase the relative nonlinearity of higher modes. However, this procedure did not generate nonzero back-coupling coefficients. Research has shown that such coefficients (though different in terms of nonlinearity), may be found for different structures [9, 18]. To determine whether a string resonator may ever show FPUT behavior, one could do a topology optimization study that is focused on finding structures that have such nonzero back-coupling coefficients as well as the required frequency ratios. Before this optimization is initiated, one should expand the current software for the STEP method, such that this software may also account for more accurate displacement models (e.g. beam elements). Additionally, one should include the coupling between the (degenerate) vertical and transverse modes of square or circular cross-sectioned strings, as these appear to be strongly coupled, as is shown in App. B.8.

In summary, this research has shown that to observe FPUT behavior, one should design a resonator that has certain modal coefficients. This resonator should have non-integer frequency ratios, a nonzero back-coupling coefficient and it should be placed in an environment where Q-factors are sufficiently high. Simulations of experimentally obtained frequency responses have shown that continuous cross-section string resonators generate the desired dynamics. Additionally, this research has shown that the nonlinearity of string resonators may be tuned by varying the ratio of E over σ_0 and a non-constant cross-sectional area along the length of the string. Expansion of the STEP method to include more displacement formulations and geometries may result in structures which could show FPUT behavior. These structures could then be used for various applications, e.g. sensors with non-constant measurement characteristics, filters, and possibly many more applications.

References

[1] Principles of lock-in detection. URL https://www.zhinst.com/europe/en/resources/principles-of-lock-in-detection.

[2] G.V. Anand. Large-Amplitude Damped Free Vibration of a Stretched String. *The Journal of the Acoustical Society of America*, 45(5):1089–1096, 1969. ISSN 0001-4966. doi: 10.1121/1.1911578.

[3] A. Barnard, M. Zhang, G. Wiederhecker, M. Lipson, and P.L. McEuen. Real-time vibrations of a carbon nanotube. *Nature*, (7742): 89–93. ISSN 14764687. doi: 10.1038/s41586-018-0861-0.

[4] G. P. Berman and F. M. Izrailev. The Fermi-Pasta-Ulam problem: Fifty years of progress. *Chaos*, 15(1), 2005. ISSN 10541500. doi: 10.1063/1.1855036.

[5] V. Bos. Nonlinear dynamics of graphene membranes. Master's thesis, Delft University of Technology, 1 2020.

[6] B. V. Chirikov, F. M. Izrailev, and V. A. Tayursky. Numerical experiments on the statistical behaviour of dynamical systems with a few degrees of freedom. *Computer Physics Communications*, 5(1):11–16, 1973. ISSN 00104655. doi: 10.1016/0010-4655(73)90003-9.

[7] T. Dauxois, M. Peyrard, and S. Ruffo. The Fermi-Pasta-Ulam 'numerical experiment': History and pedagogical perspectives. *European Journal of Physics*, 26(5):3–11, 2005. ISSN 01430807. doi: 10.1088/0143-0807/26/5/S01.

[8] D. Davidovikj, F. Alijani, S. J. Cartamil-Bueno, H. S.J. Van Der Zant, M. Amabili, and P. G. Steeneken. Nonlinear dynamic characterization of two-dimensional materials. *Nature Communications*, (1):1–7. ISSN 20411723. doi: 10.1038/s41467-017-01351-4.

[9] S. Dou, B.S. Strachan, S.W. Shaw, and J.S. Jensen. Structural optimization for nonlinear dynamic response. *Philosophical Transactions of the Royal Society A: Mathematical, Physical and Engineering Sciences*, 373(2051), 2015. ISSN 1364503X. doi: 10.1098/rsta.2014.0408.

[10] N. Engelsen, A. Ghadimi, S. Fedorov, T. Kippenberg, M. Bereyhi, R. Schilling, and D. Wilson. Elastic Strain Engineering for Ultralow Mechanical Dissipation. *International Conference on Optical MEMS and Nanophotonics*, 2018-July(May):1–6, 2018. ISSN 21605041. doi: 10.1109/OMN.2018.8454645.

[11] E. Fermi, P Pasta, S Ulam, and M Tsingou. Studies of the nonlinear problems. doi: 10.2172/4376203. URL https://www.osti.gov/biblio/4376203.

[12] J. Ford. The fermi-pasta-ulam problem: paradox turns discovery. *Physics Reports*, 213(5):271–310, 1992.

[13] A. H. Ghadimi, D. J. Wilson, and T. J. Kippenberg. Dissipation engineering of high-stress silicon nitride nanobeams. 2016.

[14] J. Güttinger, A. Noury, P. Weber, A. Eriksson, C. Lagoin, J. Moser, C. Eichler, A. Wallraff, A. Isacsson, and A. Bachtold. Energy-dependent path of dissipation in nanomechanical resonators. *Nature Nanotechnology*, 12(7):631–636, 2017. ISSN 17483395. doi: 10.1038/nnano.2017.86.

[15] G.A. Holzapfel. *Nonlinear Solid Mechanics: A Continuum Approach for Engineering*. Wiley, 2000. ISBN 9780471823193.

[16] Daniel J. Inman. *Engineering Vibrations*. Pearson, 2014.

[17] A. Keşkekler, O. Shoshani, M. Lee, H. van der Zant, P. Steeneken, and F. Alijani. Tuning nonlinear damping in graphene nanoresonators by parametric–direct internal resonance. *Nature Communications*, 12 (1):1–7, 2021. ISSN 20411723. doi: 10.1038/s41467-021-21334-w.

[18] L. Li, P. Polunin, S. Dou, O. Shoshani, B. Strachan, J.. Jensen, S. Shaw, and K. Turner. Tailoring the nonlinear response of MEMS resonators using shape optimization. *Applied Physics Letters*, 110(8), 2017. ISSN 00036951. doi: 10.1063/1.4976749.

[19] R. Lifshitz and M. C. Cross. Nonlinear Dynamics of Nanomechanical and Micromechanical Resonators. *Reviews of Nonlinear Dynamics and Complexity*, pages 1–52, 2009. doi: 10.1002/9783527626359.ch1.

[20] L. Meirovitch. *Fundamentals of Vibrations*. Waveland Press, 2010. ISBN 9781577666912.

[21] D. Midtvedt, A. Croy, A. Isacsson, Z. Qi, and H. S. Park. Fermi-pasta-ulam physics with nanomechanical graphene resonators: Intrinsic relaxation and thermalization from flexural mode coupling. *Physical Review Letters*, 112(14):1–5, 2014. ISSN 10797114. doi: 10.1103/PhysRevLett.112.145503.

[22] A.A. Muravyov and S.A. Rizzi. Determination of nonlinear stiffness with application to random vibration of geometrically nonlinear structures. *Computers Structures*, 81(15):1513 – 1523, 2003. ISSN 0045-7949. doi: https://doi.org/10.1016/S0045-7949(03)00145-7.

[23] A. Mussot, C. Naveau, M. Conforti, A. Kudlinski, F. Copie, P. Szriftgiser, and S. Trillo. Fibre multi-wave mixing combs reveal the broken symmetry of Fermi-Pasta-Ulam recurrence. *Nature Photonics*, (5): 303–308. ISSN 17494893. doi: 10.1038/s41566-018-0136-1.

[24] A.H. Nayfeh. Applied nonlinear dynamics: analytical, computational, and experimental methods. *Choice Reviews Online*, 32(11):32–6286–32–6286, 1995. ISSN 0009-4978. doi: 10.5860/choice.32-6286.

[25] A.H. Nayfeh. *Nonlinear Oscillations*, chapter 7, pages 444–543. John Wiley Sons, Ltd, 1995. ISBN 9783527617586. doi: https://doi.org/10.1002/9783527617586.ch7.

[26] H. Nelson, M.A. Porter, and Bhaskar Choubey. Variability in Fermi-Pasta-Ulam-Tsingou arrays can prevent recurrences. *Physical Review E*, 98(6):1–10, 2018. ISSN 24700053. doi: 10.1103/PhysRevE.98.062210.

[27] R.A. Norte, J.P. Moura, and S. Gröblacher. Mechanical Resonators for Quantum Optomechanics Experiments at Room Temperature. *Physical Review Letters*, 116(14):1–6, 2016. ISSN 10797114. doi: 10.1103/PhysRevLett.116.147202.

[28] S.D. Pace and D.K. Campbell. Behavior and breakdown of higher-order Fermi-Pasta-Ulam-Tsingou recurrences. *Chaos*, 29(2), 2019. ISSN 10541500. doi: 10.1063/1.5079659.

[29] S. Schmid and C. Hierold. Damping mechanisms of single-clamped and prestressed double-clamped resonant polymer microbeams. *Journal of Applied Physics*, 104(9), 2008. ISSN 00218979. doi: 10.1063/1.3008032.

[30] S. Schmid, K. D. Jensen, K. H. Nielsen, and A. Boisen. Damping mechanisms in high-Q micro and nanomechanical string resonators. *Physical Review B - Condensed Matter and Materials Physics*, 84 (16):1–6, 2011. ISSN 10980121. doi: 10.1103/PhysRevB.84.165307.

[31] S. Schmid, L.G. Villanueva, and M.L. Roukes. *Fundamentals of nanomechanical resonators*. 2016. ISBN 9783319286914. doi: 10.1007/978-3-319-28691-4.

[32] R. Munnig Schmidt, G. Schitter, A. Rankers, and J. Van Eijk. *The Design of High Performance Mechatronics: High-Tech Functionality by Multidisciplinary System Integration*. IOS Press, NLD, 2nd edition, 2014. ISBN 161499367X.

[33] D.S. Sholl and B.I. Henry. Recurrence times in cubic and quartic Fermi-Pasta-Ulam chains: A shifted-frequency perturbation treatment. *Physical Review A*, 44(10):6364–6374, 1991. ISSN 10502947. doi: 10.1103/PhysRevA.44.6364.

[34] J. L. Tuck and M. T. Menzel. The superperiod of the nonlinear weighted string (FPU) problem. *Advances in Mathematics*, 9(3):399–407, 1972. ISSN 10902082. doi: 10.1016/0001-8708(72)90024-2.

[35] G. Van Simaeys and Ph Emplit. Experimental demonstration of the fermi-pasta-ulam recurrence in a modulationally unstable optical wave. *Physical Review Letters*, 87(3):33902–1–33902–4, 2001. ISSN 10797114. doi: 10.1103/PhysRevLett.87.033902.

[36] Scott S. Verbridge, Jeevak M. Parpia, Robert B. Reichenbach, Leon M. Bellan, and H. G. Craighead. High quality factor resonance at room temperature with nanostrings under high tensile stress. *Journal of Applied Physics*, 99(12), 2006. ISSN 00218979. doi: 10.1063/1.2204829.

[37] S.S. Verbridge, H.G. Craighead, and J.M. Parpia. A megahertz nanomechanical resonator with room temperature quality factor over a million. *Applied Physics Letters*, 92(1):8–11, 2008. ISSN 00036951. doi: 10.1063/1.2822406.

[38] D.M. Zhao, S.P. Li, Y. Zhang, and J.L. Liu. Nonlinear Vibration of an Elastic Soft String: Large Amplitude and Large Curvature. *Mathematical Problems in Engineering*, 2018, 2018. ISSN 15635147. doi: 10.1155/2018/7909876.

3

Conclusion, Discussion and Recommendations

3.1. Conclusion and discussion

The goal of this thesis was to determine whether a string resonator could show Fermi-Pasta-Ulam-Tsingou recurrence. The research has been summarized in the research paper. The research questions are answered in the next three subsections.

3.1.1. Requirements for FPUT behavior

The modal coefficients of the FPUT problem were determined through a modal coordinate transformation of the FPUT potential. This transformation indicated that to see FPUT behavior, one requires the non-integer linear frequency ratios (and slightly lower than the nearest internal resonance condition) and certain coupling coefficients. Specifically, the system should have a nonzero back-coupling coefficient, which will excite the third mode under pure excitation of the first mode.
FPUT behavior becomes visible as the energy of the initially excited mode is dominated by some other mode(s), before the energy returns to the initially excited mode again. It was shown that energy dominance of a certain mode does not directly imply that the modal amplitude of the dominant mode is largest. To verify that the system shows FPUT behavior, one should thus always check both amplitudes and (linear) energies of each mode. Furthermore, it was shown that the dynamics of the default FPUT problem (for $N = 16$ and $\beta = 8\text{Nm}^{-3}$) -where the first mode is excited only- is relatively insensitive to Q-factors for the first, third and fifth mode that exceed 10,000, 3333 and 2000, respectively. In addition, it was shown in A.11 that one may still observe FPUT behavior for a system with increased nonlinearity and (linear) frequency ratios lower than the internal resonance condition. The increased nonlinearity compensates the lower frequency ratios, due to the hardening nonlinearity. FPUT behavior may be observed for systems where the initial nonlinear to linear force ratios are larger than approximately 21%. Energy transfer will become more significant for systems with larger nonlinearities and initial conditions. However, for these conditions, the negligence of the nonlinear energy fraction is no longer valid.

3.1.2. Dynamics in continuous string resonators

The vibrations of continuous string resonators were approximated using three displacement models that account only for axial deformation of the resonator. Two of these models were considered in the research paper: one that accounts only for vertical (w) displacements, and another that accounts for longitudinal (u) and vertical (w) displacements. It is assumed that though the coupling between transverse and vertical modes of degenerate modes is strong (App. E.2.2), the vibrations still remain planar, since the resonator's transverse and vertical frequencies are non-degenerate.
All analytical models generate the same linear stiffness parameters (for the vertical modes of the string), which scale with the mode number n, generating integer frequency ratios. On the other hand, it was found that the w-displacement model generates significantly stronger nonlinear (coupling) coefficients than the uw-displacement model, which implies that negligence of a displacement direction will cause overestima-

tion of the stiffness. Both analytical models show that the relative nonlinearity of strings is dependent on the ratio of Young's modulus and pre-stress, as well as the mode number. Using frequency response simulations, it was shown that the uw-displacement model replicates the frequency response of a physical resonator of length 1110μm fairly accurately, as it shows slope fits of the Duffing curve and frequency locking. The w-displacement model generates similar Duffing curves for this resonator, but it does generate frequency locking. The experimentally obtained Duffing response of another string resonator (of length 700μm, and a much larger thickness) could be simulated using both displacement models, but neither model could replicate frequency locking. The simulations of this second experimental frequency response hence remain inconclusive regarding which displacement formulation is most valid, as the Duffing response could be fitted using both analytical models. The results of the experimental ringdowns (from the weakly nonlinear regime) for both resonators of this resonator do not show modal significant interactions either, as the decay is linear. This could -together with the notion that in reality, a vertical displacement is only possible for some longitudinal displacement- imply that the uw-displacement model is probably most valid. However, this conclusion should be drawn carefully, as the ringdown experiments were conducted from the linear regime.
All frequency response simulations showed qualitative agreement in the form of fits of the Duffing curve (and frequency locking for one of the two experiments), but they did not show qualitative agreement, as the Young's modulus in simulations should have been increased to values that are 1.8 times (E = 450GPa) or even 22 times larger (E = 5500GPa). This implies that there is still some error present in the analysis, which could be related to experimental data conversion, or assumptions regarding the considered deformation models of these resonators. Interestingly, the model appears to be most inaccurate for a larger resonator thickness, which could have more significant bending deformation.

3.1.3. FPUT recurrence in string resonators

A string-like resonator may potentially show FPUT behavior if certain requirements are met. One of these requirements is that the frequency ratios are non-integer, and slightly lower than the nearest internal resonance condition. Another requirement is that the system should have a nonzero back-coupling coefficient. For these criteria, the w-displacement model may potentially show FPUT behavior for an initial nonlinear to linear force ratio of 21%, which is achieved for a displacement that is nearly three times larger than the experimental displacements. To achieve a more realistic displacement, the relative nonlinearity should be increased. Though this w-displacement model may display FPUT mechanics, simulations of frequency responses show that the w-displacement model (which has this nonzero back-coupling coefficient) is the least valid analytical model. This implies that a different resonator design should be found, which either allows for negligence of the longitudinal displacements, or it should possess a nonzero back-coupling term for the uw-displacement model as well.
In this regard, STEP method was employed to show that an asymmetry in the resonator's cross-sectional area allows for shifting of the linear frequencies and variation of the relative nonlinearity. However, these designs did not generate nonzero back-coupling coefficients. Hence, to observe FPUT recurrence in string-like resonators, one should try different designs, with more complicated geometries. The current implementation of the STEP method only works for axial deformation models; it does not work for more complicated deformation models, such as those for beams or plates. The coefficients of the improved designs, where the mass density was varied, are thus computed using a simplified deformation model, which is only valid for systems with large pre-stresses, where possible bending of the structure is neglected.

3.2. Recommendations

This research has clarified why FPUT behavior may, or may not be observed in a structure. This research is not perfect, and there is certainly room for improvements. This section will elaborate upon further steps, which may taken into account when improving the nonlinearity in (string) resonators -possibly even with the target to design a system that displays FPUT recurrence. The recommendations are divided into three topics concerning the FPUT study, (simulated and experimental) string vibrations and design for FPUT behavior.

3.2.1. Recommendations regarding the FPUT study

- The present study is focused primarily on the FPUT β-model, which only includes a cubic nonlinearity. The α-model (for quadratic nonlinearities) is not considered here, since the nonlinearity of string resonators is cubic. This results in the fact that the present study may not be taken one-to-one for other structures, which could have different types of nonlinearities. Furthermore, this research neglects all

linear couplings in resonators. Subsequent studies should characterize the influence of these additional coupling methods as well, and possibly even combine them.

- The simulated FPUT study is an approximation of the original experiment, as it only accounts for the first three uneven modes (modes 1, 3 and 5). There appears to be a slight difference in the energy plots of the third and fifth modes. This could be improved by adding higher (uneven) modes to the simulation.
- The FPUT study was conducted for 16 mass elements, which basically simulates a strongly discretized string, generating linear frequency ratios that are far from integer values. It was shown that for ring-down from a certain initial nonlinear to linear force ratio, these non-integer frequency ratios generate the most significant energy transfer. The hardening nonlinearity of the resonator increases the frequency ratios, which should be taken into account during the design of a resonator. The effects of larger numbers of masses -which approach integer frequency ratios- should be characterized together with the corresponding hardening effect of the nonlinearity, to generate a design that displays the most significant energy transfer.

3.2.2. Recommendations for the experimental validation of analytical models

- The simulation method has thus far only been tested for two string resonators. The simulations of both resonators' frequency responses were found for significant increases of the Young's modulus in the simulation. Neither simulation model generated a fully conclusive result regarding which model is most valid. Additional tests on multiple string resonators with different relative nonlinearities (e.g. by decrease of the pre-stress) and thickness could fully characterize the discrepancy and limitations of the considered (analytical) models. Once these limitations are known, one can generate a more accurate simulation model (with possibly more deformation mechanisms, e.g. bending deformations). This model could then potentially be used for characterization of a material's Young's modulus [8].
- The analytical study is based on a square or circular cross-sectioned string, which was shown to have degenerate transverse and vertical eigenfrequencies, generating strong coupling between these two modes (as shown in Fig. B.27). In reality, this effect is expected to be less significant, since the resonators' cross-sections is are rectangular, and thus these frequencies will not be degenerate. However, this effect should be characterized first, before it may be safely neglected. In addition, such structures will also posses torsional modes, of which the coupling with respect to the transverse modes is unknown. Experimental measurements in combination with modelling of the frequency response of the resonator for transverse and torsional motion could validate the true coupling between these transverse, vertical and torsional modes. This way, the assumption that vibrations remain planar can be verified or rejected.

3.2.3. Recommendations for the design of resonators showing FPUT behavior

- It was shown that string resonators with constant cross-sectional areas do not posses the required coupling coefficients, nor do they have the required non-integer frequency ratios. A string-like resonator with a local increase in cross-sectional can be designed to have non-integer frequency ratios and improved (relative) nonlinearity, but it does not have the required coupling coefficients. These results should be experimentally verified.
- Similarly to the recommendation about the analytical deformation models, the STEP method only works for string-like resonators that allow for simulation using truss models, which account for axial deformations only. This method should be expanded to account for additional deformation formulations, such bending deformations.
- Once a solid numerical framework has been established, additional geometries should be tested for improvement of the coupling coefficients. This could be done efficiently using topology optimization, which could then be used to extract the modal coefficients of various designs. The goal would then be to find a system which has non-integer frequency ratios (below the internal resonance condition) and a nonzero back-coupling term. However, the nonlinear problem that is solved to yield the nonlinear modal coupling coefficients, may complicate this topology optimization study significantly.

A

The FPUT β-model

This chapter will first characterize the modal interactions in the FPUT β-model through a modal coordinate transformation. A subsequent study will explore the limitations for occurrence of FPUT behavior. Finally, requirements are formulated for systems to show FPUT behavior.

A.1. The default FPUT β-model

The original FPUT study analysed several models; quadratic (α-model), cubic (β-model) and broken linear models. All of these models resulted in significant energy transfer, followed by recurrence of the initial condition [11]. Fig. A.1a depicts a result for the β-model, which is analysed in this section. This model consists of 16 mass elements ($N = 16$) of $m = 1$kg, a linear stiffness of $k = 1\text{Nm}^{-1}$, and a nonlinear stiffness of $\beta = 8\text{Nm}^{-3}$. The equations of motion are are shown in Eq. A.1.

$$\ddot{x}_i = (x_{i+1} + x_{i-1} - 2x_i) + \beta[(x_{i+1} - x_i)^3 - (x_i - x_{i-1})^3], \text{ where } i = 1,2,...N \tag{A.1}$$

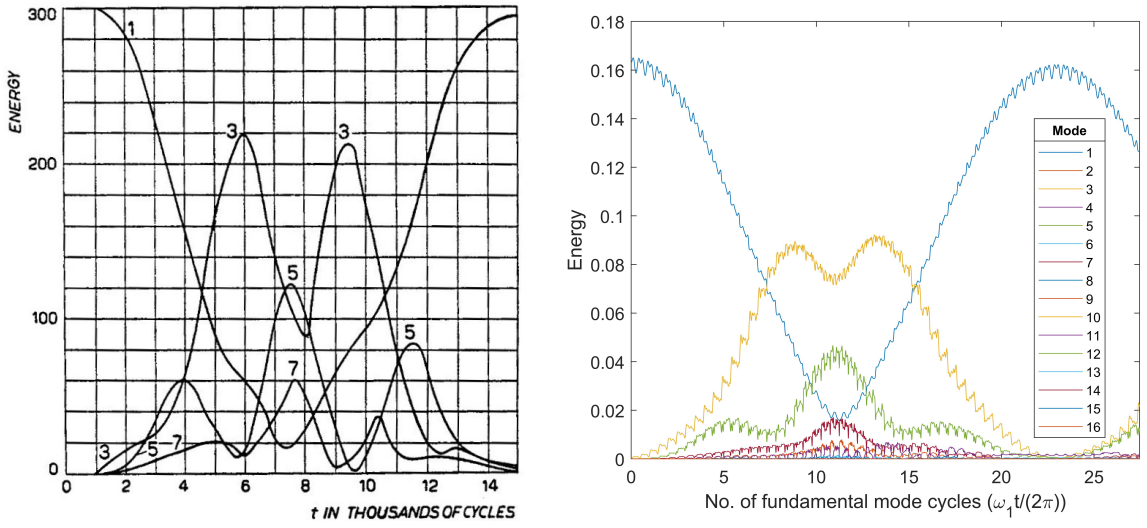

(a) (b)

Figure A.1: FPUT β-model simulations, for $N = 16$, $\beta = 8$, $\delta t^2 = \frac{1}{8}$ and the initial conditions were half a sine wave (similar to the first mode of a string). A.1a depicts the result from the original report [11]. A.1b depicts a reproduction that is based on Dauxois' paper [7].

Fig. A.1 depicts a plot from the original report of the FPUT study, as well as a reproduction of the original experiment, which is produced using a modified code from Dauxois' paper on FPUT mechanics [7].
In the FPUT experiment, the linear modal energy (consisting of a kinetic and a potential part) is monitored

under the assumption that the nonlinearities remain small; the energy residing in each involved mode k is calculated using the Fourier transforms of the amplitudes, as is shown in Eq. A.2.

$$E_{a_k}^{lin} = E_{a_k}^{kin} + E_{a_k}^{pot} = \frac{1}{2}\dot{a}_k^2 + 2a_k^2 \sin^2\left(\frac{\pi k}{2N}\right) \text{ where } a_k = \sum_{n=1}^{N} \sin\left(\frac{nk\pi}{N}\right) \tag{A.2}$$

These Fourier functions map the displacement of each individual mass element i (given by x_i) to the modal displacement of mode k of the system, a_k. Several differences may be distinguished from both graphs. The first is that the recurrent behavior is present in Fig. A.1b, but the quantities along the horizontal and vertical axes of the plots do not seem to match. This could be due to some scaling of the time response in the original experiment. Secondly, the energy versus time graph from the original experiment is smooth, whereas the reproduced experimental plot shows a rough graph. This is due to the fact that the original plot was drawn manually, which generated these smooth graphs [34]. In addition, it is clear that the local minimum of the third mode's energy (and corresponding local maximum of the fifth mode's energy) at $t = 8$ in Fig. A.1a is not of the same magnitude as the same behavior in Fig. A.1b. This difference could have various origins: for example, different integration tolerances may be used in the left and right simulations, or a (slightly) different magnitude of the initial conditions could have been used in either computation. The difference may also be present due a slight shift in the linear frequencies. The full effect of shifted linear frequencies will be shown later in this chapter. Though the exact origin of these differences is not known, the author of this report will continue with the same simulation scheme, as the reproduced experiment still reproduces FPUT behavior with sufficient accuracy.

A.2. The β-model in terms of modal coordinates

To determine the origin of the recurrent behavior, it is convenient to transform the physical coordinates x_i of each mass element to modal coordinates, which represent state of the system in terms of its eigenmodes. This will generate linear and nonlinear modal coefficients, which will show what relations are present between all considered modes.

A.2.1. Relation of considered modes and initial conditions

The number of considered modes (or degrees of freedom) in the model determines the accuracy of the modeled dynamics. Tuck and Menzel (née Tsingou) [34] stated that for FPUT behavior to become visible, the imposed initial condition should not generate nonlinear forces that exceed 10% of the linear force:

$$r_{NLvsL} = \frac{F_{NL}}{F_L} = \frac{\beta[(x_{i+1} - x_i)^3 - (x_i - x_{i-1})^3]}{(x_{i+1} + x_{i-1} - 2x_i)} < 0.1, \text{ where } i = 1, 2, ...N \tag{A.3}$$

Which implies that for a decreased number of elements N, the difference between the initial coordinates $(x(n) - x(n-1))$ increases.

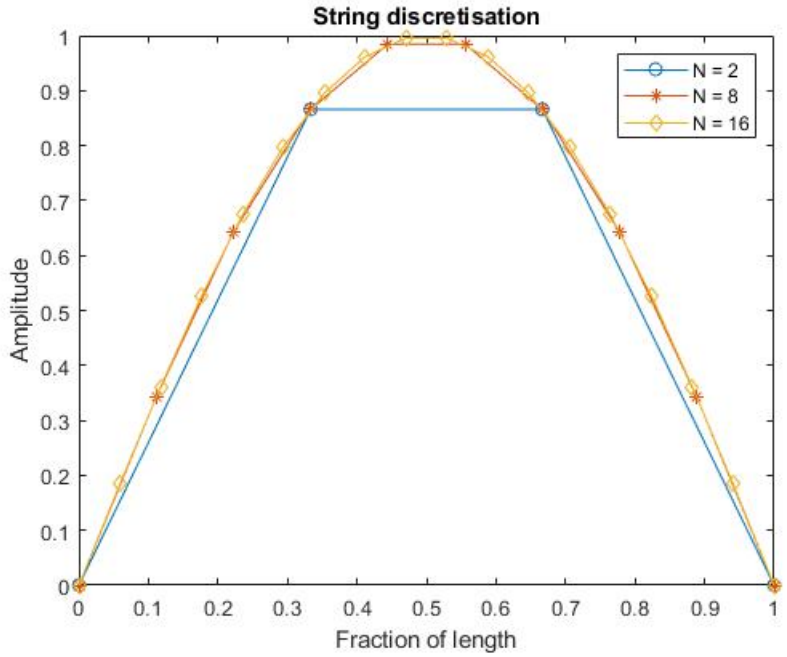

Figure A.2: Discretisation of a string's first mode shape. Shown are discretisations for $N = 2$, $N = 8$ and $N = 16$.

Decreasing the mode number N will result in a large difference between the initial amplitudes, as is depicted in Fig. A.2. Comparing the amplitudes of the first point (denoted by A_1) along the string for the $N = 2$ and the $N = 16$ cases, shows that the initial amplitudes are $A_1 = \frac{\sqrt{2}}{2} = 0.71$ and $A_1 = 0.18$ respectively. These amplitudes generate cubic nonlinear forces ($F_{NL} = \beta A_1^3$). Comparing these nonlinear forces with each linear counterpart, by dividing the nonlinear force over the linear force ($F_L = kA_1$), the following nonlinear to linear force relation is found:

$$\frac{F_{NL}}{F_L} = \frac{\beta A_1^3}{kA_1} = \beta A_1^2. \tag{A.4}$$

For $N = 2$ and $N = 16$, these nonlinear-to-linear force ratios equal:

$$\text{N = 2: } \left(\frac{\sqrt{2}}{2}\right)^2 \beta \approx 0.50\beta \text{ and for N = 16: } (0.18)^2\,\beta \approx 0.03\beta \tag{A.5}$$

which amounts to 50% and 3%, respectively. Hence, discretising the string into N elements might have significant influence in the computational efficiency, as the initial nonlinearity increases significantly with a decrease in the number of elements.

A.2.2. Modal coupling coefficients of the FPUT β-model

If one were to take into account the comments that were made in the above paragraph, it would be sensible to continue with system with a number of elements that does not exceed this 10%-threshold. Clearly, the $N = 16$ case obeys this condition, and hence we could derive the modal coupling coefficients of this model, by first writing the kinetic and potential energies of this system, which derive from the equations of motion from Eq. A.1.

$$T = \sum_{i=1}^{N} \frac{1}{2} m\ddot{x}_i, \text{ where } i = 1,2,...N \tag{A.6}$$

$$V = \sum_{i=1}^{N+1} \frac{1}{2} k(x_i - x_{i-1})^2 + \frac{1}{4}\beta(x_i - x_{i-1})^4, \text{ where } i = 1,2,...N \tag{A.7}$$

Where the boundary conditions imply that $x_0 = 0$ and $x_{N+1} = 0$.
The physical coordinates of the mass elements i (denoted above in terms of x_i) do not provide information about the interaction between the eigenmodes of the system. It is hence convenient to convert the FPUT

equations of motion from these physical coordinates (in terms of x_i) into modal coordinates (in terms of q_i) to derive the modal coefficients. These coefficients indicate what interaction is present between the modes of the system. These coefficients could generate requirements (e.g. required frequency ratios) for FPUT behavior.

To determine these modal coupling coefficients of this system, one should substitute the mode shapes into the energy formulation and take the derivatives to find the *modal* equations of motion. This method is employed, because if the opposite procedure would be followed, where first the equations of motion (in physical coordinates) are derived and subsequently the mode shapes are substituted, the energy potential will change, resulting in equations of motion that derive from different energy potentials.

The linear and nonlinear elastic (modal) forces are dependent only on the potential energy of the system (scleronomic system) and they may be derived by taking the derivative with respect to the considered modal degree-of-freedom q_n:

$$F_{el}^{(n)} = \frac{dV}{dq_n} \tag{A.8}$$

The modal potential energies may be computed by substituting the following relations into the potential energy of the system:

$$x = \phi_u^T \mathbf{q}_u = \phi_m^T \mathbf{q} = \alpha \phi_u^T \mathbf{q}. \tag{A.9}$$

Where α is a parameter that scales the max-1 eigenvectors ($\max(\phi_u) = 1$ and associated displacement q_u) to the mass-normalized eigenvectors, ϕ_m (and its associated displacement $q_m = q$). The displacement of a single mass element -in terms of modal displacements- is given by Eq. A.10.

$$x_i = \alpha \sum_{n=1}^{N} \sin\left(\frac{\pi n i}{N+1}\right) q_n. \tag{A.10}$$

First, the modal coefficients of the first mode ($n = 1$) mode may be derived, this results in the following potential:

$$V_{mode1} = 0.017027 k q_1^2 + 0.000026 \beta q_1^4. \tag{A.11}$$

Using Eq. A.8, this will generate the following elastic force:

$$F_{El}^{(1)} = 0.034054 k q_1 + 0.000102 \beta q_1^3. \tag{A.12}$$

The first six modes are considered here, as they generate the most significant dynamics. Repeating the procedure for modes 2 to 6 will then result the single-mode coefficients from Table A.1, where $k = 1\text{Nm}^{-1}$ and $\beta = 8\text{Nm}^{-3}$.

Table A.1: Single mode coefficients for the FPUT β-model, normalized with respect to the first mode (n = 1).

n	**(1)**	**(2)**	**(3)**	**(4)**	**(5)**	**(6)**
k_n	0.0341	0.1351	0.2996	0.5220	0.8518	1.1085
$\tilde{k}_n$	1.00	3.97	8.80	15.33	25.0	32.56
$\frac{\omega_n}{\omega_1}$	1.00	1.99	2.97	3.92	5.00	5.71
$\tilde{b}_{nnn}$	1.00	15.73	77.39	236.39	625.60	1059.65

The validity of these linear variables may be verified by conducting an eigenvalue analysis of the mass and stiffness matrices that result from the original equations of motion (Eq. A.1). This yields a slightly different result for the fifth mode, as is shown in Table A.2.

Table A.2: Linear stiffness for the FPUT β-model (from an eigenvalue analysis).

n	**(1)**	**(2)**	**(3)**	**(4)**	**(5)**	**(6)**
k_n	0.0341	0.1351	0.2996	0.5220	0.7947	1.1085
$\tilde{k}_n$	1.00	3.97	8.80	15.33	23.34	32.55
$\frac{\omega_n}{\omega_1}$	1.00	1.99	2.97	3.92	4.83	5.71

Which shows that the employed method for computing the modal coefficients of the FPUT model is at least valid for the first four modes, as it shows some discrepancy with the fifth mode's eigenfrequency.
This eigenfrequency analysis is considered to be the most accurate approximation of the linear variables of the FPUT model, as these are derived directly from the original equations of motion. The linear variables from Table A.1 are calculated indirectly, as they are transformed into modal coordinates first, which could lead to approximation errors. Dauxois [7] and Pace [28] have shown that the frequencies of the FPUT chain follow the following relation:

$$\omega_n = 2\sin\left(\frac{\pi n}{2(N+1)}\right) \tag{A.13}$$

Which exactly generates the frequencies from Table A.2. The effects of such inaccuracies in the linear stiffness are elucidated in section A.2.4.

A.2.3. Modal coupling coefficients of the FPUT β-model

Table A.3 displays the modal coupling coefficients for the FPUT β-model, which are derived by first prescribing displacements of multiple modes into the potential energies of the system and subsequently deriving the modal equations of motion by taking the modal derivatives (Eq. A.8). Eventually, this will generate all terms for the following equations of motion from Eq. A.14.

$$m^{(r)}\ddot{q}_r + k^{(r)}q_r + \sum_{j=1}^{6}\sum_{k=j}^{6}\sum_{l=k}^{6} b_{jkl}^{(r)} q_j q_k q_l = 0,\ r = 1,2,...,6 \tag{A.14}$$

Table A.3 displays the modal coupling coefficients for any β. This does not generate much insight, and hence one should normalize these coefficients with respect to the $b_{111}^{(1)}$-term to find the *ratios* of these coupling coefficients. The resulting normalized variables are shown in Table A.4. This table is quite crowded: it contains quite some nonzero values. Most of these values are non-integer, which likely results from the discretization of system. Still, there is a trend visible in these modal coupling coefficients: they appear to follow -with some margin, and certainly some exceptions- the scaling law with the considered linear frequency ratio, which is denoted by n_r for mode r. For strings (App. B), there is no difference between the mode numbers and the frequency ratios, as these follow an integer relationship. Contrary to the model that is considered here -the FPUT model-, there is such a difference. This likely results from the discretization, and there is thus a likelihood of disappearance of this difference once more elements are considered, as the frequencies approach integer values as N is increased in Eq. A.13. The relation between the coupling coefficients and the normalized mode frequencies is as follows:

$$\tilde{b}_{ijk}^{(r)} = 2n_r n_j n_j n_l. \tag{A.15}$$

One of the aforementioned exceptions is present for the cases where $j = k$ and $l \neq j$. For example for the $\tilde{b}_{113}^{(1)}$-term:

$$\tilde{b}_{jkl}^{(r)} = 2n_r n_j n_k n_l :\ \tilde{b}_{113}^{(1)} = 1.00 \times 1.00 \times 1.00 \times 2.97 = 2.97. \tag{A.16}$$

This shows that the coupling coefficients, though calculated for a discretized model, follow the relation where the coupling coefficients have a dependency on the frequency ratios.

A.2.4. Accuracy of the linear modal stiffness

Now that the nonlinear coefficients are known, one may check the accuracy of the conversion from physical to modal coordinates, by checking if the calculated modal coefficients actually show FPUT behavior. The linear energy formulation of mode n is given by Eq. A.17.

$$E_{lin} = \frac{1}{2}\dot{q}_n^2 + \frac{1}{2}k_n q_n^2 \text{ where } n = 1,...,N \tag{A.17}$$

Fig. A.3 shows the linear energy versus time plots of two simulations, for two sets of linear stiffness coefficients: one simulation is run for the linear coefficients that result from the method where the modal displacements are substituted into the potential energy, and another simulation with the linear coefficients that result from an eigenfrequency analysis of the linear part of the FPUT equations of motion. These simulations are conducted using Matlab's ODE45 solver. The difference is present only in the frequency ratio for the fifth mode; 5.00 for the first method (Table A.1) and 4.83 for the second method (Table A.2). However, there is

Table A.3: Modal coupling coefficients for the $N = 16$ FPUT β-model, for the first 6 modes.

Eq.	**(1)**	**(2)**	**(3)**	**(4)**	**(5)**	**(6)**
b_{111}	0.000102323β	0	0.000101162β	0	0	0
b_{112}	0	0.000811615β	0	0.000797796β	0	0
b_{113}	0.000303485β	0	0.00180024β	0	0.00151779β	0
b_{114}	0	0.000797796β	0	0.00313685β	0	0.00228564β
b_{115}	0	0	0.00151779β	0	0.00511861β	0
b_{116}	0	0	0	0.00228564β	0	0.00666166β
b_{122}	0.000811615β	0	0.0012036β	0	0.00202953β	0
b_{123}	0	0.00240721β	0	0.00473244β	0	0.00689652β
b_{124}	0.00159559β	0	0.00473244β	0	0.00797988β	0
b_{125}	0	0.00405905β	0	0.00797988β	0	0.011629β
b_{126}	0	0	0.00689652β	0	0.011629β	0
b_{133}	0.00180024β	0	0	0	0.00450168β	0
b_{134}	0	0.00473244β	0	0	0	0.0135582β
b_{135}	0.00303558β	0	0.00900335β	0	0	0
b_{136}	0	0.00689652β	0	0.0135582β	0	0
b_{144}	0.00313685β	0	0	0	0	0
b_{145}	0	0.00797988β	0	0	0	0
b_{146}	0.00457128β	0	0.0135582β	0	0	0
b_{155}	0.00511861β	0	0	0	0	0
b_{156}	0	0.011629β	0	0	0	0
b_{166}	0.00666166β	0	0	0	0	0
b_{222}	0	0.00160941β	0	0	0	0.00153696β
b_{223}	0.0012036β	0	0.00713965β	0	0	0
b_{224}	0	0	0	0.0124406β	0	0
b_{225}	0.00202953β	0	0	0	0.0203001β	0
b_{226}	0	0.00461088β	0	0	0	0.0264198β
b_{233}	0	0.00713965β	0	0.00701808β	0	0
b_{234}	0.00473244β	0	0.0140362β	0	0.0236679β	0
b_{235}	0	0	0	0.0236679β	0	0.0344909β
b_{236}	0.00689652β	0	0	0	0.0344909β	0
b_{244}	0	0.0124406β	0	0	0	0.0178208β
b_{245}	0.00797988β	0	0.0236679β	0	0	0
b_{246}	0	0	0	0.0356416β	0	0
b_{255}	0	0.0203001β	0	0	0	0
b_{256}	0.011629β	0	0.0344909β	0	0	0
b_{266}	0	0.0264198β	0	0	0	0
b_{333}	0	0	0.0079182β	0	0	0
b_{334}	0	0.00701808β	0	0.0275943β	0	0
b_{335}	0.00450168β	0	0	0	0.0450276β	0
b_{336}	0	0	0	0	0	0.0586016β
b_{344}	0	0	0.0275943β	0	0.0232649β	0
b_{345}	0	0.0236679β	0	0.0465298β	0	0.0678072β
b_{346}	0.0135582β	0	0	0	0.0678072β	0
b_{355}	0	0	0.0450276β	0	0	0
b_{356}	0	0.0344909β	0	0.0678072β	0	0
b_{366}	0	0	0.0586016β	0	0	0
b_{444}	0	0	0	0.0240411β	0	0
b_{445}	0	0	0.0232649β	0	0.0784589β	0
b_{446}	0	0.0178208β	0	0	0	0.102111β
b_{455}	0	0	0	0.0784589β	0	0.0571685β
b_{456}	0	0	0.0678072β	0	0.114337β	0
b_{466}	0	0	0	0.102111β	0	0
b_{555}	0	0	0	0	0.0640134β	0
b_{556}	0	0	0	0.0571685β	0	0.166622β
b_{566}	0	0	0	0	0.166622β	0
b_{666}	0	0	0	0	0	0.108426β

Table A.4: Modal coupling coefficients for the first 6 modes of the $N = 16$ FPUT β-model, normalized with respect to $b^{(1)}_{111}$.

Eq.	**(1)**	**(2)**	**(3)**	**(4)**	**(5)**	**(6)**
b_{111}	1	0	0.99	0	0	0
$\tilde{b}_{112}$	0	7.93	0	7.80	0	0
$\tilde{b}_{113}$	2.97	0	17.59	0	14.83	0
$\tilde{b}_{114}$	0	7.80	0	30.66	0	22.34
$\tilde{b}_{115}$	0	0	14.83	0	50.024	0
$\tilde{b}_{116}$	0	0	0	22.34	0	65.10
$\tilde{b}_{122}$	7.93	0	11.76	0	19.83	0
$\tilde{b}_{123}$	0	23.53	0	46.25	0	67.40
$\tilde{b}_{124}$	15.59	0	46.25	0	77.99	0
$\tilde{b}_{125}$	0	39.67	0	77.99	0	113.65
$\tilde{b}_{126}$	0	0	67.40	0	113.65	0
$\tilde{b}_{133}$	17.59	0	0	0	43.99	0
$\tilde{b}_{134}$	0	46.25	0	0	0	132.50
$\tilde{b}_{135}$	29.67	0	87.99	0	0	0
$\tilde{b}_{136}$	0	67.40	0	132.50	0	0
$\tilde{b}_{144}$	30.67	0	0	0	0	0
$\tilde{b}_{145}$	0	77.99	0	0	0	0
$\tilde{b}_{146}$	44.68	0	132.50	0	0	0
$\tilde{b}_{155}$	50.02	0	0	0	0	0
$\tilde{b}_{156}$	0	113.65	0	0	0	0
$\tilde{b}_{166}$	65.10	0	0	0	0	0
$\tilde{b}_{222}$	0	15.73	0	0	0	15.02
$\tilde{b}_{223}$	11.76	0	69.78	0	0	0
$\tilde{b}_{224}$	0	0	0	121.58	0	0
$\tilde{b}_{225}$	19.83	0	0	0	198.39	0
$\tilde{b}_{226}$	0	45.06	0	0	0	258.20
$\tilde{b}_{233}$	0	69.78	0	68.59	0	0
$\tilde{b}_{234}$	46.25	0	137.8	0	231.31	0
$\tilde{b}_{235}$	0	0	0	231.31	0	337.08
$\tilde{b}_{236}$	67.40	0	0	0	337.08	0
$\tilde{b}_{244}$	0	121.58	0	0	0	174.16
$\tilde{b}_{245}$	77.99	0	231.31	0	0	0
$\tilde{b}_{246}$	0	0	0	348.32	0	0
$\tilde{b}_{255}$	0	198.39	0	0	0	0
$\tilde{b}_{256}$	113.65	0	337.08	0	0	0
$\tilde{b}_{266}$	0	258.20	0	0	0	0
$\tilde{b}_{333}$	0	0	77.38	0	0	0
$\tilde{b}_{334}$	0	68.59	0	269.68	0	0
$\tilde{b}_{335}$	43.99	0	0	0	440.05	0
$\tilde{b}_{336}$	0	0	0	0	0	572.71
$\tilde{b}_{344}$	0	0	269.68	0	227.37	0
$\tilde{b}_{345}$	0	231.31	0	454.73	0	662.68
$\tilde{b}_{346}$	132.50	0	0	0	662.68	0
$\tilde{b}_{355}$	0	0	440.05	0	0	0
$\tilde{b}_{356}$	0	337.08	0	662.68	0	0
$\tilde{b}_{366}$	0	0	572.71	0	0	0
$\tilde{b}_{444}$	0	0	0	234.95	0	0
$\tilde{b}_{445}$	0	0	227.37	0	766.78	0
$\tilde{b}_{446}$	0	174.16	0	0	0	997.93
$\tilde{b}_{455}$	0	0	0	766.78	0	558.71
$\tilde{b}_{456}$	0	0	662.68	0	1117.41	0
$\tilde{b}_{466}$	0	0	0	997.93	0	0
$\tilde{b}_{555}$	0	0	0	0	625.60	0
$\tilde{b}_{556}$	0	0	0	558.71	0	1628.39
$\tilde{b}_{566}$	0	0	0	0	1628.39	0
$\tilde{b}_{666}$	0	0	0	0	0	1059.64

still a clear difference in the resulting dynamics. Fig. A.3a(i) indicates some energy transfer between only the uneven modes, though none of the higher modes seem to dominate the first mode's energy at any point in the considered time frame. Fig. A.3b(i) shows dominance in terms of energy, where the behavior is similar to the original experiment for the FPUT β-model from Fig. A.1a, where energy is distributed among only the uneven modes. Figures A.3a(ii) and A.3b(ii) depict the modal amplitudes of each simulation. The left figure shows that the small energy of the higher modes is related to small amplitudes of modes 3 and 5. The right figure shows that higher amplitudes *do* relate to this energy transfer, though the difference in magnitude of the modal amplitudes for the left and right figures is small. This implies that though a system shows modulations in the modal amplitudes (beatings), one cannot discern whether a system shows energy transfer between modes. One should there always calculate the linear energy of each mode, to verify any presence of modal energy dominance.
The difference in the two energy plots of Fig. A.3 clearly indicates that an non-integer frequency ratio (which is slightly smaller than the internal resonance condition, which requires an integer relation: $\omega_5 = 5\omega_0$) for the fifth mode is required to generate the classical FPUT behavior. This could mean that one of the possible origins of the FPUT behavior lies in these non-integer frequency ratios. This FPUT behavior is closely related to quasiperiodic behavior, which requires a system with N modes to have incommensurate (irrational) frequency ratios [24]. These frequencies should follow the relation from Eq. A.18, where all n_r-terms are integers.

$$n_1\omega_1 + n_2\omega_2 + ... + n_N\omega_N = 0 \tag{A.18}$$

This relation should only be valid if all n_r-terms are zero. To observe quasiperiodic behavior, none of the frequency ratios should be integer. The FPUT phenomenon, where energy is seen to be transferred from the fundamental mode to higher modes, before it returns to the fundamental mode essentially results from some quasiperiodicity in the amplitude of the system. In subsequent steps, the linear values from the eigenfrequency analysis (Table A.2) will be employed as these are calculated accurately and the resulting dynamics agree very well with the original experiments.

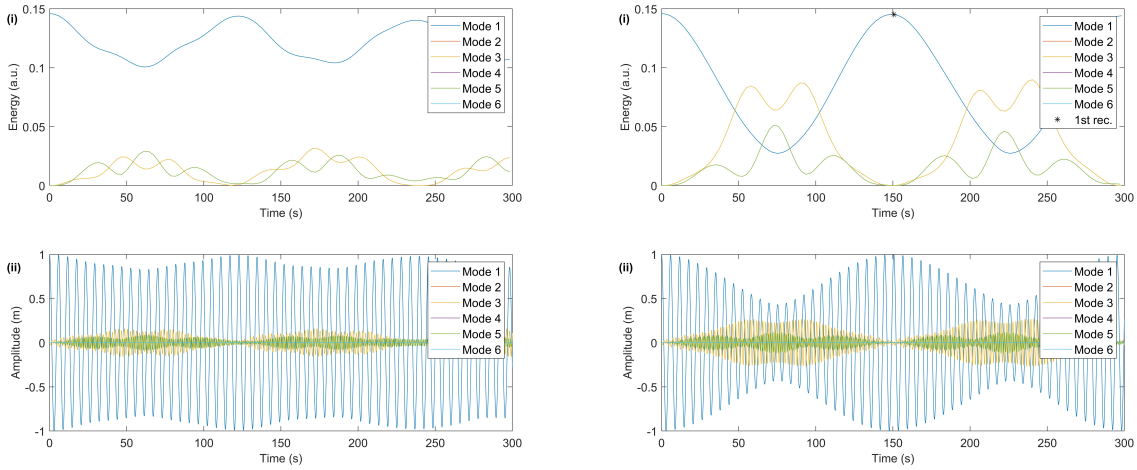

(a) $\frac{\omega_i}{\omega_0} = 1.00, 1.99, 2.97, 3.92, 5.00$ and 5.71.

(b) $\frac{\omega_i}{\omega_0} = 1.00, 1.99, 2.97, 3.92, 4.83$ and 5.71.

Figure A.3: Ringdown simulations from an initial displacement of the first mode for the undamped FPUT system. The model consists of the first six eigenmodes. The nonlinear coefficients from Table A.3 for $\beta = 8\text{Nm}^{-3}$ are used here. A.3a depicts the results for the linear variables from the potential substitution method in Table A.1. A.3a(i) depicts the energy, A.3a(ii) depicts the amplitude. A.3b depicts the results with linear variables that follow from an eigenfrequency analysis of the FPUT equations (Table A.2). A.3b(i) depicts the energy, A.3b(ii) depicts the amplitude. The star indicates the first recurrence of energy at approximately 150 seconds. 99.8% of the initial energy is recovered in this point.

A.2.5. Required coupling coefficients

The equations of motion consist of nonlinear terms, which result in energy transfer through cross-terms (i.e. b_{ijk}-terms where $i \neq j$ and/or $j \neq k$). This energy transfer is most dominant for the cases where the internal resonance condition is satisfied (as is shown in Section B.5). The nonlinear coupling coefficients from Table A.4 show that the amount of nonzero cross-terms is quite large. Before determining which these terms are

the origin of the FPUT behavior, it is important to note that the total nonlinear energy may be found by integrating any of the six modal equations of motion, according to the following formula for the total energy:

$$E_{tot} = \int_0^{q_r} \left[\sum_{j=1}^{N} \sum_{k=j}^{N} \sum_{l=k}^{N} b_{jkl}^{(r)} q_j q_k q_l \right] dq_r \text{ where } n = 1,2,...,N \text{ and } r = 1 \text{ or } 2 \text{ or } ... \text{ or } N \tag{A.19}$$

which is valid for any choice of the variable r, because all equations of motion basically result from the same energy potential, which consists of all considered modes. The variable r basically sets which modal equation of motion is integrated; it determines which column of Table A.4 is used for integration. The integration will generate a pre-factor, which will generate certain relations between these coupling coefficients. One of these relations is shown in Eq. A.20.

$$\begin{aligned} E_{jjl}^{(j)} &= \frac{1}{3} b_{jjl}^{(j)} q_j^3 q_l \\ E_{jjj}^{(l)} &= b_{jjj}^{(l)} q_j^3 q_l \\ E_{jjl}^{(j)} = E_{jjj}^{(l)} &\rightarrow \frac{1}{3} b_{jjl}^{(j)} q_j^3 q_l = b_{jjj}^{(l)} q_j^3 q_l \end{aligned} \tag{A.20}$$

This implies that the following relation should always be valid:

$$b_{jjl}^{(j)} = 3 b_{jjj}^{(l)}. \tag{A.21}$$

Using a similar method, it can be proven that the following relations should also be valid:

$$b_{jkl}^{(r)} = b_{rkl}^{(j)} = b_{rjk}^{(l)} = b_{rjl}^{(k)}. \tag{A.22}$$

The total energy may be considered to consist of two parts: a part that accounts for the energy that resides in only *one* mode (i.e. if $r = j = k = l = 1$, this term is denoted by $\frac{1}{4} b_{111}^{(1)} q_1^4$) and a part that allows for energy transfer between several modes; the coupling energy. The coupling energy -for the first mode- may be written as E_{coupling}:

$$E_{\text{coupling}} = \int_0^{q_1} \left[\sum_{j=1}^{N} \sum_{k=j}^{N} \sum_{l=k}^{N} b_{jkl}^{(1)} q_j q_k q_l \right] dq_1 \text{ where } l > 1 \tag{A.23}$$

The variable l should be larger than one, such that only the nonlinear *coupling* energy is considered. For the default FPUT system (where $\beta = 8\text{Nm}^{-3}$), the coupling energy may be found at each time integration point. Plotting all three quantities over time, which are (1) the linear energy per mode $E_{lin.n} = \frac{1}{2} m \dot{q}_n + \frac{1}{2} k^{(n)} q_n^2$, (2) the total single mode energy ($E_{tot.n} = \frac{1}{2} m \dot{q}_n + \frac{1}{2} k^{(n)} q_{ni}^2 + \frac{1}{4} b_{nnn}^{(n)} q_n^4$) and (3) the coupling energy (Eq. A.23), will generate the following plots:

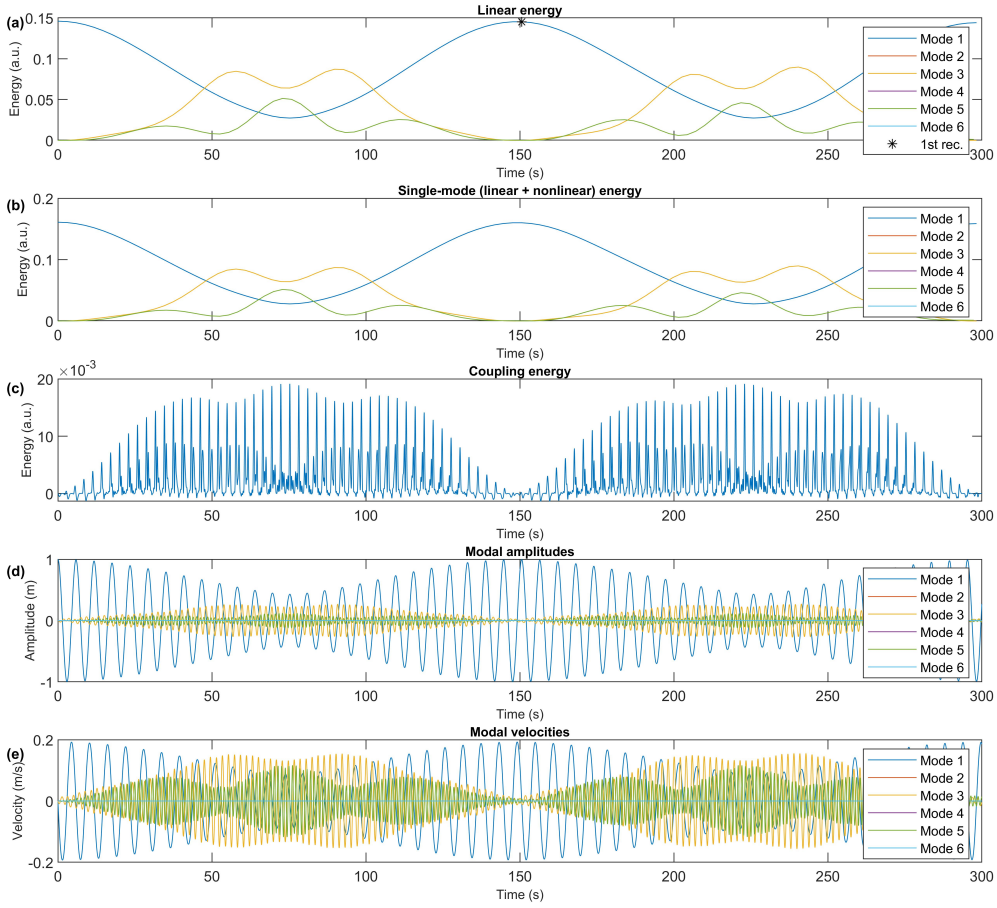

Figure A.4: Several plots of quantities over time. (a) depicts the linear energy, (b) shows the total single-mode energy, (c) depicts the coupling energy, (d) depicts the modal amplitudes and (e) depicts the modal velocity.

Fig. A.4 reveals several interesting topics:

- Only the uneven modes are excited: the even modes appear to remain zero during the entire simulation.
- The linear modal energy and the single mode energy (which also accounts for the nonlinear energy fraction) do not differ much: their difference is hardly visible in these plots. This could be due to the small magnitudes of the nonlinear coefficients, as well as amplitudes that remain smaller than one, resulting in small nonlinear energy fractions;
- The coupling energy follows an expected trend: this quantity increases as the first mode's energy decreases, indicating that energy flows from the first mode to the higher modes. On the contrary, once the first mode's energy increases, the coupling energy decreases. The trend of the maxima of the coupling energy is likely to show the total coupling energy, where the lower peaks (e.g. the one between 0 and 50s) could indicate that energy flows to the third mode. These trends are accompanied by the local increase of the amplitude of the third mode (and similarly for the fifth mode). This observation is in agreement with Eq. A.23: the coupling energy may only increase as the amplitude of the higher modes increase.
- The amplitude plot indicates that the amplitudes are modulated (generating beatings). As was mentioned before, this energy dominance of a higher mode does not necessarily imply that the modal amplitude of the corresponding mode dominates. FPUT behavior may hence be present in structures for

which these beatings are visible in the amplitude signal. The modal velocity does show this dominance: the FPUT behavior may thus be predicted for systems that show beatings in both the modal amplitudes and modal velocities.

The coupling energy (as mentioned before) is dependent on the amplitudes of at least two modes. To determine which terms are required to see FPUT behavior, the coupling energy should be analyzed. Keeping only the nonzero coupling terms (from Table A.3) results in Eq. A.24.

$$E_{\text{coupling.1}} = \frac{1}{3}b^{(1)}_{113}q_1^3q_3 + \frac{1}{2}b^{(1)}_{122}q_1^2q_2^2 + \frac{1}{2}b^{(1)}_{124}q_1^2q_2q_4 + \frac{1}{2}b^{(1)}_{133}q_1^2q_3^2 + \frac{1}{2}b^{(1)}_{135}q_1^2q_3q_5 +$$
$$\frac{1}{2}b^{(1)}_{144}q_1^2q_4^2 + \frac{1}{2}b^{(1)}_{146}q_1^2q_4q_6 + \frac{1}{2}b^{(1)}_{155}q_1^2q_5^2 + \frac{1}{2}b^{(1)}_{166}q_1^2q_6^2 + b^{(1)}_{223}q_1q_2^2q_3 + b^{(1)}_{225}q_1q_2^2q_5 + b^{(1)}_{234}q_1q_2q_3q_4 + b^{(1)}_{236}q_1q_2q_3q_6 +$$
$$b^{(1)}_{245}q_1q_2q_4q_5 + b^{(1)}_{256}q_1q_2q_5q_6 + b^{(1)}_{335}q_1q_3^2q_5 + b^{(1)}_{346}q_1q_3q_4q_6 \tag{A.24}$$

For this problem, where the even modes always have zero amplitude (Fig. A.4), there is no coupling energy generated by any term that dependent on the amplitude of an even mode, since $q_2(t) = 0$, $q_4(t) = 0$ and $q_6(t) = 0$ for $t \geq 0$, Eq. A.24 may thus be simplified to Eq. A.25.

$$E_{\text{coupling.1}} = \frac{1}{3}b^{(1)}_{113}q_1^3q_3 + \frac{1}{2}b^{(1)}_{133}q_1^2q_3^2 + \frac{1}{2}b^{(1)}_{135}q_1^2q_3q_5 + \frac{1}{2}b^{(1)}_{155}q_1^2q_5^2 + b^{(1)}_{335}q_1q_3^2q_5 \tag{A.25}$$

This shows that there are only five terms which are responsible for this coupling energy. Of course, the nonlinear parameter of a single mode (for cubic nonlinearity, this is the Duffing term), also excites the other modes' harmonics, as is shown in Section B.5. However, the energy that is associated to this Duffing behavior has no dependency on the amplitudes of the other modes. Hence, should these terms (the $b^{(1)}_{113}$-, $b^{(1)}_{133}$-, $b^{(1)}_{135}$-, $b^{(1)}_{155}$- and the $b^{(1)}_{335}$-terms) not be present, it is likely that this FPUT phenomenon cannot be observed. It is however important to note that this simplification (from Eq. A.24 to Eq. A.25) is only valid in the regimes where these even modes are not excited. Any other initial condition, where one of these even modes does have nonzero initial amplitude, most likely results in different dynamics, as the even modes will most likely also receive energy.

The required coupling terms (from Table A.3) may be determined by checking which coefficients generate a nonzero force from the nonzero coupling coefficients multiplied by the nonzero modal amplitudes (in this case, this is $q_1(t), q_3(t)$ and $q_5(t)$, as was shown in Fig. A.4). This results Equations A.26, A.27 and A.28 for the first, third and fifth equation of motion, respectively.

$$\ddot{q}_1 + k^{(1)}_1 q_1 + b^{(1)}_{111}q_1^3 + b^{(1)}_{113}q_1^2q_3 + b^{(1)}_{133}q_1q_3^2 + b^{(1)}_{135}q_1q_3q_5 + b^{(1)}_{155}q_1q_5^2 + b^{(1)}_{335}q_3^2q_5 = 0 \tag{A.26}$$

$$\ddot{q}_3 + k^{(3)}_3 q_3 + b^{(3)}_{111}q_1^3 + b^{(3)}_{113}q_1^2q_3 + b^{(3)}_{115}q_1^2q_5 + b^{(3)}_{135}q_1q_3q_5 + b^{(3)}_{333}q_3^3 + b^{(3)}_{355}q_3q_5^2 = 0 \tag{A.27}$$

$$\ddot{q}_5 + k^{(5)}_5 q_5 + b^{(5)}_{113}q_1^2q_3 + b^{(5)}_{115}q_1^2q_5 + b^{(5)}_{133}q_1q_3^2 + b^{(5)}_{335}q_3^2q_5 + b^{(5)}_{555}q_5^3 = 0 \tag{A.28}$$

The nonlinear parts of the equations consist of Duffing parameters ($b^{(1)}_{111}, b^{(3)}_{333}$ and $b^{(5)}_{555}$), coupling parameters which were be found using Equations A.21, A.22 and A.25, and coupling coefficients between the third and fifth modes ($b^{(3)}_{355}$ and $b^{(5)}_{335}$, which are only present in the equations of motion for the third and fifth modes). Table A.5 shows (in the highlighted terms) which coefficients are thus required to see this FPUT behavior.

Table A.5: Modal coupling coefficients for the first 6 modes of the N = 16 FPUT β-model, normalized with respect to $b^{(1)}_{111}$. The coefficients that generate a nonzero force for the amplitude condition $q_1(t) \neq 0, q_2(t) = 0, q_3(t) \neq 0, q_4(t) = 0, q_5(t) \neq 0$ and $q_6(t) = 0$ are highlighted here. The coefficients that are highlighted in yellow are the Duffing terms, the terms which are highlighted in green are the coupling terms.

Eq.	**(1)**	**(2)**	**(3)**	**(4)**	**(5)**	**(6)**
$\tilde{b}_{111}$	1	0	0.99	0	0	0
$\tilde{b}_{112}$	0	7.93	0	7.80	0	0
$\tilde{b}_{113}$	2.97	0	17.59	0	14.83	0
$\tilde{b}_{114}$	0	7.80	0	30.66	0	22.34
$\tilde{b}_{115}$	0	0	14.83	0	50.024	0
$\tilde{b}_{116}$	0	0	0	22.34	0	65.10
$\tilde{b}_{122}$	7.93	0	11.76	0	19.83	0
$\tilde{b}_{123}$	0	23.53	0	46.25	0	67.40
$\tilde{b}_{124}$	15.59	0	46.25	0	77.99	0
$\tilde{b}_{125}$	0	39.67	0	77.99	0	113.65
$\tilde{b}_{126}$	0	0	67.40	0	113.65	0
$\tilde{b}_{133}$	17.59	0	0	0	43.99	0
$\tilde{b}_{134}$	0	46.25	0	0	0	132.50
$\tilde{b}_{135}$	29.67	0	87.99	0	0	0
$\tilde{b}_{136}$	0	67.40	0	132.50	0	0
$\tilde{b}_{144}$	30.67	0	0	0	0	0
$\tilde{b}_{145}$	0	77.99	0	0	0	0
$\tilde{b}_{146}$	44.68	0	132.50	0	0	0
$\tilde{b}_{155}$	50.02	0	0	0	0	0
$\tilde{b}_{156}$	0	113.65	0	0	0	0
$\tilde{b}_{166}$	65.10	0	0	0	0	0
$\tilde{b}_{222}$	0	15.73	0	0	0	15.02
$\tilde{b}_{223}$	11.76	0	69.78	0	0	0
$\tilde{b}_{224}$	0	0	0	121.58	0	0
$\tilde{b}_{225}$	19.83	0	0	0	198.39	0
$\tilde{b}_{226}$	0	45.06	0	0	0	258.20
$\tilde{b}_{233}$	0	69.78	0	68.59	0	0
$\tilde{b}_{234}$	46.25	0	137.8	0	231.31	0
$\tilde{b}_{235}$	0	0	0	231.31	0	337.08
$\tilde{b}_{236}$	67.40	0	0	0	337.08	0
$\tilde{b}_{244}$	0	121.58	0	0	0	174.16
$\tilde{b}_{245}$	77.99	0	231.31	0	0	0
$\tilde{b}_{246}$	0	0	0	348.32	0	0
$\tilde{b}_{255}$	0	198.39	0	0	0	0
$\tilde{b}_{256}$	113.65	0	337.08	0	0	0
$\tilde{b}_{266}$	0	258.20	0	0	0	0
$\tilde{b}_{333}$	0	0	77.38	0	0	0
$\tilde{b}_{334}$	0	68.59	0	269.68	0	0
$\tilde{b}_{335}$	43.99	0	0	0	440.05	0
$\tilde{b}_{336}$	0	0	0	0	0	572.71
$\tilde{b}_{344}$	0	0	269.68	0	227.37	0
$\tilde{b}_{345}$	0	231.31	0	454.73	0	662.68
$\tilde{b}_{346}$	132.50	0	0	0	662.68	0
$\tilde{b}_{355}$	0	0	440.05	0	0	0
$\tilde{b}_{356}$	0	337.08	0	662.68	0	0
$\tilde{b}_{366}$	0	0	572.71	0	0	0
$\tilde{b}_{444}$	0	0	0	234.95	0	0
$\tilde{b}_{445}$	0	0	227.37	0	766.78	0
$\tilde{b}_{446}$	0	174.16	0	0	0	997.93
$\tilde{b}_{455}$	0	0	0	766.78	0	558.71
$\tilde{b}_{456}$	0	0	662.68	0	1117.41	0
$\tilde{b}_{466}$	0	0	0	997.93	0	0
$\tilde{b}_{555}$	0	0	0	0	625.60	0
$\tilde{b}_{556}$	0	0	0	558.71	0	1628.39
$\tilde{b}_{566}$	0	0	0	0	1628.39	0
$\tilde{b}_{666}$	0	0	0	0	0	1059.64

To verify that these terms generate this behavior, the green highlighted terms are set to zero, and another ringdown simulation is run. This results in Fig. A.5.

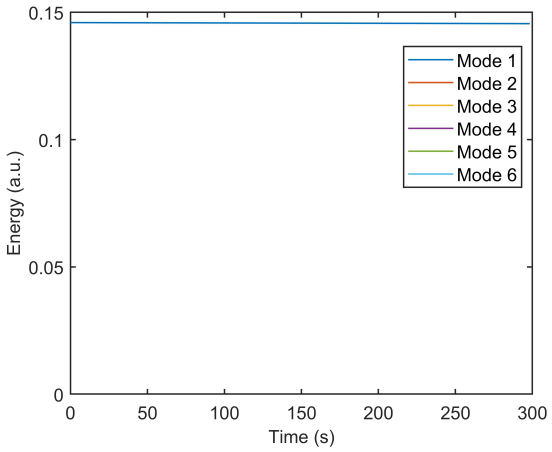

Figure A.5: Simulated ringdown for the first 6 modes of the FPUT β-problem. The initial condition is an initial amplitude of the first mode. $\beta = 8\text{Nm}^{-3}$ and all green variables in Table A.5 are zero.

This clearly shows that all energy remains in the first mode. The energy of the higher modes does not increase, indicating that the energy is not transferred. It may hence be concluded that the green highlighted terms in Table A.5 and/or the coupling terms from Eq.'s A.26, A.27 and A.28 are required to see this FPUT behavior.

Effect of initial conditions

Tuck and Menzel stated that this behavior was sensitive of the initial force ratio, which was (in terms of spatial coordinates) given by Eq. A.4 [34]. Its modal equivalent may be written as:

$$r_{\text{NLvsL}} = \frac{F_{NL}}{F_L} = \frac{b_{111}^{(1)} q_{0.1}^3}{k_1^{(1)} q_{0.1}} = \frac{b_{111}^{(1)}}{k_1^{(1)}} q_{0.1}^2 \tag{A.29}$$

Substitution of these variables from Table A.1 combined with $q_{0.1} = \frac{q_{u_{0.1}}}{\alpha_{FPUT}} = 2.93$ m gives a initial force ratio that equals 0.21. This implies that for the default problem, this *modal* initial nonlinear force equals 21% of the initial linear force.

For the initial condition where only the first mode is excited, this will only generate nonzero forces for the terms which are only dependent on the amplitude of the first mode. Plugging the initial condition $q_1 = q_{0.1}$, $q_3 = 0$ and $q_5 = 0$ into the equations A.26, A.27 and A.28 gives:

$$\ddot{q}_1 + k_1^{(1)} q_{0.1} + b_{111}^{(1)} q_{0.1}^3 = 0 \tag{A.30}$$

$$\ddot{q}_3 + b_{111}^{(3)} q_{0.1}^3 = 0 \tag{A.31}$$

$$\ddot{q}_5 = 0. \tag{A.32}$$

These equations show that the first equation of motion is excited through the linear stiffness ($k_1^{(1)}$) and the Duffing term ($b_{111}^{(1)}$). The fifth mode's equation of motion remains zero. However, for the third equation of motion, there is a term that is excited as well: the term that scales with $b_{111}^{(3)}$. This generates an excitation of the third mode, through an initial excitation of the first mode. This could be the term that is responsible for the initial energy transfer from the first mode to the third mode. Again, to verify that this term is responsible for the initial energy transfer, the simulation may be run once more, though this time with $b_{111}^{(3)}$, (and thus $b_{113}^{(1)}$) equal to zero. The results are depicted in Fig. A.6. This shows that no energy is transferred to the other modes. This $b_{111}^{(3)}$-term (referred to as the back-coupling term) may thus be seen as the "catalyst"-term: the term that initiates excitation of another mode under pure excitation of a single mode, as is verified by Sholl [33].

The origin of the $b_{111}^{(3)}$-term may be traced by checking the potential that is associated to a prescribed displacement that is a function of both the first and third mode. This procedure is shown for two analytical

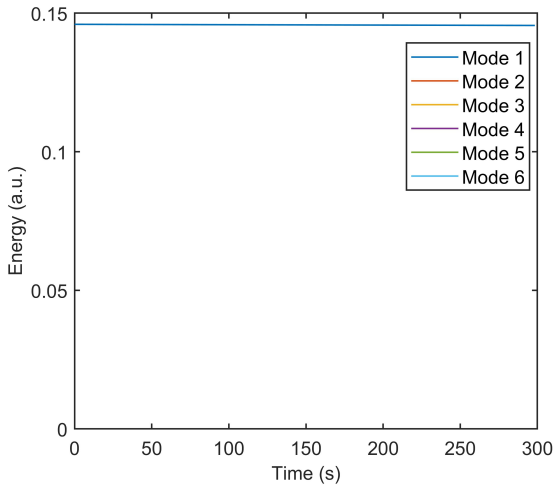

Figure A.6: Simulated ringdown for the first 6 modes of the FPUT β-problem. The initial condition is an initial amplitude of the first mode. $\beta = 8$ and $b^{(3)}_{111} = 0$ and $b^{(1)}_{113} = 0$.

string models in Section B.7; for the FPUT model, this is basically identical to the w-displacement string model.

A.2.6. Conclusions

From this study on the default FPUT β-model, the following conclusions may be drawn:

- FPUT behavior may become visible through energy transfer from the initially excited mode to other modes and subsequent recurrence of energy to the initially excited mode. To generate this in- and decrease in the energy, local modulations of the modal amplitudes (beatings) are required. However, though beatings in the amplitude signal of a mode could mean that energy is transferred to other modes, it is not sufficient to *only* check amplitude versus time plots to determine whether a system shows FPUT behavior. To verify whether a system shows FPUT recurrence, one should check both the modal amplitude versus time plots, the modal velocity versus time plots and preferably the energy versus time plots.
- The conversion from physical to modal parameters is done with sufficient accuracy: the converted variables generate FPUT behavior. However, the linear frequencies from this conversion do not equal those of a linear eigenfrequency analysis of the equations of motion in terms of the physical coordinates. Therefore, in this section, the frequency ratio from this eigenfrequency analysis (Table A.2) was used in combination with the found nonlinear modal coefficients in Table A.3.
- In addition to the previous point one may conclude that to generate FPUT behavior, one should have linear frequency ratios which are non-integer and slightly lower than the nearest internal resonance condition.
- The modal coupling coefficients seem to show a relation to these frequency ratios. Note that this is not related to the (integer) mode number.
- For the studied nonlinearity ($\beta = 8\text{Nm}^{-3}$) and magnitude of the initial conditions, it is sufficient to only account for the linear fraction of the total energy, as the nonlinear energy remains fairly small (Fig. A.4(a) vs. Fig. A.4(b)).
- Though it was shown that the nonlinear energy remains small, this nonlinear energy is responsible for the energy transfer, as was shown in Fig. A.4(c). The coupling energy follows an expected trend: it increases as energy is transferred from the first mode to others, and it decreases for cases where energy is transferred from the higher modes to the first mode.
- To see FPUT-behavior, a coupling between the uneven modes is required. This coupling may be established through nonzero modal coupling terms, which couple the amplitudes of several (in this case,

uneven) modes of vibration. Eq.'s A.26, A.27 and A.28 display the required nonzero coefficients. It was shown that without these coefficients, especially the $b^{(3)}_{111}$-term (the back-coupling term) there would not be any energy transfer. This $b^{(3)}_{111}$-term may be seen as the "catalyst"-term, which produces a nonzero force in the equation of motion of the third mode, under excitation of only mode 1. Hence, to see FPUT behavior, these terms should be nonzero.

- The study in this section shows FPUT behavior under exactly the same conditions as the original experiment [11]: the initial conditions, damping, linear stiffness and nonlinear stiffness were all identical. To see whether this behavior may be visible for different conditions, another study should be conducted. This will be done in the next section.

A.3. Limiting conditions of the FPUT β-problem

The previous section comprised a study of the default FPUT problem, using initial conditions and linear versus nonlinear relations which were in agreement with the original experiment. This study showed -among many others- that the linear frequency ratios should not be integer, as well as the necessity for certain modal coupling coefficients to be nonzero. This section will explore the limits of this behavior: this will generate insight into which conditions should be met in order to see the desired behavior. These conditions aim to answer the following questions, regarding what damping, linear strength, nonlinear strength or initial condition should be present to see FPUT-like behavior:

1. What quality-factor (Q) is needed?
2. What linear frequency ratio is required?
3. What ratio of linear to nonlinear stiffness is required?
4. What initial ratio of the nonlinear versus linear force is required?

The first question accounts for damping, which is not present in the original FPUT experiment. Should a mechanical system allow for the required energy transfer, then the damping should be small enough to be able to observe this exchange [21]. This question is answered independently of the three other questions, as this has no direct relation to the others: a change in the magnitude of damping does not immediately generate large difference in the linear, nonlinear and initial condition of the system. The second question is formulated such that the required linear frequency ratios may be determined. The third question aims to quantify the required strength of nonlinearity. Finally, the last question generates insight into what the initial force ratio (nonlinear versus linear) should be. Tuck and Menzel claimed that this ratio should not exceed 10% for the default FPUT problem [34]. The previous section has shown that in terms of modal coordinates, this is more: about 20%. Since the present study goes beyond this default problem (in different regimes of nonlinearity), this condition may no be valid. The latter three questions are all related to one another, as e.g. any change in the linear stiffness will impact the initial force ratio (Eq. A.29) as well.

A.3.1. The influence of linear damping on FPUT mechanics

This paragraph will aim to answer the question which quality factor is required to see FPUT-like behavior. This may be done quite easily by adding a modal damping coefficient to the default FPUT β-problem. The present analysis will assume linear damping, which is expressed in terms of the Q-factor of the first mode, where the Q-factors of the higher modes are assumed to scale with the inverse of the mode number ($Q_n = \frac{Q_1}{n}$), this appears to be approximately valid for strings, as is shown in Section B.4. By setting the quality factor of the first mode (Q_1), the modal damping may thus be tuned. The equations of motion (from Eq. D.16) become, with inclusion of this additional damping factor and exclusion of the quadratic coupling coefficients:

$$\ddot{q}_r + k_r^{(r)} q_r + \frac{\omega_r}{Q_r}\dot{q}_r + \sum_{j=1}^{N}\sum_{k=j}^{N}\sum_{l=k}^{N} b^r_{jkl} q_j q_k q_l = 0,\ r = 1,2,...,N. \tag{A.33}$$

Where $k_r^{(r)} = \omega_r^2$ and again, the first six modes are considered: $N = 6$. These equations are solved using the linear stiffness parameters from Table A.2, in combination with the nonlinear variables from Table A.3 for $\beta = 8\text{Nm}^{-3}$. The quality factor is swept for 20 logarithmically spaced variables between 500 and 1 million. This produces the energy evolution over time that is depicted in Fig. A.7. Evidently, the recurrent behavior is still visible, though is is suppressed heavily for quality factors below 1000. From Q-factors of 8230 and higher,

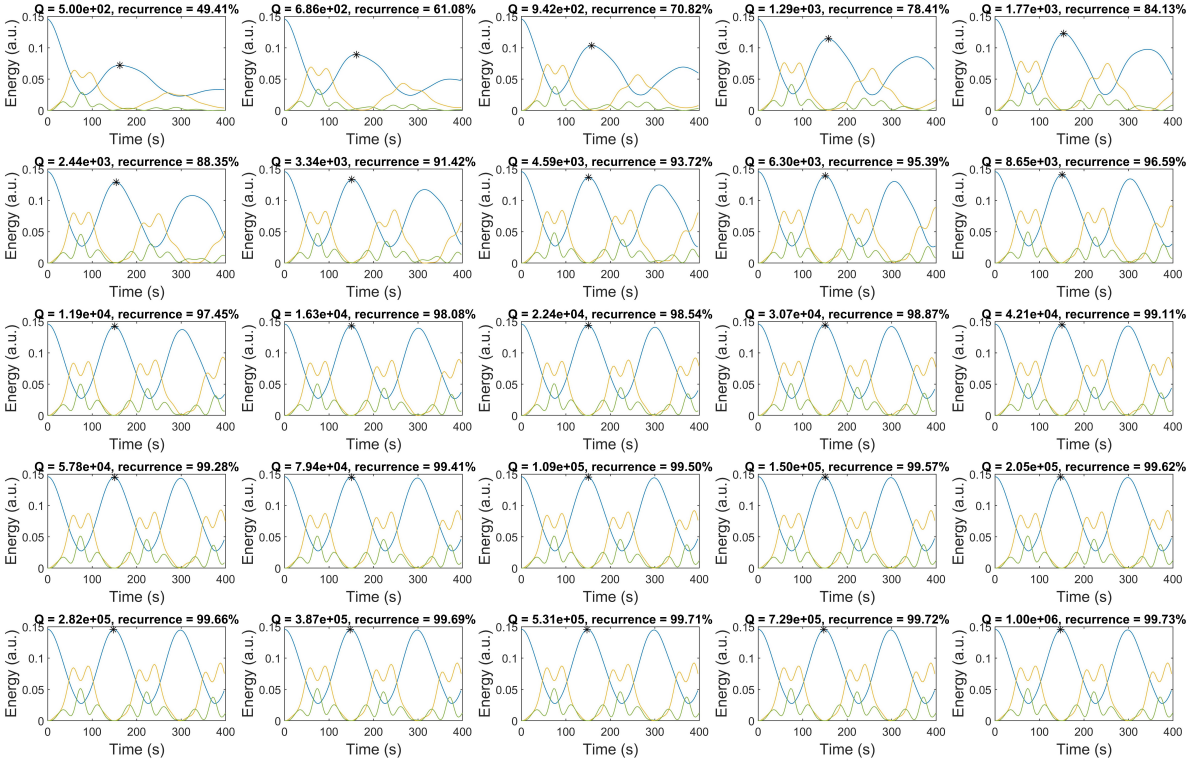

(a) Modal energy versus time for the first six modes of the FPUT β-model with $\beta = 8\text{Nm}^{-3}$ and initial excitation of the first mode. These plots were generated for simulations with 20 logarithmically spaced Q-factors between 500 and 1 million.

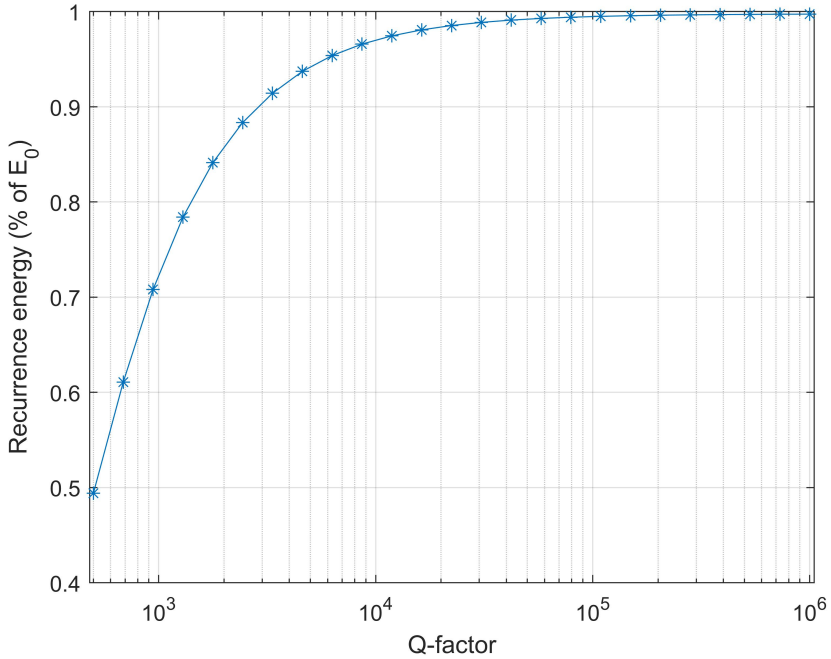

(b) Fraction of initial energy returning to the first mode at the first recurrent peak.

Figure A.7: Modal energy versus Q-factor plots. A.7a depicts the versus time for the first six modes of the FPUT β-model for $\beta = 8$ and initial excitation of only the first mode. These plots were generated for simulations with 20 logarithmically spaced Q-factors between 500 and 1 million. A.7b depicts the fraction of energy returning to the initially excited mode.

more than 95% of the initial energy returns to the first mode. For quality factors of approximately 135,000, this has increased to nearly 99.5%, which shows that for Q-factors higher than approximately 100,000, the

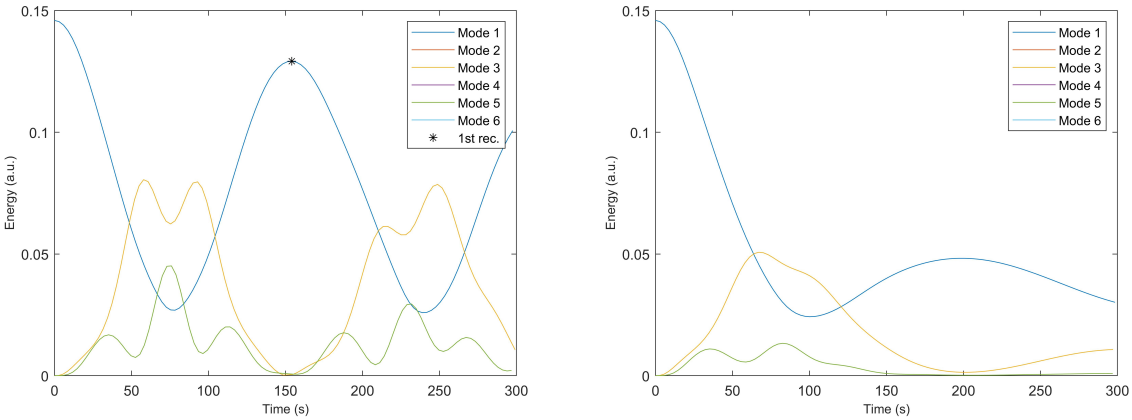

Figure A.8: Simulations of the damped default FPUT problem for a first mode Q-factor of 100,000. In 1.8a $Q_3 = 1000$ and $Q_5 = 200$. In A.8b $Q_3 = 100$ and $Q_5 = 20$.

effect of damping on this default FPUT problem (where $N = 16$ and $\beta = 8\text{Nm}^{-3}$) may be assumed to be very small. Note that this is observed for Q-factors of the higher modes that scale with the inverse of the mode number. For lower Q-factors of the higher modes, part of the transferred energy will dissipate to the environmental bath. This dissipation will influence the recurrent peak of the first mode, as the total energy dissipates quickly for these cases. Fig. A.8 depicts two iterations, where the Q-factors of modes 3 and 5 have deteriorated significantly. Figures A.8(a) and A.8(b) show that less energy is present in the first recurrence peaks, indicating that part of the energy that is distributed among these higher modes is dissipated sooner than that it is returned to the first mode. Fig. shows that for $Q_3 = 1000$ and $Q_5 = 200$, a large amount of energy returns to the initial condition, indicating that recurrence is still present. Now, if one were to manufacture a Si_3N_4 string-like resonator, it is very likely that a Q of 100,000 can be achieved in high vacuum. In the subsequent iterations in this section, the effect of damping is however not neglected. Rather, the fundamental Q-factor is set to 100,000, and the Q-factors of the higher modes are assumed with the inverse of the mode number.

A.3.2. Linear frequency ratios

The second question that was set-up in the beginning of this section considered the required frequency ratio to observe FPUT behavior. Table A.2 and Fig. A.3 have previously shown that the FPUT behavior for the default FPUT system is most significant for non-integer frequency ratios near the internal resonance condition. Although it may be clear that these linear frequency ratios should be non-integer, it is not clear by how much. This may be checked by manually varying the linear stiffness. Nine options for these stiffness ratios will be analyzed in this section. These nine values are expressed in terms of the percentage of the default FPUT problem parameters. This percentage ranges between 90% and 110%. The higher modes (modes 2, 3, 4, 5 and 6) are multiplied by this percentage only, to check the influence with respect to the first mode. The following procedure shows how these linear stiffness values are swept:

1. The non-dimensional linear stiffness parameters of the default FPUT system are (from Table A.2):

$$\tilde{k} = [1.00,\ 3.97,\ 8.80,\ 15.33,\ 23.34,\ 32.55]. \tag{A.34}$$

2. The higher modes (2, 3, 4, 5 and 6) are multiplied by the sweep percentage p, using the following formula:

$$\tilde{k}_p = [1.00,\ 3.97p,\ 8.80p,\ 15.33p,\ 23.34p,\ 32.55p]. \tag{A.35}$$

3. For example, for a percentage of $p = 90\%$, the linear parameters will become:

$$\tilde{k}_p = [1.00,\ 3.57,\ 7.92,\ 13.80,\ 21.00,\ 29.30]. \tag{A.36}$$

4. The linear frequency ratios for $p = 90\%$ are thus given by:

$$\omega = \sqrt{\tilde{k}_p} = [1.00,\ 1.89,\ 2.81,\ 3.71,\ 4.58,\ 5.41]. \tag{A.37}$$

A.3.3. Nonlinear versus linear stiffness ratio

The third question, concerning the ratio of nonlinear over linear stiffness, $\frac{b_{111}^{(1)}}{k_1^{(1)}}$, may determine the regime for which FPUT behavior may be observed. The linear and nonlinear modal variables for the default FPUT problem are listed in Table A.1. The parameter sweep that is conducted in this paragraph uses various variables of β, since the linear stiffness is swept already for the method that is shown in the previous paragraph. In this analysis, this β-variable is chosen to be in the same order of magnitude of the original variable ($\beta = 8\text{Nm}^{-3}$); the variable range consists of six linearly spaced values between 0 and 20Nm^{-3}.

A.3.4. Initial ratio of nonlinear versus linear force

The final question treats the ratio of nonlinear versus linear force. This ratio could determine what effect the initial condition may have on the resulting dynamics. This analysis is conducted on the initial force ratio generated by the first mode, it is expressed by Eq. A.29. This equation shows the dependency on three variables: the nonlinear stiffness $b_{111}^{(1)}$, the linear stiffness $k_1^{(1)}$ and the initial amplitude $q_{u_{0.1}}$. The previous two paragraphs have already set values for the first two, leaving only one "free" variable: the initial modal amplitude $q_{u_{0.1}} (= \alpha_{FPUT} q_{0.1})$. This variable is swept for several values ranging between 0.1 and 3.25m, where for small values (0.1m), the initial nonlinearity is suppressed due to the quadratic dependency in Eq. A.29: $r_{NL2L}(q_{u_{0.1}} = 0.1m) \ll 1$. On the contrary, for initial amplitudes larger than unity, the initial ratio is already strongly nonlinear: $r_{NL2L}(q_{u_{0.1}} = 3.25m) \gg 1$.

A.3.5. Three conditions to determine the sensitivity of the FPUT β-problem

The previous paragraphs have shown that four questions may be set up to define the sensitivity of the FPUT behavior to certain conditions for damping, linear stiffness, nonlinear stiffness and initial conditions. This paragraph will show several results from this sensitivity study. The study consists of three free parameters: (1) the linear frequency ratio, (2) the strength of the nonlinearity and (3) the magnitude of the initial conditions. The range of the swept variables are:

$$p = [90\%, 92.5\%, 95\%, 97.5\%, 100\%, 102.5\%, 105\%, 107.5\% \text{ and } 110\%] \tag{A.38}$$

for the linear stiffness, where the higher modes' stiffness is multiplied with this variable, according to Eq. A.35. The nonlinear stiffness is swept for 6 variables between 0 and 20Nm^{-3}:

$$\beta = 0, 4, 8, 12, 16 \text{ and } 20\text{Nm}^{-3}. \tag{A.39}$$

The last variable, the initial condition $q_{u_{0.1}} (= \alpha_{FPUT} q_{0.1})$ is swept for 8 variables between 0.1 and 3.25m:

$$q_{u_{0.1}} = 0.1, 0.55, 1.00, 1.45, 1.90, 2.35, 2.80 \text{ and } 3.25m. \tag{A.40}$$

These parameters are swept for 9, 6 and 8 magnitudes, for the linear stiffness ratio, nonlinear strength and the initial conditions, respectively. In total, there are $9 \times 6 \times 8 = 432$ combinations possible. The default FPUT problem is considered here as well: this is the combination where $p = 100\%$, $\beta = 8\text{Nm}^{-3}$ and $q_{u_{0.1}} = 1.00$m. During these sweeps, several quantities are monitored: the linear energy, the modal amplitude, the recurrence fraction in terms of the initial energy and the energy dominance of the third and fifth mode. The latter quantity is calculated as the maximum difference between the energy of the first mode (E_1) and the third (E_3) or fifth mode (E_5), with respect to the initial energy E_0 (at $t = 0$):

$$E_{dom.n}(t) = \max\left(\frac{E_n(t) - E_1(t)}{E_0}\right),\ \forall\ t, \text{ and } n = 3,\ 5. \tag{A.41}$$

The sweep results are depicted for constant initial conditions, because this allows for proper comparison of the behavior for different conditions over the simulated time. Fig. A.9 depicts the energy and amplitude versus time plots for a sweep for $q_{u_{0.1}} = 1.00$m and the values from Equations A.38 and A.39.

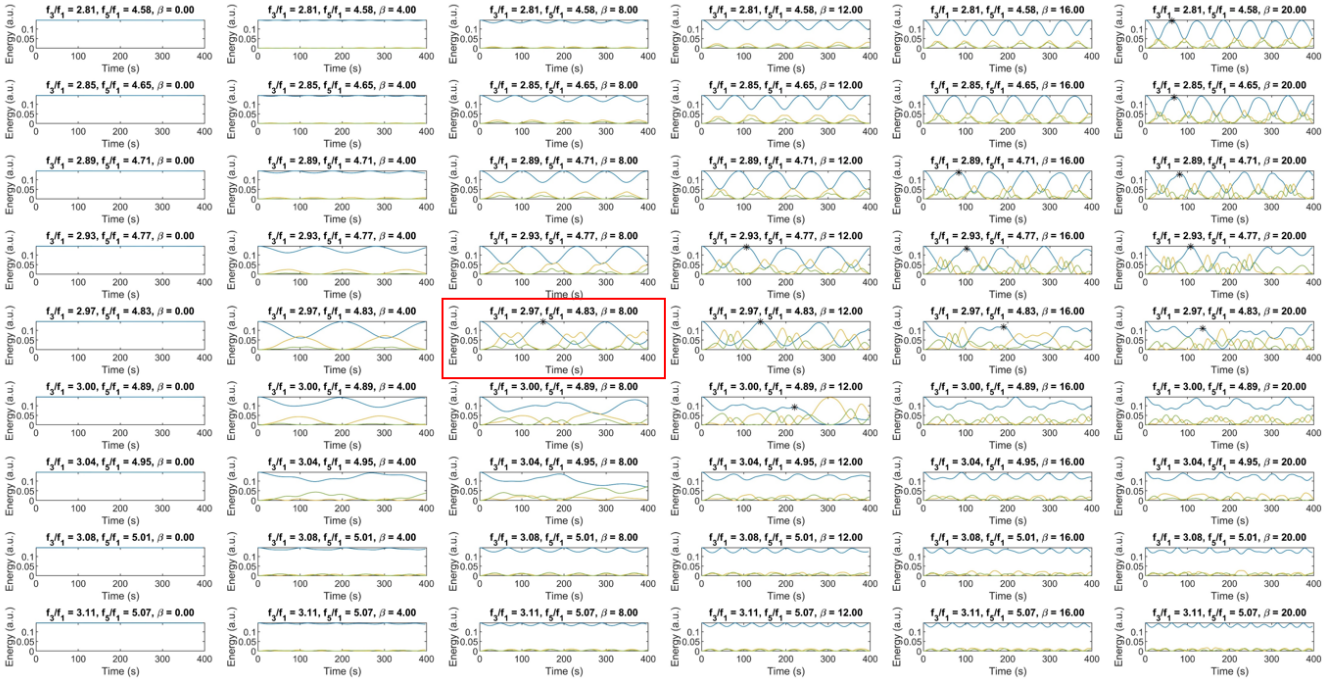

(a) Energy versus time plots for sweeps for linear frequency ratios and nonlinear stiffness and a constant initial condition $q_{0,1} = 1$m.

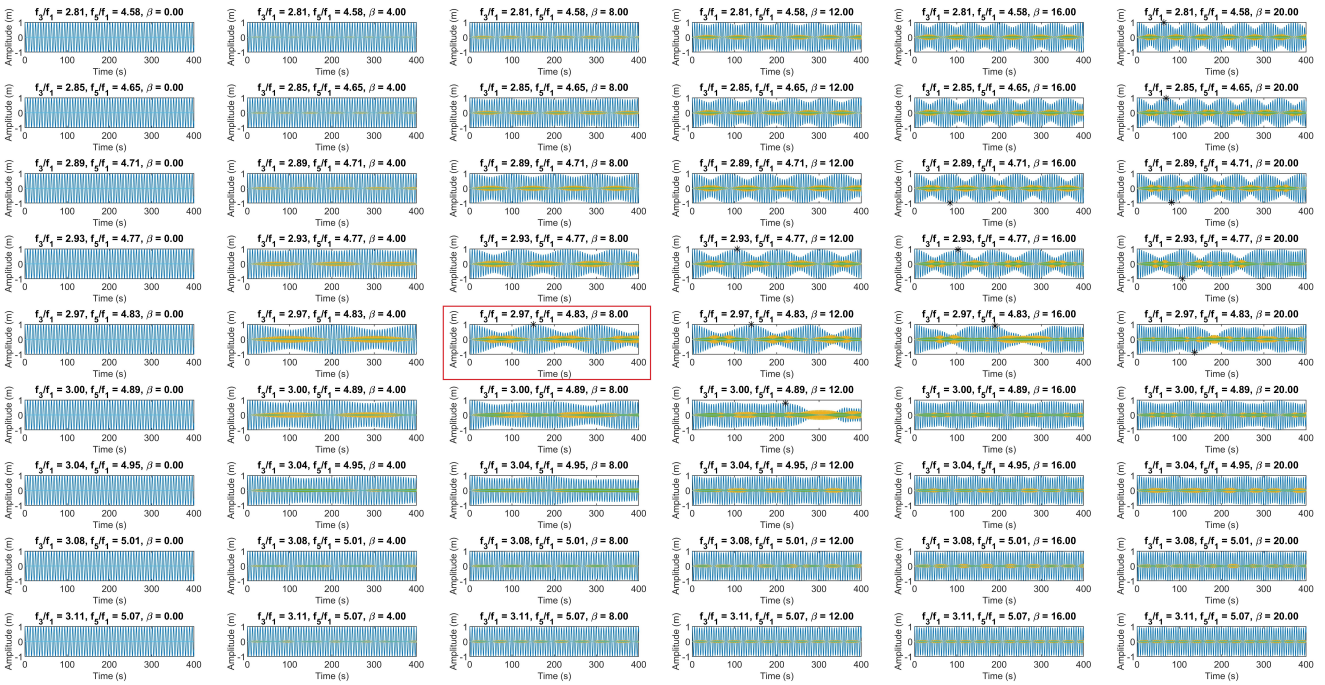

(b) Energy versus time plots for sweeps for linear frequency ratios and nonlinear stiffness and a constant initial condition $q_{0,1} = 1$m.

Figure A.9: A.9a (A.9b) depict the energy versus time (amplitude versus time) plots for various combinations of linear and nonlinear stiffness. The first mode is indicated by blue lines, the third mode is indicated by yellow lines and the fifth mode is indicated by the green lines. The rows show (from top to bottom) an increasing percentage for the linear stiffness: [90%, 92.5%, 95%, 97.5%, 100%, 102.5%, 105%, 107.5% and 110%]. The columns depict (from left to right) the sweep for β, for $\beta = 0, 4, 8, 12, 16$ and 20 Nm^{-3}, which generate an initial nonlinear force ratio of $0, 10, 21, 31, 41, 51\%$. The red rectangle annotates the default FPUT problem, for p=100% and $\beta = 8\mathrm{Nm}^{-3}$. The stars in the plots indicate the recurrence of energy of the first mode, after another mode has been dominant over the first mode.

This figure shows several interesting things:

- As expected, the energy transfer is zero for zero nonlinear stiffness ($\beta = 0\text{Nm}^{-3}$). The amplitude of the first mode remains constant.

- For low nonlinear stiffness (e.g. for $\beta = 4\text{Nm}^{-3}$, the second column) there is some energy transfer, but the energy of the third mode dominates the energy of the first mode for only one combination: the case where $p = 100\%$.

- For a nonlinear stiffness that is equal to the default FPUT variable, $\beta = 8\text{Nm}^{-3}$ (an initial force ratio of 21%), the energy transfer is stronger than for the case where $\beta = 4\text{Nm}^{-3}$ (initial force ratio of 10%). The recurrent behavior is only visible for the linear frequency ratios which are equal to the default FPUT system. Hence, this behavior (as was also shown in Fig. A.3a) appears to be quite sensitive to variations in the linear frequency ratios. The increase in energy of the higher modes is accompanied by an increase in the amplitude of these modes.

- The last three columns (for initial force ratios larger than 31%) show that the dynamics become more complicated for stronger nonlinearity, as there is more energy exchange visible. Clear modulations in amplitude are visible for all modes.

- The bottom two rows, for values of p equalling 107.5 and 110%, the energy exchange is present, though the E_1 is never dominated by E_3 nor E_5. The increasing nonlinearity does show that the energy transfer (and the amplitude of the higher modes) increase accordingly.

- The upper right plots show that there is quite some energy exchange visible, both in energy and amplitude. A trend is visible if one were to draw a (diagonal) line from the default FPUT problem to the upper right-hand corner of the figure. Along this line, the nonlinearity is increased as one moves towards the right, and the frequency ratio is decreased further as one moves upwards. This implies that for decreasing linear stiffness ratios and increasing nonlinear stiffness, the behavior remains -approximately- similar to the default problem. The decrease in the linear stiffness ratios may be thus be compensated by increasing the nonlinear stiffness, which in turn increases (hardens) the effective frequency of the modes, similar to the Duffing behavior from Section B.3.2.

- During this increase in nonlinearity, the recurrence time appears to decrease, showing that for systems with stronger nonlinearity, this behavior may occur on a smaller time scale.

Before expanding to various other initial conditions, it is important to compare the abovementioned observations with literature.

A.3.6. Literature

Nelson et. al recently presented a study that shows what the influence of tolerances to the nonlinear stiffness is [26]. They conducted numerical simulations of the FPUT α-model, where they placed tolerances (t_i) on the linear and/or nonlinear stiffness of Eq. A.42:

$$\ddot{x}_i = t_{i+1}x_{i+1} + t_{i-1}x_{i-1} - 2t_i x_i + \alpha[(t_{i+1}x_{i+1} + t_i x_i)^2 - (t_i x_i + t_{i-1}x_{i-1})^2]. \tag{A.42}$$

These tolerances were considered to cover the manufacturing tolerances which are commonly present in passive electronics; their magnitudes are claimed to vary between $\pm 0.1\%$ and $\pm 10\%$ of the considered strength. Their study covered three topics: (1) the effects of tolerances on the linear, nonlinear, or both terms; (2) the effects of tolerances on the number of elements (N) in the model, and (3) the effects of asymmetry in the coupling coefficients, where $t_i \neq t_{i-1} \neq t_{i+1}$. The study that is conducted in this report is primarily focused on Nelson's first topic, but the others may also be quite relevant during further design stages. Nelson's research showed that the effects of adding such tolerances to either the linear, nonlinear or both linear and nonlinear terms may quickly reduce the recurrent behavior of the system.

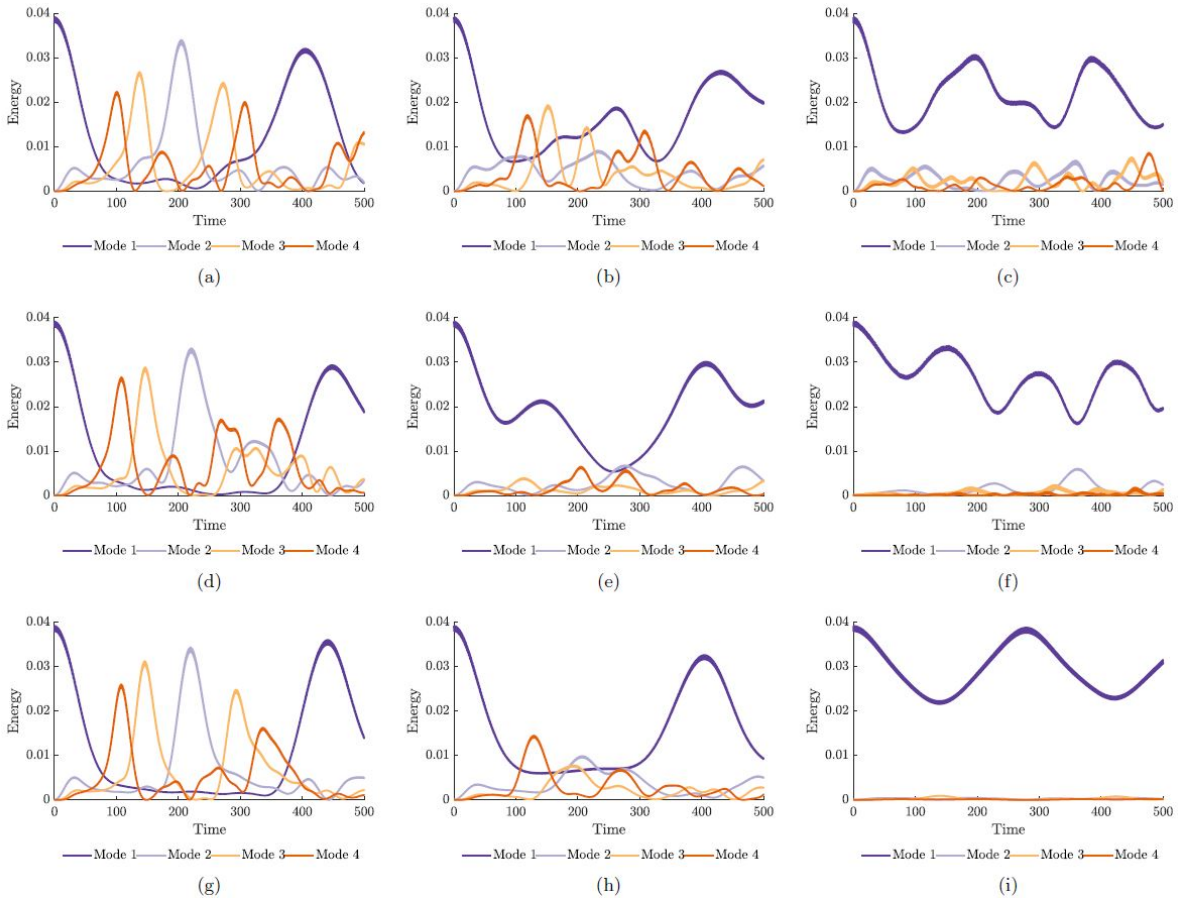

Figure A.10: From Nelson et. al, [26]. The effect of tolerance on different parts of a 1D FPUT-α array with a coupling coefficient of α = 0.25 and N = 64 oscillators. Panels (a)–(c) show examples with tolerance in both the linear and nonlinear terms, panels (d)–(f) show examples with tolerance in only the linear terms, and panels (g)–(i) show examples with tolerance in only the nonlinear terms. Observe that adding tolerance to only the linear terms has a comparable effect on recurrence to adding tolerance to only the nonlinear terms. Tolerance in both linear and nonlinear terms: (a) ±1%, (b) ±5%, and (c) ±10%. Tolerance in the linear terms: (d) ±1%, (e) ±5%, and (e) ±10%. Tolerance in the nonlinear terms: (g) ±1%, (h) ±5%, and (i) ±10%.

Figures A.10(a)-(c) from Nelson [26] depict that increase of tolerances to both the linear and nonlinear stiffness result in deteriorating recurrent behavior. For tolerances larger or equal to ±5%, in A.10 (b-c), the recurrent behavior is hardly visible. Adding tolerances only to the linear (Fig. A.10(d-f)) or nonlinear terms (Fig. A.10(g-i)) show approximately the same behavior: the energy dominance and recurrent behavior disappears as the tolerance is increased. Comparing the case where a tolerance to only the linear fraction or nonlinear fraction is added with the case where a tolerance is added both linear and nonlinear fractions, it is clear that the other modes receive more energy for the case where the tolerances are added to both. Nelson subsequently shows that asymmetry in the tolerances of the coupling elements and a lower number of elements may enhance the recurrent behavior as well. The latter statement may be verified using the results from the previous subsection, where it was shown that FPUT recurrence is most likely to occur for non-integer frequency ratios. Now, imagine one were to discretize a string into N elements: using a lot of elements (large N) will approximate a string's properties with increasing accuracy. This in turn generates frequencies that are close to the frequencies of a string, which follow integer relations. By using less elements, these frequencies will approximate the string frequencies with less accuracy, generating non-integer ratios, which were previously shown to generate strong recurrent behavior.

This research by Nelson shows that the recurrent behavior in the FPUT-α model is very sensitive to the applied tolerances, and it is shown to be most significant for the cases where the tolerances are added to both the linear and nonlinear variables. These effectively generate similar results (showing recurrent behavior) to what was shown in the upper right corner of Fig. A.9a, where both the linear and nonlinear stiffness deviated from the default problem. Though the dynamics of these FPUT-α and FPUT-β models may appear to be similar,

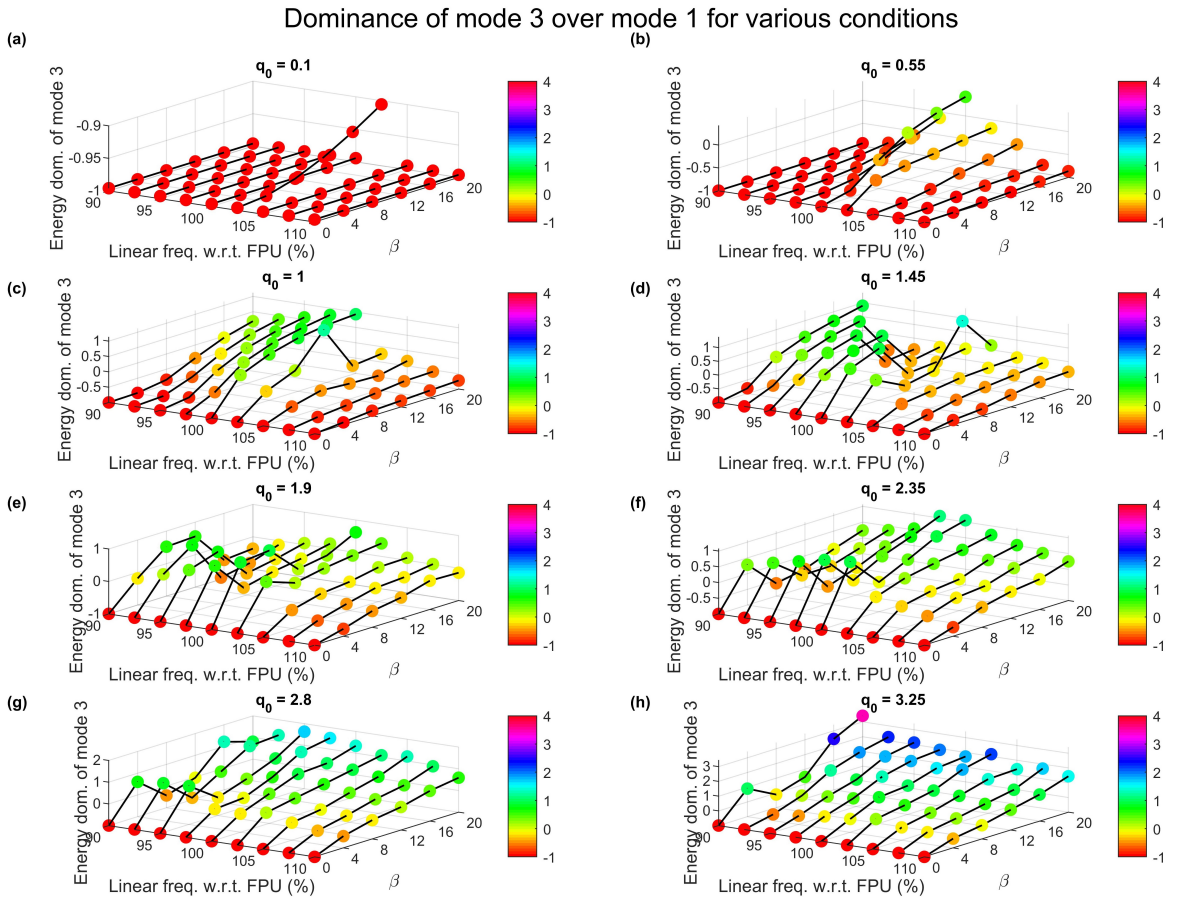

Figure A.11: Energy dominance of the third mode over the first mode, for several parameter sweeps. The results are grouped per initial condition. Each plotted point depicts a combination of 3 parameters: the magnitude of the initial condition, the percentage of the default linear stiffness and the magnitude of the nonlinearity. The output of each iteration -the magnitude of the energy dominance- is plotted along the vertical axis and plotted in different colors, depending on its magnitude.

the comparison should be executed carefully, as their global dynamics are different. For instance, in the α-model, there is a coupling between even and uneven modes, due quadratic nonlinearity.

A.3.7. Results of the sensitivity analysis

In the previous section, it was found that the quantitative dynamics of the FPUT α-model agree fairly well with the observations that were made in Fig. A.9. However, these observations should not be considered to be valid for the FPUT β-model. This section will elaborate upon the results of the parameter sweeps for linear, nonlinear stiffness and initial conditions, as were presented in Section A.3.5. The parameter sweeps are grouped per initial condition, and the results for each parameter sweep are plotted in a 3-dimensional scatter plot. The x-, y- and z-axes contain the linear frequency ratio (expressed in terms of a percentage p, Eq. A.38), the magnitude of β (Eq. A.39) and the magnitude of the energy dominance (Eq. A.41), respectively. The magnitude of the energy dominance will also be expressed in a color, which will show gradual effect of the swept parameters.

The initial force ratio of each of these initial conditions depends only on the initial amplitude of the first mode and the magnitude of β, since the first mode's linear frequency is kept constant. The initial force ratios may thus be calculated for each initial condition and value of β, using Eq. A.29. Figures A.11 and A.12 depict the results for 8 initial conditions, which are each swept for 6 values of β. Table A.6 depicts the initial force ratios, where each row indicates an initial condition from Figures A.11 and A.12.

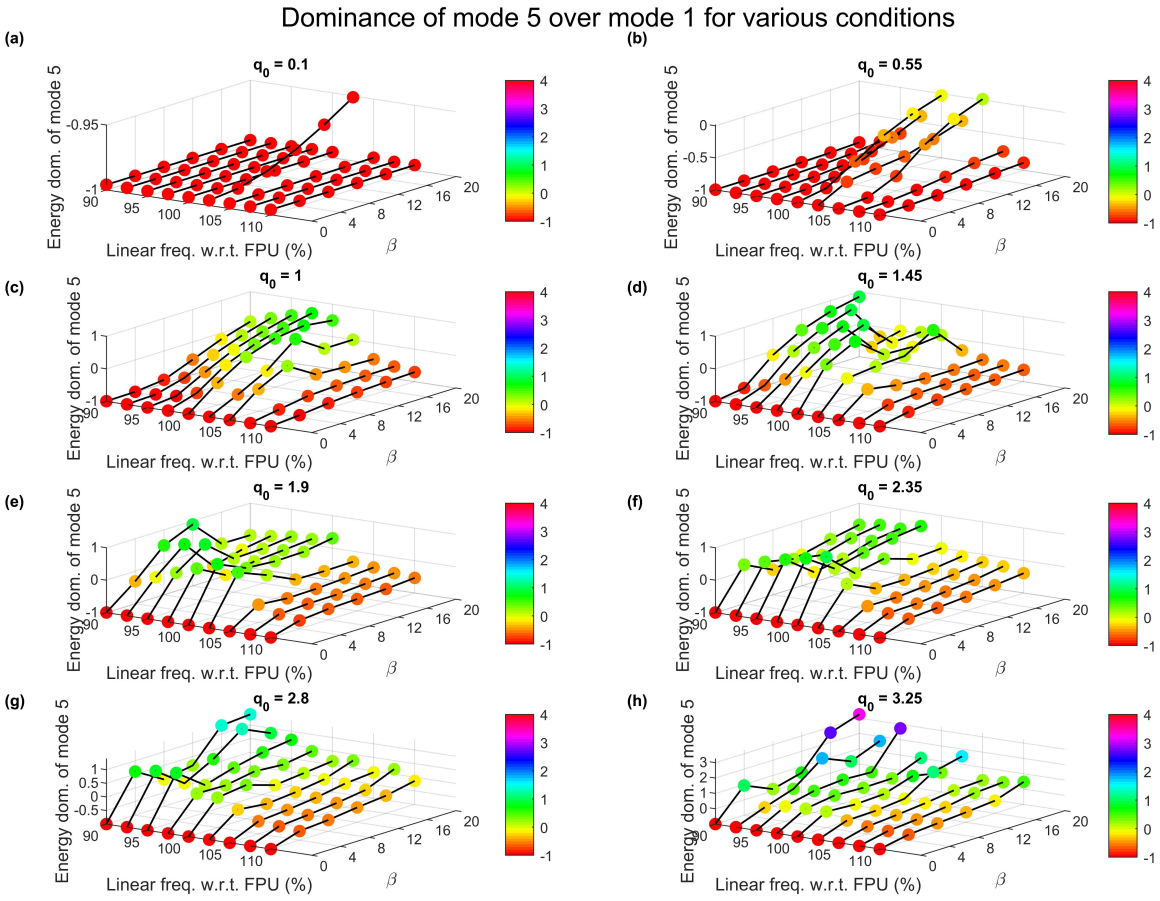

Figure A.12: Energy dominance of the fifth mode over the first mode, for several parameter sweeps. The results are grouped per initial condition. Each plotted point depicts a combination of 3 parameters: the magnitude of the initial condition, the percentage of the default linear stiffness and the magnitude of the nonlinearity. The output of each iteration -the magnitude of the energy dominance- is plotted along the vertical axis and plotted in different colors, depending on its magnitude.

Table A.6: Initial nonlinear force ratios (Eq. A.29). Rows indicate the initial force percentages for all subplots in Figures A.11 and A.12, for the nonlinearities in each column.

	β[Nm^{-3}]					
$\mathbf{q_{u_{0.1}}}$ [m]	**0**	**4**	**8**	**12**	**16**	**20**
0.10	0	0	0	0	0	1
0.55	0	3	6	9	12	16
1.00	0	10	21	31	41	51
1.45	0	22	43	65	87	108
1.90	0	37	74	111	149	186
2.35	0	57	114	170	227	284
2.80	0	81	161	242	323	403
3.25	0	109	217	326	435	543

The results for the third and fifth mode in Figures A.11(a-b) and A.12(a-b) show that for small initial conditions, where $q_{u_{0.1}} < 1$m ($F_{NL2L} \leq 16\%$), the dominance of the modal energy is small: there is little significant energy transfer for the case where $q_{u_{0.1}} = 0.1$m, since the dominance remains well below 0. The case where $q_{u_{0.1}} = 0.550$m indicates that the energy transfer is more significant. For the case where the linear frequencies equal 100% of the FPUT variables, there is energy dominance, which increases as the nonlinear strength increases. For Figures A.11(c) and A.12(c), where $q_0 = 1$m, there is significant energy transfer, which follows the trend which was already observed in Fig. A.9a: for a smaller value of p and increased nonlinearity, the energy transfer seems to increase in magnitude. Interestingly, for the cases where the linear frequencies have shifted to a higher frequency ($p > 100\%$), this energy dominance magnitude decreases, for both the third and fifth modes. Figures A.11(d-e) and A.12(d-e) show that as the magnitude of the initial condition increases (to $q_{u_{0.1}} = 1.45$m or $q_{u_{0.1}} = 1.8$m), where the initial nonlinear force ratio exceeds 37%, the energy dominance seems to be destroyed for increased nonlinearity and shifted frequencies. However, the cases where the linear stiffness is increased, we start to see more significant energy transfer. This effect is also present in the remaining Figures Fig. A.11(f-h) and A.12(f-h), though it is less significant: the energy transfer first increases before it drops for $\beta = 8$Nm^{-3}, and increases again for higher nonlinearity. The latter plots, Fig. A.11(h) and A.12(h), show that the energy transfer mostly increases for all considered conditions. Generally, large initial force ratios (exceeding 100%, for higher nonlinearities and larger magnitudes of the initial condition) increase energy transfer. For higher initial amplitudes and increased magnitudes of nonlinearities, the energy dominance increases beyond the point where $E_{dom.n}(t) > 1$ (Eq.A.41), implying that there is more energy located in the studied mode, than there was initially present in the first mode. The reason for this could be that the initial energy is defined as the initial *linear* energy. For higher nonlinearity and increasing magnitudes of the initial conditions, this linear approximation of the energy will no longer be valid, implying that the fraction of nonlinear energy will become larger and no longer negligible. Nonetheless, this analysis has shown that it is possible to see FPUT behavior for stronger nonlinearities (and magnitudes of the initial conditions), as long as the initial force ratios remain larger than 21%, which was found for the default FPUT model.

A.3.8. Conclusion

In summary, from this sensitivity study on the default FPUT system, it may be concluded that FPUT behavior is not confined to the default FPUT problem only, where $k = 1$Nm^{-1} and $\beta = 8$Nm^{-3}. In this section, the the influence of a linear damping factor on the default FPUT system (where $N = 16$ and $\beta = 8$Nm^{-3}) was investigated first. This showed that the behavior is still visible for relatively low Q-factors, where roughly 80% of the initial energy returned to the initial condition for Q-factors of the first mode of around 1,000 (and higher mode Q-factors were here assumed to scale with the inverse of the mode number). For first mode's Q-factors that exceed this 100,000, it could be observed that less than 1% of the initial energy was lost in single recurrence period. For lower Q-factors of the higher modes, part of the energy that is distributed to these modes will dissipate sooner than it can be transferred back to the first mode, which reduces the recurrent peak.
The observations that were made here are in line with the study on the α-model from Nelson [26], who reported that by increasing the tolerances of both the linear and nonlinear stiffness terms of the α-model, one will more or less conserve the FPUT mechanics. Where Nelson included maximum tolerances of 10%, the present research does not include tolerances, but it varies the magnitude of the nonlinear stiffness in larger steps than this 10%. The present research shows that for a weakly damped β-model, which includes a cubic (Duffing) nonlinearity, one may compensate the decrease of the linear frequencies by increasing the non-

linear stiffness. This model is weakly damped, the first mode's Q = 100,000 and higher modes are assume to scale with this Q and the inverse of the mode number. In addition, contrary to what Nelson reported, it can be concluded that the FPUT mechanics in these regimes for high nonlinearity are less sensitive to the changes of these nonlinearities. Fig. A.9a indicates that for example that two of the requirements for FPUT behavior (energy dominance of another mode over the initially excited mode, followed by recurrence of the initial condition) may be observed for higher magnitudes of nonlinearity. However, increasing the nonlinear magnitude of the system will also increase the nonlinear energy, which therefore should be taken into account as well, especially for large amplitudes of vibration.

B

String vibrations

This chapter elaborates upon string vibrations. First, two analytical models are presented which are subsequently compared to a numerical model. Finally, experimentally obtained frequency responses of string resonators will be simulated using these analytical models.

B.1. Analytical string models

This section will show in what form nonlinearities appear in the equations of motion of a continuous string resonator. Many theoretical studies investigate the nonlinearities in strings. The analysis that is presented here is a combination of research by Anand, Zhao and Nayfeh [2, 38, 25]. Zhao derives the equations of motion from Hamiltons priciple, but Nayfeh and Anand follow a more direct approach using force equilibrium. Eventually, both methods will generate the same equations of motion.

These string resonators may be modelled by the following system, a simply supported string of length L. The string is made of a material with density ρ and Young's modulus E. The string is under a pre-load in the longitudinal direction with magnitude T_0, which is distributed over a cross-sectional area A, resulting in a pre-stress of $\sigma_0 = \frac{T_0}{A}$.

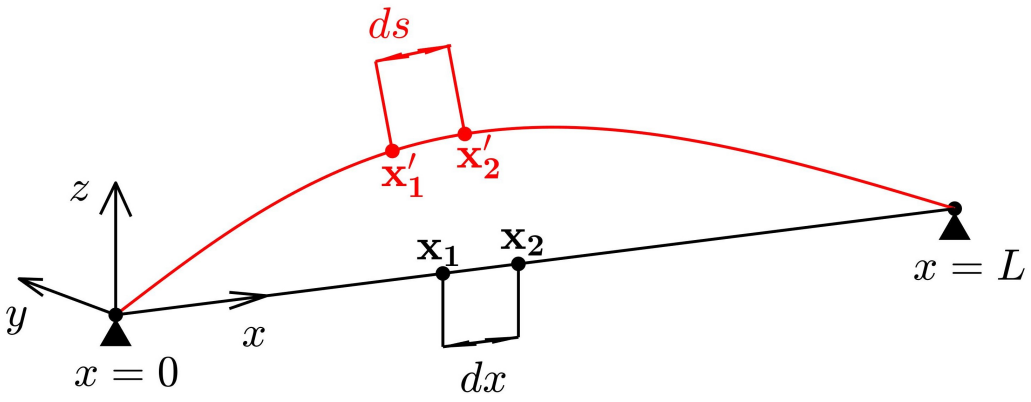

Figure B.1: Simply supported string of length L. Shown is an infinitesimal element with length dx. The initial configuration of the string is shown in black; the large deformation case is shown in red. The string is pre-loaded in the x-direction with load T_0.

Now, as can be seen in Fig. B.1, the string consists of a infinitesimal element which has length dx in the initial (black) configuration. The deformed configuration (in red) shows that the element is displaced in the vertical direction. The two points that initially were at locations $\mathbf{x_1} = [x_1,\ y_1,\ z_1]$ and $\mathbf{x_2} = [x_2 = x_1 + dx,\ y_2,\ z_2]$ have displaced to $\mathbf{x_1'} = [x_1',\ y_1',\ z_1']$ and $\mathbf{x_2'} = [x_2',\ y_2',\ z_2']$ respectively. The longitudinal displacement (in the x-direction) is denoted by u, the transverse displacement (the y-direction) is denoted by v and the vertical displacement (in the z-direction) is denoted by w. The following equations show how these displacements are formulated:

$$\begin{aligned} x_1' - x_1 &= u \\ y_1' &= v \\ z_1' &= w \\ x_2' - (x_1 + dx) &= u + du \\ y_2' &= y_1' + dv = v + dv \\ z_2' &= z_1' + dw = w + dw. \end{aligned} \tag{B.1}$$

Pythagoras' theorem is can be used to determine the length of the stretched element ds:

$$ds = \sqrt{(x_2' - x_1')^2 + (y_2' - y_1')^2 + (z_2' - z_1')^2} = \sqrt{(dx + du)^2 + dv^2 + dw^2)} = dx\sqrt{\left(1 + \frac{du}{dx}\right)^2 + \left(\frac{dv}{dx}\right)^2 + \left(\frac{dw}{dx}\right)^2}. \tag{B.2}$$

The derivatives with respect to x may be written as $\frac{du}{dx} = u_x$, $\frac{dv}{dx} = v_x$ and $\frac{dw}{dx} = w_x$:

$$ds = dx\sqrt{\left(1 + \frac{du}{dx}\right)^2 + \left(\frac{dv}{dx}\right)^2 + \left(\frac{dw}{dx}\right)^2} = dx\sqrt{(1 + u_x)^2 + v_x^2 + w_x^2} \tag{B.3}$$

The analytical models in this chapter are based on the assumption that the bending motion of the string may be neglected, as the area moment of inertia is very small for small string thickness. This area moment of inertia scales with the string thickness to the power three (for a rectangular cross-section, the area moment of inertia equals $\frac{1}{12}bh^3$, where b and h are the width and thickness, respectively). For the small thicknesses that are considered here, this will result in a magnitude that is considered to be small with respect to the energy that is associated to the axial deformation of the resonator. This latter quantity is large due to the significant pre-stress of the resonator.

Anand's method is based on the assumption that though the displacements will be relatively large, they will still be small enough for Hooke's law to be valid [2]. This assumption allows one to also assume that the derivatives of the displacement (u_x, v_x and w_x) are very small compared to unity. Assuming that $v \gg u$ and $w \gg u$ (small longitudinal displacement w.r.t. the transverse or vertical displacements) allows us to get rid of u-terms that scale with higher orders than 2 and to get rid of terms that scale with the cube of the displacement in the transverse and vertical directions: v and w respectively.

Approximating ds by Taylor expanding u_x up to second order gives:

$$ds \approx \left[\sqrt{v_x^2 + w_x^2 + 1} + \frac{u_x}{\sqrt{v_x^2 + w_x^2 + 1}} + \mathcal{O}(u_x^2)\right] dx. \tag{B.4}$$

Subsequently Taylor expanding v_x and w_x up to the power three, will then give, after some algebra:

$$ds \approx \left[1 + u_x + \frac{1}{2}v_x^2 + \frac{1}{2}w_x^2\right] dx. \tag{B.5}$$

The axial tension force that is present the string results from two parts, (1) the pretension force -denoted by T_0- and (2) the stretching force of the element from length ds to dx -denoted by $EA\frac{ds-dx}{dx}$, where E is the Young's modulus of the string material and A is the cross-sectional area of the string. This can be given by the following formula for the tension at location x and time t:

$$T(x,t) = T_0 + EA\frac{ds - dx}{dx} = T_0 + EA(u_x + \frac{1}{2}v_x^2 + \frac{1}{2}w_x^2). \tag{B.6}$$

The tension due to the stretching in the longitudinal direction is given by the ratio of the longitudinal stretching over the total stretched length ds:

$$T_x(x,t) = T(x,t)\frac{(1+u_x)dx}{ds}. \tag{B.7}$$

And similarly for the tension in the transverse (Eq. B.8) and vertical (Eq. B.9) directions.

$$T_y(x,t) = T(x,t)\frac{v_x dx}{ds} \tag{B.8}$$

$$T_z(x,t) = T(x,t)\frac{w_x dx}{ds} \tag{B.9}$$

Where the fraction $\frac{dx}{ds}$ is given by:

$$\frac{dx}{ds} = 1 - u_x - \frac{1}{2}v_x^2 - \frac{1}{2}w_x^2. \tag{B.10}$$

Force equilibrium in all directions will give us three expressions: one for the each of the three displacement directions. The linear mass density of the element is given by m and it is equal to the product of the density and the cross-sectional area: $m = \rho A$. The force that results from a change in displacement should thus be equal to the inertia terms in these directions.

$$mu_{tt} = \frac{\partial}{\partial x}\left[T(x,t)(1+u_x)\frac{ds}{dx}\right] = \frac{\partial}{\partial x}\left[[T_0 + EA\left(u_x + \frac{1}{2}v_x^2 + \frac{1}{2}w_x^2\right)](1+u_x)\left(1 - u_x - \frac{1}{2}v_x^2 - \frac{1}{2}w_x^2\right)\right] \tag{B.11}$$

$$mv_{tt} = \frac{\partial}{\partial x}\left[T(x,t)(v_x)\frac{ds}{dx}\right] = \frac{\partial}{\partial x}\left[[T_0 + EA\left(u_x + \frac{1}{2}v_x^2 + \frac{1}{2}w_x^2\right)]v_x\left(1 - u_x - \frac{1}{2}v_x^2 - \frac{1}{2}w_x^2\right)\right] \tag{B.12}$$

$$mw_{tt} = \frac{\partial}{\partial x}\left[T(x,t)(w_x)\frac{ds}{dx}\right] = \frac{\partial}{\partial x}\left[[T_0 + EA\left(u_x + \frac{1}{2}v_x^2 + \frac{1}{2}w_x^2\right)]w_x\left(1 - u_x - \frac{1}{2}v_x^2 - \frac{1}{2}w_x^2\right)\right] \tag{B.13}$$

Expanding Eq.'s B.11, B.12, B.13 and neglecting the $\mathcal{O}(u_x^2)$, $\mathcal{O}(v_x^3)$, $\mathcal{O}(w_x^3)$ and cross-terms that scale with u_x results in the equations of motion for all three directions:

$$mu_{tt} = EAu_{xx} + \frac{1}{2}(EA - T_0)\frac{\partial}{\partial x}\left[v_x^2 + w_x^2\right] \tag{B.14}$$

$$mv_{tt} = T_0 v_{xx} + (EA - T_0)[u_x v_{xx} + u_{xx}v_x + \frac{3}{2}v_x^2 v_{xx} + w_x w_{xx} v_x + \frac{1}{2}w_x^2 v_{xx}] \tag{B.15}$$

$$mw_{tt} = T_0 w_{xx} + (EA - T_0)[u_x w_{xx} + u_{xx}w_x + \frac{1}{2}v_x^2 w_{xx} + v_x v_{xx} w_x + \frac{3}{2}w_x^2 w_{xx}] \tag{B.16}$$

Several analytical models will be shown in this chapter: the first model will show how the linear resonance frequencies may be determined through linearization of the strains which result from vertical displacements of strings. Subsequently, a nonlinear model will be derived that includes only vertical displacements. Thereafter, the modal equations of motion for planar vibrations (where the transverse displacement is assumed to be zero) are derived from a model that accounts for all three displacement directions. Finally, the full modal equations of motion for strings will be derived. In the latter model, all displacement directions (longitudinal, transverse and vertical) will be considered.

B.1.1. Analytical string model for vertical displacements

Zhao recently presented an analytical string model which only accounts for vertical displacements [38]. Here, it is assumed that (1) the vibrations remain planar (in the xz-plane) and (2) that the displacement in the longitudinal direction is much smaller than that in the vertical direction: $dv = 0$ and $du \ll dw$. Therefore, it may be assumed that the displacement du is negligible with respect to the displacement dw. This then results in the following displacement directions:

$$u_x = 0,\ v_x = 0,\ \text{and}\ w_x \neq 0. \tag{B.17}$$

The equation (Eq. B.3) for the stretched element ds reduces to the following expression when these assumptions of planar vibrations and small longitudinal displacements are applied:

$$ds = dx\sqrt{1 + w_x^2}. \tag{B.18}$$

Linear string models for vertical vibrations

If it is furthermore assumed that the strain may be approximated by using that $\sqrt{1+w_x^2} \approx 1 + \frac{1}{2}w_x^2$, the following strain formulation is found:

$$\epsilon_{\text{vertical}} = \sqrt{1+w_x^2} - 1 \approx 1 + \frac{1}{2}w_x^2 - 1 = \frac{1}{2}w_x^2. \tag{B.19}$$

The equation of motion for w then becomes, after assuming that only *linear* terms in w should be kept ($\mathcal{O}(w_x^2)$ and higher are zero):

$$m w_{tt} = T_0 w_{xx}. \tag{B.20}$$

This equation could also be found from Eq. B.16 when neglecting longitudinal and vertical displacement directions ($u = 0$ and $v = 0$) and negligence of all nonlinear terms.

This equation results in the following equation of motion if the relation for the pre-tension force T_0 is substituted for $\sigma_0 A$ in Eq. B.20:

$$\frac{\partial^2 w}{\partial t^2} = \frac{\sigma_0}{\rho}\frac{\partial^2 w}{\partial x^2}. \tag{B.21}$$

This yields the familiar (linear) wave equation. This equation is a strong simplification of the vibrations of a string as it relies on the assumptions that the vibrations remain small. In subsequent (nonlinear) analyses, it will be shown that this equation becomes much more complex when the vibrations become large.

The linear frequencies of the string may be determined by separating Eq. B.21 into two parts, which are time and space dependent, respectively. If we assume that the displacement may be divided into a time-dependent part $p(t)$ and a space dependent part $W(x)$, we can rewrite the wave equation assuming that both terms equal some constant $-\omega^2$ [20], as is shown in Eq. B.22.

$$\frac{\ddot{p}(t)}{p(t)} = \frac{\sigma_0}{\rho}\frac{W''(x)}{W(x)} = -\omega^2 \tag{B.22}$$

The space-dependent part of the above equation can be rewritten as:

$$W''(x) + \omega^2 \frac{\rho}{\sigma_0} W(x) = 0. \tag{B.23}$$

This is just a harmonic ordinary differential equation with solutions of the following form:

$$W(x) = A\cos\left(\omega\sqrt{\frac{\rho}{\sigma_0}}x\right) + B\sin\left(\omega\sqrt{\frac{\rho}{\sigma_0}}x\right). \tag{B.24}$$

Imposing the boundary conditions of a simply-supported string of length L, i.e. that $W(0) = 0$ and $W(L) = 0$, we can immediately see that $A = 0$ and that the following equation should be satisfied:

$$W(L) = B\sin\left(\omega\sqrt{\frac{\rho}{\sigma_0}}L\right) = 0. \tag{B.25}$$

This requires that either $B = 0$ or that $\sin\left(\omega\sqrt{\frac{\rho}{\sigma_0}}L\right) = 0$. The latter is the only feasible solution, and hence the following relation should be satisfied:

$$\omega\sqrt{\frac{\rho}{\sigma_0}}L = n\pi,\ n = 1,2,... \tag{B.26}$$

This yields the following equation for ω_n, the string's n^{th} eigenfrequency:

$$\omega_n = \frac{n\pi}{L}\sqrt{\frac{\sigma_0}{\rho}}. \tag{B.27}$$

The space-dependent part can thus be written as,

$$W_n(x) = \sin\left(\frac{n\pi}{L}x\right). \tag{B.28}$$

Which shows that the eigenfrequencies of a string scale with mode number n, these linear frequencies thus scale with the real mode number n as well.
Now the frequencies of the system are known, a non-dimensionalization and a coordinate transformation to modal coordinates may be performed as well. The non-dimensionalisation of Eq. B.21 is conducted using the following relations D.2.2:

$$\bar{w} = \frac{w}{L},\ \bar{x} = \frac{x}{L},\ \omega_0 = \frac{\pi}{L}\sqrt{\frac{\sigma_0}{\rho}},\ \tau = \omega_0 t. \tag{B.29}$$

Substitution of these relations into Eq. B.21, gives Eq. B.30.

$$\frac{\pi^2}{L}\frac{\sigma_0}{\rho}\frac{d^2\bar{w}}{d\tau^2} - \frac{\sigma_0}{\rho}\frac{1}{L}\frac{d^2\bar{w}}{d\bar{x}^2} = 0 \rightarrow \frac{d^2\bar{w}}{d\tau^2} - \frac{1}{\pi^2}\frac{d^2\bar{w}}{d\bar{x}^2} = 0 \tag{B.30}$$

Now, in order to determine the modal equations of motion, a modal coordinate transformation should be performed. The displacement $\bar{w}$ may be written as:

$$\bar{w}(\bar{x},\tau) = \phi_{u_n}(\bar{x})\tilde{q}_n(\tau). \tag{B.31}$$

Where $\phi_{u_n}(\bar{x})$ is the linear mode shape of mode n, which has a maximum of unity:

$$\phi_{u_n}(x) = \sin(n\pi\bar{x}) = \sin(\pi\bar{x}). \tag{B.32}$$

Substitution of the mode shapes results in the following expression for the modal equations of motion:

$$\ddot{\tilde{q}}_{u_n}(\tau)\sin(n\pi\bar{x}) + \frac{1}{\pi^2}n^2\pi^2\sin(n\pi\bar{x})\tilde{q}_{u_n}(\tau) = 0. \tag{B.33}$$

Evaluating the integrals over the domain of $\bar{x}$, which ranges from 0 to 1, gives:

$$\int_0^1 (\ddot{\tilde{q}}_{u_n}(\tau)\sin(n\pi\bar{x}) + n^2\sin(n\pi\bar{x})\tilde{q}_{u_n}(\tau))d\bar{x} = \ddot{\tilde{q}}_{u_n}(\tau)(1-\cos(n\pi)) + n^2\tilde{q}_{u_n}(\tau)(1-\cos(n\pi)) = 0 \tag{B.34}$$

The first mode is considered only: $n = 1$. The linear (non-dimensional) equation of motion of a string will thus become:

$$\ddot{\tilde{q}}_{u_n}(\tau) + n^2\tilde{q}_{u_n}(\tau) = \ddot{\tilde{q}}_{u_1}(\tau) + \tilde{q}_{u_1}(\tau) = 0 \tag{B.35}$$

Which shows that the dimensionless linear modal equation of motion does not depend on any string parameters. This means that the inertia term and the linear stiffness term both scale with the same parameters, which can also be seen in Eq.'s B.21 and B.30, where all string's dimensional parameters appear to drop out. The equation in Eq. B.21 is often written as $\ddot{q}_{u_1} + \omega_n^2 q_{u_1} = 0$, where the ω-terms for a string scale linearly with mode number n. The effect of dimensional parameters on the nonlinear or large-amplitude vertical vibration of strings is examined in the next subsection.

Nonlinear string models for vertical vibrations: the w-displacement model
If one still were to take into account only the vertical vibrations w and that terms that scale nonlinearly in w_x are nonzero, (i.e. for which $\mathcal{O}(w_x^2)$ and higher are **non**zero), we arrive (using Eq. B.16) at the following equation of motion for w:

$$\rho A w_{tt} - [EA - T_0]\left(\frac{3}{2}w_{xx}w_x^2\right) - T_0 w_{xx} = 0 \tag{B.36}$$

After division with the mass density, the constants in this equation can be rewritten as $c_0 = \sqrt{\frac{T_0}{\rho A}} = \sqrt{\frac{\sigma_0}{\rho}}$ and $c_1 = \sqrt{\frac{EA}{\rho A}} = \sqrt{\frac{E}{\rho}}$, which are the vertical and longitudinal wave velocities in a string. Their ratio, $\frac{c_1^2}{c_0^2} \gg 1$, as the Young's Modulus is much larger than the pre-stress of the strings that are considered in this research (250

GPa vs. 1 GPa, respectively). Hence, it is assumed that $c_1^2 - c_0^2 \approx c_1^2$ for the considered string characteristics. Finally, this simplification will generate the following equation of motion:

$$w_{tt} - (c_1^2 - c_0^2)\left(\frac{3}{2} w_{xx} w_x^2\right) - c_0^2 w_{xx} = 0 \rightarrow w_{tt} - c_1^2 \left(\frac{3}{2} w_{xx} w_x^2\right) - c_0^2 w_{xx} = 0. \tag{B.37}$$

Now, in order to compute the modal variables, current (physical) coordinates should be transformed to modal coordinates, which allow for separation of space and time, similarly to the previous section. This may be done using the following equation:

$$w(x,t) = \sum_{n=1}^{N} \phi_{u_n}(x) q_{u_n}(t) \tag{B.38}$$

where the (dimensional) displacement w is written as a combination of N eigenmodes. Here, $\phi_{u_n}(x)$ is gives the max-1 shape of the eigenmode n, and $q_{u_n}(t)$ is the time dependent modal amplitude of mode n. The modal shape function may be assumed to be a function that is equal to one of the eigenmodes of the string. In this case, this is a Sine-function (according to Eq. B.32), the mode shape of mode n may be written as follows:

$$\phi_{u_n}(x) = \sin\left(\frac{n\pi x}{L}\right) \tag{B.39}$$

To determine the modal parameters of the system, we should imply the Galerkin method, where the equation is first multiplied by a certain weight function, before it is integrated over the length of the string [20]. This weight function is just another mode shape of the system; this allows one to decompose the modal variables into parts that are only present in the equation for mode r. This weight function is denoted by ϕ_{u_r}, the mode shape of mode number r. Note that the mode numbers r and n are not necessarily equal: if not, this method allows for computation of the influence of mode n onto mode r.

$$\phi_{u_r}(x) = \sin\left(\frac{r\pi x}{L}\right) \tag{B.40}$$

To determine the modal parameters of mode n in equation of motion r (i.e. the modal equation of mode r), one should evaluate the following integral (where $q_{u_n}(t)$ is written as q_{u_n} for simplicity). For $r = n$, the integral from Eq. B.41 should be solved to arrive at Eq. B.42.

$$\int_0^L \phi_{u_r}(x)\left(w_{tt} - c_0^2 w_{xx} - \frac{3}{2} c_1^2 w_x^2 w_{xx}\right) dx = 0 \tag{B.41}$$

$$\frac{L}{2}\ddot{q}_{u_n} + \frac{\pi^2 n^2 c_0^2}{2L} q_{u_n} + \frac{3\pi^4 n^4 c_1^2}{16 L^3} q_{u_n}^3 = 0 \tag{B.42}$$

Which generated the modal mass, stiffness and nonlinear stiffness (all normalized with the linear mass-density, ρA). This shows that the modal mass is independent of the mode number, where the linear and nonlinear stiffness are dependent of the mode number.

$$\ddot{q}_{u_n} + \frac{\pi^2 n^2 c_0^2}{L^2} q_{u_n} + \frac{3\pi^4 n^4 c_1^2}{8 L^4} q_n^3 = \ddot{q}_{u_n} + \omega_n^2 q_{u_n} + b_{nnn}^{(n)} q_{u_n}^3 = 0 \tag{B.43}$$

The equation may then be normalized with respect to the length of the string for the space variable q, and the fundamental mode frequency ω_0 for the time t.

$$\tilde{q}_{u_n} = \frac{q_{u_n}}{L},\ \tau = t\omega_0, \text{ where } \omega_0 = \frac{\pi}{L}\sqrt{\frac{\sigma_0}{\rho}} \tag{B.44}$$

If these variables are substituted into Eq. B.64, the following non-dimensional equation is found:

$$\omega_0^2 L \tilde{q}''_{u_n} + \frac{\pi^2 n^2 c_0^2}{L} \tilde{q}_{u_n} + \frac{3\pi^4 n^4 c_1^2}{8L} \tilde{q}_{u_n}^3 = 0 \tag{B.45}$$

Normalization with respect to the inertia term then gives:

$$\tilde{q}''_{u_n} + n^2 \tilde{q}_{u_n} + \frac{3}{8}\pi^2 n^4 \frac{c_1^2}{c_0^2} \tilde{q}_{u_n}^3 = \tilde{q}''_{u_n} + n^2 \tilde{q}_{u_n} + \frac{3}{8}\pi^2 n^4 \frac{E}{\sigma_0} \tilde{q}_{u_n}^3 = 0 \tag{B.46}$$

Where it is clear that the nonlinearity (for one mode, this is the Duffing parameter) is dependent on ratio of Young's modulus (E) over the pre-stress (σ_0), and the mode number. The Duffing strength of a mode may hence be improved by either decreasing the pre-stress or increasing the Young's modulus. Additionally, the relation with the mode number shows that the higher the mode number, the larger the relative nonlinearity (the linear stiffness scales with n^2, and the Duffing parameter with n^4). This results in the following terms for $n = 1$:

$$\tilde{q}''_{u_1} + \tilde{q}_{u_1} + \frac{3\pi^2}{8}\frac{E}{\sigma_0}\tilde{q}^3_{u_1} = 0. \tag{B.47}$$

Which generates the following modal variables:

$$\tilde{k}^{(1)}_1 = 1,\ \tilde{b}^{(1)}_{111} = \frac{3\pi^2}{8}\frac{E}{\sigma_0} = 1\tilde{b}^{(1)}_{111}. \tag{B.48}$$

Repeating the same procedure for the higher modes, where $n = 1,2,..,6$, generates the following modal parameters:

$$\begin{aligned}
\tilde{k}^{(2)}_2 = 2^2 = 4,\ \tilde{b}^{(2)}_{222} &= \frac{3\pi^2 2^4}{8}\frac{E}{\sigma_0} = 16\tilde{b}^{(1)}_{111} \\
\tilde{k}^{(3)}_3 = 3^2 = 9,\ \tilde{b}^{(3)}_{333} &= \frac{3\pi^2 3^4}{8}\frac{E}{\sigma_0} = 81\tilde{b}^{(1)}_{111} \\
\tilde{k}^{(4)}_4 = 4^2 = 16,\ \tilde{b}^{(4)}_{444} &= \frac{3\pi^2 4^4}{8}\frac{E}{\sigma_0} = 256\tilde{b}^{(1)}_{111} \\
\tilde{k}^{(5)}_5 = 5^2 = 25,\ \tilde{b}^{(5)}_{555} &= \frac{3\pi^2 5^4}{8}\frac{E}{\sigma_0} = 625\tilde{b}^{(1)}_{111} \\
\tilde{k}^{(6)}_6 = 4^2 = 36,\ \tilde{b}^{(6)}_{666} &= \frac{3\pi^2 6^4}{8}\frac{E}{\sigma_0} = 1296\tilde{b}^{(1)}_{111}
\end{aligned} \tag{B.49}$$

The modal coupling terms can be computed by letting $w(x,t)$ be a combination of all considered modes. For example, if modes 1 and 2 are considered, one can compute the magnitudes of terms such as $\tilde{b}^{(1)}_{122}$, which quantifies the coupling between mode 1 and 2 on mode 1. If the first three modes are considered ($N = 3$), $w(x,t)$ writes (using Eq. B.38):

$$w(x,t) = \sum_{n=1}^{3} \phi_{u_n}(x) q_{u_n}(t) = \sin\left(\frac{\pi x}{L}\right) q_{u_1} + \sin\left(\frac{2\pi x}{L}\right)\tilde{q}_{u_2} + \sin\left(\frac{3\pi x}{L}\right) q_{u_3} \tag{B.50}$$

This, together with the space and time normalization, will generate the following equation of motion for the first mode ($k = 1$):

$$\tilde{q}''_{u_1} + 1^2\tilde{q}_{u_1} + \frac{3}{8}\pi^2\frac{E}{\sigma_0}\left[1^4\tilde{q}^3_{u_1} + 8\tilde{q}_{u_1}\tilde{q}^2_{u_2} + 3\tilde{q}^2_{u_1}\tilde{q}_{u_3} + 12\tilde{q}^2_{u_2}\tilde{q}_{u_3} + 18\tilde{q}_{u_1}\tilde{q}^2_{u_3}\right] = 0 \tag{B.51}$$

The nonzero coupling terms appear to follow the following relations:

$$\tilde{b}^{(r)}_{rrn} = r^3 n\frac{3\pi^2}{8}\frac{E}{\sigma_0} \text{ and } \tilde{b}^{(r)}_{rnn} = 2r^2 n^2\frac{3\pi^2}{8}\frac{E}{\sigma_0} \tag{B.52}$$

Which shows that these nonzero coupling terms are dependent on the mode numbers of these coupled modes (r and n). The equation delivered the following modal coefficients (note that the coupling terms have been normalized with respect to $\tilde{b}^{(1)}_{111}$):

$$\begin{aligned}
\tilde{k}^{(1)}_1 = 1,\ \tilde{b}^{(1)}_{111} &= \frac{3\pi^4}{8}\frac{E}{\sigma_0} = 1\tilde{b}^{(1)}_{111} \\
\tilde{b}^{(1)}_{113} = 3\tilde{b}^{(1)}_{111},\ \tilde{b}^{(1)}_{122} = 8\tilde{b}^{(1)}_{111},\ \tilde{b}^{(1)}_{133} &= 18\tilde{b}^{(1)}_{133},\ \tilde{b}^{(1)}_{223} = 12\tilde{b}^{(1)}_{111}
\end{aligned} \tag{B.53}$$

Once the same procedure has been repeated for $r = 2$ and $r = 3$, the following nonlinear modal coefficients may be obtained:

Table B.1: Linear modal coefficients for a string model that includes only vertical displacements. These values are normalized with respect to $k_1^{(1)}$.

Eq.	(1)	(2)	(3)
$\tilde{k}_1$	1	0	0
$\tilde{k}_2$	0	4	0
$\tilde{k}_3$	0	0	9

Table B.2: Modal coupling coefficients for a string. Note that the coefficients are scaled with respect to $\tilde{b}_{111}^{(1)}$

Eq.	(1)	(2)	(3)
$\tilde{b}_{111}$	1	0	1
$\tilde{b}_{112}$	0	8	0
$\tilde{b}_{113}$	3	0	18
$\tilde{b}_{122}$	8	0	12
$\tilde{b}_{123}$	0	24	0
$\tilde{b}_{133}$	18	0	0
$\tilde{b}_{222}$	0	16	0
$\tilde{b}_{223}$	12	0	72
$\tilde{b}_{233}$	0	72	0
$\tilde{b}_{333}$	0	0	81

The results of the procedure for an inclusion of up to six modes is shown in Table E.2 in E.1.1.

Conclusion
The analytical model that accounts only for the linearized vertical displacements of a string generates the linear wave equation, which may give insight into the linear frequencies of a string. A more advanced model, which uses a nonlinear strain formulation for the vertical displacements, generates identical linear frequencies. Additionally, this model contains nonlinear terms which have a cubic dependency on the modal coordinates. A string with this cubic nonlinearity will thus contain Duffing terms. The relative strength of this Duffing parameter is dependent on the ratio of Young's modulus over the pre-stress ($\frac{E}{\sigma_0}$), and scales with the mode number (to the power four). The higher the mode number, the higher the relative nonlinearity of this mode. The linear stiffness scales with n^2 and the Duffing nonlinearity scales with n^4. The modal coupling coefficients are also dependent on the mode numbers of the modes that are involved; for the $\tilde{b}_{jkl}^{(r)}$-term, scales with $n_r n_j n_k n_l$, which shows the dependency on the mode numbers for the coupling coefficients.

B.1.2. Nonlinear equations of motion including vertical, transverse and longitudinal displacements

Equations B.14, B.15 and B.16 showed a string's equations of motion for all three directions. Before diving into the equations where one of these displacements may be neglected, one could approximate these equations under the assumption that the longitudinal inertia (u_{tt}) is most likely to be small under excitation of one of the first transverse or vertical modes. If this inertia is neglected, and it is again assumed that the ratio of pre-tension over Young's modulus will still be very small ($EA \gg T_0$ and thus $EA - T_0 \approx EA$), Eq. B.14 can be simplified to the following expression:

$$u_{xx} = -\frac{1}{2}\left(1 - \frac{T_0}{EA}\right)\frac{\partial}{\partial x}[v_x^2 + w_x^2] = -\frac{1}{2}\frac{\partial}{\partial x}[v_x^2 + w_x^2] = -v_x v_{xx} - w_x w_{xx}. \tag{B.54}$$

This expression should also obey the boundary conditions of a pinned-pinned string, where the displacement in both directions is zero at $x = 0$ and $x = L$, as follows:

$$u(0,t) = v(0,t) = w(0,t) = 0 \text{ and } u(L,t) = v(L,t) = w(L,t) = 0 \tag{B.55}$$

Integration then gives:

$$u_x = -\frac{1}{2}\left(v_x^2 + w_x^2\right) + \frac{1}{2L}\int_0^L \left(v_x^2 + w_x^2\right) dx \tag{B.56}$$

And the second integration gives:

$$u = -\frac{1}{2L}\int_0^x \left(v_x^2 + w_x^2\right) dx + \frac{x}{2L}\int_0^L \left(v_x^2 + w_x^2\right) dx. \tag{B.57}$$

This generates the following equations of motion:

$$mv_{tt} = T_0 v_{xx} + EA[u_x v_{xx} + u_{xx} v_x + \frac{3}{2} v_x^2 v_{xx} + w_x w_{xx} v_x + \frac{1}{2} w_x^2 v_{xx}] =$$

$$mv_{tt} = T_0 v_{xx} + EA\left[\left(-\frac{1}{2}\left(v_x^2 + w_x^2\right) + \frac{1}{2L}\int_0^L \left(v_x^2 + w_x^2\right) dx\right) v_{xx} + \left(-v_x v_{xx} - w_x w_{xx}\right) v_x + \frac{3}{2} v_x^2 v_{xx} + w_x w_{xx} v_x + \frac{1}{2} w_x^2 v_{xx}\right] =$$

$$mv_{tt} = T_0 v_{xx} + EA\left[\frac{1}{2L}\int_0^L \left(v_x^2 + w_x^2\right) dx\right] v_{xx} \tag{B.58}$$

$$mw_{tt} = T_0 w_{xx} + EA[u_x w_{xx} + u_{xx} w_x + \frac{1}{2} v_x^2 w_{xx} + v_x v_{xx} w_x + \frac{3}{2} w_x^2 w_{xx}] =$$

$$mw_{tt} = T_0 w_{xx} + EA\left[\left(-\frac{1}{2}\left(v_x^2 + w_x^2\right) + \frac{1}{2L}\int_0^L \left(v_x^2 + w_x^2\right) dx\right) w_{xx} + \left(-v_x v_{xx} - w_x w_{xx}\right) w_x + \frac{1}{2} v_x^2 w_{xx} + v_x v_{xx} w_x + \frac{3}{2} w_x^2 w_{xx}\right] =$$

$$mw_{tt} = T_0 w_{xx} + EA\left[\frac{1}{2L}\int_0^L \left(v_x^2 + w_x^2\right) dx\right] w_{xx} \tag{B.59}$$

Which decouples the dependency of the vertical and transverse equations from the longitudinal displacements.

Nonlinear string models for longitudinal and vertical vibrations: the uw-displacement model

This subsection will show what the equations of motion are for strings which include both vertical and longitudinal displacements. These vibrations are still assumed to remain planar ($v = v_x = v_{xx} = 0$), but they account for stretching in the longitudinal direction (u_x) as well. This assumption is valid only when the eigenfrequencies in the transverse direction are sufficiently far away, or for transverse frequencies which are very weakly excited through internal resonance. The governing equation for this uw-displacement model, which accounts for vertical and longitudinal vibrations will thus be equal to Eq. B.60.

$$mw_{tt} - T_0 w_{xx} - EA\left(\frac{1}{2L}\int_0^L w_x^2 dx\right) w_{xx} = 0 \tag{B.60}$$

After division with the linear mass density, we can again rewrite the constants in this equation as $c_0 = \sqrt{\frac{T_0}{m}}$ and $c_1 = \sqrt{\frac{EA}{m}}$, the transverse and longitudinal wave velocities in the string. Their difference, i.e. $c_1^2 - c_0^2$ may (again) be approximated by c_1^2, generating the following equation of motion:

$$w_{tt} - c_0^2 w_{xx} - c_1^2\left(\frac{1}{2L}\int_0^L w_x^2 dx\right) w_{xx} = 0. \tag{B.61}$$

This equation of motion is thus a function of both the longitudinal and transverse wave speeds, which in turn depend on the Young's modulus and the pre-stress of the material, respectively. Now, in order to compute the modal variables, it is important to change to modal coordinates, which allow for separation of space and time. The modal coordinates may be written as follows using Equations B.38, B.39 and B.40, to arrive at the single-mode equation of motion ($r = n$):

$$\int_0^L \phi_{u_r}(x)\left(mw_{tt} - T_0 w_{xx} - EA\left(\frac{1}{2L}\int_0^L w_x^2 dx\right) w_{xx}\right) dx = 0$$

$$\int_0^L \sin\left(\frac{r\pi x}{L}\right)\left[m\sin\left(\frac{n\pi x}{L}\right)\ddot{q}_{u_n} + T_0\frac{n^2\pi^2}{L^2}\sin\left(\frac{n\pi x}{L}\right) q_{u_n} + EA\left(\frac{1}{2L}\int_0^L (\frac{n^2\pi^2}{L^2}\cos^2\left(\frac{n\pi x}{L}\right) q_{u_n}^2) dx\right)\frac{n^2\pi^2}{L^2}\sin\left(\frac{n\pi x}{L}\right) q_{u_n}\right] dx = 0$$

$$\frac{mL}{2}\ddot{q}_{u_n} + \frac{\pi^2 n^2 T_0}{2L} q_{u_n} + \frac{\pi^4 n^4 EA}{8L^3} q_{u_n}^3 = 0 \tag{B.62}$$

Which provided us with the modal mass, stiffness and nonlinear stiffness. This again shows that the modal mass is constant for each mode, whereas the linear and nonlinear stiffness are dependent of the mode number.

$$\begin{aligned} \ddot{q}_{u_n} + \omega_n^2 q_{u_n} + b_{nnn} q_{u_n}^3 &= 0 \\ \ddot{q}_{u_n} + \frac{\pi^2 n^2 T_0}{L^2 m} q_{u_n} + \frac{\pi^4 n^4 EA}{4L^4 m} q_{u_n}^3 &= 0 \end{aligned} \tag{B.63}$$

After substitution of the linear mass density $m = \rho A$ and the tension force as a function of the pre-stress and the cross-sectional area ($T_0 = \sigma_0 A$), we will arrive at the following modal equation of motion for mode n:

$$\ddot{q}_{u_n} + \frac{\pi^2 n^2 \sigma_0}{L^2 \rho} q_{u_n} + \frac{\pi^4 n^4 E}{4L^4 \rho} q_{u_n}^3 = 0 \tag{B.64}$$

The following non-dimensional variables may then be used: $\tilde{q}_n = \frac{q_n}{L}$ and $\tau = t\omega_0$, where $\omega_0 = \frac{\pi}{L}\sqrt{\frac{\sigma_0}{\rho}}$: the fundamental mode frequency. The derivatives may then be computed as follows, using the non-dimensional time τ:

$$\frac{dq}{dt} = \frac{dq}{d\tau}\frac{d\tau}{dt} = \omega_0 \frac{dq}{d\tau}, \; \frac{d^2 q}{dt^2} = \frac{d}{d\tau}\left[\frac{dq}{d\tau}\frac{d\tau}{dt}\right] = \omega_0^2 \frac{d^2 q}{d\tau^2}. \tag{B.65}$$

Also using the space scaling, $q = \tilde{q}L$:

$$\frac{dq}{dt} = \frac{d(\tilde{q}L)}{d\tau}\frac{d\tau}{dt} = L\omega_0 \frac{d\tilde{q}}{d\tau} = L\omega_0 \tilde{q}', \; \frac{d^2 \tilde{q}L}{dt^2} = \frac{d}{d\tau}\left[L\frac{d\tilde{q}}{d\tau}\frac{d\tau}{dt}\right] = \omega_0^2 L \frac{d^2 \tilde{q}}{d\tau^2} = \omega_0^2 L \tilde{q}''. \tag{B.66}$$

Substitution of these relations into Eq. B.64, generates the non-dimensional equation in Eq. B.67.

$$\omega_0^2 L \tilde{q}''_{u_n} + \frac{\pi^2 n^2 \sigma_0}{L\rho} \tilde{q}_{u_n} + \frac{\pi^4 n^4 E}{4L\rho} \tilde{q}_{u_n}^3 = 0 \tag{B.67}$$

Normalization with respect to the inertia term then gives:

$$\tilde{q}''_{u_n} + n^2 \tilde{q}_{u_n} + \frac{1}{4}\pi^2 n^4 \frac{E}{\sigma_0} \tilde{q}_{u_n}^3 = 0. \tag{B.68}$$

Here, it is clear that the nonlinearity (for one mode, this is the Duffing parameter) is also dependent on ratio of Young's modulus (E) over the pre-stress (σ_0). The Duffing strength may hence be improved by either decreasing the pre-stress or increasing the Young's modulus. This Duffing parameter is 1.5 times smaller than that of the previous model, the w-displacement model.

This results in the following terms for $n = 1$:

$$\tilde{q}''_{u_1} + \tilde{q}_{u_1} + \frac{\pi^2}{4}\frac{E}{\sigma_0} \tilde{q}_{u_1}^3 = 0 \tag{B.69}$$

Which generates the following modal variables:

$$\tilde{k}_1^{(1)} = 1, \; \tilde{b}_{111}^{(1)} = \frac{\pi^2}{4}\frac{E}{\sigma_0} = 1\tilde{b}_{111}^{(1)} \tag{B.70}$$

For $n = 1, 2, .., 6$, this results in:

$$\begin{aligned} \tilde{k}_2^{(2)} = 2^2 = 4, \; \tilde{b}_{222}^{(2)} &= \frac{\pi^2 2^4}{4}\frac{E}{\sigma_0} = 16\tilde{b}_{111}^{(1)} \\ \tilde{k}_3^{(3)} = 3^2 = 9, \; \tilde{b}_{333}^{(3)} &= \frac{\pi^2 3^4}{4}\frac{E}{\sigma_0} = 81\tilde{b}_{111}^{(1)} \\ \tilde{k}_4^{(4)} = 4^2 = 16, \; \tilde{b}_{444}^{(4)} &= \frac{\pi^2 4^4}{4}\frac{E}{\sigma_0} = 256\tilde{b}_{111}^{(1)} \\ \tilde{k}_5^{(5)} = 5^2 = 25, \; \tilde{b}_{555}^{(5)} &= \frac{\pi^2 5^4}{4}\frac{E}{\sigma_0} = 625\tilde{b}_{111}^{(1)} \\ \tilde{k}_6^{(6)} = 6^2 = 36, \; \tilde{b}_{666}^{(6)} &= \frac{\pi^2 6^4}{4}\frac{E}{\sigma_0} = 1296\tilde{b}_{111}^{(1)} \end{aligned} \tag{B.71}$$

Eq. B.50 can also be used to write $w(x,t)$ as a combination of all considered modes; this will then generate the coupling terms. If this transformation is conducted, and a subsequent non-dimensionalization is conducted, we will get the following modal coefficients, for $r = 1$ (note that the coupling terms have been normalized with respect to $\tilde{b}^{(1)}_{111}$):

$$\begin{gathered}\tilde{k}^{(1)}_1 = 1,\ \tilde{b}^{(1)}_{111} = \frac{\pi^4}{4}\frac{E}{\sigma_0} = 1\tilde{b}^{(1)}_{111} \\ \tilde{b}^{(1)}_{122} = 4\tilde{b}^{(1)}_{111},\ \tilde{b}^{(1)}_{133} = 9\tilde{b}^{(1)}_{111}\end{gathered} \tag{B.72}$$

If the same procedure is repeated for $r = 2$ and $r = 3$, the following parameters will be found:

$$\begin{gathered}\tilde{k}^{(2)}_2 = \frac{4\pi^2}{L^2}\frac{\sigma_0}{\rho},\ \tilde{b}^{(2)}_{222} = \frac{64\pi^4}{4L^4}\frac{E}{\rho} = 16\tilde{b}^{(1)}_{111} \\ \tilde{b}^{(2)}_{112} = 4\tilde{b}^{(1)}_{111},\ \tilde{b}^{(2)}_{233} = 36\tilde{b}^{(1)}_{111}\end{gathered} \tag{B.73}$$

$$\begin{gathered}\tilde{k}^{(3)}_3 = \frac{9\pi^2}{L^2}\frac{\sigma_0}{\rho},\ \tilde{b}^{(3)}_{333} = \frac{324\pi^4}{4L^4}\frac{E}{\rho} = 81\tilde{b}^{(1)}_{111} \\ \tilde{b}^{(3)}_{113} = 9\tilde{b}^{(1)}_{111},\ \tilde{b}^{(3)}_{223} = 36\tilde{b}^{(1)}_{111}\end{gathered} \tag{B.74}$$

Table B.3: Linear modal coefficients for a string model that includes vertical and longitudinal displacements. These values are normalized with respect to $k^{(1)}_1$.

Eq.	**(1)**	**(2)**	**(3)**
$\tilde{k}_1$	1	0	0
$\tilde{k}_2$	0	4	0
$\tilde{k}_3$	0	0	9

Table B.4: Modal coupling coefficients for a string model that includes vertical and longitudinal displacements Note that the coefficients are scaled with respect to $\tilde{b}^{(1)}_{111}$

Eq.	**(1)**	**(2)**	**(3)**
$\tilde{b}_{111}$	1	0	0
$\tilde{b}_{112}$	0	4	0
$\tilde{b}_{113}$	0	0	9
$\tilde{b}_{122}$	4	0	0
$\tilde{b}_{123}$	0	0	0
$\tilde{b}_{133}$	9	0	0
$\tilde{b}_{222}$	0	16	0
$\tilde{b}_{223}$	0	0	36
$\tilde{b}_{233}$	0	36	0
$\tilde{b}_{333}$	0	0	81

The results of the procedure for an inclusion of up to six modes are shown in Table E.4 in E.1.2.

Nonlinear string models for non-planar vibrations, the uvw-displacement model

In the previous analyses, the influence of the modes in the transverse direction was neglected, since the assumption was made that the vibrations of the string remained planar as the transverse mode frequencies were assumed to be of negligible influence. For strings with a square or circular cross-section, this may not be a safe assumption, since the modes will likely be resonant since the modal frequencies of both modes are degenerate. To determine the modal coupling coefficients of a string while accounting for vertical, longitudinal *and* transverse vibrations, one cannot further simplify Equations B.58 and B.59. The vertical (modal) displacements are still assumed to be well approximated by Equations B.38, B.39 and B.40. However, the transverse (modal) displacements should now also be formulated. This may be done by assuming that the mode shapes are still of the same function ($\phi_{u_n}(x)$), since the transverse and vertical modes are identical in

terms of mode shape, but they are perpendicular to each other. The modal displacement in the transverse direction is written as p_{u_n}.

$$v(x,t) = \sum_{n=1}^{N} \phi_{u_n}(x)\, p_{u_n}(t) \tag{B.75}$$

Substitution of equations B.38, B.75, B.39 and B.40 into equations B.59 and B.58 and applying the Galerkin method once again, one will arrive at the modal variables from Tables B.5 and B.6.

Table B.5: Linear modal coupling coefficients for a string model that includes vertical, longitudinal and transverse displacements. These values are normalized with respect to $k_1^{(1)}$. Note that the uneven (even) modes are the vertical (transverse) modes.

Eq.	**(1)**	**(2)**	**(3)**	**(4)**
$\tilde{k}_1$	1	0	0	0
$\tilde{k}_2$	0	1	0	0
$\tilde{k}_3$	0	0	4	0
$\tilde{k}_4$	0	0	0	4

Table B.6: Modal coupling coefficients for a string model that includes vertical, longitudinal and transverse displacements. The coefficients are scaled with respect to $\tilde{b}_{111}^{(1)}$. Note that the uneven (even) modes are the vertical (transverse) modes.

Eq.	**(1)**	**(2)**	**(3)**	**(4)**
$\tilde{b}_{111}$	1	0	0	0
$\tilde{b}_{112}$	0	1	0	0
$\tilde{b}_{113}$	0	0	9	0
$\tilde{b}_{114}$	0	0	0	9
$\tilde{b}_{122}$	1	0	0	0
$\tilde{b}_{123}$	0	0	0	0
$\tilde{b}_{124}$	0	0	0	0
$\tilde{b}_{133}$	9	0	0	0
$\tilde{b}_{134}$	0	0	0	0
$\tilde{b}_{144}$	9	0	0	0
$\tilde{b}_{222}$	0	1	0	0
$\tilde{b}_{223}$	0	0	9	0
$\tilde{b}_{224}$	0	0	0	9
$\tilde{b}_{233}$	0	9	0	0
$\tilde{b}_{233}$	0	0	0	0
$\tilde{b}_{244}$	0	9	0	0
$\tilde{b}_{333}$	0	0	81	0
$\tilde{b}_{334}$	0	0	0	81
$\tilde{b}_{344}$	0	0	81	0
$\tilde{b}_{444}$	0	0	0	81

B.2. Comparison of three models

Three models may be used to simulate the planar dynamics of strings. These models are as follows:

1. The analytical model (w-displacement model), which only considers vertical displacements from Section B.1.1;

2. The analytical model (uw-displacement model), which that considers both longitudinal and vertical displacements from Section B.1.2;

3. The numerical model that is based on the STEP method from Section D.1.1.

To determine what the differences are between each method, a high stress Silicon-Nitride string with the material properties and dimensions from Table B.7 is considered.

Table B.7: Si_3N_4 string variables

Variable	Symbol	Magnitude
Density	ρ	3100 $\frac{\text{kg}}{\text{m}^3}$
Young's modulus	E	250 GPa
Poisson's ratio	ν	0.23
Pre-stress	σ_0	849.2 MPa
Length	L	1110 μm
Width	w	4 μm
Thickness	t	92 nm

The modal coefficients of a Silicon-Nitride string

For the considered string variables, these three models generate the modal parameters from Tables B.8 and B.9.

Table B.8: Si_3N_4 string frequencies

Variable	w-displacement	uw-displacement	STEP
f_1 [kHz]	235.76	235.76	235.77
f_2 [kHz]	471.52	471.52	471.60
f_3 [kHz]	707.28	707.28	707.54

Table B.9: Modal nonlinear coupling strength (normalized by $\frac{\pi^2}{4}\frac{E}{\sigma_0}$) for a Si_3N_4 string, computed by a model that only considers vertical displacement (w-displacement model), an analytical model that considers both vertical and longitudinal displacements (uw-displacement) and a numerical model that considers both transverse and longitudinal displacements (STEP).

	w-**displacement**			uw-**displacement**			**STEP**		
Eq.	**(1)**	**(2)**	**(3)**	**(1)**	**(2)**	**(3)**	**(1)**	**(2)**	**(3)**
$\tilde{a}_{11}$	0	0	0	0	0	0	0	0	0
$\tilde{a}_{12}$	0	0	0	0	0	0	0	0	0
$\tilde{a}_{13}$	0	0	0	0	0	0	0	0	0
$\tilde{a}_{22}$	0	0	0	0	0	0	0	0	0
$\tilde{a}_{23}$	0	0	0	0	0	0	0	0	0
$\tilde{a}_{33}$	0	0	0	0	0	0	0	0	0
Eq.	**(1)**	**(2)**	**(3)**	**(1)**	**(2)**	**(3)**	**(1)**	**(2)**	**(3)**
$\tilde{b}_{111}$	1.5	0	1.5	1	0	0	1.00	-0.00	0.00
$\tilde{b}_{112}$	0	4.5	0	0	4	0	-0.00	4.04	0.00
$\tilde{b}_{113}$	4.5	0	27	0	0	9	0.02	0.00	9.09
$\tilde{b}_{122}$	12	0	18	4	0	0	4.04	0.00	0.13
$\tilde{b}_{123}$	0	36	0	0	0	0	0.00	0.26	0.00
$\tilde{b}_{133}$	27	0	0	9	0	0	9.09	0.00	0.00
$\tilde{b}_{222}$	0	24	0	0	16	0	0.00	16.00	0.00
$\tilde{b}_{223}$	18	0	108	0	0	36	0.13	0.00	36.37
$\tilde{b}_{233}$	0	108	0	0	36	0	0.00	36.37	0.00
$\tilde{b}_{333}$	0	0	121.5	0	0	81	0.00	0.00	80.99

The linear frequencies of all three models are approximately equal, as was shown in Table B.8. It is hence expected that the w-displacement model shows a stronger nonlinear response than the other models.

B.3. Experimental results of a 1110μm string resonator

A. Keşkekler and M. Xu conducted experiments on a Si_3N_4 string resonator with the following characteristics:

Table B.10: Characteristics of the experimentally tested string resonator of length 1110μm. * This is the stress in the axial direction.

Quantity	Variable	Magnitude
length	L	1110 um
width	w	4 um
thickness	t	92 nm
Young's modulus	E	250 GPa
pre-stress	σ_0	850 MPa*
density	ρ	3100 kg/m^3

This string was initially manufactured out of a Silicon Nitride film which was at an initial pre-stress of 1100 MPa, in both the x- and y-directions of the film. After etching the string, the stress redistributed to an unidirectional stress of approximately 850 MPa.

The forced and free response of this string was monitored using the (simplified) set-up that is displayed in Fig. B.2.

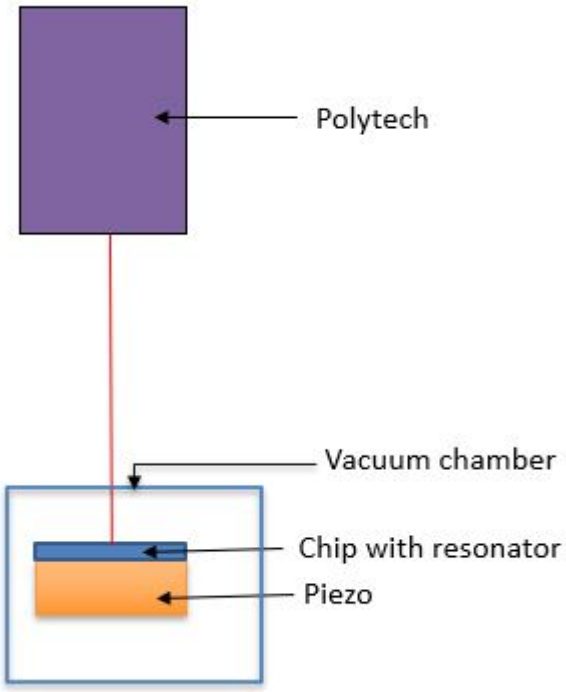

Figure B.2: Simplified experimental set-up, showing the Polytech, the vacuum chamber, the piezo-element and the chip which contains the string specimen.

The set-up consists of a measurement device (the Polytech), which monitors the vibrations of the string. The figure also depicts a vacuum chamber, which houses a piezo-element. The chip that contains the string resonator is connected to the piezo-element (using tape) for excitation. The pressure in the vacuum chamber -for this specimen- was brought to 2.69×10^{-6}mbar.

B.3.1. Verification of the mode shapes

Frequency response experiments were conducted to characterize the response at the first mode's resonance frequency. Once the system is brought into the nonlinear regime, Duffing characteristics may start to influence the displacement and stiffness of the string, which will also influence its mode shapes. For a system

that shows hardening (and thus an increase in the stiffness), the mode shapes of the system could change with respect to the previously assumed linear mode shapes. Though the maximum amplitude will probably increase in the nonlinear regime, it can be expected that the mode shape becomes slightly flattened (due to increased tension in the nonlinear regime) when comparing it to the linear mode shapes.
The response of the first mode was measured for three locations along the string. These three points were at 0.175L, 0.364L and 0.506L respectively. One of the measurements (at 0.506L) was conducted near the center of the string, which may be considered as the centre position of the string. Two other measurements are -due to the symmetry of the first mode- mirrored about this centre point. This generates a total of five points, for which the experimental mode shapes may be compared to the linear mode shapes. Fig. B.3 depicts the amplitude for several force levels at these five measurement points.

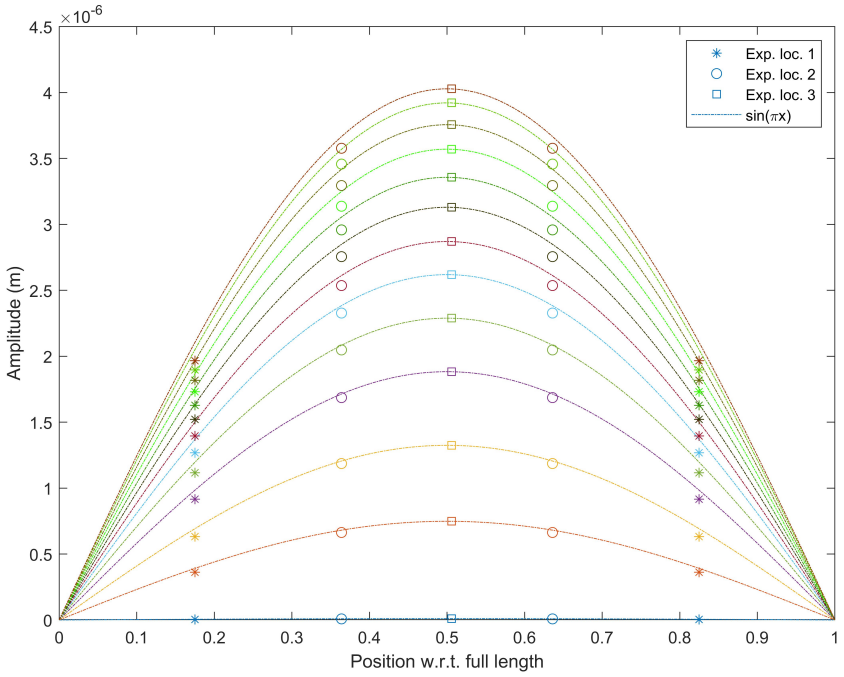

Figure B.3: Experimental amplitude at positions 1, 2, 3, 4 and 5 at x= 0.175 (stars), 0.364 (circles), 0.506 (squares), 0.636 (stars) and 0.825 (squares), respectively. A sine shape is plotted using the maximum amplitude (at 0.506L).

The plot clearly shows that though the string is driven to large amplitudes, the first mode's linear mode shape fits quite well, indicating that it is safe to assume that the amplitude in this nonlinear regime follows this linear mode shape. This mode shape can thus be used in the simulations, to determine modal amplitudes and modal forces.

B.3.2. Experimental Duffing response

The frequency response of the string is analyzed for 20 force levels; expressed in the applied voltage to the piezo-element. These voltage levels are linearly spaced between 0.001 and 0.5 Volts. The piezo-force is assumed to scale linearly with the applied voltage [32]. Fig. B.4 depicts the frequency response for three locations, for each of the 20 force levels.

The first mode's resonance frequency is located at approximately 182.7kHz, which implies that the pre-stress of the string has decreased significantly. For a pre-stress of 850MPa, one would expect (from Eq. B.27) a resonance frequency at approximately 268 kHz. The pre-stress has thus decreased significantly, from 850 to 509MPa. The underlying mechanism of this reduction of pre-stress is suspected to be a creep-like phenomenon, which causes the strength of a strained material to deteriorate over time. The response clearly displays the Duffing behavior, where the frequency increases as the amplitude increases under larger driving voltages. However, for drive levels higher than approximately 0.32V, this increase in amplitude and frequency ceased: the frequency appears to be "locked" at 185.5 kHz. This phenomenon is known as frequency locking;

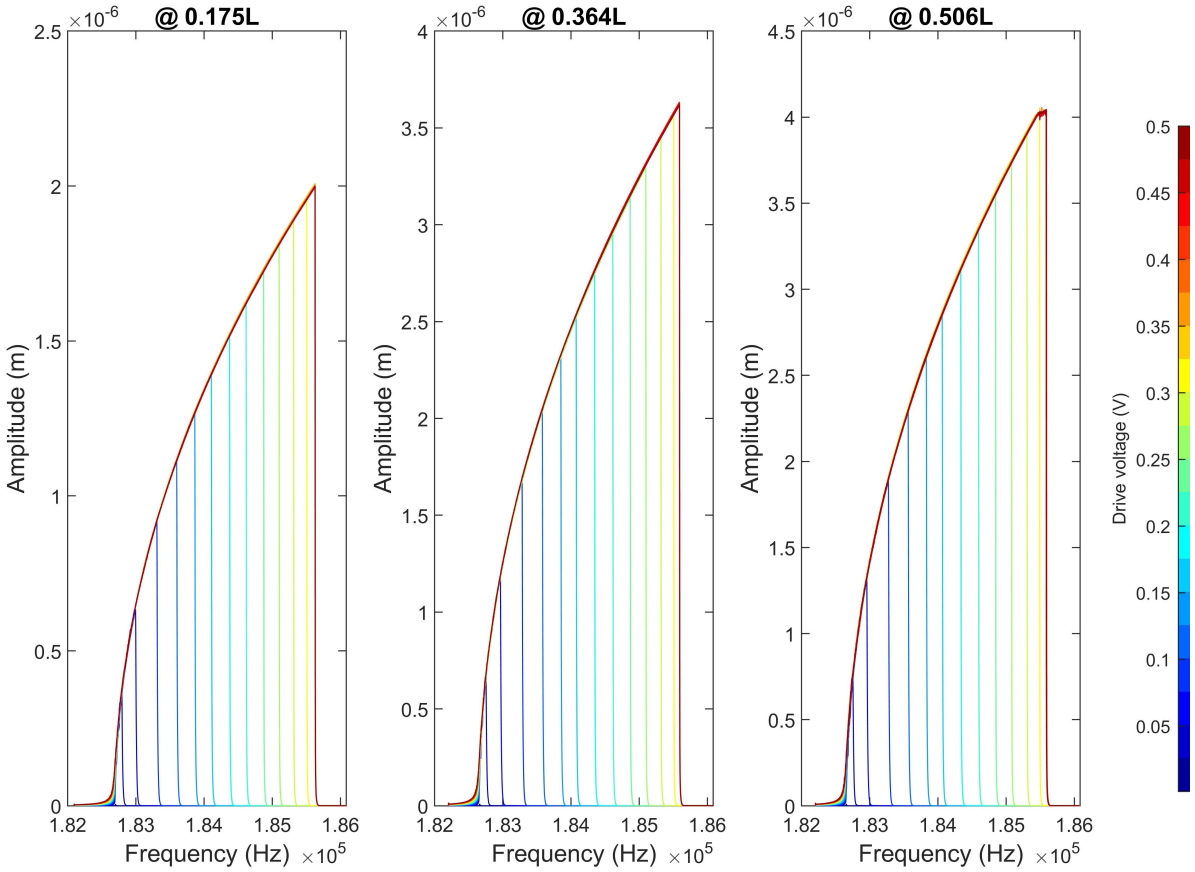

Figure B.4: Experimental frequency of an 1110μm Si_3N_4 string resonator, measured at three locations. The driving voltage ranged from 1mV to 0.5V.

where the frequency is seen to "lock" at a certain frequency while the drive power is increased. By plotting the compliance of this response, one can determine if there is any type of nonlinear dissipation process in this system. Fig. B.5 shows the compliance, which is the ratio of the amplitude and the driving voltage of the response (from Fig. B.4).

The compliance clearly decreases, indicating that there is some form of (nonlinear) dissipation present in the system. This dissipation could have several origins, among which the two most likely options are nonlinear damping or mode coupling [17]. The first option is an irreversible process, where energy is dissipated to an external bath. The latter option, mode coupling, allows for energy transfer from one mode to another, which is a reversible process (as is shown in the FPUT experiment). To verify which of these processes is the present here, one should check the ringdown data and the frequency response for the harmonics of the higher modes. This ringdown data serves three purposes: it will show whether or not nonlinear damping is present in the system. Otherwise, it will allow for fitting of the Q-factor, which may then be used in simulations to simulate this frequency response. Lastly, the exchange of energy to the other modes may be verified, to see to what degree this system shows FPUT behavior.

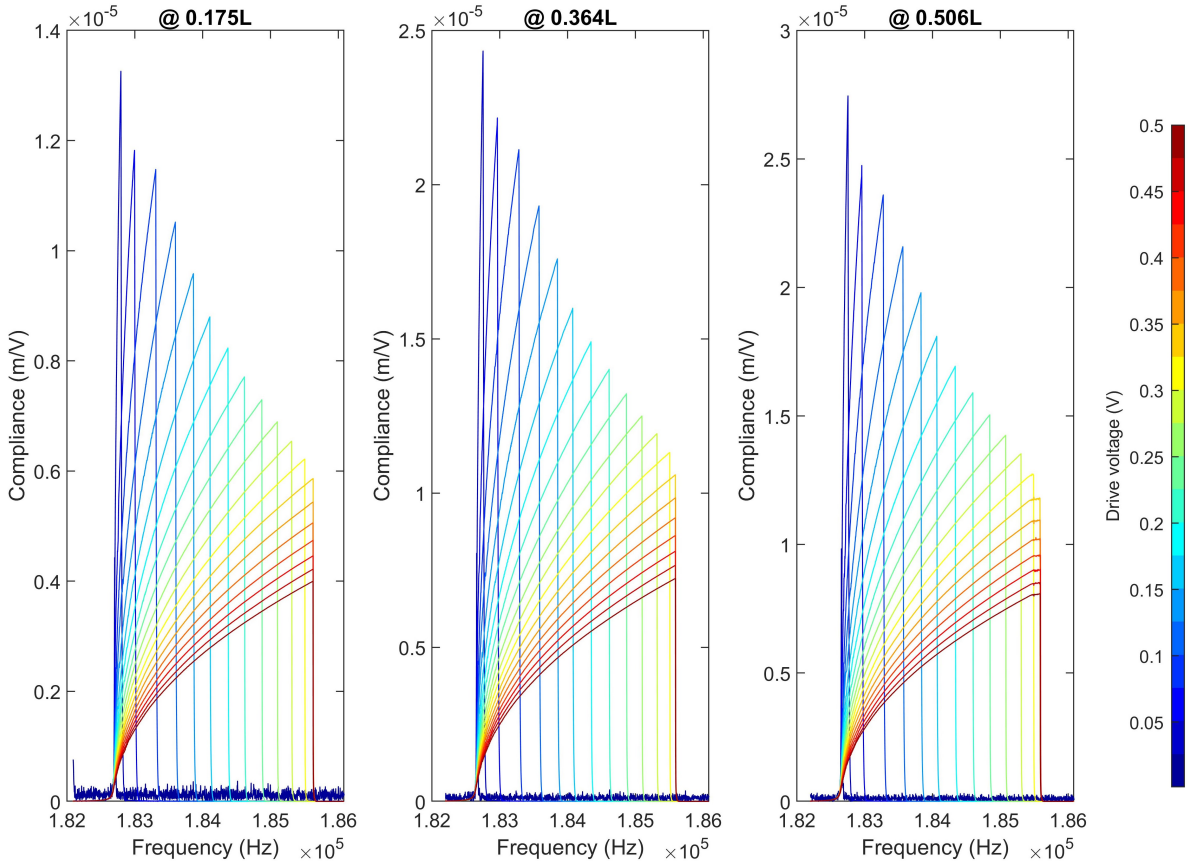

Figure B.5: Compliance of an experimental frequency response for an 1110μm Si_3N_4 string resonator, measured at three locations. The driving voltage ranged from 1mV to 0.5V.

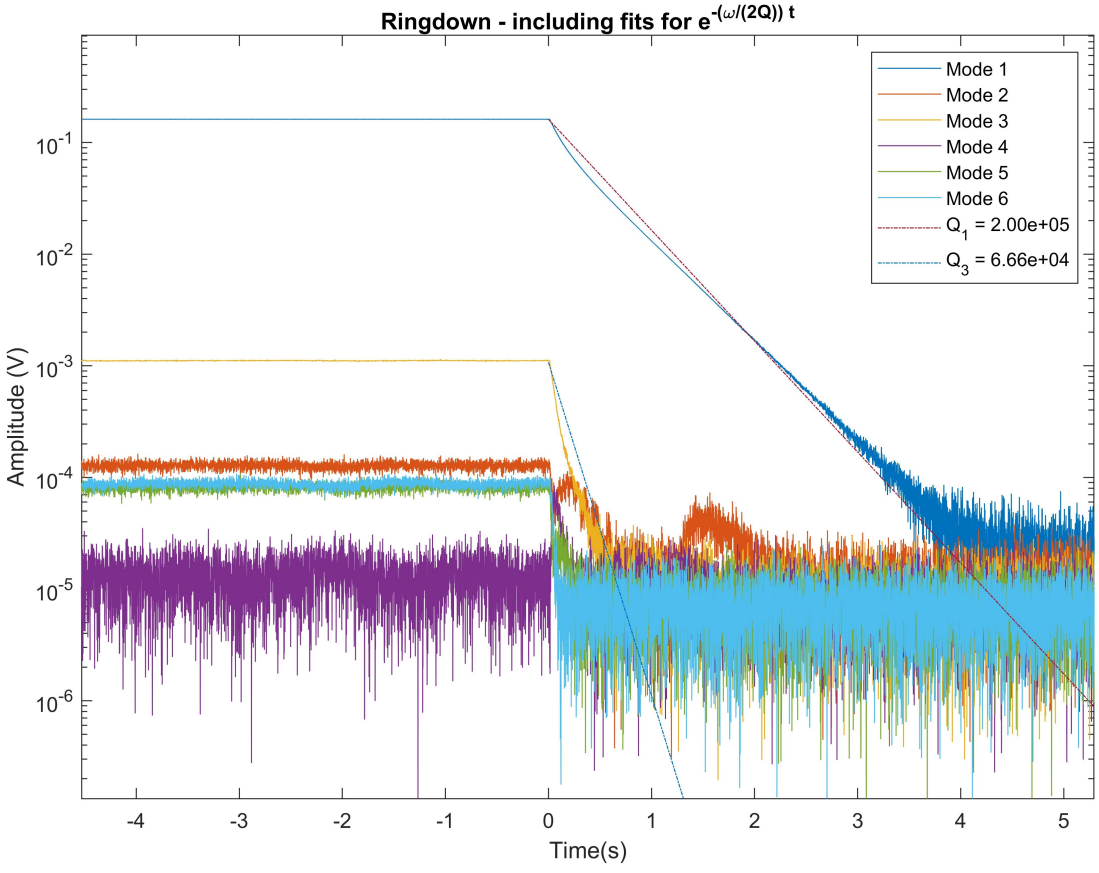

Figure B.6: Ringdown of a string, showing the response for the first six modes and fits for the quality factors for the first and third modes. This ringdown was conducted from a weakly nonlinear initial condition.

This ringdown plot (from a weakly nonlinear initial condition) shows that (1) there is little energy transfer (the second mode, in red, does appear to increase somewhat during the ringdown) and (2) that -on a logarithmic scale- the decay of the amplitude appears to remain linear. Finally, (3), no energy recurrence is visible, as most modal amplitudes appear to decrease over the entire interval. To see significant energy transfer, one would expect the amplitude of other modes to increase significantly with respect to that of the initially excited (in this case the first) mode, which is not present in this figure. The second mode's amplitude appears to increase slightly, but this is negligible as it still significantly lower than the first mode's amplitude. Possibly, the initial condition is not far enough into the nonlinear regime to generate significant nonlinear effects. The first mode's decay appears to be fitted for a Q-factor of approximately 2×10^5, at a pressure of 2.69×10^{-6}mbar. The Q-factor for the third mode appears to scale with that of the first mode and the inverse of the mode number: $Q_n = \frac{Q_1}{n}$. The other Q-factors are assumed to scale accordingly in subsequent simulations.

B.3.3. Simulated frequency response of a string

The STEP method (Section D.1.1) is used to find the modal quantities of the string. This method determines the modal coefficients for longitudinal and vertical displacement directions (identical to the uw-displacement model). The nonlinear modal parameters of the w-displacement model may be substituted in the results from STEP by multiplying the Duffing coefficient of the first mode by 1.5 and subsequently substituting the nonlinear variables by those of Table E.2. The frequency response is simulated (using AUTO, App. D.1.2) for the linear variables from Table B.11.

Table B.11: Simulated modal variables (for the first six vertical modes) of the experimentally tested string specimen.

Eq.	**(1)**	**(2)**	**(3)**	**(4)**	**(5)**	**(6)**
$\frac{m_n}{m_{tot}}$	0.4999	0.4997	0.4993	0.5007	0.4979	0.4970
$\frac{\omega_n}{\omega_1}$	1.0000	1.9998	2.9990	4.0054	4.9951	5.9914
$\frac{Q_i}{Q_1}$	1.0000	0.5001	0.3334	0.2497	0.2002	0.1669

The modal mass is -by approximation- constant to half the total string mass. The normalized frequencies (with respect to the fundamental mode) nearly follow the linear relationship with the mode number n. It was shown in the previous paragraph that the Q-factor of the fundamental mode was found to equal approximately 2×10^5 and that the higher modes may be assumed to scale with the inverse of the mode number. The cubic nonlinear variables follow the relation that is shown in Table E.2 and Table E.8 for the w- and uw-displacement models, respectively. All quadratic nonlinear variables ($a_{jk}^{(r)}$) are zero for this system. All modal variables may be substituted in the following equation of motions, where $F^{(r)}$ is nonzero only for $r = 1$:

$$m^{(r)}\ddot{q}_r + k^{(r)}q_r + c^{(r)}\dot{q}_r + \sum_{k=1}^{6}\sum_{l=1}^{6} a_{jk}^{(r)} q_j q_k + \sum_{j=1}^{6}\sum_{k=j}^{6}\sum_{l=k}^{6} b_{jkl}^{(r)} q_j q_k q_l = F^{(r)}\sin(\omega_f t),\ r = 1,2,...,6 \tag{B.76}$$

The fitting procedure is shown in Section D.3. The results for simulations for a force level of 0.32V are depicted in Figures B.7 and B.8. These fits were achieved for the w- and uw-displacement models for Young's moduli of 450GPa and 675GPa, which both exceed the default Young's modulus of Si_3N_4 of 250GPa significantly.

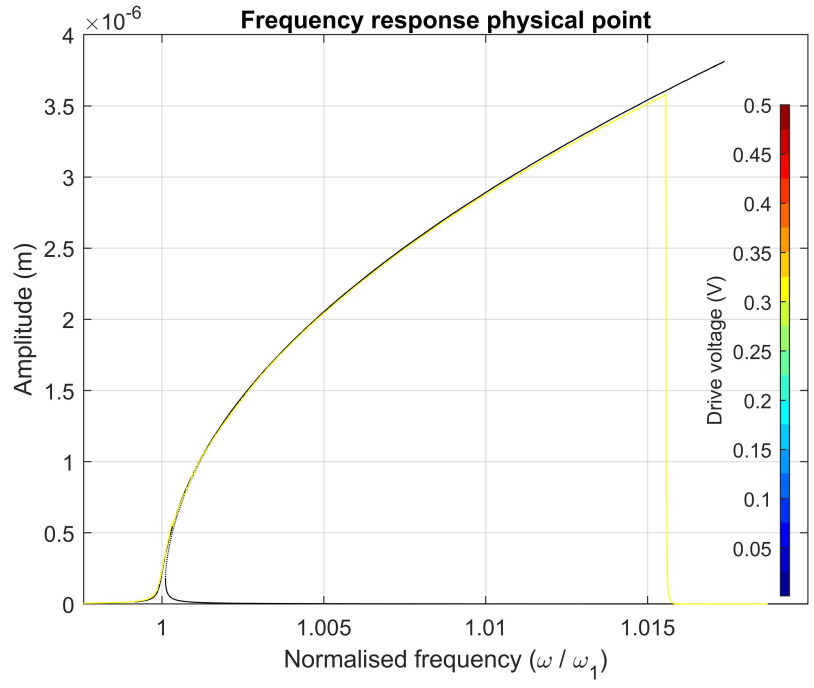

(a)

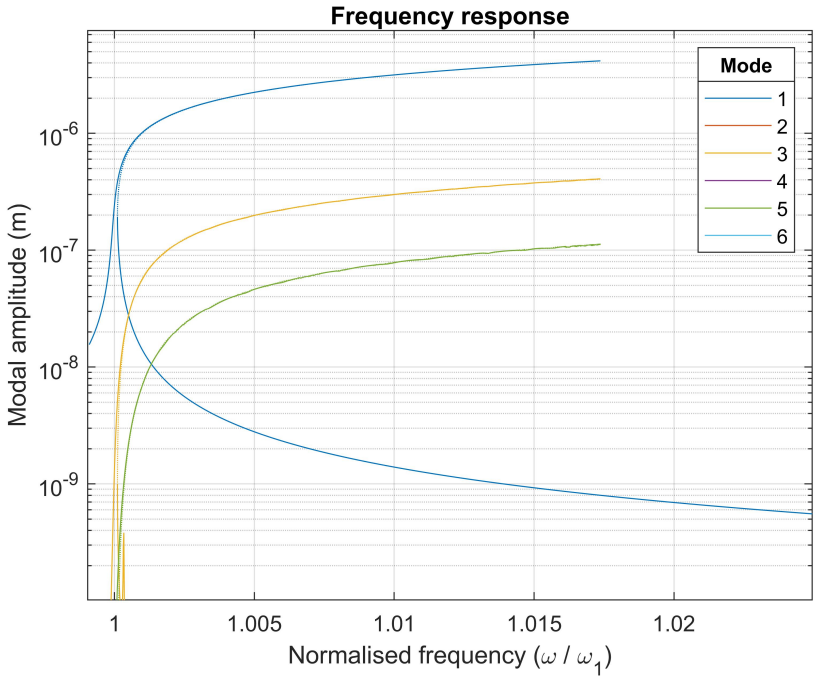

(b)

Figure B.7: Simulated (black) vs. experimentally obtained frequency response (yellow), for a drive voltage of 0.32V. The simulation was conducted for the **w**-displacement model, accounting for the first six vertical eigenmodes. B.7a depicts the response at 0.364L. B.7b depicts the modal contributions.

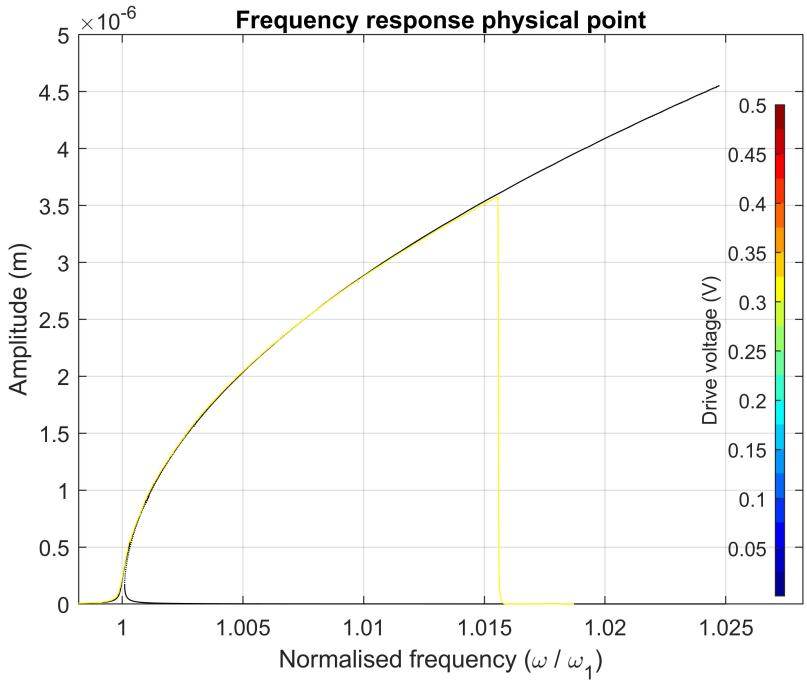

(a)

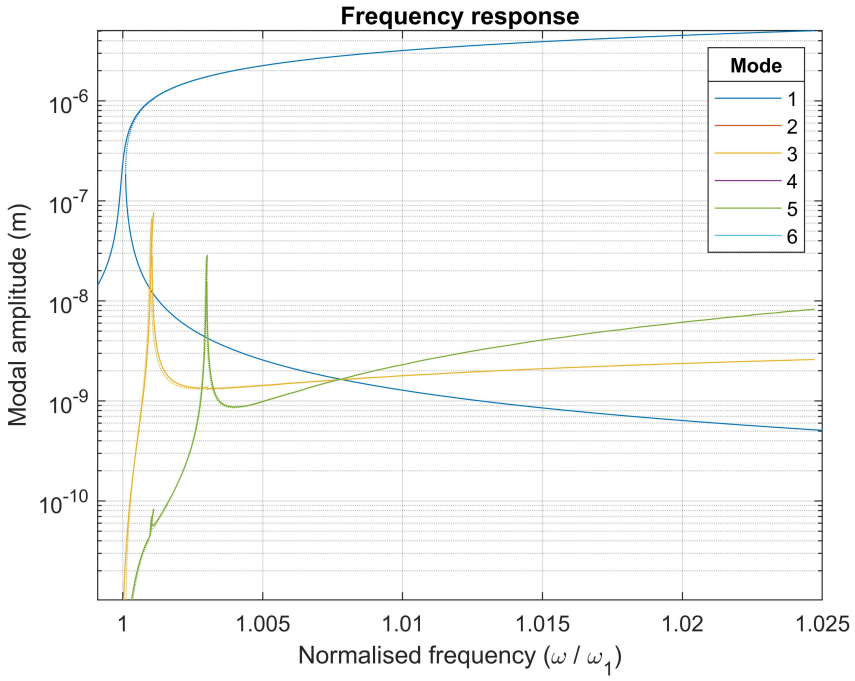

(b)

Figure B.8: Simulated (black) vs. experimentally obtained frequency response (yellow), for a drive voltage of 0.32V. The simulation was conducted for the **uw**-displacement model, accounting for the first six vertical eigenmodes. B.8a depicts the response at 0.364L. B.8b depicts the modal contributions.

Although the Young's moduli are significantly higher than the default value, these simulations do produce decent fits. The experimental results show that the Duffing behavior of the first mode is the most significant nonlinearity. Both the w- and the uw-displacement models generate a Duffing nonlinearity, which may thus be fitted easily, as long as the modal interactions are ignored. The Duffing nonlinearities of the analytical models show a 1.5 factor difference, which is clearly conveyed in the fitted Young's moduli as well: $E = 450$GPa

and $1.5E = 675$GPa for the w- and uw-displacement models, respectively. Clearly, the simulated responses does not show the locking behavior of the experimental result; both overshoot the locking frequency from the experimental results at approximately a normalized frequency of 1.016. To find accurate fits, one should apply some nonlinear dissipation mechanism to the simulation. Generally, two methods could be used for this: the first method is to add nonlinear damping, but as was shown in Fig. B.6, the decay does not show two slopes: it is linear [14]. The second method is probably more valid, as it assumes that energy is likely to be extracted from this first mode through a modal coupling, supplying other modes with energy.
By allowing modes to become resonant at a certain frequency, the energy of the fundamental mode may be supplied to the higher harmonics of the fundamental mode. This will then cause the first mode's energy (and hence amplitude) to remain (approximately) constant, while the modes that coincide with these harmonics are supplied with energy.
To replicate the experimental behavior, and especially the locking behavior, the linear frequencies in the numerical models could be shifted, such that the resonant terms are strongest at this locking frequency. By looking at the resonant terms of the equation of motion of the first mode, one may determine which (nonlinear) parameters influence this coupling (Eq. B.77) for the uw-displacement model.

$$F_{lq}^{(1)} = \frac{1}{4} b_{111}^{(1)} [3\cos(\omega_1 t) + \cos(3\omega_1 t)] + \frac{1}{4} b_{122}^{(1)} [2\cos(\omega_1 t) + \cos(3\omega_1 t) + \cos(5\omega_1 t)] + \frac{1}{4} b_{133}^{(1)} [2\cos(\omega_1 t) + \cos(5\omega_1 t) + \cos(7\omega_1 t)] \tag{B.77}$$

This equation originates from Section B.5, which results from negligence of all coupling terms that equal zero. It is shown there that excitation at the first mode's frequency may result in excitation of harmonics of the first mode as well. Here, these nonzero coupling terms result in excitation of the (uneven) modes at integer harmonics of the first mode: $3\omega_1$, $5\omega_1$ and $7\omega_1$, as is depicted in the simulated frequency response in Fig. B.8b. This shows that there is some interaction between the first, third and fifth modes, which is dependent on the amplitude of the first mode: increasing the amplitude of the first mode results in a stronger coupling. Fig. B.8b clearly depicts that the amplitude at $\omega/\omega_1 = 1.015$ is much larger than the amplitude at $\omega/\omega_1 = 1.000$. The normalized locking frequency is at approximately 1.016, as is depicted in Figures B.7 and B.8. The simulated integer frequency ratios of the string (from Table B.11) hence should be shifted such that the resonant terms are stronger at this frequency of 1.016.
Iterations have shown that the uw-displacement model is highly sensitive to these (small) frequency shifts, where the w-displacement models do not show this sensitivity: it does not show significant effects for values of ω_s between -0.05 and 0.05. Fig. B.9 depicts a simulated response (for the uw-displacement model) where the resonance frequencies of all modes (except the fundamental modes) have been shifted by a small value ω_s, according Eq. B.78.

$$\omega_n^* = (1 + \omega_s)\omega_n, \text{ where } n = 2, 3, ..., N \tag{B.78}$$

In Figures B.8a and B.9, this shift (ω_s) is equal to 0.000 and 0.005 respectively. The latter value implies that the frequencies have been shifted by 0.5% of the fundamental mode's frequency. The experimentally obtained frequency response is simulated using the uw-displacement model with these shifted linear frequencies, to result in response from Fig. B.10; this replicates the experimental results quite well, as the Duffing curves and the frequency locking are simulated quite accurately. Aside from the large Young's moduli, it is thus possible to find good fits for the uw-displacement model by shifting the linear frequencies of the higher modes. The w-displacement model appears to remain fairly insensitive to these slight frequency shifts.

These frequency responses show that the solution becomes unstable from approximately $\omega/\omega_1 = 1.016$. Typically, the onset of instability is caused by a bifurcation of some type (e.g. Period Doubling or Torus bifurcations). These bifurcations are associated with a change in the solution: it may for example become quasiperiodic through either a Period Doubling or Torus bifurcation [24]. The periodicity of the solution may be checked easily by selecting a data point along the frequency response curve, and subsequently checking the steady state motion by solving the forced equations of motion for these points as initial conditions.

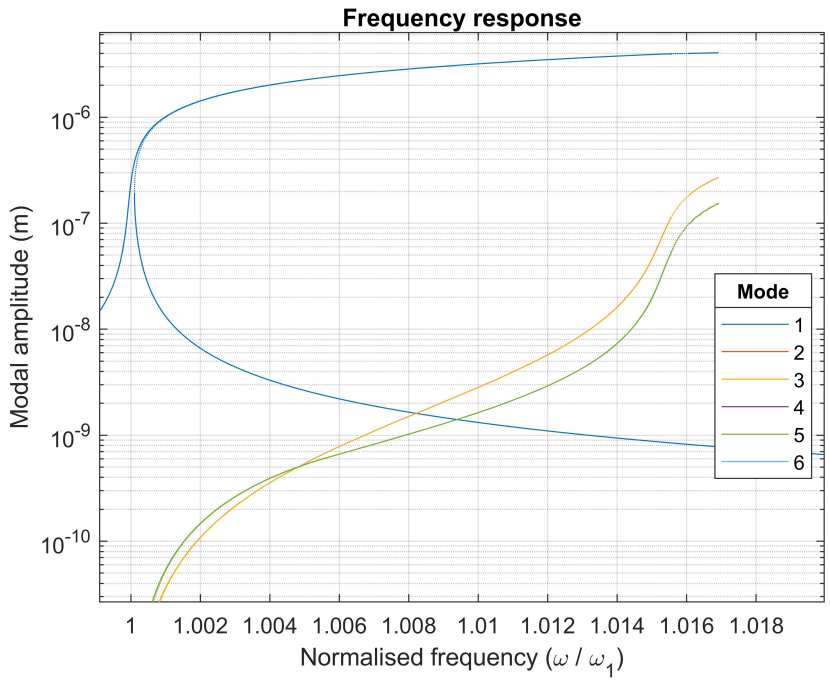

Figure B.9: Simulated frequency response graph for the **uw**-displacement model, accounting for the first six vertical eigenmodes. The linear frequencies are shifted by $\omega_s = 0.005$. The drive voltage is approximately 0.32V. The uneven harmonics have clearly increased in magnitude. Solid lines denote stable solutions, dotted lines denote unstable solutions.

B.3.4. Forced vibrations from the frequency response curve

The steady state response of a string to continuous forcing may possibly show quasiperiodic motion of this string under constant forcing frequencies (and force levels). By selecting a data point on the frequency response curve, one may integrate the equations of motion at the considered force level, amplitude and frequency of the selected data point. The equations of motion from Eq. B.76 are integrated using Matlab's ODE45 solver. Since the uw-displacement model can replicate the experimental response quite well (it shows slope-fits and frequency locking), this model is used here. Again, all variables $a_{jk}^{(r)}$ are zero. The force vector, $F^{(r)}$ is only nonzero for $r = 1$, implying that only the first mode is excited. Fig. B.10a depicts two points: a fully stable solution (denoted by the red star) and a solution at the onset of instability (denoted by the black star). These two points will be analyzed in the next sections.

Forced vibrations for a stable solution on the resonance curve

The response at the red star is checked first. The normalised frequency driving frequency for this star is at approximately 1.01 (Fig. B.10a). The force level is 0.32V. The time response to the constant driving is depicted in Fig. B.11. The total amplitude plot shows that there are amplitude modulations (beatings) visible: the minima and maxima of the amplitude in- and decrease as the time progresses. This implies that the amplitude consists of (at least) two (sinusoidal) signals of two different frequencies: when they are out-of-phase, their sum is of a small magnitude, generating the minima. Oppositely, when these signals are in-phase, the sum is of a larger magnitude, generating the maxima.

The FFT plot in Fig. B.11 shows more than two frequency peaks; it depicts four peaks (labeled from left to right as $\tilde{\omega}_A, \tilde{\omega}_B, \tilde{\omega}_C$ and $\tilde{\omega}_D$), at normalised frequencies of approximately $\tilde{\omega}_A = 0.97$, $\tilde{\omega}_B = 1.01$, $\tilde{\omega}_C = 1.05$ and $\tilde{\omega}_D = 1.09$. The magenta color is visible only, indicating that the frequency content of this fourth time frame is equal to that of the previous three. This implies that the frequency content is approximately constant over the four considered time periods. The peak at $\tilde{\omega}_B = 1.01$ may be attributed to the forcing frequency. The peaks are spaced at a constant frequency difference, namely $\tilde{\omega}_C - \tilde{\omega}_B = 0.04$, which implies that the peak at $\tilde{\omega}_C = 1.05$ is the average of $\tilde{\omega}_B$ and $\tilde{\omega}_D$: $\tilde{\omega}_C = \frac{\tilde{\omega}_B + \tilde{\omega}_D}{2} = 1.05$. The peak at $\tilde{\omega}_A$ may thus be approximated by $\omega_A = \frac{3\omega_B - \omega_D}{2} = 0.97$. It is uncertain what the origin is of these peaks, but it is likely to be present a nonlinear effect. It may for example be a result of some harmonics of the first mode. To verify that this is the case, the

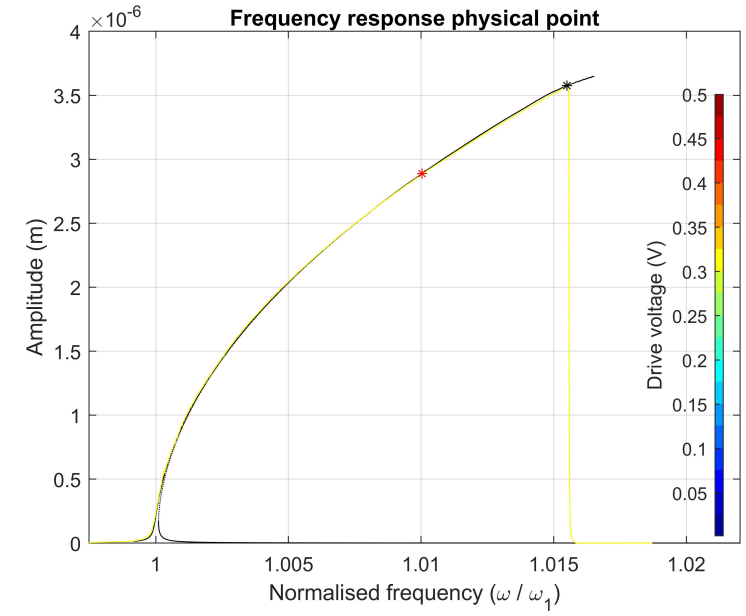

(a)

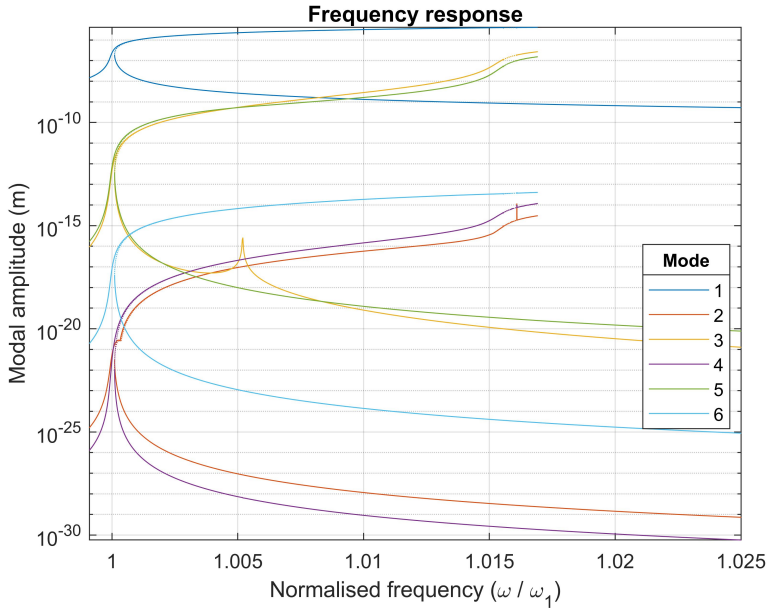

(b)

Figure B.10: Simulated frequency response graph for the **uw**-displacement model, accounting for the first six vertical eigenmodes. The linear frequencies were shifted slightly, by $\omega_s = 0.005$. The drive voltage is approximately $0.32V$. Solid lines denote stable solutions, dotted lines denote unstable solutions. B.10a depicts the total response when measuring at one point along the length of the string. B.10b displays all modal contributions. Note that there is an unstable branch generated at the maximum of all modal amplitudes.

simulation is run once more, though this time for the case where only one mode is considered: the first mode. Fig. B.12 depicts the resulting amplitude and the frequency content.

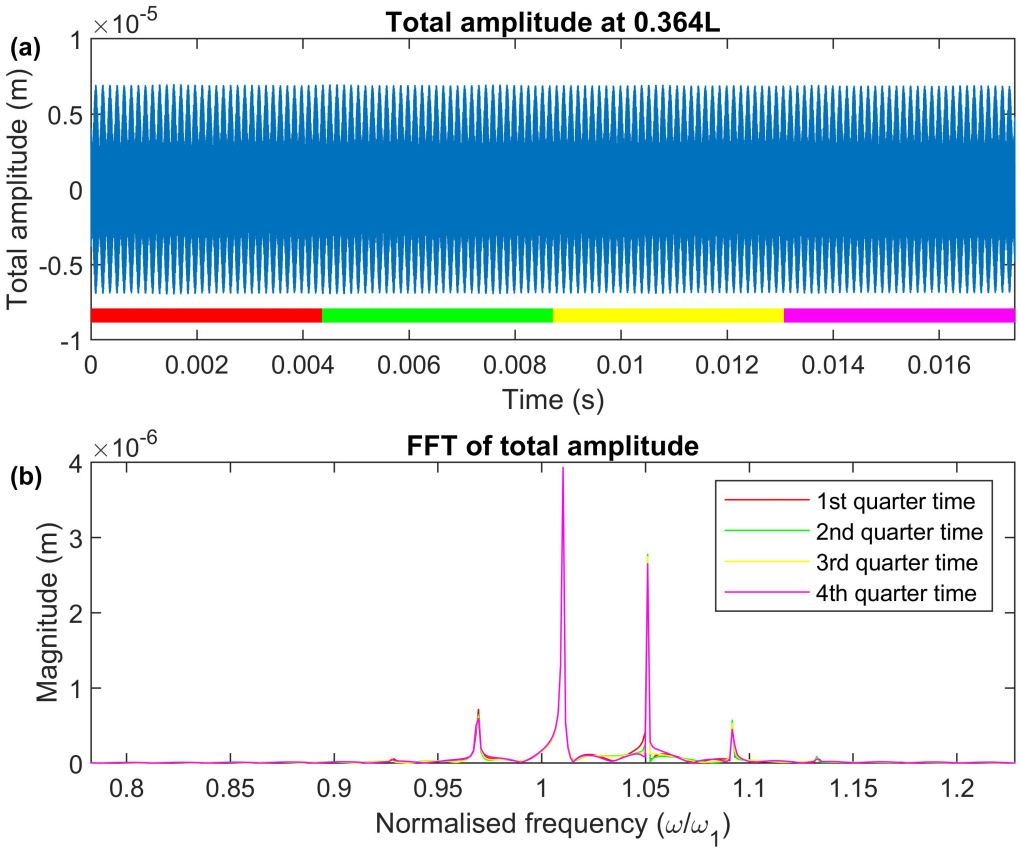

Figure B.11: Simulated time response of forced oscillations from the stable (red) point on Fig. B.10a at $\frac{\omega_f}{\omega_1} = 1.01$. The simulation model is the **uw**-displacement model, it consists of the first **six** vertical modes of the string. **(a)** Depicts the total amplitude of the string at 0.364L. The colored bars on the bottom of the plot indicate four time windows, for which **(b)** depicts the FFT of each time window.

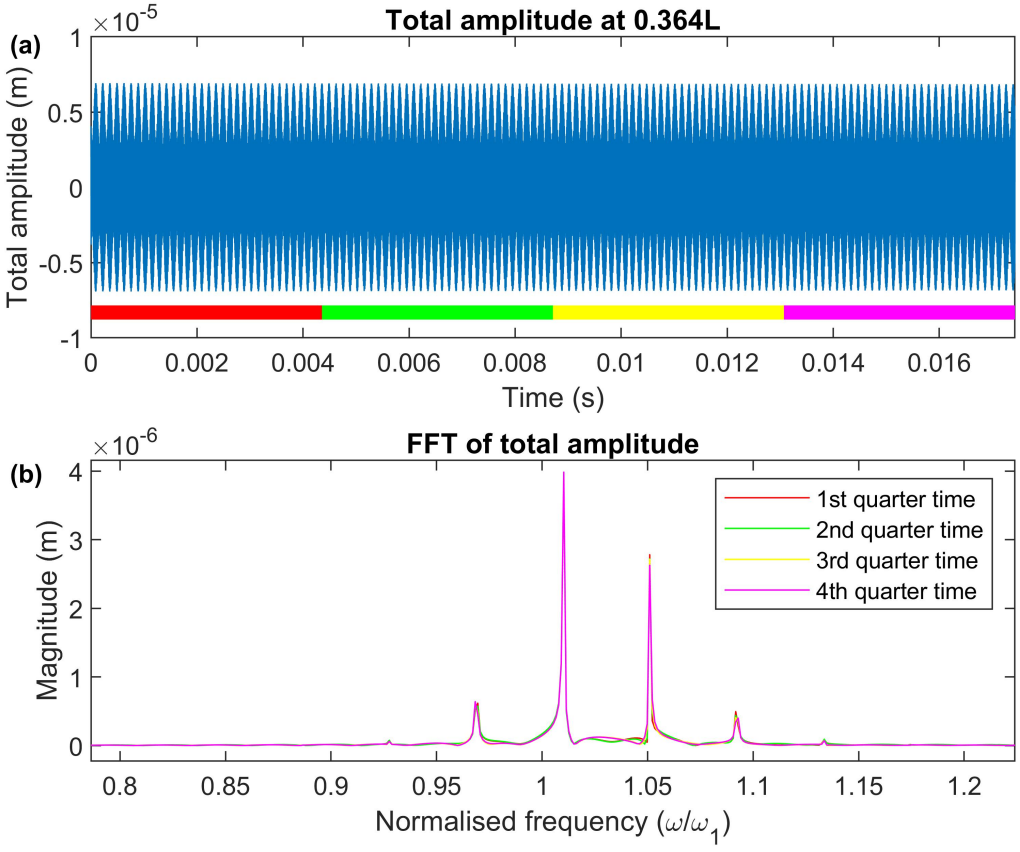

Figure B.12: Simulated time response of forced oscillations from the stable (red) point on Fig. B.10a at $\frac{\omega_f}{\omega_1} = 1.01$. The simulation model is the **uw**-displacement model, it consists of the only the **first** vertical mode of the string. **(a)** depicts the total amplitude of the string at a point at 0.364L. **(b)** depicts the FFT of the signal from **(a)**.

The amplitude versus time plot of Fig. B.12 depicts two interesting topics. The first is that -to the eye- the total amplitude remains approximately similar to Fig. B.11, showing that the first mode is the dominant over the higher modes. Secondly, it is clear that the frequency content has not changed significantly. This implies that the contribution of the higher modes is very small. The peaks at $\tilde{\omega}_A, \tilde{\omega}_B, \tilde{\omega}_C$ and $\tilde{\omega}_D$ are thus likely to result from the nonlinearity of the first mode. This may be verified by checking the response of the *linear* equations for the first mode ($b^{(1)}_{111} = 0$), as is depicted in Fig. B.13.

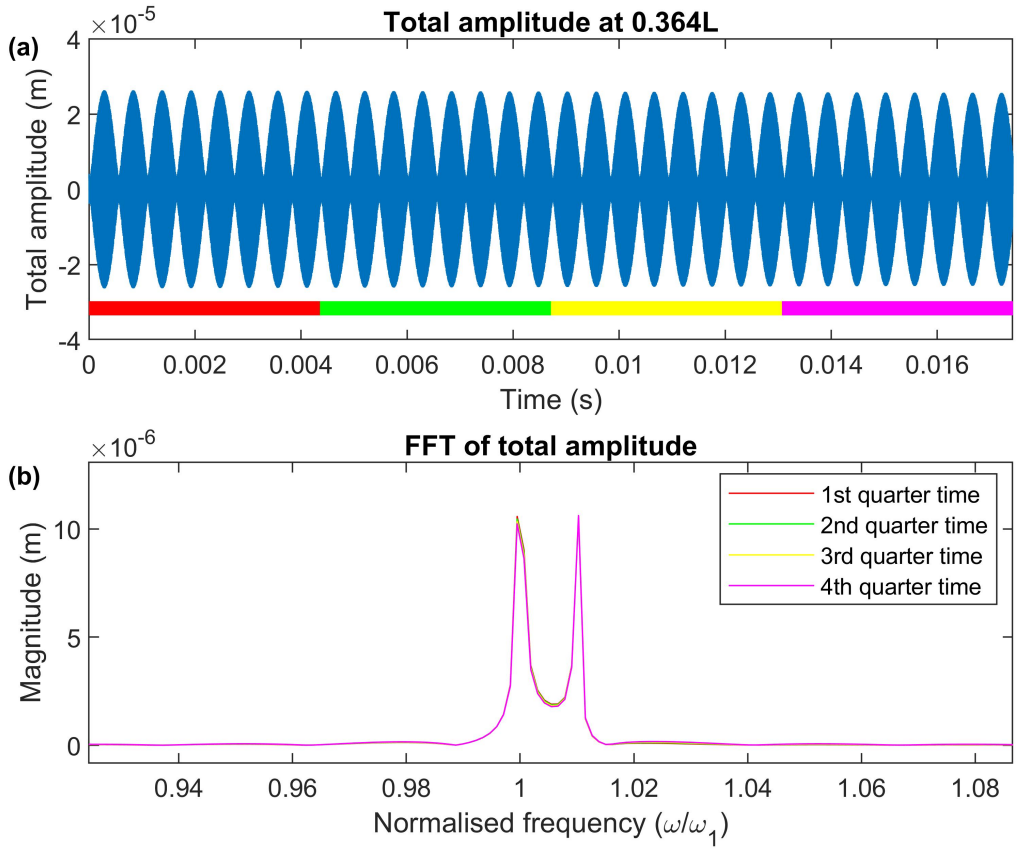

Figure B.13: Simulated time response of **linear** forced oscillations for an initial condition at $\frac{\omega_f}{\omega_1} = 1.01$. The simulation model is a linear displacement model, it consists of the only the **first** vertical mode of the string. **(a)** depicts the total amplitude of the string at a point at 0.364L. **(b)** depicts the FFT of the signal from **(a)**.

The beatings in the amplitude seem to have become more distinct: the oscillations in the amplitude are now clearly visible. Additionally, the maximum of the total amplitude has increased from $7\mu m$ in Fig. B.11 to approximately $25\mu m$. This could imply that the nonlinearity drains quite some energy (as was shown in Fig. B.11), which suppresses the amplitude significantly, by distributing energy to multiple harmonics of the first mode. Additionally, it could be due to the nonlinearity, which shifts the resonance frequency: driving the system slightly outside the resonance frequency could already generate less significant amplitudes. Lastly, the FFT in Fig. B.13(b) depicts two clear peaks: one at a normalised frequency of 1.00 and another at 1.01. These could both be clarified by the linear resonance and the driving frequency, which are at 1.00 and 1.01 respectively. The latter observations imply that the driving near the resonance frequency of a nonlinear system that includes just one mode of vibration, will generate modulations (beatings) of the amplitude signal.
The resulting behavior may be further analysed by checking what the origin of these modulations is, through an analysis of a single-degree-of-freedom linear mass-spring-damper system under harmonic sine-wave excitation, as is shown in Appendix B.6. Eq. B.99 shows that -under the assumption of negligible influence from

damping and dependency of the initial conditions-, a solution may be formulated as follows:

$$q_{\text{est}}(t) = \frac{f}{\omega_0^2 - \omega_f^2}\left[2\cos\left(\frac{\omega_f + \omega_0}{2}\right)\sin\left(\frac{\omega_f - \omega_0}{2}\right)\right] \tag{B.79}$$

This shows that two signals determine the estimated solution: a Cosine signal which is dependent on the average of the drive (ω_f) and resonance (ω_0) frequencies and a Sine-signal that is dependent on the difference between the two frequencies. The first signal (represented by the Cosine-function), oscillates at a high frequency (small period), and the second signal (the Sine-function) oscillates at a low frequency (long period). This results in the beatings that are shown in Figures B.23 and B.24. Comparison of these two figures shows that the closer one excites near resonance, the slower the period of the slow oscillation, as is verified by Eq. B.79. Fig. B.14 depicts the extimated (linear) solution (for zero initial conditions) of the simulated string from this section. The analysis of an undamped linear system shows that the estimated solution is approximately

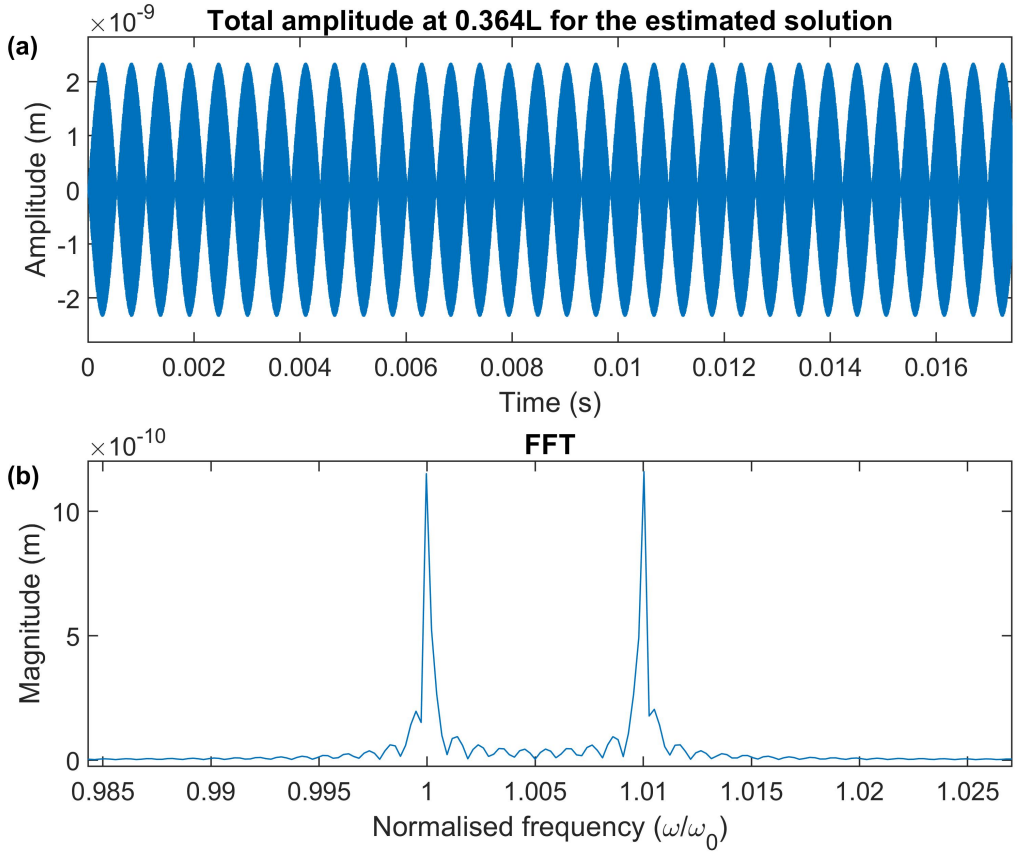

Figure B.14: The estimated solution for the amplitude of a linear (undamped) string. The normalised forcing frequency is equal to 1.01. **(a)** depicts the amplitude (at a point at 0.364L) versus time. **(b)** depicts the FFT of the amplitude signal.

correct: the total amplitude shows similar behavior to that of the nonlinear string from Fig. B.12. Note that the amplitudes in the estimated (from Eq. B.79) and simulated solutions do not match. This could have several origins; first, the initial conditions are zero for the estimated solution, where they are nonzero and quite large in the simulation model (the total amplitude is approximately 3.6μm in Fig. B.10a). Additionally, this initial condition is for strong driving power in the nonlinear regime.
Generally, it may be concluded that the simulated oscillations (from a stable point on the resonance curve) of a nonlinear and weakly damped (Q = 200,000) string under constant excitation remain fairly well understood through the comparison with single-mode nonlinear and linear models. The single-mode nonlinear model shows that some of the peaks in the FFT plots of the simulated oscillations may be attributed to the linear resonance and forcing frequencies. Additional peaks may hence be attributed to harmonics of the first mode, as they are also present in the single-mode model. Lastly, a linear undamped model shows qualitative agreement with the linear single-mode model, indicating that -for the linear system- the influence of damping is

negligible for the considered fundamental mode Q-factor (of 200,000). For the nonlinear model, this negligible damping assumption cannot be made with certainty. However, one can deduct that the nonlinear effects of the first mode are dominant, as they are present in both the multi-mode, as well as the single mode model: these nonlinear effects generate a more complex amplitude modulation, originating from multiple frequency peaks.

Forced vibrations for a solution at the onset of instability

The results of the forced response from the black star (at the onset of intstability) in Fig. B.10a are depicted in Fig. B.15.

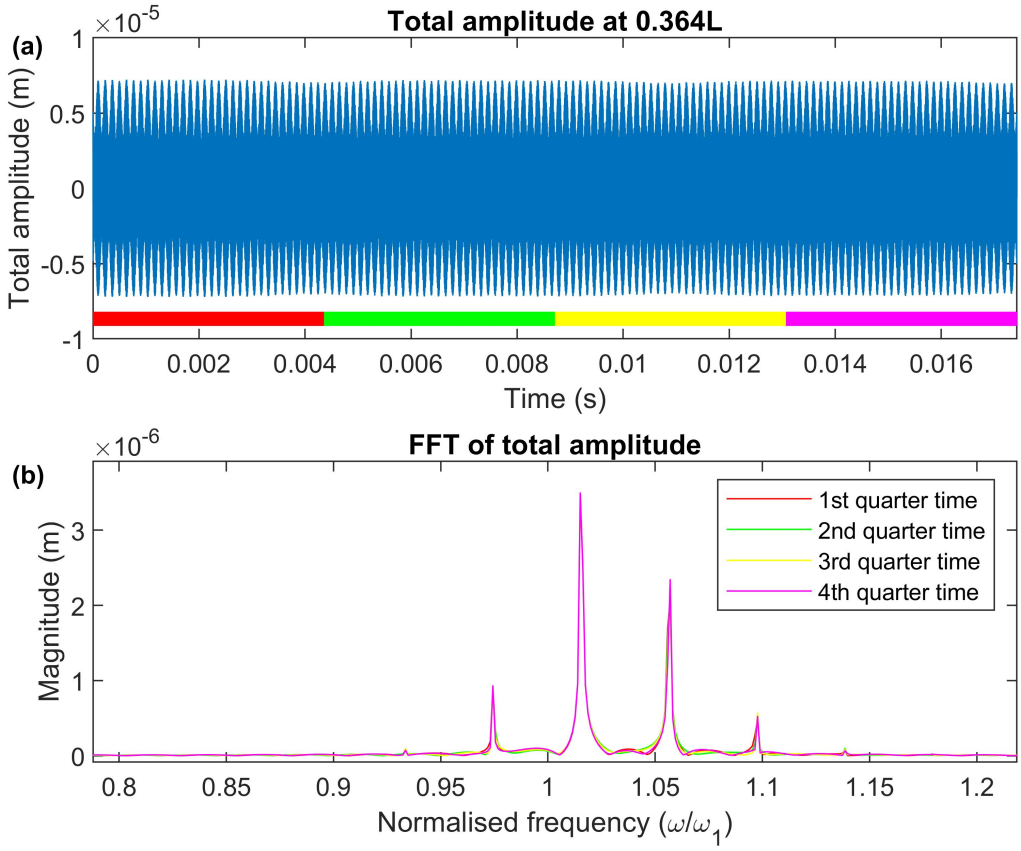

Figure B.15: Simulated time response of forced oscillations from the unstable (black) point on Fig. B.10a at $\frac{\omega_f}{\omega_1} = 1.016$. The simulation model consists of the first six eigenmodes. **(a)** Depicts the total amplitude of the string at 0.364L. The colored bars on the bottom of the plot indicate four time windows, for which **(b)** depicts the FFT of each time window.

The amplitude versus time plot shows similar behavior to that of Fig. B.11(a), where amplitude modulations are visible in the amplitude signal. Similar to the response on the stable solution, these modulations occur on a relatively small time frame. Hence, though the excitation frequency is further from resonance, the slow period of these modulations did not change significantly. The frequency content is similar to that from Fig. B.11, though the peaks in the FFT in B.15(b) seem to have shifted slightly. This may be due to larger effect of the nonlinearity, as the system is brought further into the nonlinear regime. The increase in the amplitude in this nonlinear regime will result in higher frequencies (as was shown in B.10a), which will in turn generate a difference in the period of the beatings. The relations between the four peaks are identical to those from Fig. B.11.

Altogether, this implies that the response near the onset of instability does not show much different results compared to those along the stable branch. Further analyses of a single mode nonlinear model or a undamped linear model will hence not generate much (more) insight, as the phenomena that are elucidated

here correspond very well to those of the previously analysed point (Section B.3.4).

B.3.5. Conclusion - simulations of of 1110μm string

This section has shown that the experimentally obtained frequency response of the first mode of a Si_3N_4 string is largely dominated by a Duffing-like behavior. Increase of the driving power in experiments has shown that at some point, the frequencies and amplitudes "lock", where both measured quantities appear to remain constant. Simulated solutions of a numerical uw-displacement model (STEP) show that this may be explained by interaction with the uneven eigenmodes in the system, which have been shifted slightly (by approximately 0.5% of the first mode's frequency). On the other hand, it is found that the w-displacement shows decent slope fits, but it cannot not generate the locking behavior. To achieve these slope fits, the Young's moduli have been increased from the default value of 250GPa to 675GPa and 450GPa for the uw- and w-displacement models (D.3), respectively. This could result from either an error in the conversion of the experimental data, or that the assumption that the strings' dynamics can be reproduced using only axial deformation models is invalid, as other deformation mechanisms could generate additional nonlinearities.

Two solutions along the nonlinear resonance curve were analysed (using the uw-displacement model) to determine whether the system would show any (nonlinear) quasiperiodic motion. This quasiperiodic motion could originate from various bifurcations in the frequency response figures. Two points were analysed: a stable nonlinear solution and a solution near the onset of instability (the bifurcation point). The solutions indicate that the behavior may be well explained through the nonlinearity of only the first mode, since the results for a single-mode system are similar to those of a multi-mode system. The beating behavior is expected, since an undamped linear system that is excited near resonance also produces these beatings, consisting of two distinct frequencies. A added nonlinearity, though small (the maximum frequency shift is only by 1.6%) generates a different frequency content, where more peaks are visible.
It may thus be concluded that the forced oscillations from the two analysed points remain dominated by the first mode's nonlinearity, though the frequency response curves show locking: a multi-modal interaction. It is probable that the effect of the higher modes is still too small to become significant in the forced oscillations.

B.4. Experimental results on a 700μm string resonator

Zichao Li conducted similar experiments on a second Si_3N_4 string resonator with the characteristics from Table B.12.

Table B.12: Characteristics of the experimentally tested string specimen of length 700mum. * This is the stress in the axial direction.

Quantity	Variable	Magnitude
length	L	700 um
width	w	4 um
thickness	t	344 nm
Young's modulus	E	250 GPa
pre-stress	σ_0	850 MPa*
density	ρ	3100 kg/m^3

While the pre-stress and the width of this string are equal to the previously studied string resonator (Table B.10), this string has a significantly larger thickness than the previous experimentally tested resonator: 344nm versus 92nm. This implies that the string's bending area moment of inertia (which scales with the thickness to the power 3) has increased by $\left(\frac{344}{92}\right)^3 = 52.3$ times, increasing the resistance to bending. The assumption that bending may be neglected could thus become less valid for this particular string resonator.

B.4.1. Verification of the mode shapes

Five force measurements were conducted at three points along the length of the string: $\frac{L}{6}$, $\frac{L}{3}$ and $\frac{L}{2}$. The mode shapes for each of these points may be verified by mirroring the measurements at $\frac{L}{6}$, $\frac{L}{3}$ about the centre point. For each of these five sweeps, a sine function in the form of the first mode with a maximum amplitude equal to the amplitude at $\frac{L}{2}$ is fitted. The measurements and the fitted functions are depicted in Fig. B.16.

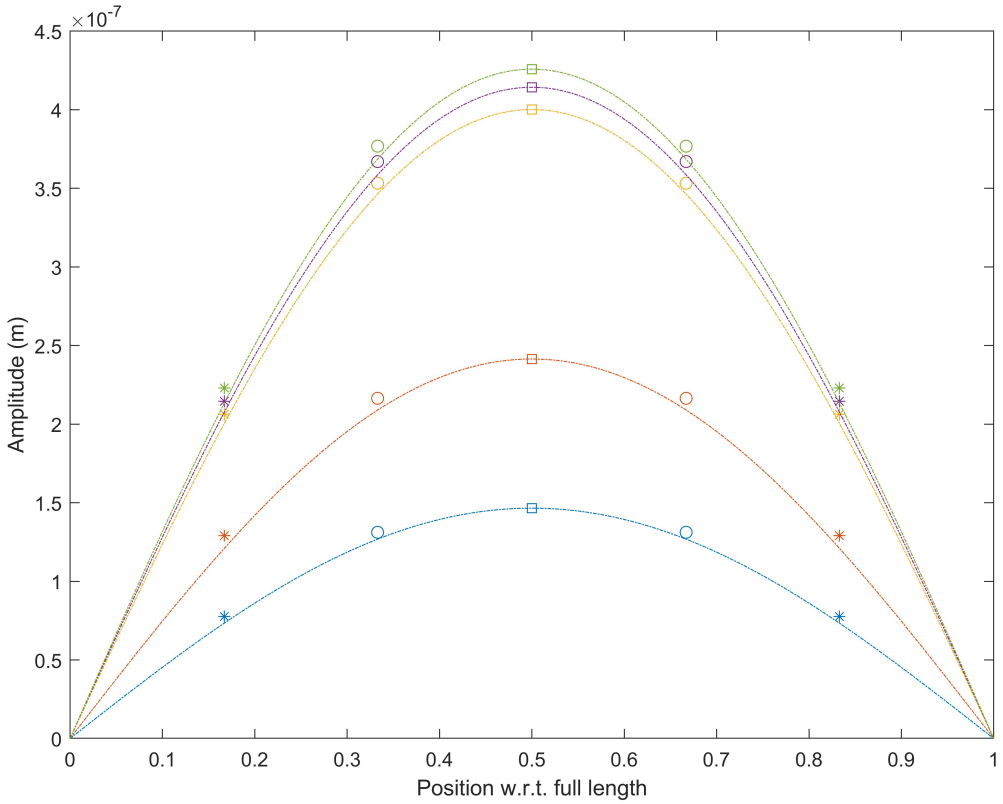

Figure B.16: Fitted mode shapes in the form of a Sine function for five measurement locations along the length of the string: $\frac{L}{6}$ (stars), $\frac{L}{3}$ (circles), $\frac{L}{2}$ (squares), $\frac{2L}{3}$ (circles) and $\frac{5L}{6}$ (stars).

This shows that the linear mode shapes agree quite well, also in the nonlinear regime.

B.4.2. Experimental Duffing response

This experiment consists of five force sweeps ranging between 0.03 and 0.15V. The measurements were conducted for air pressures of approximately 9.81×10^{-5}mbar: slightly higher than that of the experiments on the 1110μm string (2.69×10^{-6}mbar). The experimental frequency response and the corresponding compliance are depicted in Figures B.17 and B.18. The responses show Duffing behavior. Contrary to the Duffing response of the 1110μm string, this response does not show such perfect locking, where the amplitude and frequency cease to increase under increase of the driving voltage. However, these experimental results show a smaller increase in frequency and amplitude from driving voltages larger than 0.09V, showing that there is probably some locking present. Interestingly, the frequency shift for this specimen is quite low: it is approximately 0.2% of the fundamental mode frequency.

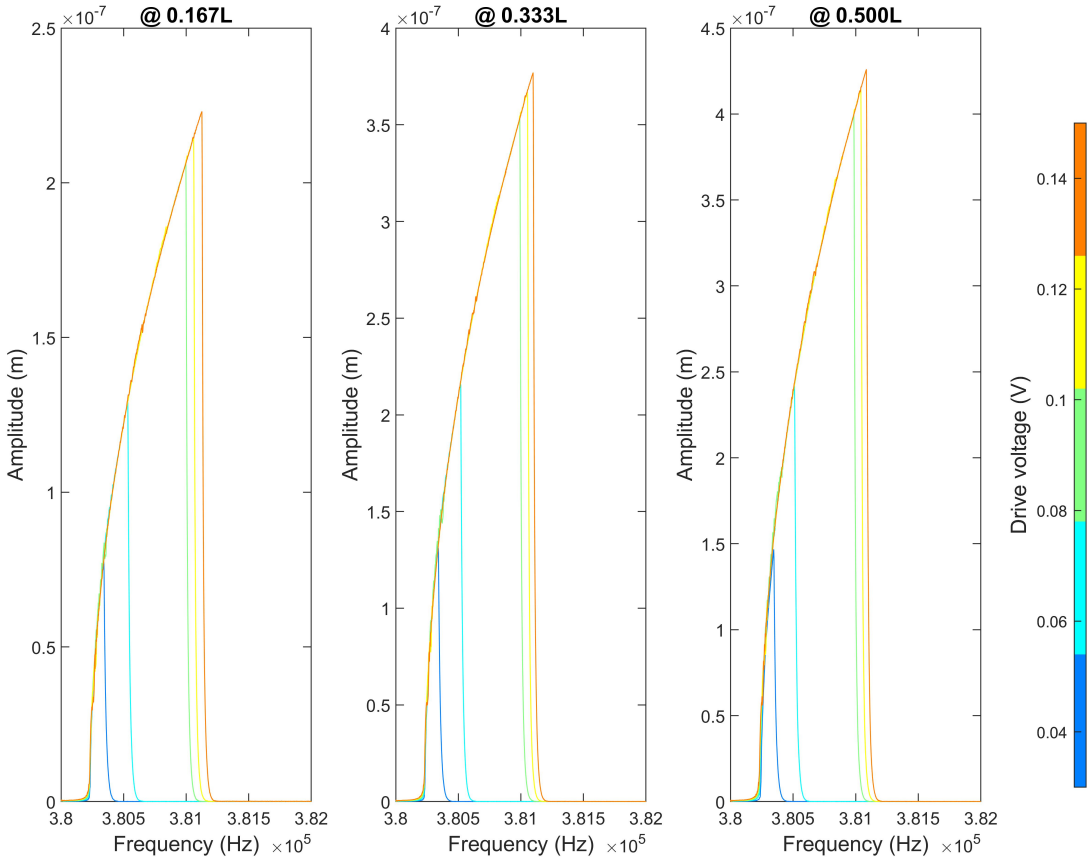

Figure B.17: Experimentally obtained frequency response for three measurement locations.

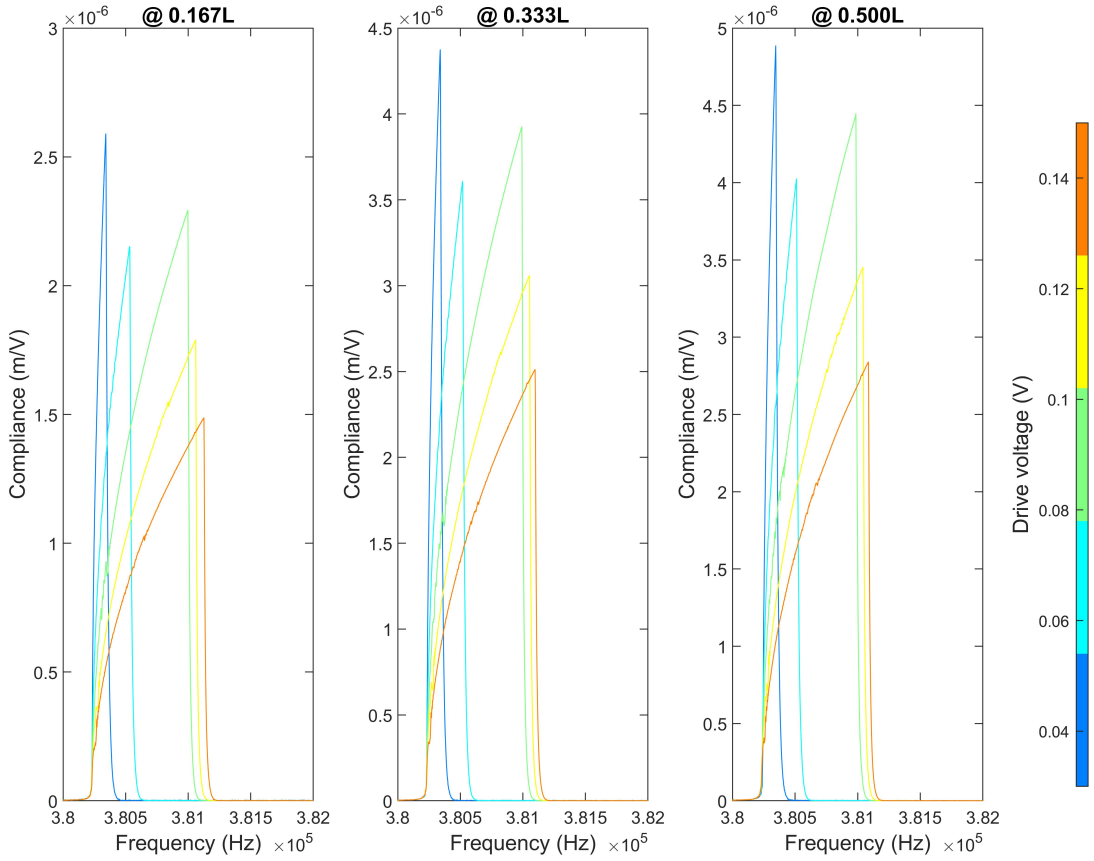

Figure B.18: Experimentally obtained compliance for three measurement locations.

The compliance appears to decrease for increasing driving voltages, but for a drive level of 0.09V, the compliance suddenly increases for all three measurement points. The origin of this behavior may become clear from frequency response simulations, which will be shown in the next section. To conduct proper simulations, one should first determine the Q-factor of the considered mode. A ringdown experiment shows that this fundamental mode's decay is linear with a Q-factor of 1.326×10^6 (Fig. B.19). This is a significantly larger Q-factor than the 1110μm string, which was found for an even lower air pressure: in theory, a higher air pressure generates lower Q-factors.

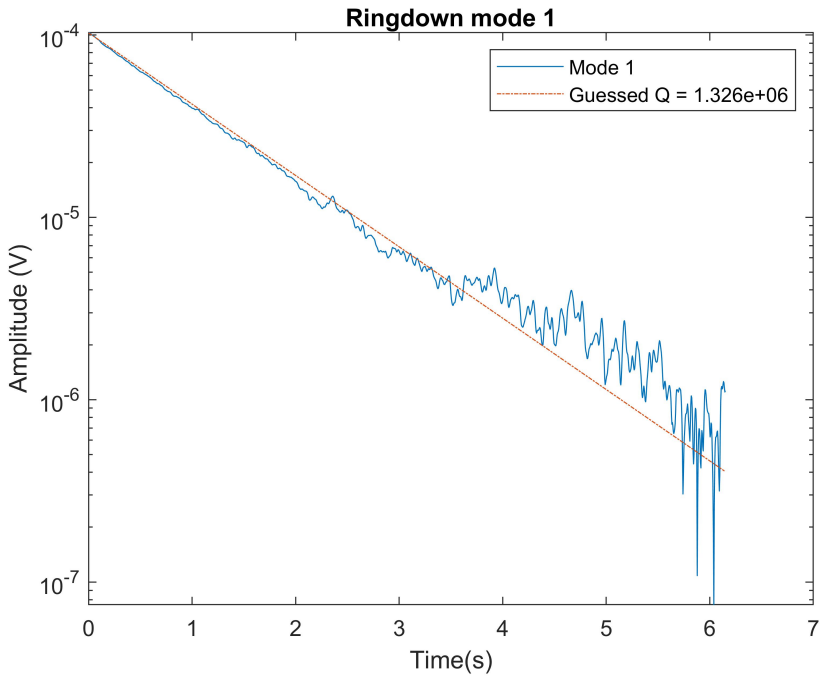

Figure B.19: Ringdown of the first mode for a $L = 700\mu$m string.

From Eq. B.80, one would expect the Q-factor to decrease with increased thickness [31].

$$Q_{\text{str}} = \left[\frac{n^2\pi^2}{12} \left(\frac{t}{L}\right)^2 \frac{E}{\sigma} + \frac{1}{\sqrt{3}} \frac{t}{L} \sqrt{\frac{E}{\sigma}} \right]^{-1} Q_{\text{intr}} \tag{B.80}$$

Here, Q_{intr} is the intrinsic Q-factor of the resonator. The left and right terms inside the square brackets denote the Sine-shape bending and the edge bending respectively. For strings, where $t \ll L$, the edge bending is proportional to $\left(\frac{t}{L}\right)^2$; it is much larger than the Sine-shape bending ($\propto \frac{t}{L}$). The Q-factor for this thicker 700μm string would thus be expected to have decreased with respect to that of the 1110μm string ($Q \approx 200{,}000$). Rather, the Q-factor has increased significantly for an increased thickness. This could be related to the decrease in pre-stress of the 1110μm string resonator, which decreases the Q-factor due to a decrease of the denominator of Eq. 1.9. Furthermore, the 1110μm string resonator already was quite old, which could have accumulated more (dust) particles from the environment, which limit the Q-factor.
An additional effect of this higher pre-stress is that it limits the relative nonlinearity of the resonator, which depends on the ratio of $\frac{E}{\sigma_0}$. This may clarify the limited frequency shift.

B.4.3. Simulated frequency response

Though the frequency response does not show significant frequency shifts, it does show some weak locking behavior, where the amplitude and frequency increase at a much slower rate. This is the result of system slowly losing its sensitivity to the applied force, where any energy is transferred from the first mode into the higher order modes. The uw-displacement model showed good agreement with the locking behavior for the 1110μm string, and thus it was used to simulate the frequency response of this second string as well. This uw-displacement model (including the first six vertical eigenmodes) was fitted for a Young's modulus of 5500GPa, approximately 22 times larger than the default Young's modulus of 250GPa. Fig. B.20a depicts the fit for the uw-displacement model, Fig. B.20b depicts the magnitudes of each of the involved modes.

To determine whether this simulation model can show locking, the linear frequency was perturbed by the parameter ω_s. Many combinations were analysed (ranging from -0.05 to 0.05), but this did not generate the desired locking behavior. A possible explanation of this may be sought in the small magnitude of the relative nonlinearity in the simulation model: this does not generate sufficient excitation of the higher modes to cause significant modal coupling. Comparing Fig. B.20b to Fig. B.10a shows that the higher modes increase

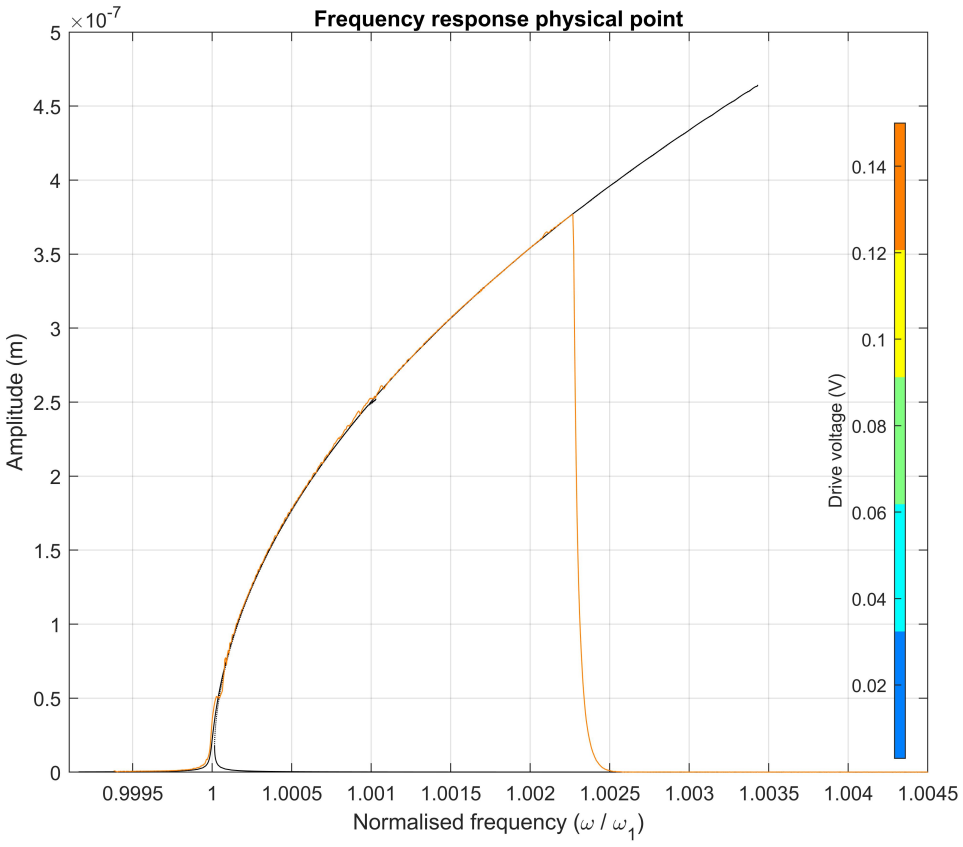

(a)

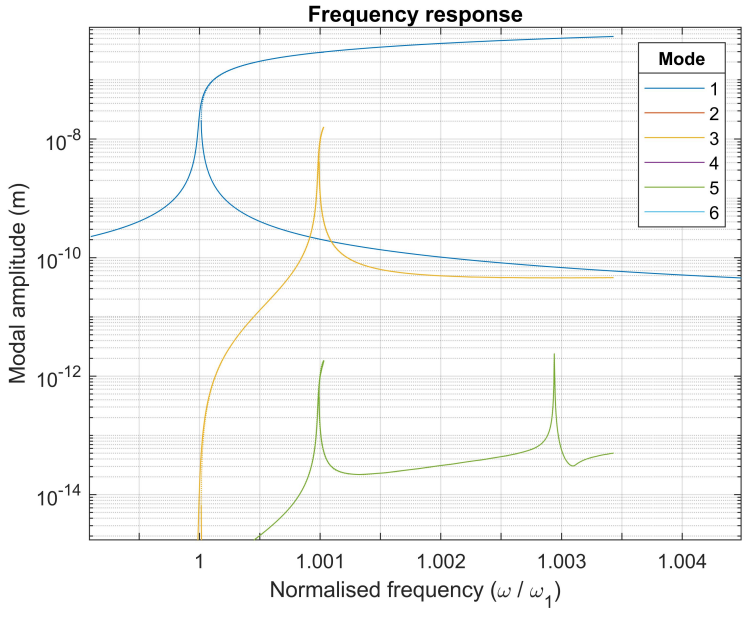

(b)

Figure B.20: Simulated frequency responses for a (**uw**-displacement) string model accounting for the first six vertical eigenfrequencies. The drive power is estimated to be approximately $0.15V$. Solid lines denote stable solutions, dotted lines denote unstable solutions. B.20a depicts the total response when measuring at one point along the length of the string. B.20b displays all modal contributions. Note that there is an unstable branch generated at the maximum of all modal amplitudes.

in magnitude when the system is brought further into the nonlinear regime. Should this condition not be achieved, one cannot reproduce this behavior using this uw-displacement model.

Since it was previously found that the w-displacement model generates stronger nonlinearities *and* (perhaps for this simulation most importantly) stronger coupling coefficients, this model was fitted as well. A decent fit was found for a Young's modulus of 3667GPa; reviewing Table B.9 shows that the first mode's Duffing stiffness for this model is 1.5 times larger than that of the uw-displacement model. The same relation holds between the fitted Young's moduli of both models: 5500GPa = $\frac{3}{2}$3667GPa. Fig. B.21a clearly does not show locking either. Unfortunately, for this w-displacement model, no suitable frequency shift parameter could be found. Hence, although the third and fifth modes' magnitudes at $\tilde{\omega} = 1$ are significantly higher than that of the uw-displacement model (Fig. B.20b), this is still not sufficient to generate the locking behavior, probably due to the stronger coupling term and the nonzero back-coupling term.

B.4.4. Conclusion - simulations of a 700μm string resonator

This section has shown that a large part of the pre-stress was still present in the 700μm string. This results weakly nonlinear response, were small frequency shifts of maximum 0.2% of the fundamental mode frequency were obtained. Both simulation models were fitted for very high -unphysical- Young's moduli. The locking behavior was not observed in either model, possibly due to the small excitation of the higher modes in this weakly nonlinear regime. Other possible effects may be that the estimated damping coefficients of these higher modes do not scale with the inverse of the mode number, which could possibly significantly influence modal contributions.
The simulations for this 700μm string resonator are thus inconclusive regarding which displacement formulation model is most appropriate, as the Duffing behavior can be fitted using both models. However, ringdown results of the first mode do not depict significant energy transfer to other modes, which would generate a different (a much faster, nonlinear) decay of the first mode. Should this significant energy transfer be present, this could be related to a nonzero back-coupling term, and thus a fit for the w-displacement model. On the contrary, a linear decay would suggest that the uw-displacement model is probably more valid. However, since this ringdown was conducted from the weakly nonlinear regime, this modal coupling will be small (and probably invisible) for both models, invigorating the statement about the inconclusiveness of the most appropriate displacement formulation.

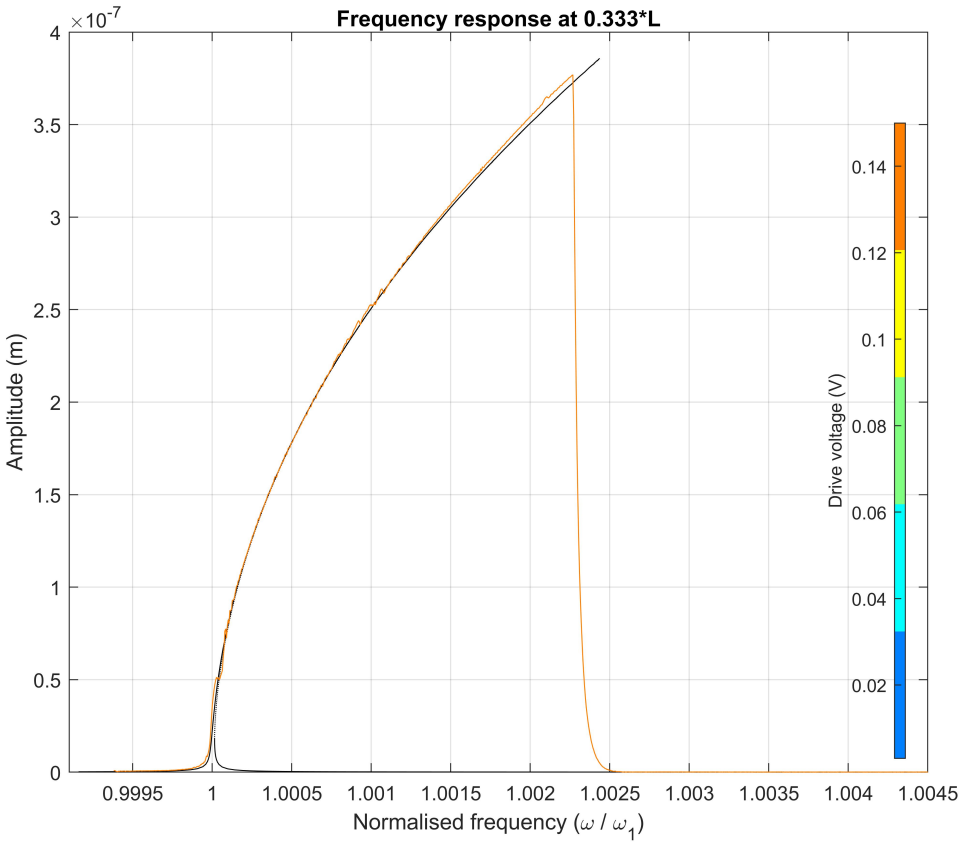

(a)

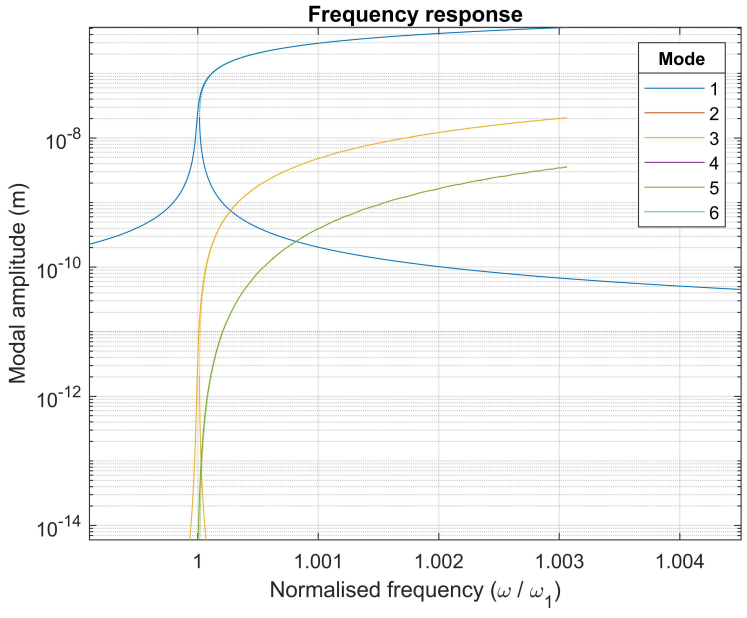

(b)

Figure B.21: Simulated frequency responses for a (**w**-displacement) string model accounting for the first six vertical eigenfrequencies. The drive power is estimated to be approximately $0.15V$. Solid lines denote stable solutions, dotted lines denote unstable solutions. B.21a depicts the total response when measuring at one point along the length of the string. B.21b displays all modal contributions. Note that there is an unstable branch generated at the maximum of all modal amplitudes.

B.5. Appendix - Resonant terms in strings

If it is assumed that the solutions of Eq.'s B.76 (for $r = 3$) are of the form $q_1(t) = \cos(\omega_1 t)$, $q_2(t) = \cos(\omega_2 t)$ and $q_3(t) = \cos(\omega_3 t)$ (where, since it is assumed that the system is a string resonator: $\omega_n = n\omega_1$) and if we substitute this to determine the nonlinear coefficients that cause the strongest (resonant) coupling, Eq. B.81 is found. Note here that the quadratic coupling coefficients of this system are zero.

$$\begin{gathered} F^{(r)} = k_r^{(r)} q_r + b_{111}^{(r)} q_1^3 + b_{112}^{(r)} q_1^2 q_2 + b_{113}^{(r)} q_1^2 q_3 + b_{122}^{(r)} q_1 q_2^2 + \\ b_{123}^{(r)} q_1 q_2 q_3 + b_{133}^{(r)} q_1 q_3^2 + b_{222}^{(r)} q_2^3 + b_{223}^{(r)} q_2^2 q_3 + b_{233}^{(r)} q_2 q_3^2 + b_{333}^{(r)} q_3^3 = \\ k_1^{(r)} \cos(\omega_1 t) + b_{111}^{(r)} \cos(\omega_1 t)^3 + b_{112}^{(r)} \cos(\omega_1 t)^2 \cos(\omega_2 t) + b_{113}^{(r)} \cos(\omega_1 t) \cos(\omega_2 t) \cos(\omega_3 t) + \\ b_{122}^{(r)} \cos(\omega_1 t) \cos(\omega_2 t)^2 + b_{123}^{(r)} \cos(\omega_1 t) \cos(\omega_2 t) \cos(\omega_3 t) + b_{133}^{(r)} \cos(\omega_1 t) \cos(\omega_3 t)^3 + \\ b_{222}^{(r)} \cos(\omega_2 t)^3 + b_{223}^{(r)} \cos(\omega_2 t)^2 \cos(\omega_3 t) + b_{233}^{(r)} \cos(\omega_2 t) \cos(\omega_3 t)^2 + b_{333}^{(r)} \cos(\omega_3 t)^3 \end{gathered} \tag{B.81}$$

The trigonometric relations from Equations B.82 and B.83 show how a nonlinear equation will generate excitation of the harmonics of a mode.

$$\cos(\omega t)^3 = \frac{1}{4}(3\cos(\omega t) + \cos(3\omega t)) \tag{B.82}$$

$$\cos(\omega_i t)^2 \cos(\omega_j t) = \frac{1}{4}(\cos((2\omega_i - \omega_j) t) + 2\cos(\omega_j t) + \cos((2\omega_i + \omega_j) t) \tag{B.83}$$

To reduce the length of the Eq. B.81, the following notation is defined: $F^{(r)} - k_r^{(r)} q_r = F_{lq}^{(r)}$, which may be assumed to be linear in q_r. Using this simplification, together with the relations from equations B.82 and B.83 and substituting $\omega_n = n\omega_1$ into Eq. B.81 results in Eq. B.84.

$$\begin{gathered} F_{lq}^{(r)} = \frac{1}{4} b_{111}^{(r)} [3\cos(\omega_1 t) + \cos(3\omega_1 t)] + \frac{1}{4} b_{112}^{(r)} [2\cos(2\omega_1 t) + \cos(4\omega_1 t) + 1] + \frac{1}{4} b_{113}^{(r)} [cos(\omega_1 t) + 2\cos(3\omega_1 t) + \cos(5\omega_1 t)] + \\ \frac{1}{4} b_{122}^{(r)} [2\cos(\omega_1 t) + \cos(3\omega_1 t) + \cos(5\omega_1 t)] + \frac{1}{4} b_{123}^{(r)} [\cos(2\omega_1 t) + \cos(4\omega_1 t) + \cos(6\omega_1 t) + 1] + \\ \frac{1}{4} b_{133}^{(r)} [2\cos(\omega_1 t) + \cos(5\omega_1 t) + \cos(7\omega_1 t)] + \frac{1}{4} b_{222}^{(r)} [3\cos(2\omega_1 t) + \cos(6\omega_1 t)] + \frac{1}{4} b_{223}^{(r)} [\cos(\omega_1 t) + 2\cos(3\omega_1 t) + \cos(7\omega_1 t)] + \\ \frac{1}{4} b_{233}^{(r)} [2\cos(2\omega_1 t) + \cos(4\omega_1 t) + \cos(8\omega_1 t)] + \frac{1}{4} b_{333}^{(r)} [3\cos(3\omega_1 t) + \cos(9\omega_1 t)] \end{gathered} \tag{B.84}$$

This shows that shows that the $b_{112}, b_{222}, b_{123}$ and b_{233}-terms only excite harmonics of the even modes. The other terms; the $b_{111}, b_{113}, b_{122}, b_{133}, b_{223}$ and b_{333}-terms only harmonics of the uneven.

Now, one may check which modes are (resonantly) coupled with the first mode, by setting $r = 1$ and keeping only the nonzero terms for the first modal equation of motion (Tables E.3 and E.4):

$$\begin{gathered} F_{lq}^{(1)} = \frac{1}{4} b_{111}^{(1)} (3\cos(\omega_1 t) + \cos(3\omega_1 t)) + \frac{1}{4} b_{122}^{(1)} (2\cos(\omega_1 t) + \cos(3\omega_1 t) + \cos(5\omega_1 t)) + \\ \frac{1}{4} b_{133}^{(1)} (2\cos(\omega_1 t) + \cos(5\omega_1 t) + \cos(7\omega_1 t)). \end{gathered} \tag{B.85}$$

This equation shows that if an external excitation would be present at the first mode's frequency, these resonant terms will cause excitation of the higher harmonics as well. In this model, where cubic coefficients are present only, the uneven modes will be excited through excitation of the first mode.

B.6. Appendix - Single DoF forced mass-spring-damper system

This section will show what dynamics may be visible for a one-dimensional mass-spring-damper system that is under harmonic excitation. This analysis is based on an analysis from Inman [16].

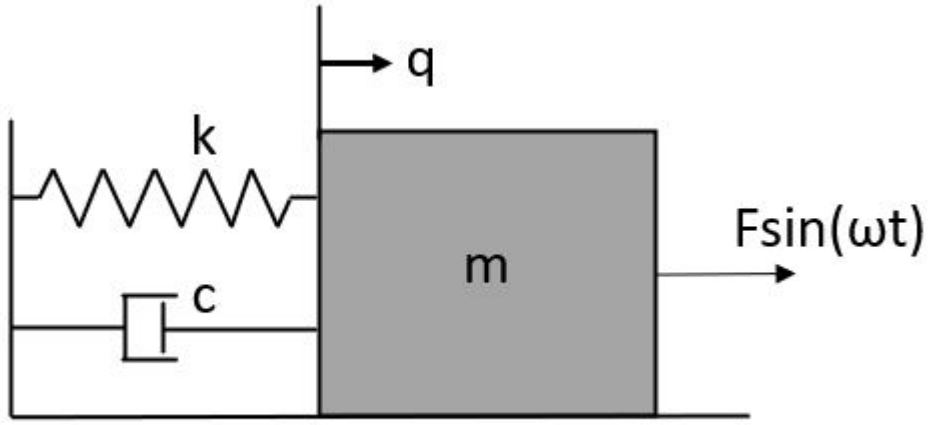

Figure B.22: One-dimensional mass spring damper system under a harmonic forcing.

The single degree-of-freedom (SDOF) system in Fig. B.22 consists of a block with mass m, the stiffness of the (massless) spring is k, the damping coefficient is c and a forcing is present at amplitude F and frequency ω_f. The equation of motion for the degree of freedom q writes:

$$m\ddot{q} + c\dot{q} + kq = F\sin(\omega_f t) \tag{B.86}$$

Mass-normalization gives:

$$\ddot{q} + \frac{c}{m}\dot{q} + \frac{k}{m}q = \frac{F}{m}\sin(\omega_f t) \tag{B.87}$$

Where $\omega_0 = \sqrt{\frac{k}{m}}$, $f = \frac{F}{m}$, and it may be assumed that the damping c -for now- is zero, resulting in the equation of motion:

$$\ddot{q} + \omega_0^2 q = f\sin(\omega_f t) \tag{B.88}$$

To solve this equation, one should assume that there are two types of solutions: a homogeneous solution ($q_h(t)$), which is the solution in absence of the forcing term, and a particular solution ($q_p(t)$), which is the solution of the forcing term. The total solution is hence written as a combination of the two:

$$q(t) = q_h(t) + q_p(t) \tag{B.89}$$

$q_p(t)$ may be assumed to be of the same form of the forcing equation: $q_p(t) = X_0\sin(\omega_f t)$, substitution of this equation into the Eq. B.88 results in:

$$\begin{aligned} \ddot{q}_p + \omega_0^2 q_p &= f\sin(\omega_f t) \\ -\omega_f^2 X_0\sin(\omega_f t) + \omega_0 X_0\sin(\omega_f t) &= f\sin(\omega_f t). \end{aligned} \tag{B.90}$$

The equality allows for cancellation of the $\sin(\omega_f t)$-terms, to generate the following equation:

$$-\omega_f^2 X_0 + \omega_0^2 X_0 = f. \tag{B.91}$$

Where X_0 may be written as Eq. B.92.

$$X_0 = \frac{f}{\omega_0^2 - \omega_f^2} \tag{B.92}$$

Which is hence dependent on the "closeness" of the resonance and the forcing frequency. The particular equation is given by:

$$q_p(t) = \frac{f}{\omega_0^2 - \omega_f^2}\sin(\omega_f t) \tag{B.93}$$

The homogeneous equation is assumed to be a function of both Cosine- and Sine-terms: $q_h(t) = A\cos\omega_0 t + B\sin(\omega_0 t)$. The total solution (from Eq. B.89) is given by Eq. B.94.

$$\begin{aligned} q(t) &= q_h(t) + q_p(t) \\ q(t) &= A\cos(\omega_0 t) + B\sin(\omega_0 t) + \frac{f}{\omega_0^2 - \omega_f^2}\sin(\omega_f t) \end{aligned} \tag{B.94}$$

The variables A and B may be determined using the initial conditions, $q(0) = q_0$ and $\dot{q}(0) = \dot{q}_0$.

$$\begin{aligned} q(0) &= A\cos(\omega_0 0) + B\sin(\omega_0 0) + \frac{f}{\omega_0^2 - \omega_f^2}\sin(\omega_f 0) \\ q_0 &= A \rightarrow A = q_0 \end{aligned} \tag{B.95}$$

$$\begin{aligned} \dot{q}(t) &= -\omega_0 q_0 \sin(\omega_0 t) + \omega_0 B\cos(\omega_0 t) + \frac{f\omega_f}{\omega_0^2 - \omega_f^2}\cos(\omega_f 0) \\ \dot{q}(0) = \dot{q}_0 &= -\omega_0 q_0 \sin(\omega_0 0) + \omega_0 B\cos(\omega_0 0) + \frac{f\omega_f}{\omega_0^2 - \omega_f^2}\cos(\omega_f 0) \\ \dot{q}_0 &= \omega_0 B + \frac{f\omega_f}{\omega_0^2 - \omega_f^2} \\ \rightarrow B &= \frac{\dot{q}_0}{\omega_0} - \frac{\omega_f}{\omega_0}\left[\frac{f}{\omega_0^2 - \omega_f^2}\right] \end{aligned} \tag{B.96}$$

The total solution is thus:

$$q(t) = q_0\cos(\omega_0 t) + \left[\frac{\dot{q}_0}{\omega_0} - \frac{\omega_f}{\omega_0}\left(\frac{f}{\omega_0^2 - \omega_f^2}\right)\right]\sin(\omega_0 t) + \frac{f}{\omega_0^2 - \omega_f^2}\sin(\omega_f t) \tag{B.97}$$

Then, if the excitation frequency ω_f is close to the resonance frequency of the undamped, unforced system ω_0, it is valid to assume that $\frac{\omega_f}{\omega_0} \approx 1$. In addition, if it is assumed that the initial conditions are -for now- zero, the solution will equate to:

$$\begin{aligned} q(t) &= -\left(\frac{f}{\omega_0^2 - \omega_f^2}\right)\sin(\omega_0 t) + \frac{f}{\omega_0^2 - \omega_f^2}\sin(\omega_f t) \\ q(t) &= \frac{f}{\omega_0^2 - \omega_f^2}\left[\sin(\omega_f t) - \sin(\omega_0 t)\right]. \end{aligned} \tag{B.98}$$

Using the trigonometric identity, which states that $\sin(x) - \sin(y) = 2\cos\left(\frac{x+y}{2}\right)\sin\left(\frac{x-y}{2}\right)$, the solution may be re-written as follows:

$$\begin{aligned} q_{\text{est}}(t) &= \frac{f}{\omega_0^2 - \omega_f^2}\left[\sin(\omega_f t) - \sin(\omega_0 t)\right] \\ q_{\text{est}}(t) &= \frac{f}{\omega_0^2 - \omega_f^2}\left[2\cos\left(\frac{\omega_f + \omega_0}{2}\right)\sin\left(\frac{\omega_f - \omega_0}{2}\right)\right]. \end{aligned} \tag{B.99}$$

The latter equation of Eq. B.99 shows that the solution consists of two functions, which both oscillate at different frequencies. The Cosine-term oscillates at a frequency of $\frac{\omega_f+\omega_0}{2}$, where the Sine-term oscillates at a frequency of $\frac{\omega_f+\omega_0}{2}$. This implies that the Cosine-term oscillates at a much higher frequency than the Sine-term.

The produced response is thus a function of two frequencies: a fast frequency and a slow frequency, which generate a total response that consists of an oscillation that slowly changes in amplitude, while these slow changes in amplitude consist of rapid oscillations. For a system with $m = 1kg$, $k = 1\text{Nm}^{-1}$, $F =$ and ω_f between 0.9 and 1.01, this results in the amplitude versus time plots of Fig. B.23.

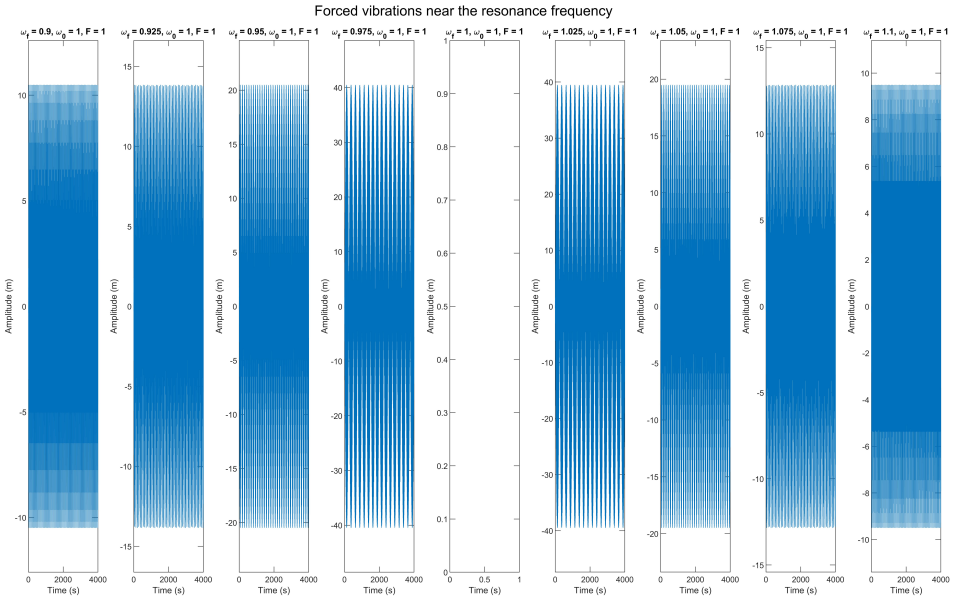

Figure B.23: Plots of $q_{\text{est}}(t)$ for $\omega_0 = 1 rad/s$, $\omega_0 = 0.9, 0.825, 0.85, 0.975, 1.00, 1.025, 1.05$ or 1.1 rad/s for $F = 1$N.

Which shows that there are indeed two frequencies present in the system, as beatings are present, For forcing frequencies even closer to the resonance frequencies, e.g. for $\omega_0 = 1$ rad/s, this phenomenon is more pronounced, as is depicted in Fig. B.24.

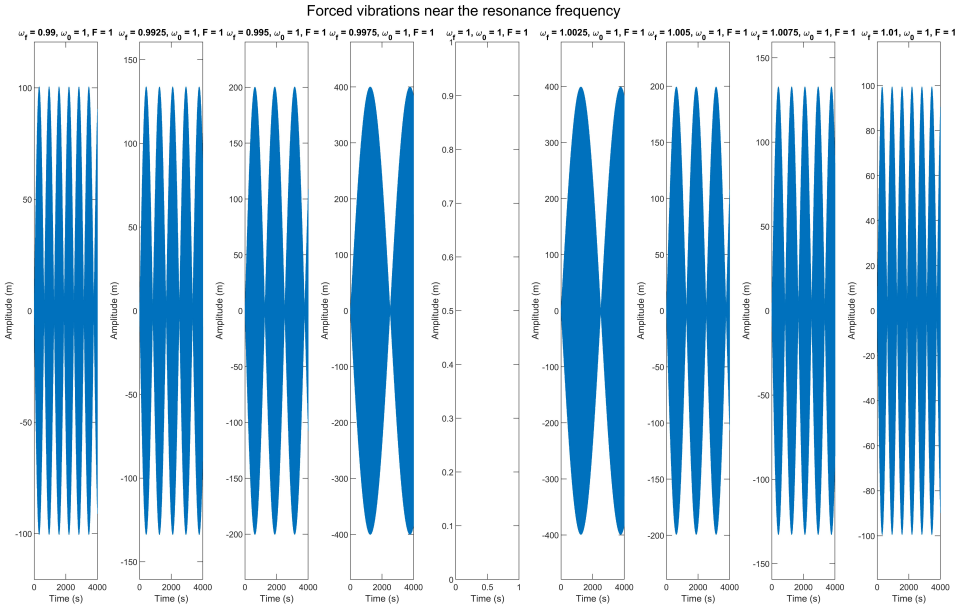

Figure B.24: Plots of $q_{\text{est}}(t)$ for $\omega_0 = 0.9900, 0.9925, 0.9950, 0.9975, 1.0000, 1.0025, 1.0050, 1.0075$ or 1.0100 rad/s rad/s for $F = 1$N.

B.7. Appendix - Origin of coupling terms

B.7.1. Origin of the coupling terms of the w-displacement model

The coupling terms from Tables B.1 and B.2 seem to follow the relation from Eq. B.52. This section will elaborate upon the coupling terms that are generated between the first and third modes. It was shown that the modal coupling coefficients of the FPUT problem resemble those w-displacement analytical model. It was shown that the behavior that is typical for FPUT -the immediate energy exchange to the third mode from an initial excitation of the first mode- is related to a nonzero $b_{111}^{(3)}$-term.

The origin of these coupling terms will become clear after revisiting the equation of motion of the analytical model that accounts for vertical displacements only (Eq. B.37):

$$w_{tt} - c_0^2 w_{xx} - c_1^2 \left(\frac{3}{2} w_{xx} w_x^2 \right) = 0 \tag{B.100}$$

The first two terms of this equation generate terms which are linear in the modal displacement (due to the linear relation with w), as has been shown for the linear model in Equations B.21 and B.35. The latter (nonlinear) term hence produces the nonlinear coupling terms. This section will hence focus solely on the part of the equations of motion that follow from this nonlinear part:

$$-c_1^2 \frac{3}{2} w_{xx} w_x^2. \tag{B.101}$$

The modal coefficients may be found by substitution of Equations B.38 and B.39 and through integration of the mode shape from Eq. B.40. Assuming that the displacements can be written in terms of the first and third modes, the displacement can be written as:

$$w(x,t) = \phi_{u_1}(x) q_1(t) + \phi_{u_3}(x) q_3(t), \text{ where } \phi_{u_1} = \sin\left(\frac{\pi x}{L}\right) \text{ and } \phi_{u_3} = \sin\left(\frac{3\pi x}{L}\right) \tag{B.102}$$

and its derivatives with respect to x equal:

$$\begin{aligned} w_x &= \frac{dw}{dx} = \frac{d\phi_{u_1}(x)}{dx} q_1(t) + \frac{d\phi_{u_3}(x)}{dx} q_3(t) = \frac{\pi}{L} \cos\left(\frac{\pi x}{L}\right) q_1(t) + \frac{3\pi}{L} \cos\left(\frac{3\pi x}{L}\right) q_3(t) \\ w_{xx} &= \frac{d^2 w}{dx^2} = \frac{d^2\phi_{u_1}(x)}{dx^2} q_1(t) + \frac{d^2\phi_{u_3}(x)}{dx^2} q_3(t) = -\frac{\pi^2}{L^2} \sin\left(\frac{\pi x}{L}\right) q_1(t) - \frac{9\pi^2}{L^2} \sin\left(\frac{3\pi x}{L}\right) q_3(t) \end{aligned} \tag{B.103}$$

The weight function of the third mode is given by Eq. B.104.

$$\phi_{u_3}(x) = \sin\left(\frac{3\pi x}{L}\right) \tag{B.104}$$

The nonlinear part of the equation of motion is then found using the following equation:

$$\begin{aligned} &\int_0^L \phi_{u_3}(x) \left[-c_1^2 \frac{3}{2} w_{xx} w_x^2 \right] dx = \\ &c_1^2 \frac{3}{2} \int_0^L \sin\left(\frac{3\pi x}{L}\right) \left[\left(\frac{\pi^2}{L^2} \sin\left(\frac{\pi x}{L}\right) q_1 + \frac{9\pi^2}{L^2} \sin\left(\frac{3\pi x}{L}\right) q_3 \right) \left(\frac{\pi}{L} \cos\left(\frac{\pi x}{L}\right) q_1 + \frac{3\pi}{L} \cos\left(\frac{3\pi x}{L}\right) q_3 \right)^2 \right] = \\ &c_1^2 \frac{3}{2} \frac{\pi^4}{L^4} \int_0^L \left[\sin\left(\frac{\pi x}{L}\right) \sin\left(\frac{3\pi x}{L}\right) \cos^2\left(\frac{\pi x}{L}\right) q_1^3 + \left(9 \sin^2\left(\frac{3\pi x}{L}\right) \cos^2\left(\frac{\pi x}{L}\right) + 6 \sin\left(\frac{\pi x}{L}\right) \sin\left(\frac{3\pi x}{L}\right) \cos\left(\frac{\pi x}{L}\right) \cos\left(\frac{3\pi x}{L}\right) \right) q_1^2 q_3 + \right. \\ &\left(9 \sin\left(\frac{\pi x}{L}\right) \sin\left(\frac{3\pi x}{L}\right) \cos^2\left(\frac{3\pi x}{L}\right) + 54 \sin^2\left(\frac{3\pi x}{L}\right) \cos\left(\frac{\pi x}{L}\right) \cos\left(\frac{3\pi x}{L}\right) \right) q_1 q_3^2 + \\ &\left. 81 \sin^2\left(\frac{3\pi x}{L}\right) \cos^2\left(\frac{3\pi x}{L}\right) q_3^3 \right] dx. \end{aligned} \tag{B.105}$$

The equation may be split up in various modal contributions and using that $\frac{x}{L} = \bar{x}$ results in more simple equations, as is shown by Equations B.106 to B.109.

$$c_1^2 \frac{3}{2} \frac{\pi^4}{L^3} \int_0^1 \left[\sin(\pi\bar{x}) \sin(3\pi\bar{x}) \cos^2(\pi\bar{x}) \right] d\bar{x} q_1^3 = c_1^2 \frac{3}{2} \frac{\pi^4}{L^3} \left(\int_0^1 \text{MNLD}_{3111} \right) d\bar{x} q_1^3 \tag{B.106}$$

$$c_1^2 \frac{3}{2} \frac{\pi^4}{L^3} \int_0^1 \left[9 \sin^2(3\pi\bar{x}) \cos^2(\pi\bar{x}) + 6 \sin(\pi\bar{x}) \sin(3\pi\bar{x}) \cos(\pi\bar{x}) \cos(3\pi\bar{x})\right] d\bar{x} q_1^2 q_3 = c_1^2 \frac{3}{2} \frac{\pi^4}{L^3} \left(\int_0^1 \text{MNLD}_{3113} d\bar{x} \right) q_1^2 q_3 \tag{B.107}$$

$$c_1^2 \frac{3}{2} \frac{\pi^4}{L^3} \int_0^1 \left[\left(9 \sin(\pi\bar{x}) \sin(3\pi\bar{x}) \cos^2(3\pi\bar{x}) + 54 \sin^2(3\pi\bar{x}) \cos(\pi\bar{x}) \cos(3\pi\bar{x})\right)\right] d\bar{x} q_1 q_3^2 = c_1^2 \frac{3}{2} \frac{\pi^4}{L^3} \left(\int_0^1 \text{MNLD}_{3133} d\bar{x} \right) q_1 q_3^2 \tag{B.108}$$

$$c_1^2 \frac{3}{2} \frac{\pi^4}{L^3} \int_0^1 \left[81 \sin^2(3\pi\bar{x}) \cos^2(3\pi\bar{x})\right] d\bar{x} q_3^3 = c_1^2 \frac{3}{2} \frac{\pi^4}{L^3} \left(\int_0^1 \text{MNLD}_{3333} d\bar{x} \right) q_3^3 \tag{B.109}$$

The terms inside the integration terms may be seen as the modal nonlinear displacement function, this function is dependent on the modal displacements and their derivatives with respect to the axial coordinate $\bar{x}$. Fig. B.25 depicts the magnitudes of these functions as a function of $\bar{x}$. In these figures, the modal nonlinear displacement functions of modes j, k, and l onto mode r are defined as MNLD_{rjkl}.

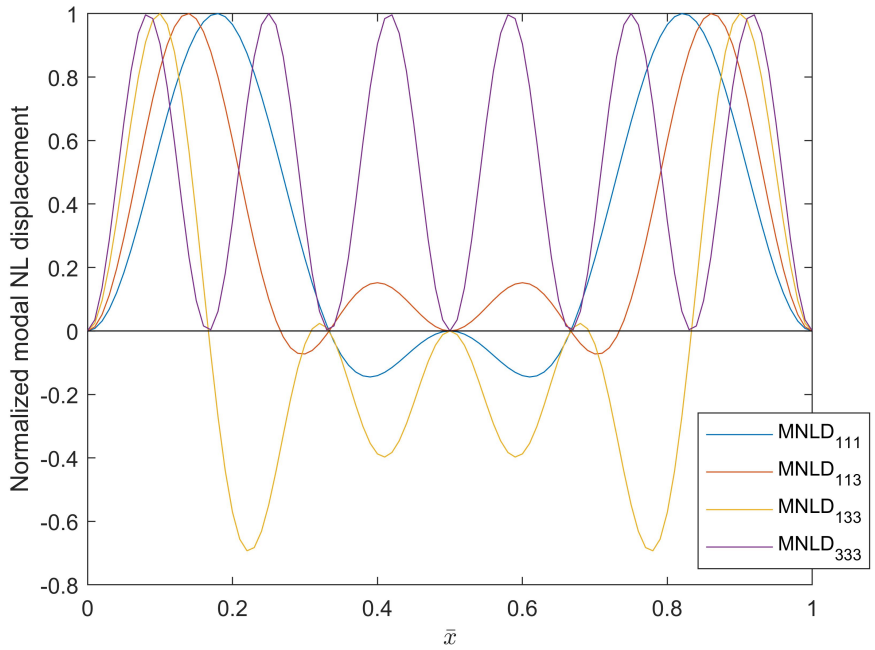

Figure B.25: The normalized modal nonlinear displacement functions with respect to the fractional length of the string. The colors blue, red, yellow and purple depict the magnitudes of the to be integrated functions in B.106 to B.109.

This figure shows that the integral that is represented by Equation B.106 (which basically is surface between the blue line and the zero displacement line), is larger than zero, which will generate a positive coupling term. The same may be said for the red and purple lines, which generate the b_{113}- and b_{333}-terms. The surface under the yellow line will most likely be zero. Solving the integrals confirm this, and the following terms are found:

$$c_1^2 \frac{3}{2} \frac{\pi^4}{L^3} \int_0^1 \left[\sin(\pi\bar{x}) \sin(3\pi\bar{x}) \cos^2(\pi\bar{x})\right] d\bar{x} q_1^3 = \frac{3}{16} c_1^2 \frac{\pi^4}{L^3} q_1^3 = b_{111}^{(3)} q_1^3 \tag{B.110}$$

$$c_1^2 \frac{3}{2} \frac{\pi^4}{L^3} \int_0^1 \left[9 \sin^2(3\pi\bar{x}) \cos^2(\pi\bar{x}) + 6 \sin(\pi\bar{x}) \sin(3\pi\bar{x}) \cos(\pi\bar{x}) \cos(3\pi\bar{x})\right] d\bar{x} q_1^2 q_3 = \frac{27}{8} c_1^2 \frac{\pi^4}{L^3} q_1^2 q_3 = b_{113}^{(3)} q_1^2 q_3 \tag{B.111}$$

$$c_1^2\frac{3}{2}\frac{\pi^4}{L^3}\int_0^1\left[9\left(\sin(\pi\bar{x})\sin(3\pi\bar{x})\cos^2(3\pi\bar{x})+54\sin^2(3\pi\bar{x})\cos(\pi\bar{x})\cos(3\pi\bar{x})\right)\right]d\bar{x}q_1q_3^2= \\ 0q_1q_3^2=b_{133}^{(3)}q_1q_3^2 \tag{B.112}$$

$$c_1^2\frac{3}{2}\frac{\pi^4}{L^3}\int_0^1\left[81\sin^2(3\pi\bar{x})\cos^2(3\pi\bar{x})\right]d\bar{x}q_3^3=\frac{243}{16}c_1^2\frac{\pi^4}{L^3}q_3^3=b_{333}^{(3)}q_3^3 \tag{B.113}$$

Normalization with respect the $b_{111}^{(1)}$-term (from Eq. B.42) results in the expected normalized variables:

$$b_{111}^{(3)}=1b_{111}^{(1)},\ b_{113}^{(3)}=18b_{111}^{(1)},\ b_{133}^{(3)}=0\,,b_{333}^{(3)}=81b_{111}^{(1)}. \tag{B.114}$$

The relations with respect to the mode numbers may also be discerned from Equations B.110, B.111, B.112 and B.113.
The origin of the nonzero $b_{111}^{(3)}$-term hence lies in the formulation of the displacement. For this term to become nonzero, one should hence have a term in the equation of motion that follows the relation from Eq. B.101. The uw-displacement model follows a different displacement relation, due to the inclusion of the in-plane (longitudinal) displacements in the strain formulation. The next section will elaborate upon this equation and it will show the modal coupling terms for this model.

B.7.2. Origin of the coupling terms of the uw-displacement model

The previous section served as a means to show the origin of the coupling between the first and third mode for the w-displacement model. This section will show why the terms that are nonzero in the w-displacement model, could become zero in the uw-displacement model. Revisiting the equation of motion for w of the uw-displacement model in Eq. B.115 (from Eq. B.61) will show what the difference is.

$$w_{tt}-c_0^2w_{xx}-c_1^2\left(\frac{1}{2L}\int_0^L w_x^2dx\right)w_{xx}=0 \tag{B.115}$$

For this displacement model, the nonlinear part is given by the $-c_1^2\left(\frac{1}{2L}\int_0^L w_x^2dx\right)w_{xx}$-term. Similar to the previous section, this analysis will study the third equation of motion under the influence of the first and third modes as well. Using Equations B.102, B.103 and B.104 will generate the following equation for the nonlinear part of the equation of motion:

$$\int_0^L\phi_{u_3}(x)\left[-c_1^2\left(\frac{1}{2L}\int_0^L w_x^2dx\right)w_{xx}\right]dx= \\ \int_0^L\sin\left(\frac{3\pi x}{L}\right)\left[c_1^2\left(\frac{1}{2L}\int_0^L\left(\frac{\pi}{L}\cos\left(\frac{\pi x}{L}\right)q_1+\frac{3\pi}{L}\cos\left(\frac{3\pi x}{L}\right)q_3\right)^2dx\right)\left(\frac{\pi^2}{L^2}\sin\left(\frac{\pi x}{L}\right)q_1+\frac{9\pi^2}{L^2}\sin\left(\frac{3\pi x}{L}\right)q_3\right)\right]dx \tag{B.116}$$

The integral term inside the square brackets of Eq. B.116 may be solved to find Eq. B.117.

$$c_1^2\frac{1}{2L}\frac{\pi^2}{L^2}\int_0^L\left(\cos^2\left(\frac{\pi x}{L}\right)q_1^2+6\cos\left(\frac{\pi x}{L}\right)\cos\left(\frac{3\pi x}{L}\right)q_1q_3+9\cos^2\left(\frac{3\pi x}{L}\right)q_3^2\right)dx=c_1^2\frac{\pi^2}{4L^2}\left(q_1^2+9q_3^2\right) \tag{B.117}$$

Substitution of this result into Eq. B.116 generates the following integral:

$$c_1^2\frac{\pi^4}{4L^3}\int_0^1\left[\left(\sin(\pi\bar{x})\sin(3\pi\bar{x})q_1^3+9\sin(\pi\bar{x})\sin(3\pi\bar{x})q_1q_3^2+9\sin^2(3\pi\bar{x})q_1^2q_3+81\sin^2(\pi\bar{x})q_3^3\right)\right]d\bar{x}. \tag{B.118}$$

This may be split up in the following terms:

$$c_1^2\frac{\pi^4}{4L^3}\int_0^1\left(\sin(\pi\bar{x})\sin(3\pi\bar{x})\right]d\bar{x}q_1^3=c_1^2\frac{\pi^4}{4L^3}\left(\int_0^1\mathrm{MNLD}_{3111}d\bar{x}\right)q_1^3=0q_1^3=b_{111}^{(3)}q_1^3 \tag{B.119}$$

$$c_1^2\frac{\pi^4}{4L^3}\int_0^1 9\sin^2(3\pi\bar{x})d\bar{x}q_1^2q_3=c_1^2\frac{\pi^4}{4L^3}\left(\int_0^1\mathrm{MNLD}_{3113}d\bar{x}\right)=\frac{9}{8}c_1^2\frac{\pi^4}{L^3}q_1^2q_3=b_{113}^{(3)}q_1^2q_3 \tag{B.120}$$

$$c_1^2\frac{\pi^4}{4L^3}\int_0^1 9\sin(\pi\bar{x})\sin(3\pi\bar{x})d\bar{x}q_1q_3^2=c_1^2\frac{\pi^4}{4L^3}\left(\int_0^1\mathrm{MNLD}_{3133}d\bar{x}\right)=0q_1^2q_3^2=b_{133}^{(3)}q_1q_3^2 \tag{B.121}$$

$$c_1^2 \frac{\pi^4}{4L^3} \int_0^1 81 \sin^2(\pi\bar{x}) d\bar{x} q_3^3 = c_1^2 \frac{\pi^4}{4L^3} \left(\int_0^1 \text{MNLD}_{3333} d\bar{x} \right) = \frac{81}{8} c_1^2 \frac{\pi^4}{4L^3} q_3^3 = b_{333}^{(3)} q_3^3. \tag{B.122}$$

Normalization with respect the $b_{111}^{(1)}$-term (from Eq. B.62) results in the expected following normalized nonlinear variables:

$$b_{111}^{(3)} = 0 b_{111}^{(1)},\ b_{113}^{(3)} = 9 b_{111}^{(1)},\ b_{133}^{(3)} = 0\ ,\ b_{333}^{(3)} = 81 b_{111}^{(1)}. \tag{B.123}$$

This shows that the $b_{111}^{(3)}$-term is zero. Fig. B.26 depicts the (normalized) magnitudes of the modal nonlinear displacement functions over $\bar{x}$.

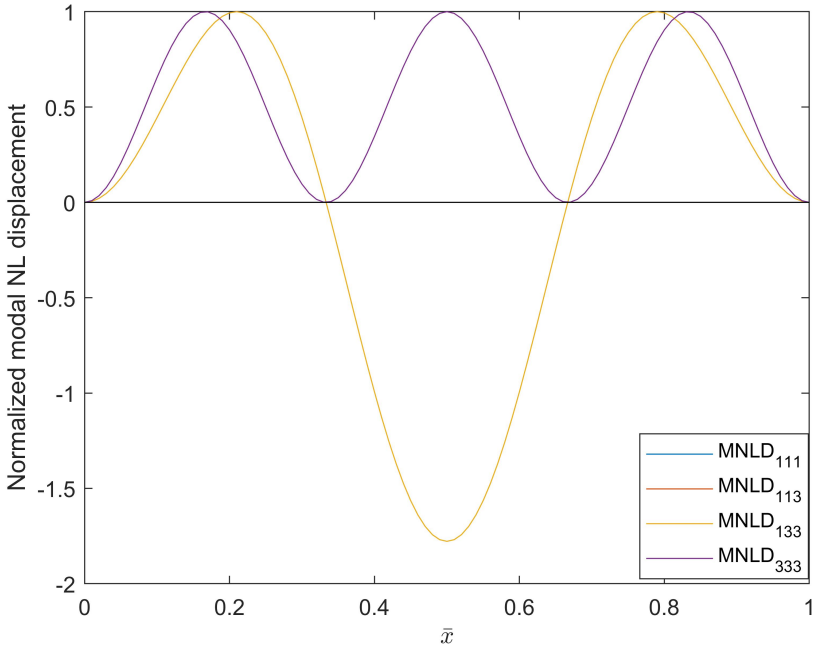

Figure B.26: The normalized modal nonlinear displacement functions with respect to the fractional length of the string. The blue, red, yellow and purple lines the magnitudes of the to be integrated functions in B.119 to B.122.

The figure shows that the purple and the red lines overlap. The integral of these functions over the region $0 \leq \bar{x} \leq 1$, results in the nonzero $b_{333}^{(3)}$- and $b_{113}^{(3)}$-terms, respectively. The blue line is overlapped by the yellow which appears to have an equal surface above the zero-displacement line, as well as below the zero-displacement line. These $b_{111}^{(3)}$- and $b_{133}^{(3)}$-terms are thus zero.

B.7.3. Conclusion

The coupling terms were shown to result from different displacement functions, which in turn generate different dependencies on the modal displacements (here, this is presented by the modal nonlinear displacement functions). In theory, one should be able to change these coupling terms using two methods: changing the nonlinear part of the equation of motion, and through variance of the mode shapes of the resonator. A change in the nonlinear part of the equation of motion would require different strain formulations, which could become different for varying cross-sections in the resonator. Additionally, one should be able to tune the nonlinear coefficients with different mode shapes, which may be achieved in a similar method; by local variance of the cross-section of the resonator, which locally change the mass and (nonlinear) stiffness, this will definitely influence the linear and nonlinear stiffness coefficients of the resonator.

B.8. Appendix - frequency response of the uvw-displacement model

The string vibrations which are analysed in this research are based on the assumption that the vibrations remain planar (in the xz-plane), where the displacement of the string in the transverse direction is zero ($v = 0$). This assumption is approximately valid for systems where the transverse and vertical mode frequencies are

sufficiently apart, such that they are not resonantly coupled. However, for square or circular strings, these (theoretical) frequencies are always degenerate (of equal values, but different direction). To determine what the influence of these degenerate modes is, the frequency response is simulated using the variables from section E.2.2 for the 1100μm string which was analysed in section B.4. This results in the frequency response graphs in Fig. B.27. Fig. B.27 depicts a strong interaction between the these vertical and transverse modes,

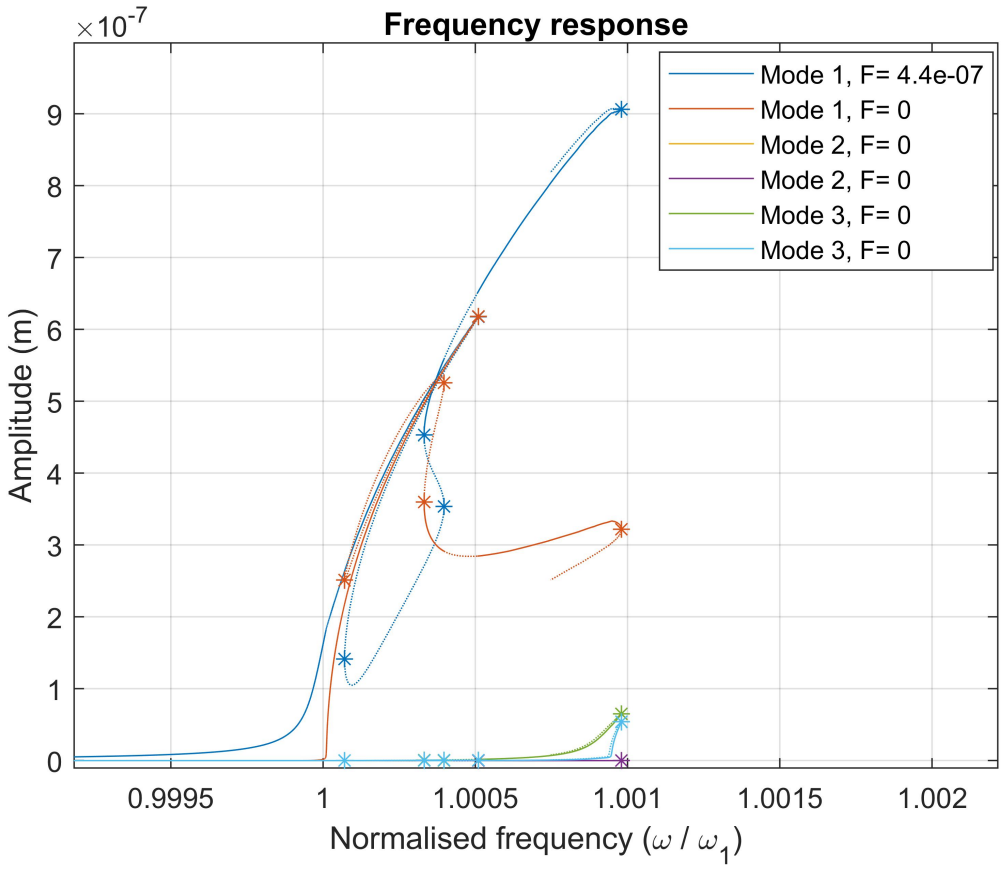

Figure B.27: Frequency response of a model that includes **uvw**-displacements. The uneven modes are the vertical modes, the even modes are the transverse modes.

while the transverse modes are initially not excited. Their excitation results from the modal coupling between the transverse and vertical modes. The coupling is quite significant, as both perpendicular modes are of the same order of magnitude. This coupling will generate out-of-plane or transverse displacement of the string, resulting in a whirling motion.

C

FPUT mechanics in string resonators

The present chapter will show how, and for which type of string resonators, FPUT mechanics may be observed. This chapter will first compare the FPUT and string models, before the requirements to string systems are set. Lastly, some string designs will be tested for their (improved) nonlinearity and frequency ratios.

C.1. The FPUT β-model verus string models

The difference in behavior for the FPUT β-model and string models have several origins, which will be elaborated in this section. Section B.1 presented three (analytical) string models: a model which accounts only for vertical displacements (w-displacement model), a model that accounts for both vertical and longitudinal displacements (uw-displacement model) and finally a model which accounts all three displacement directions (the uvw-displacement model). This section will first compare the linear string variables with the FPUT-model, before comparing the nonlinear (coupling) coefficients of strings to the FPUT model. The FPUT model is based on a hypothetical system, for which a physical equivalent has yet been found. The analysis in this section will mostly consist of comparison of the ratios of the modal coefficients, as evidently, the magnitudes of these coefficients are entirely different.

C.1.1. Linear variables

The normalized linear coefficients of the vertical modes of all analytical string models are shown in Table C.1. The linear stiffness has a linear dependency on the mode number according to Eq. B.27).

Table C.1: The linear stiffness and frequency ratios of the simple string model versus the linear stiffness ratios for FPUT β-model (from an eigenvalue analysis).

n	**(1)**	**(2)**	**(3)**	**(4)**	**(5)**	**(6)**
string: $\tilde{k}_{\text{string}}$	1.00	4.00	9.00	16.00	25.00	36.00
string: $\tilde{\omega}_{\text{string}}$	1.00	2.00	3.00	4.00	5.00	6.00
FPUT: $\tilde{k}_{\text{FPU}}$	1.00	3.97	8.80	15.33	23.34	32.55
FPUT: $\tilde{\omega}_{\text{string}}$	1.00	1.99	2.97	3.92	4.83	5.71

The table shows that the frequency ratios of strings are integer, where the frequency ratios of the FPUT model (from Section A) are non-integer. Furthermore, it was shown that the frequencies of the third and fifth mode should be 2.97 and 4.83 (and thus lower than the nearest internal resonance condition) to generate FPUT behavior, as is depicted in Fig. A.3. Hence, to observe FPUT-like behavior in strings, one should design a string system which contains these non-integer frequency ratios. Though the difference in the frequency ratios is only several per-cents e.g. $\left(\frac{5.00-4.83}{5.00} \times 100\% = 3.4\%\right)$, the effect on the dynamics is still significant. Analytical models for continuous strings (with constant cross-sectional areas) generally follow this integer frequency relation, which also generate certain relations between the coupling terms. A string system which would have these non-integer frequency ratios could hence also generate modal coupling parameters of a different magnitude.

Until now, the comparison mostly consisted of analyses of frequency ratios, and it has yet included an analysis of the magnitudes of the linear variables, as these are dependent on the geometry of the structure.

C.1.2. Nonlinear variables

The nonlinear modal variables consist of two types. The first type of variables are the Duffing coefficient (denoted by the $b^{(n)}_{nnn}$-terms), which generates a force that is only dependent on the amplitude of the considered mode (of number n). The second type are the modal coupling coefficients, which generate a force that depends on the amplitudes of several modes. The Duffing coefficients are studied first, before the coupling coefficients are compared.

Duffing coefficients

The Duffing coefficients of the analytical models were shown to be dependent on the amount of displacement directions that were considered. It was shown that the Duffing coefficients of the w-displacement model were 1.5 times larger than those of the uw- and uvw-displacement models. This may be an important requirement for FPUT dynamics (which was shown to be dependent on the ratio of nonlinear versus linear forces for the initial conditions). Comparison of the Duffing nonlinearities of the FPUT model and the analytical models may be done through normalization with respect to the first mode. This yields Table C.2.

Table C.2: Normalized Duffing nonlinearities, for the first six (vertical) modes, for the FPUT β model and three analytical string models. The last row shows the Duffing coefficients of the uneven (even) vertical (transverse) modes.

n	**(1)**	**(2)**	**(3)**	**(4)**	**(5)**	**(6)**
FPU: $\tilde{b}_{\text{FPUT}}$	1.00	15.73	77.39	236.39	625.6	1059.69
string.u: $\tilde{b}_{\text{string}}$	1.00	16.00	81.00	256.00	625.00	1096.00
string.uw: $\tilde{b}_{\text{string}}$	1.00	16.00	81.00	256.00	625.00	1096.00
string.uvw: $\tilde{b}_{\text{string}}$	1.00	1.00	16.00	16.00	81.00	81.00

This shows that the ratios of the Duffing coefficients for the FPUT problem nearly resemble those of the string models that include the w- or uw-displacements. The discrepancy between the FPUT and string models is likely to result from the discretization into N elements. The FPUT model shows that the Duffing nonlinearity approximately follows the same trend as the w- and uw-displacement models: it scales with the frequency ratio to the power four. The uvw-displacement model is included here as well, because this may also show desired dynamics: perpendicular modes were shown to be strongly coupled in Table E.6.

Modal coupling coefficients

This section will compare the modal coupling coefficients of string models to those of the FPUT model. Reference will often be made to Tables E.2, E.4 and E.6. The modal coupling coefficients of the FPUT model are shown in Table A.4.

Table C.3: Coupling coefficients for the first three uneven modes: 1, 3 and 5. From left to right: the required coupling coefficients for the FPUT β-model, the coupling coefficients of the w-displacement string model, and the uw-displacement string model. The uvw-displacement string model is excluded here, since these modes are defined differently.

	FPUT model			String model (w)			String model (uw)		
Eq.	**(1)**	**(3)**	**(5)**	**(1)**	**(3)**	**(5)**	**(1)**	**(3)**	**(5)**
$\tilde{b}_{111}$	1.00	0.99	0	1.00	1.00	0	1.00	0	0
$\tilde{b}_{113}$	2.97	17.59	14.83	3.00	18.00	15.00	0	9.00	0
$\tilde{b}_{115}$	0	14.83	50.02	0	15.00	50.00	0	0	25.00
$\tilde{b}_{133}$	17.59	0	43.99	18.00	0	45.00	9.00	0	0
$\tilde{b}_{135}$	29.67	87.99	0	30.00	90.00	0	0	0	0
$\tilde{b}_{155}$	50.02	0	0	50.00	0	0	25.00	0	0
$\tilde{b}_{333}$	0	77.38	0	0	81.00	0	0	81.00	0
$\tilde{b}_{335}$	43.99	0	440.05	45.00	0	450.00	0	0	225.00
$\tilde{b}_{355}$	0	440.05	0	0	450.00	0	0	225.00	0
$\tilde{b}_{555}$	0	0	625.60	0	0	625.00	0	0	625.00

Section A.2.5 showed that FPUT behavior may only be observed for systems with a nonzero back-coupling coefficient (the $\tilde{b}^{(3)}_{111}$-term). This term causes excitation of the third mode through initial excitation of the first mode. Table C.3 shows that $\tilde{b}^{(3)}_{111.w}$ is nonzero, where it is zero for uw-model ($\tilde{b}^{(3)}_{111.uw} = 0.00$). This implies that the w-displacement model is the only string model that satisfies this requirement. Additionally, none of the higher modes contain nonzero $\tilde{b}^{(r)}_{jjj}$-terms (here, $r > j$). This implies these modes do not cause excitation of mode r through excitation of *only* mode j.
Interestingly, the three-dimensional (uvw-displacement) model, which includes an additional displacement direction, shows coupling between perpendicular (vertical and transverse) degenerate modes (Table E.6), but these are not directly excited for the default FPUT initial condition, reducing the possibility to see FPUT behavior for this uvw-displacement model. In summary, it may be stated that the simplest string model, the w-displacement model, is the only model that could potentially show FPUT behavior, since its coupling coefficients are in good agreement with those of the FPUT β-model. However, (as was shown in section B.4) this model does not capture all experimentally observed dynamics. To observe FPUT behavior in a string-like resonator, one may thus concluded that a string system should be designed for which the assumption may be made that the longitudinal and transverse displacements remain negligible.

C.1.3. Comparison of modal quantities

Where previous subsections have shown comparison of the modal coefficients in terms of their ratios with respect to the first modes of each model, this section will compare the actual quantities of the FPUT model and the w-displacement string model.
The FPUT model is a hypothetical model, of which no mechanical equivalent has (yet) been found. The default FPUT problem that was studied in Section A consisted of 16 elements with mass $m = 1kg$, connected to springs with a linear stiffness of $k = 1\text{Nm}^{-1}$ and a nonlinear perturbation to the stiffness of $\beta = 8\text{Nm}^{-3}$. The total mass of the system would thus be $m_{tot} = mN = 16kg$.
The modal equation of motion for the first mode of the FPUT β-model was found to write:

$$\ddot{q}_1 + 3.41 \times 10^{-2} k q_1 + 1.02 \times 10^{-4} \beta q_1^3 = 0. \tag{C.1}$$

Where the total equation has been normalized with respect to the modal mass, which -by approximation- equals half the total mass of the system: $\frac{m_{\text{tot}}}{2} \approx \frac{16}{2} = 8\text{kg}$. For a Si_3N_4 nanostring, this modal mass will be multiple orders of magnitude lower, due to its significantly smaller size. The dimensions and properties of a Si_3N_4 nanostring with similar properties to those of the experimentally tested specimen of length 1110μm are (once more) tabulated in Table C.4.

Table C.4: Characteristics of the experimentally tested string specimen.

Quantity	Variable	Magnitude
length	L	1110 um
width	w	4 um
thickness	t	92 nm
Young's modulus	E	250 GPa
pre-stress	σ_0	509 MPa
density	ρ	3100 kg/m^3
cross-sectional area	$A = tw$	3.68×10^{-13} m^2
total mass	$m_{\text{string}} = \rho AL$	1.27×10^{-12} kg

The modal coefficients of the w-displacement string model were found in Section B.1. For a single mode, the following modal equations of motion were found (from Eq. B.42). This equation, here once again multiplied with the mass density ρA, equates to:

$$\frac{\rho AL}{2} \ddot{q}_{u_n} + \frac{\pi^2 n^2 T_0}{2L} q_{u_n} + \frac{3\pi^4 n^4 EA}{8L^3} q_{u_n}^3 = 0. \tag{C.2}$$

This equation shows that for strings, the modal mass is defined by $\frac{\rho AL}{2} = \frac{m_{\text{string}}}{2}$: half the total mass. After the mass normalization, using mass-normalized eigenvectors (according to the method that is shown in Section

D.2.1), the following equation of motion is found for the first mode:

$$\ddot{q}_{u_1} + \frac{\pi^2\sigma_0}{L^2\rho} q_{u_1} + \frac{2}{\rho AL}\frac{3\pi^4 E}{8L^4\rho} q_{u_1}^3 = 0. \tag{C.3}$$

The mass-normalized coefficients of both the FPUT model and the string's equations of motion are tabulated in Table C.5.

Table C.5: Mass-normalized modal coefficients for the FPUT β-model (left) and the coupling coefficients for the simple string model, which only accounts for vertical displacements (right).

Variable	Unit	FPUT-model	String model (w)
$m^{(1)}$	$[-]$	1	1
α	$[-]$	$\sqrt{\frac{2\,\mathrm{kg}}{m_{tot}}} = 0.35$	$\sqrt{\frac{2\,\mathrm{kg}}{\rho AL}} = 1.26 \times 10^6$
$k_1^{(1)} = \omega_0^2$	$\left[\frac{1}{s^2}\right]$	$3.41 \times 10^{-2} k = 3.41 \times 10^{-2}$	$\frac{\pi^2 n^2 \sigma_0}{\rho L^2} = 1.32 \times 10^{12}$
$b_{111}^{(1)}$	$\left[\frac{1}{m^2 s^2}\right]$	$1.02 \times 10^{-4}\beta = 8.19 \times 10^{-4}$	$\alpha^2 \frac{3\pi^4 E}{8L^4\rho} = \alpha^2 1.94 \times 10^{21} = 3.07 \times 10^{33}$
h	$[m]$	$\sqrt{\frac{\omega_0^2}{b_{111}^{(1)}}} = 6.45$	$\sqrt{\frac{\omega_0^2}{b_{111}^{(1)}}} = 2.07 \times 10^{-11}$

The table depicts a difference in relative nonlinearity, which may be defined through the ratio of $\frac{b_{111}^{(1)}}{k_1^{(1)}}$: this value is much larger for strings than for the FPUT model, since $b_{111}^{(1)} >> k_1^{(1)}$ for a string, whereas for the FPUT model, this is the opposite. However, since the amplitudes of both systems are on very different orders of magnitude, it is more useful to compare the non-dimensionalized quantities. This non-dimensionalization is conducted using the equations from Section D.2.2.

$$t = \frac{\tau}{\omega_0},\ q_n = \tilde{q}_n h, \text{ where } h = \sqrt{\frac{\omega_0^2}{b_{111}^{(1)}}}. \tag{C.4}$$

In this non-dimensionalization, time is scaled from dimensional variable t to non-dimensional time τ using the time constant ω_0. Space is scaled through the introduction of the variable h, which chosen such that the non-dimensional $\tilde{b}_{111}^{(1)}$-term is unity.
Recall from Section A that the initial force ratio should be approximately 21% for the default FPUT system, for $N = 16$ and $\beta = 8\mathrm{Nm}^3$. The initial force ratio quantifies the relative nonlinearity of the initial condition, and it may be written as the ratio of these the nonlinear and linear forces:

$$r_{\mathrm{NL2L}} = \frac{\tilde{F}_{\mathrm{nonlin}}}{\tilde{F}_{\mathrm{lin}}} = \frac{\tilde{b}_{111}^{(1)}\tilde{q}_1^3}{\tilde{k}_1^{(1)}\tilde{q}_1} = \frac{\tilde{b}_{111}^{(1)}}{\tilde{k}_1^{(1)}}\tilde{q}_1^2 \tag{C.5}$$

The initial displacement is -for the default FPUT problem- defined as half a sine wave, or the mode shape of the first mode of a string. This mode shape is maximum at its center ($\frac{L}{2}$): the vertical displacement of this point is defined as w_c. For the FPUT problem, this centre-point displacement was defined to be one meter: $w_{c.FPU} = 1m$. The displacement may be scaled to the (mass-normalized) modal displacement using the following formula:

$$w = \phi_{u_1}^T q_{u1} = \phi_{m_1}^T q_1 = \alpha\phi_{u_1}^T q_1. \tag{C.6}$$

The max-1 eigenvectors, which are denoted by the Φ_{u_k}-terms, have a maximum of 1 ($\max(\Phi_{u_1}) = 1$). The maximum (mass-normalized) non-dimensional modal displacement (Eq. C.7) may thus be written as a function of the maximum string displacement (w_c), the maximum of the max-1 eigenmode and the parameter that scales the eigenvectors from max-1 eigenvectors to mass-normalized eigenvectors, α.

$$\tilde{q}_1 = \frac{w_c}{\max(\Phi_{u_1})}\frac{1}{\alpha h}. \tag{C.7}$$

Finally, the comparison of both models can be made. For a string system to generate the same initial force ratio as the FPUT model, the following equation needs to be satisfied:

$$r_{NL2L.\mathrm{FPUT}} = r_{NL2L.\mathrm{string}} \tag{C.8}$$

Since $\tilde{b}^{(1)}_{111.\text{FPUT}}$ and $\tilde{k}^{(1)}_{1.\text{FPUT}}$ are scaled such that $\tilde{b}^{(1)}_{111.\text{FPUT}} = 1$ and $\tilde{k}^{(1)}_{1.\text{FPUT}} = 1$, Eq. C.5 may be simplified, which results in a dependency on the square of the initial (non-dimensional) amplitude:

$$r_{\text{NL2L.FPUT}} = \frac{\tilde{b}^{(1)}_{111.\text{FPUT}}}{\tilde{k}^{(1)}_{1.\text{FPUT}}} \tilde{q}^2_{1.FPUT} = \tilde{q}^2_{1.FPUT}. \tag{C.9}$$

The same normalization has been applied to the string model, which implies that $\tilde{k}^{(1)}_{\text{FPUT}} = \tilde{k}^{(1)}_{\text{string}}$ and $\tilde{b}^{(1)}_{111.\text{FPUT}} = \tilde{b}^{(1)}_{111.\text{string}}$. This thus implies that the following relation should be satisfied:

$$\begin{gathered} r_{\text{NL2L.FPUT}} = r_{\text{NL2L.string}} = \\ \tilde{q}^2_{1.\text{FPUT}} = \tilde{q}^2_{1.\text{string}} \rightarrow \tilde{q}_{1.\text{FPUT}} = \tilde{q}_{1.\text{string}}. \end{gathered} \tag{C.10}$$

The latter equation states that the non-dimensional (mass-normalized) amplitudes should be equal. This equation is subsequently combined with Eq. C.7 to find the relation between the string and the FPUT models.

$$\begin{gathered} \tilde{q}_{1.\text{FPUT}} = \tilde{q}_{1.\text{string}} = \frac{w_{\text{FPUT}}}{\alpha_{\text{FPUT}} h_{\text{FPUT}}} = \frac{w_{\text{string}}}{\alpha_{\text{string}} h_{\text{string}}} \\ \rightarrow w_{\text{string}} = w_{\text{FPUT}} \frac{\alpha_{\text{string}} h_{\text{string}}}{\alpha_{\text{FPUT}} h_{\text{FPUT}}} \end{gathered} \tag{C.11}$$

C.1.4. FPUT mechanics for the w-displacement string model

Substitution of the variables from Table C.5 and assuming again that $w_{\text{FPUT}} = 1\text{m}$, gives the following required displacement for the string model:

$$w_{\text{string}} = w_{\text{FPUT}} \frac{\alpha_{\text{string}} h_{\text{string}}}{\alpha_{\text{FPUT}} h_{\text{FPUT}}} = 11.82 \times 10^{-6} = 11.82 \mu m \tag{C.12}$$

Which implies that -to generate the same initial force ratio- for the w-displacement string model, an initial displacement of centre point in the form of the first mode with a magnitude of 11.82 micron is required.

Fig.C.1 depicts a (damped, $Q_1 = 100,000, Q_3 = 33,333$ and $Q_5 = 20,000$) ringdown simulation for this initial condition (and the parameters from E.1.1), it generates energy transfer, but it does not generate FPUT behavior. Though the linear energy is exchanged among the higher modes, no energy dominance is visible. In addition, comparison of the linear and nonlinear energy magnitudes shows that the magnitude of the nonlinear energies still is small (Fig. C.1(b and c)). The modal amplitudes and velocities (Fig. C.1(d and e)) show beatings, but the effect not significant. This simulation was run for the linear frequency ratios from Table E.1, which follow an integer relation with the mode number. Section A has shown that non-integer frequency ratios generate more significant energy transfer than integer frequency ratios. This simulation is therefore run again, but this time for the frequency ratios of the default FPUT problem; the results are depicted in Fig. C.2.

The energy and amplitude plots show that this weakly damped (w-displacement) string model can show FPUT-like behavior. This FPUT behavior is visible in the linear energy plot, which only accounts for part of the total energy. Fig. C.2(b) shows this behavior is still present when accounting for the nonlinear energy fraction, which is associated to only this mode (the Duffing energy). Though the nonlinear stiffness has increased significantly, the nonlinear energy thus remains small. This is due to the small orders of magnitude of the vibrations, which basically suppress magnitude of the nonlinear energy.
The remaining nonlinear energy, which is associated to the coupling terms, is depicted in Fig. C.2(c). This plot clearly shows that while the first mode's energy decreases, the coupling energy increases, increasing the energy of the higher modes. Similar to what was shown for the default FPUT model, the highest peaks in the coupling energy seem to follow a similar trend as the third and fifth modes combined. In addition, the lower peaks in the coupling energy depict the trends which follow from solely the third or fifth mode.
The modal amplitude and velocity plots clearly show beatings, where the first mode decreases while the other modes strongly increase, up to the point where the higher modes' amplitudes and velocities are of the same order of magnitude.
The magnitude of this initial displacement could require some further attention, as the maximum displacement that is required for this string equals nearly 12 micron. Comparing this value to the amplitudes which

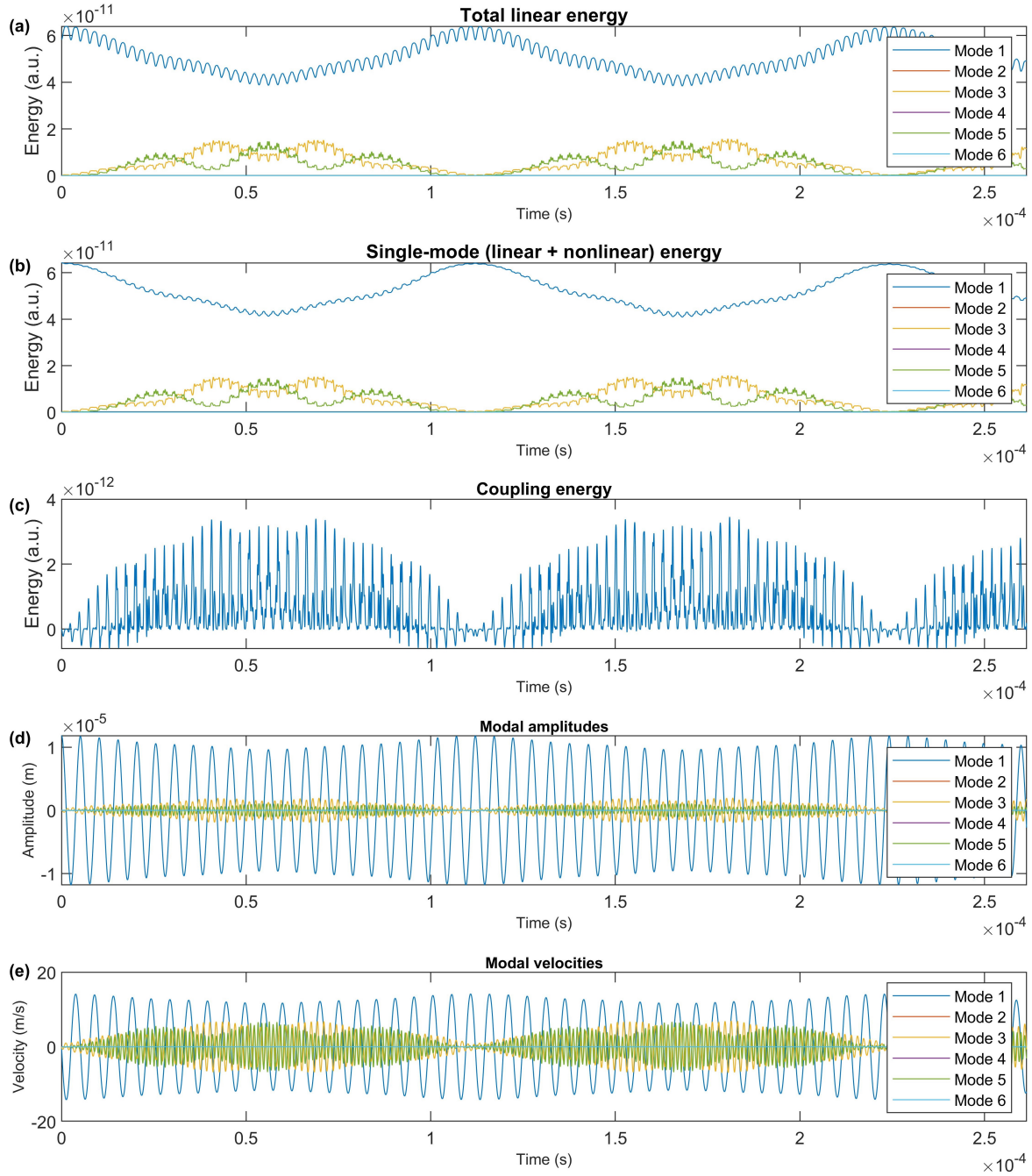

Figure C.1: Numerical simulation for a string model that includes only vertical displacements. The linear stiffness ratios are integer. The initial condition resembles the first mode with a maximum displacement of 11.82μm. This simulation was run with a quality factor of the fundamental mode of 100,000, the Q-factors of the higher modes scale with the inverse of the mode number. Shown in (a), (b) and (c) are the linear, single mode and coupling energies, respectively. The modal amplitudes and velocities in are shown in (d) and (e).

were found in the experiments, e.g. Fig. B.4, one may deduct that the required amplitudes for this FPUT behavior are significantly higher than those of the experiments: 11.82μm versus 4μm respectively. Achieving such a displacement without breaking the resonator is likely to be impossible. However, simulations of the frequency response of this 1110μm resonator (Section B.4) indicate that the Young's modulus should be much higher than the estimated Young's modulus of Si_3N_4: 450GPa (for the w-displacement model) versus the estimated 250GPa. For a larger Young's modulus, the nonlinearity increases (through Eq. C.3), increasing the ratio of $\frac{b_{111}^{(1)}}{k_1^{(1)}}$. The required initial amplitude should thus be lower to generate the required initial force ratio.

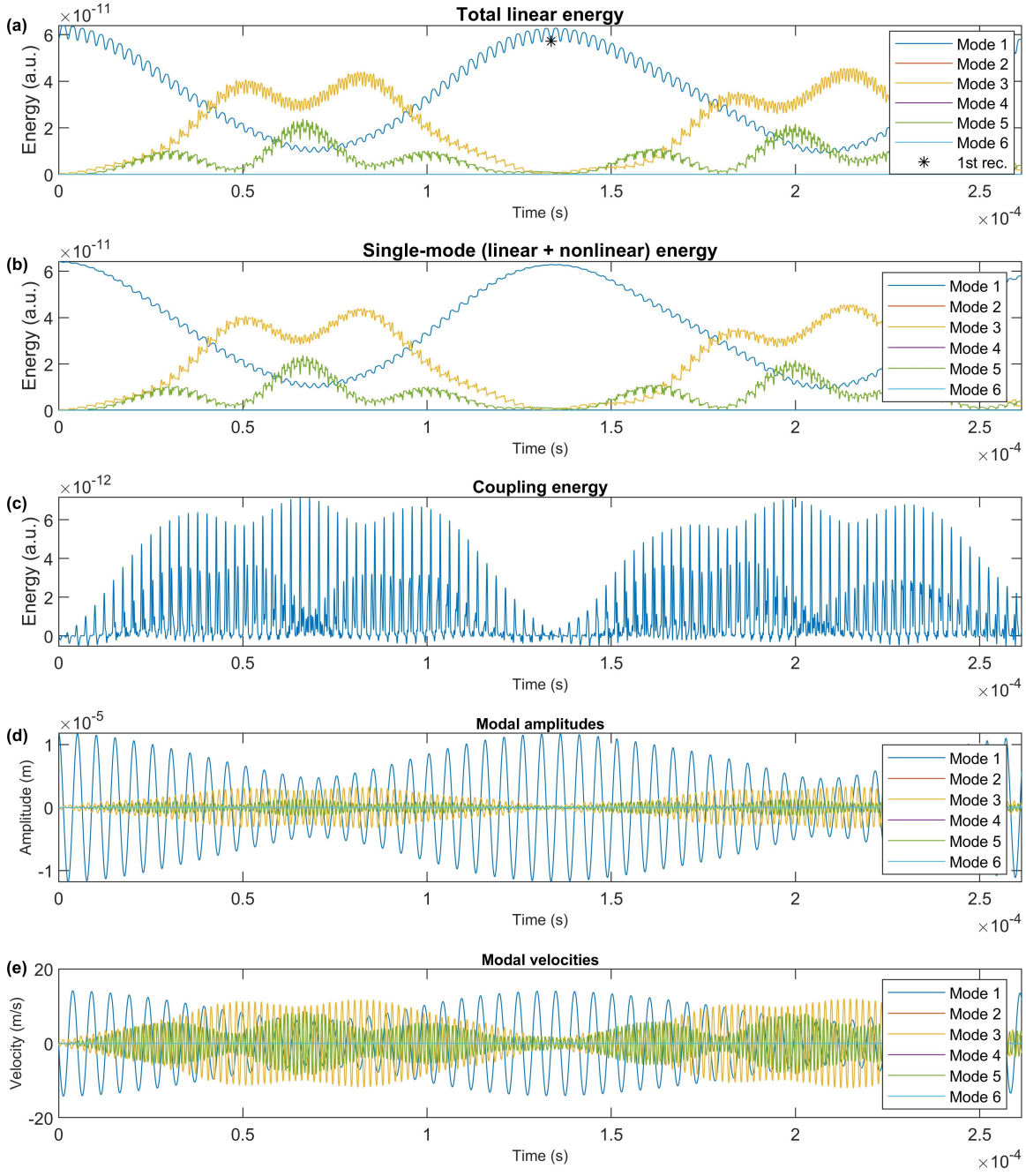

Figure C.2: Numerical simulation for a string model that includes only vertical displacements. The linear stiffness ratios are **non-integer** and equal to those of the FPUT problem ([1.00, 1.97, 2.97, 3.92, 4.83 and 5.71]). The initial condition resembles the first mode with a maximum displacement of 11.82μm. This simulation was run with a quality factor of the fundamental mode of 100,000, the Q-factors of the higher modes scale with the inverse of the mode number. Shown in (a), (b) and (c) are the linear, single mode and coupling energies, respectively. The modal amplitudes and velocities in are shown in (d) and (e).

For a Young's modulus of 450GPa, one an initial displacement of 8.81 micron is required, which appears to be about double the maximum midpoint amplitude that is seen in experiments on strings (B.4). This displacement of 8.81 micron would equal 0.79% of the resonator's length.
This latter analysis has shown that for an increased nonlinearity, which could be present in strings, a smaller initial displacement is required. The section on the analytical string models has shown that this effective nonlinearity is dependent on the ratio of Young's modulus and pre-stress: $\frac{E}{\sigma_0}$. The effective nonlinearity may thus be increased through either increasing the Young's modulus, or decreasing the pre-stress.

Sensitivity of initial conditions
The previous subsection has shown that FPUT behavior may be observed for string resonators that are represented by the w-displacement string model for an initial condition that resembled the first mode's mode shape. This is a static initial condition, as the amplitudes and velocities of all other modes is assumed to be zero. Should a resonator be manufactured that suits the requirements, one may still never exactly replicate this initial condition in experiments. This is due to the fact that little (simple) non-destructive methods exist that can statically displace these nanoresonators. This section will therefore explore the sensitivity to an initial velocity for the first mode, as well as some displacement of the first modes uneven harmonics (the third and fifth mode).

First, the dynamic first mode's initial condition may be considered, where an initial velocity is added to the first mode, to replicate ringdown from an initial condition where the system is driven near the first mode's resonance frequency. The initial velocity is assumed to be related to the initial amplitude through Equations C.13 and C.14, where it is assumed that the displacement is a function of a trigonometric function.

$$w(t) = \sum_{n=0}^{N} A_n \sin(\omega_n t) \tag{C.13}$$

$$\dot{w} = \frac{dw}{dt} = \frac{d}{dt}\left[\sum_{n=0}^{N} A_n \sin(\omega_n t)\right] = \sum_{n=0}^{N} A_n \omega_n \cos(\omega_n t) \tag{C.14}$$

For a pure initial displacement of the first mode, $A_1 = w_0$ and $A_n = 0$ for $n \geq 2$. The velocity is then given by: $\dot{w} = w_0\omega_1$.
To see FPUT behavior in a string-like resonator, one requires an initial displacement of 11.82 micron. For a string-like resonator with a fundamental mode frequency of $\omega_0 = \omega_1 = \sqrt{1.32 \times 10^{12}} = 1.15 \times 10^6$ rad/s, this initial modal velocity should thus be $\dot{w} = w_0\omega_1 = 13.59$m/s. Such an initial condition will generate the dynamics from Fig. C.3

For this dynamic initial condition, there is immediate energy transfer, but no immediate energy dominance. Before this dominance occurs, the first mode's energy first decreases (in the first 0.1ms, under increase of the higher modes), it subsequently increases and then decreases before the higher modes start to dominate the first mode's energy. After this dominance, the first recurrence of the first mode (at approximately 0.18ms) is not as "perfect" as that for a static initial condition: at this time, the higher modes still have quite some energy due to the nonzero amplitude of the higher modes. The amplitudes of the higher modes decrease to smaller magnitudes at around 0.78ms. The first mode then increases and generates near full recurrence (note that the system is weakly damped) at 0.78ms, which is significantly longer than the first recurrence from Fig. C.2. At this time point, the coupling energy is also very small. FPUT-like behavior is thus still visible for dynamic initial conditions, where both the velocity and amplitude of the first mode are nonzero.
However, to achieve such large initial conditions (e.g. the required 11.82 micron), one will have to force the system far into the nonlinear regime. It was shown in the experimental section that in this nonlinear regime, one will also see excitation of higher modes through harmonics of the first mode. The subsequent ringdown simulation will thus be run for nonzero amplitudes (and velocities) of the first, third and fifth modes. It is assumed that the third and fifth mode have no larger magnitude than 15% and 5% of the initial amplitude, respectively, generating the following initial amplitudes (and velocities):

$$\begin{gathered} A_1 = 80\%w_0 = 9.46\mu m,\ A_2 = 0\mu m,\ A_3 = 15\%w_0 = 1.77\mu m,\ A_4 = 0\mu m,\ A_5 = 5\%w_0 = 0.59\mu m,\ A_6 = 0\mu m \\ \dot{A}_1 = A_1 w_0 = 10.85 m/s,\ \dot{A}_2 = A_2\omega_2 = 0 m/s,\ \dot{A}_3 = A_3\omega_3 = 6.04 m/s, \\ \dot{A}_4 = A_4\omega_4 = 0 m/s,\ \dot{A}_5 = A_5\omega_5 = 3.28 m/s,\ \dot{A}_6 = A_6\omega_6 = 0 m/s \end{gathered} \tag{C.15}$$

The results of such initial conditions are presented in Fig. C.4. Initial weak excitation of the higher uneven

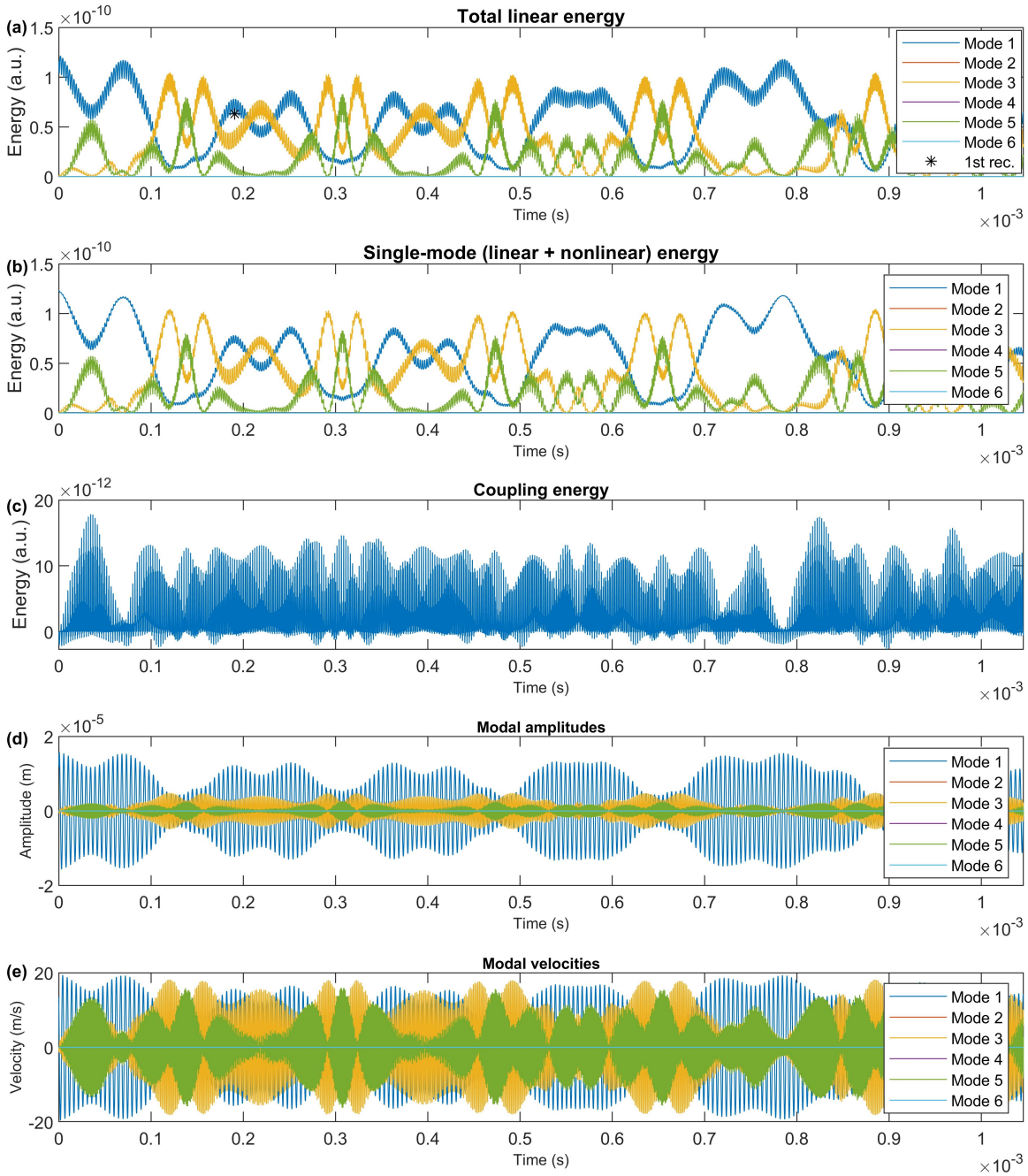

Figure C.3: Numerical simulation for a string model that includes only vertical displacements. The linear stiffness ratios are **non-integer** and equal to those of the FPUT problem. The initial condition resembles the first mode with a maximum displacement of 11.82μm and an initial velocity of 13.59m/s. This simulation was run with a quality factor of the fundamental mode of 100,000, the Q-factors of the higher modes scale with the inverse of the mode number. Shown in (a), (b) and (c) are the linear, single mode and coupling energies, respectively. The modal amplitudes and velocities in are shown in (d) and (e).

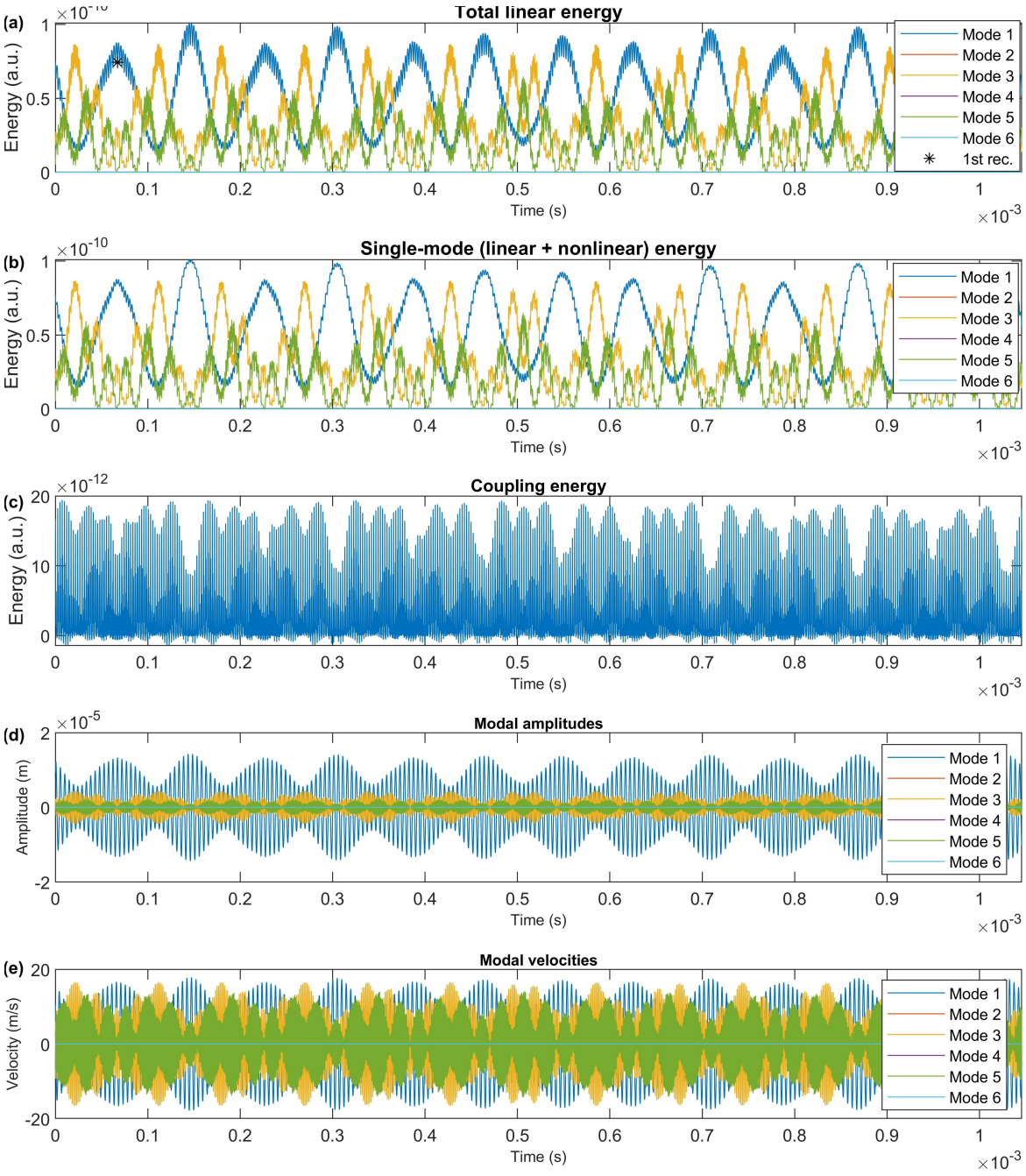

Figure C.4: Numerical simulation for a string model that includes only vertical displacements. The linear stiffness ratios are **non-integer** and equal to those of the FPUT problem. The initial condition resembles dynamic excitation of the first, third and fifth modes, as is shown in Eq. C.15. This simulation was run with a quality factor of the fundamental mode of 100,000, the Q-factors of the higher modes scale with the inverse of the mode number. Shown in (a), (b) and (c) are the linear, single mode and coupling energies, respectively. The modal amplitudes and velocities in are shown in (d) and (e).

modes still generates energy transfer (as expected, since all these modes are initially excited), as well as dominance. The initial energy (at t = 0s) is distributed among all three uneven modes through a nonzero initial condition. A large fraction of the energy is located in the first mode after approximately 0.06ms. Thereafter, the third and fifth mode dominate the first mode for some time, before some of the energy is returned to the first mode at 0.15ms, but this time for a larger amount of energy, since the amplitudes of the third and fifth modes have decreased (Fig. C.4(d)).
Later, at approximately 0.23ms, the energy, amplitude and velocity states from 0.065ms are achieved again. Similarly, the state at approximately 0.15ms appears to return at around 0.30ms. The previous analysis shows that energy exchange may still be observed for less "perfect" initial conditions, where the higher modes have a nonzero initial energy. The typical FPUT phenomenon; the immediate recurrent behavior in the energy plot is more difficult to define. For these initial conditions, one should distinguish between recurrence of the initial conditions, or recurrence of a certain state (e.g. where all energy is located in the first mode). Nonetheless, both types of recurrence may be observed here.

C.1.5. Conclusion

This section has shown that though the magnitudes of the modal coefficients of the w-displacement string model and the FPUT model do not match, they could display similar behavior for some non-integer frequency ratios and certain sets of initial conditions. The linear and single-mode energy still show that there is recurrent behavior visible, which is verified by the modulations of the amplitude. This single-mode energy is assumed to sufficiently represent the modal energies since the (nonlinear) terms only become significant when the amplitudes of the associated modes are large.

C.2. Design for FPUT behavior

The previous sections have shown that FPUT behavior may be observed for a string model which only accounts for vertical displacements. However, experiments have shown that for at least one resonator, this model probably does not replicate the string's dynamics accurately, as this requires the inclusion of longitudinal displacements. To design a resonator that could potentially show FPUT behavior, one should thus optimize the structures which account for displacements in vertical and longitudinal directions. This section will show methods that may be used to improve the nonlinearity of these string resonators. The requirements of the system will be elaborated upon first. Thereafter, a method which could improve the nonlinearity of beams in literature will be presented, before the STEP method is employed to test this method.

C.2.1. Requirements for FPUT behavior

Other than the requirement that Q-factors should be sufficiently large, two requirements have previously been established, which determine whether a structure could show FPUT-like behavior:

1. The frequency ratios should be a non-integer value; slightly lower than the integer frequency ratios for strings.

2. A back-coupling term (the $b_{111}^{(n)}$-term) should be nonzero, this will cause initial excitation of mode n through excitation of the first mode.

Section B.1 has shown that the continuous cross-sectional strings do not posses all these requirements, since its frequency ratios are integer. It was previously shown that a system that is represented by the w-displacement model with non-integer frequency ratios may show FPUT behavior; this model is only valid for resonators for which it is safe to ignore the longitudinal displacements. Experimental results have however shown that it is likely that this w-displacement model is not entirely accurate for the considered string resonators; from a mechanics point of view, it is sensible to include the longitudinal displacements of a system. Hence, a method should be sought that can generate the required modal coupling coefficients and frequency ratios for a system that *does* include longitudinal displacements. This section will therefore -numerically- show which methods may be employed to design a resonator that will generate such coefficients. The origin of the nonzero back-coupling coefficients was shown in Section B.7, it essentially depends on the mode shape and the nonlinear displacement formulation. The mode shapes of these resonators may be easily changed by local variance of the cross-sectional area of the string. The next section will show some theories on improvement of the nonlinearity in literature.

C.2.2. Literature - improvement of the nonlinearity of beam resonators

Several studies (e.g. those by Dou and Li [9, 18]) have shown that the Duffing nonlinearity of clamped-clamped beam resonators may be enhanced by local variance of the beams' geometries. Dou and Li found that the nonlinearity of a constant cross-sectional area beam (Fig. C.5a) could be improved by locally increasing the beam's thickness, specifically at approximately 0.25L and 0.75L (Fig. C.5b). Oppositely, by decreasing the thickness at certain locations (Fig. C.5c), the Duffing nonlinearity can be decreased. The results of these iterations show that the resonance frequency decreases with increasing nonlinearity and vice versa. Li has experimentally validated the results for Dou's designs, showing that by locally varying the thickness, one may tune the resonators behavior: one may increase the size of the linear regime by decreasing the magnitude of the nonlinearity and vice versa for a smaller linear regime [18]. The design optimization was constrained through a condition on the frequency ratios, which was set to remain close to the (integer) internal resonance conditions.

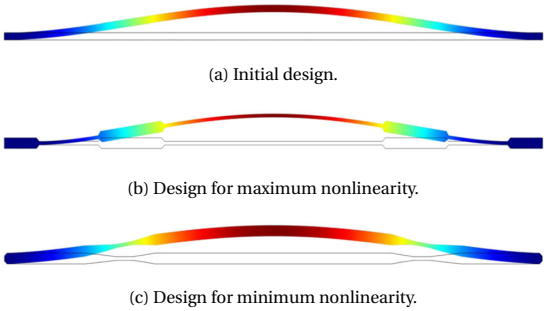

(a) Initial design.

(b) Design for maximum nonlinearity.

(c) Design for minimum nonlinearity.

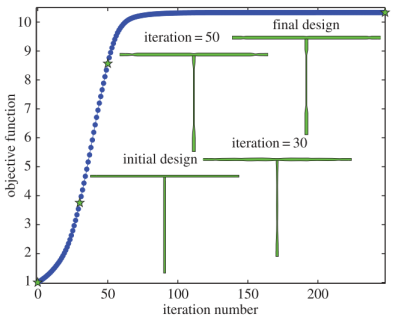

(d) Design for maximum modal coupling.

Figure C.5: Four designs which have been analysed for their nonlinear behavior. C.5a-C.5c depict three designs for clamped-clamped beam structures which have been designed for a certain Duffing nonlinearity. C.5a depicts the initial design, C.5b shows a design for maximum nonlinearity and C.5c shows a design for minimum nonlinearity. C.5d depicts the results of the iterations to find the strongest coupling between two modes (which are in 2:1 IR) of the T-structure. Adopted from [18].

The coupling terms of these improved clamped-clamped beam structures are not reported. However, Li does report a modal coupling optimization scheme for a T-structure (Fig. C.5d). This optimization is focused on the coupling between two modes, and it is sought for the condition where these modes are in 2:1 internal resonance. Fig. C.5d depicts initial and final designs; the latter was found to have the largest modal coupling. This structure is claimed to have a quadratic (passive back-)coupling term ($a_{11}^{(2)}$). This $a_{11}^{(2)}$-term passively excites mode 2 through excitation of mode 1. This method may be employed to find structures that display FPUT behavior. However, the nonlinearity should be cubic for the FPUT β-model (and, through the theory of resonant terms, the coupled mode should be located at mode 3). Regardless, this T-structure may be tested to see if it replicates FPUT behavior that is similar to the FPUT α-model.
It is important to note here that the studies by Dou and Li are based on beam elements, which account for more strain formulations (e.g. mid-plane stretching and bending) than the truss-structures in the current research [9, 18]. This assumption may be valid for the dimensions and pre-stress of the present structures. The next sections will first attempt to verify (using the STEP method) the results form Figures C.5a and C.5b, before attempting more complex geometries.

C.2.3. Limitations of the STEP method

Before attempting to verify the results from Dou and Li using STEP, it is paramount to first characterize the limitations of this method.
The STEP method allows for rapid computation of the modal variables for various designs. The system has

shown to work for strings (including longitudinal and transverse displacements), square and circular membranes, fully clamped plates and cantilevers. The STEP method (in its present form) may thus be used for fully constrained systems, such as the fully clamped strings and membranes/plates which are clamped on all sides.
The STEP method produces reliable results for (continuous) strings: the linear as well as nonlinear variables agree very well with the analytical (uw- and uvw-displacement) models. However, these string systems are modelled based on some assumptions. The first is that the cross-section of the string is assumed to be constant and square. For the Si_3N_4 resonators that are considered in the present study, this is not the case, but this model generated sufficient agreement with experiments on continuous strings, since the axial deformation is assumed to be the governing displacement model. A string-like resonator with non-integer frequency ratios may be generated by varying the cross-sectional area along the length of the string (i.e. by making the string's cross-sectional area discontinuous).
Such designs would be most sufficiently represented by a model that includes the non-uniform tension along the length of the string. Plate deformation models allow for such non-uniform tension due to the inclusion of additional displacement directions in the strain formulation, causing an inhomogeneous stress distribution along the width of the resonator [15]. However, the present STEP software does not allow for this, as the prescribed displacements of plates (clamped on 2 edges) are not sufficiently constrained, generating incorrect displacements and subsequently incorrect coupling coefficients. The modelling method is hence restricted to the use of truss models (which account only for axial deformations due to a displacement), for systems which are pinned at each end.
Such a discontinuous cross-sectioned string may however be modelled through discretization of string models. This discetization entails that a single string is divided into multiple string elements, where the cross-sectional area of each element may be varied. Fig. C.6 depicts a structure which consists of several cross-sections. The structure consists of 5 elements, of which three have dimensions L_1, w_1 and two have dimensions L_2 and w_2; the thickness is assumed to remain constant.

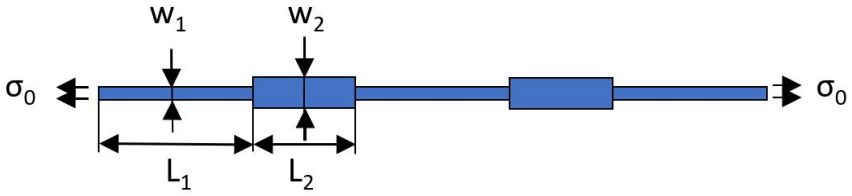

Figure C.6: A string design consisting of 5 elements, of which 3 have have dimensions L_1, w_1 and two have dimensions L_2 and w_2. The system is pre-stressed on the edges with a pre-stress of σ_0. The system has a constant thickness (into the paper) of t.

The pre-stress generates a force that is assumed to scale linearly with the the cross-sectional area ($A_i = tw_i$). This force is constant over the length of the resonator.

$$F_{pre} = \sigma_1 t w_1 = \sigma_0 t w_1 = \sigma_2 t w_2 \tag{C.16}$$

The thickness is constant, and σ_1 is equal to the pre-stress at the edges: $\sigma_1 = \sigma_0$. The constant force allows for computation of the pre-stress in the second element, as follows:

$$\sigma_2 = \sigma_0 \frac{t w_1}{t w_2} = \sigma_0 \frac{w_1}{w_2}. \tag{C.17}$$

This method allows one to check whether this method of locally varying a string's cross-sectional area can generate (1) shifted frequencies and (2) additional coupling coefficients. The next section will show how this is modelled using COMSOL.

C.2.4. Design method

The design from Fig. C.7 consists of 100 truss elements. It is assumed that the length and thickness of each of these elements is constant. The width of each element may be varied, generating a different cross-section and thus different stresses in these elements. Additionally, through this variance in the width, the mass and stiffness of each element is varied, which will influence the modal quantities. Tables E.11 and E.12 depict the

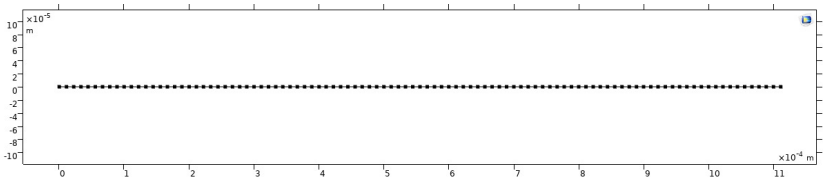

Figure C.7: A COMSOL model of a string design. The design consists of 100 elements (with constant length and width), the width may be varied per element.

linear and nonlinear modal coefficients, which show that there is some small (negligible) discrepancy with the continuous model (from Tables E.7 and E.8). In addition, there are some coefficients that are nonzero which should be zero, though their influence is assumed to remain small due to the small magnitudes of these coefficients with respect to the others; these terms are multi-mode coefficients, of which the effect will be negligible when the amplitude of one of these modes remains small.

Comparison of beam elements and truss elements

The present form of STEP cannot accurately replicate the results that were found by Dou, since it can only account for axial deformations in truss models. This simplification -from beam elements to truss elements- will probably result in different results, since some deformation mechanisms (e.g. mid-plane stretching due to bending) are neglected. However, the qualitative results from Dou and Li [9, 18], may be compared to those for truss models, to see whether this theory will still hold for systems that account only for axial deformations.

The designs from Li have considerably larger ratio of width versus thickness ($\frac{w}{t} = \frac{20\mu m}{6\mu m} = 3.33$ for Li, and $\frac{w}{t} = \frac{4\mu m}{92nm} \approx 40$ for the considered 1110μm string), generating much larger bending stiffness for Li's structures. Modelling these beam designs using truss elements would hence be very inaccurate. The present analysis will therefore compare the qualitative results of local variance of a systems cross-sectional area (i.e. beam elements versus string elements); this will generate insight on how the eigenfrequencies and Duffing nonlinearities change for string systems. Another difference is that Dou and Li vary the thickness, where for truss models, one should change the cross-sectional area, which is achieved in this (truss) analysis through variance of the width.

The resulting coefficients of several designs similar to those in Fig.'s C.5a, C.5b and C.5c are shown in Table C.6. All modal coefficients (up to the sixth mode) are shown in Sections E.3.1, E.3.2 and E.3.3, respectively.

Table C.6: Single mode coefficients for the first 3 vertical modes of a discretized string of 100 elements. The characteristics of the string are similar to Table C.4. The coefficients are tabulated for three designs: the default design (constant width), a design for increased width near the clamping points and at 0.25L and 0.75L (similar to Fig. C.5b, and $w_{\text{spring}} = 4\mu$m and $w_{\text{mass}} = 3w_{\text{spring}} = 12\mu$m) and a design for decreased width near at 0.25L and 0.75L (similar to Fig. C.5c and $w_{\text{spring}} = 4\mu$m and $w_{\text{mass}} = \frac{1}{3}w_{\text{spring}} = 1.33\mu$m.). The coefficients were found using STEP.

Design	Default (const. width)			Max			Min		
Eq.	**(1)**	**(2)**	**(3)**	**(1)**	**(2)**	**(3)**	**(1)**	**(2)**	**(3)**
k_n [s^{-2}]	1.32×10^{12}	5.26×10^{12}	1.18×10^{13}	2.55×10^{12}	7.34×10^{12}	2.24×10^{13}	1.57×10^{12}	8.03×10^{12}	1.66×10^{13}
ω_n [rads^{-1}]	1.15×10^{6}	2.29×10^{6}	3.44×10^{6}	1.60×10^{6}	2.71×10^{6}	4.73×10^{6}	1.25×10^{6}	2.83×10^{6}	4.08×10^{6}
b_{nnn} [ms^{-2}]	2.05×10^{33}	3.27×10^{34}	1.66×10^{35}	1.17×10^{33}	9.66×10^{33}	9.01×10^{34}	1.83×10^{33}	4.80×10^{34}	2.05×10^{35}
$\frac{b^{(n)}_{nnn}}{k_n}$ [m]	1.55×10^{21}	6.22×10^{21}	1.41×10^{22}	4.59×10^{20}	1.32×10^{21}	4.02×10^{21}	1.17×10^{21}	5.98×10^{21}	1.23×10^{22}
$\tilde{k}_n$	1.00	4.00	9.00	1.00	2.88	8.78	1.00	5.11	10.58
$\tilde{\omega}_n$	1.00	2.00	3.00	1.00	1.70	2.96	1.00	2.26	3.25
$\tilde{b}_{nnn}$	1.00	16.00	80.98	1.00	8.26	76.97	1.00	26.17	111.95

The modal coefficients of the string designs based on local in- or decrease of the cross-sectional area are shown in Tables E.13 and E.15. Clearly, these string-like structures do not follow the same trend as beam structures: locally increasing or decreasing the width results in higher frequencies than the default model. The nonlinearity of the first mode is decreased as well, for both designs. The linear frequency ratios appear to decrease with a local increase of the width, and vice versa. The ratios of the Duffing coefficients follow the same trend, and the relative nonlinearity ($\frac{b^{(n)}_{nnn}}{k_n}$) also decreases with the variance of the dimensions. The effect of the coupling coefficients, which may be found by comparison of Tables E.12, E.14 and E.16, is small. Some parameters slightly increase, where some slightly decrease. It is however clear that the coupling coefficients

(especially those of the higher modes) increase the most trough the local decrease in width. However, the $b^{(3)}_{111}$-term is zero for all designs, implying that these designs do not generate coupling terms that can generate FPUT behavior.

Zipper-like designs

Another method that may be (numerically) tested is a zipper-like design. This design is similar to what is depicted in Fig. C.6, but it may contain more thin (referred to as string elements) and thick (referred to as mass elements) elements, generating a chain of such elements. This system replicates the (hypothetical) FPUT system trough the alternating spring-mass elements, which represents a discretized string. An example of such a zipper-like design is depicted in Fig. C.8. This design consists of 16 masses (each mass consists of 2 elements of width w_{mass}) and 17 springs (here, each of these strings consists of 4 elements of width w_{spring}). Two designs were tested: one with $w_{\text{spring}} = 4\mu$m and $w_{\text{mass}} = 4w_{\text{spring}} = 16\mu$m and another with a larger mass width: $w_{\text{spring}} = 4\mu$m and $w_{\text{mass}} = 10w_{\text{spring}} = 40\mu$m. The single-mode coefficients of each iteration are tabulated in Table C.7.

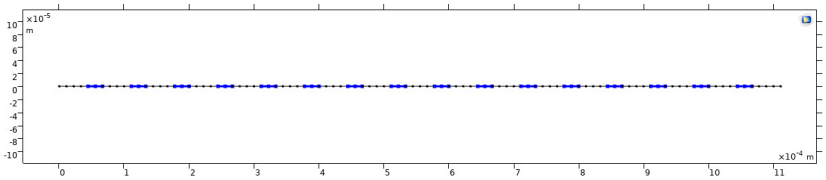

Figure C.8: A string design in COMSOL. The design consists of 100 elements (with constant length and width). The black elements are the spring elements with w_{spring} and the blue elements have width w_{mass}. All other design characteristics are similar to Table C.4.

Table C.7: Single mode coefficients for the first 3 vertical modes of a discretized string of 100 elements. The coefficients are tabulated for two zipper-like designs: a design $w_{\text{spring}} = 4\mu$m and $w_{\text{mass}} = 4w_{\text{spring}} = 16\mu$m) and a for $w_{\text{spring}} = 4\mu$m and $w_{\text{mass}} = 10w_{\text{spring}} = 40\mu$m.). All other design characteristics are similar to Table C.4. The coefficients were found using STEP.

Design	$w_{\text{mass}} = 4w_{\text{spring}}$			$w_{\text{mass}} = 10w_{\text{spring}}$		
Eq.	**(1)**	**(2)**	**(3)**	**(1)**	**(2)**	**(3)**
k_n [s^{-2}]	6.57×10^{11}	2.63×10^{12}	5.90×10^{12}	3.29×10^{11}	1.31×10^{12}	2.94×10^{12}
ω_n [rads^{-1}]	8.11×10^{5}	1.62×10^{6}	2.43×10^{6}	5.73×10^{5}	1.14×10^{6}	1.71×10^{6}
b_{nnn} [ms^{-2}]	6.72×10^{32}	1.07×10^{34}	5.41×10^{35}	1.79×10^{32}	2.85×10^{33}	1.43×10^{34}
$\frac{b^{(n)}_{nnn}}{k_n}$ [m]	1.02×10^{21}	4.07×10^{21}	9.17×10^{22}	5.44×10^{20}	2.19×10^{21}	4.86×10^{21}
$\tilde{k}_n$	1.00	4.00	8.97	1.00	3.99	8.94
$\tilde{\omega}_n$	1.00	2.00	3.00	1.00	2.00	2.99
$\tilde{b}_{nnn}$	1.00	15.96	80.48	1.00	15.92	79.92

The results are shown in Tables E.17, E.18, E.19 and E.20 which indicate that the linear frequencies ratios have not changed much: they have only decreased for a couple per cents. The same is visible for the ratios of the nonlinear coupling coefficients: the influence is hence very small; they are close to those of a constant width design.

These two designs show that the zipper-like designs with 16 mass elements of width w_{mass} and 17 spring elements of width w_{spring} do not have a significant influence on the modal parameter ratios. The linear variables seem to decrease with an increase width of the masses, which tends to the required non-integer frequency ratios for the default FPUT system. However, the effect on the nonlinear coefficients is small: the coefficients hardly change with respect to those of a continuous cross-sectioned string. The reason behind this small effect may be that the mode shapes of such resonators remain fairly similar to those of continuous strings, which will generate modal variables that are similar to those of continuous strings. The mass and stiffness are uniformly distributed over the length of the string, which generates symmetrical mode shapes. Appendix B.7 shows that the origin of the coupling is in the displacement formulation, which in turn generates coupling terms from the nonlinear displacement formulations. These nonlinear displacement formulations depend on the shape of each mode, where symmetry along the length of the mode shapes may result in zero coupling coefficients. Theoretically, by tuning the shapes of the modes, one should thus be able to generate different coupling coefficients. These mode shapes may be tuned by introducing asymmetry to the system, by inhomogeneously distributing the mass or stiffness over the length of the string. This may be achieved by locally increasing the number of "mass" elements, as will be shown in the next section.

Asymmetric designs

An asymmetrical mode shape may be generated by inhomogeneously distributing the mass (or stiffness) along the length of the string. Fig. C.9a depicts such a design, where (from left to right) the first 10 elements have width w_{spring}, the following 30 elements have width w_{mass}, and the last 60 elements have width w_{spring}. The mode shapes are shown in C.9b to C.9g. The mode shapes clearly show asymmetry.

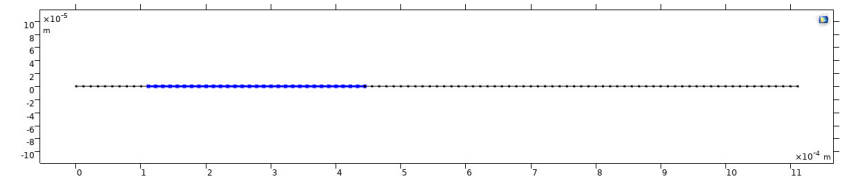

(a) Asymmetrical string design.

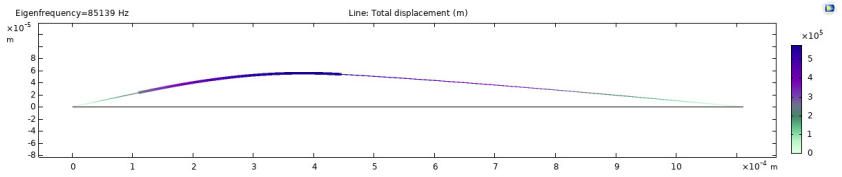

(b) First mode shape.

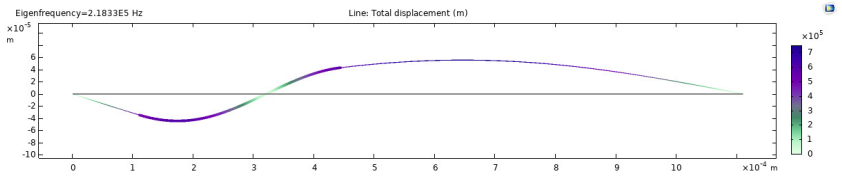

(c) Second mode shape.

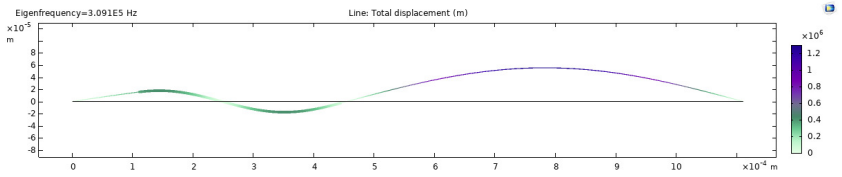

(d) Third mode shape.

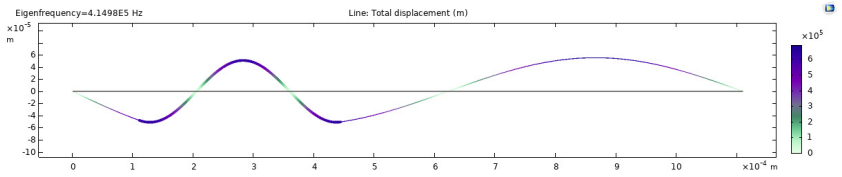

(e) Fourth mode shape.

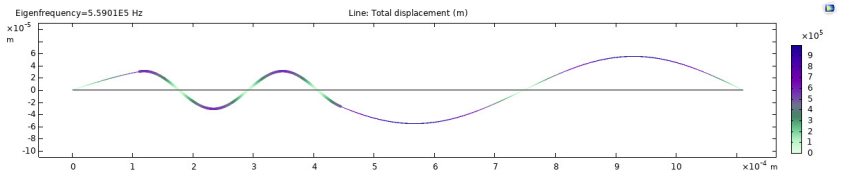

(f) Fifth mode shape.

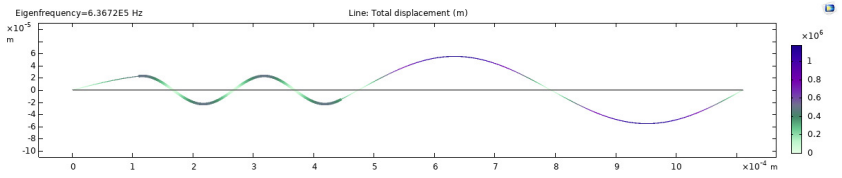

(g) Sixth mode shape.

Figure C.9: Design and mode shapes of an asymmetrical string design. C.9a depicts a design where the black elements (the first 10 from the left and the last 60 elements from the right) have width $w_{\text{spring}} = 4\mu$m, elements 11 to 40 (in blue) have width $w_{\text{mass}} = 40\mu$m. All other design characteristics are similar to Table C.4.

Table C.8: Linear stiffness and Duffing coefficients for the first 6 modes of an asymmetrical discretized string of 100 elements from Fig. C.9. The coefficients were found using STEP. $w_{\text{spring}} = 4\mu$m and $w_{\text{mass}} = 40\mu$m. All other design characteristics are similar to Table C.4.

Eq.	**(1)**	**(2)**	**(3)**	**(4)**	**(5)**	**(6)**
k_n [s^{-2}]	2.86×10^{11}	1.88×10^{12}	3.77×10^{12}	6.80×10^{12}	1.23×10^{13}	1.60×10^{13}
ω_n [rad s^{-1}]	5.35×10^{5}	1.37×10^{6}	1.94×10^{6}	2.61×10^{6}	3.51×10^{6}	4.00×10^{6}
b_{nnn} [m^{-2}s^{-2}]	1.33×10^{32}	5.75×10^{33}	2.30×10^{34}	7.52×10^{34}	2.47×10^{35}	4.15×10^{35}
$\frac{b_{nnn}^{(n)}}{k_n}$ [m]	4.65×10^{20}	3.06×10^{21}	6.10×10^{21}	1.11×10^{22}	2.01×10^{22}	2.59×10^{22}
$\tilde{k}_n$	1.00	6.58	13.18	23.76	43.11	55.93
$\tilde{\omega}_n$	1.00	2.56	3.63	4.87	6.57	7.48
$\tilde{b}_{nnn}$	1.00	43.32	173.50	566.05	1860.76	3127.26

The results of the STEP analysis of this design are tabulated in Tables C.8, E.21 and E.22. These indicate that the linear stiffness (and hence the linear resonance frequencies) have dropped to non-integer ratios. The relative nonlinearity has increased significantly with respect to the mode number, showing that the (relative) nonlinearity of a mode may in fact be engineered in this manner. However, though most of the modal coupling coefficients have increased, none of the $b_{111}^{(n)}$-coefficients are nonzero for $n > 0$. It is hence likely that these coefficients generate little initial energy transfer, which reduce the likelihood of observing FPUT behavior for these structures.

C.2.5. Conclusion

This section showed that through variance of the cross-sectional area of string-like systems, one may tune the frequency ratios, tune the (Duffing) nonlinearity of especially the higher modes while the coupling ratios hardly improve. Nonetheless, the method that is employed here is far from perfect, as it is limited to string-like resonators, which can be modelled by truss elements only. This implies that deformations of these systems only generate axial deformation in the resonator, while in reality, much more displacement mechanisms may be present. Expansion of this method is thus necessary, such that all possible displacements are accounted for in the computation of the modal variables. Dou and Li found that a structure consisting of two perpendicular beams may also have nonzero quadratic back-coupling coefficients [9, 18]. This STEP method should be expanded to work for such designs as well. Lastly, since the possibilities for geometries are endless, a topology optimization or machine learning algorithm could be linked to the STEP software, such that the modal coefficients of each design may be efficiently analysed. Such study would have several constraints, among which two should be as follows: (1) the frequency ratios of the system should be non-integer (and lower than the mode number) and (2) the method should find nonzero back-coupling coefficients.

D

Methods

This section will elaborate on some of the methods that are employed in this research, these consist of numerical methods, analytical (scaling) methods and numerical simulations. The numerical methods will first elaborate upon a method which is used to determine the modal coefficients: the STEP method. Subsequently, the resulting numerical integration methods are shown, which allow for solving of the differential equations and subsequent analysis of the resulting dynamics. Three clear distinctions in the integration methods may be made: (1) frequency characterization, (2) forced vibrations and (3) free vibrations (ringdown). All three methods -though somewhat similar- will be explained in this section. The analytical methods will show some scaling methods, which are used for further analyses. The last section will highlight the procedure for numerical simulation of experimental results.

D.1. Numerical methods

D.1.1. Numerical determination of the modal coefficients

Nonlinear effects may become visible in structures if a (large-amplitude) out-of-plane displacement is applied to this structure. A (geometric) nonlinearity becomes apparent in the fact that the imposed out-of-plane displacement does not only result in an vertical (out-of-plane) deformation, rather it also shows deformation in a plane perpendicular to this out-of-plane displacement: the longitudinal (in-plane) direction. A common -though simple- example is that of applying a transverse load to an elastic band: here, the band will deflect in the transverse (out-of-plane) direction, but it will also show some deformation in the longitudinal (in-plane) direction. Now, if we would consider a linear model, where all displacements follow a linear relationship, we cannot capture this effect; the system should be expanded to higher orders to find an equation that suits this (nonlinear) behavior sufficiently. The dynamics of a resonator may be approximated by the following modal equations of motion, if two modes are considered and the nonlinearity is approximated up to third order:

$$\begin{aligned} &\ddot{q}_1 + k_1^{(1)} q_1 + a_{11}^{(1)} q_1^2 + a_{12}^{(1)} q_1 q_2 + a_{22}^{(1)} q_2^2 + b_{111}^{(1)} q_1^3 + b_{112}^{(1)} q_1^2 q_2 + b_{122}^{(1)} q_1 q_2^2 + b_{222}^{(1)} q_2^3 = F^{(1)} \\ &\ddot{q}_2 + k_2^{(2)} q_2 + a_{11}^{(2)} q_1^2 + a_{12}^{(2)} q_1 q_2 + a_{22}^{(2)} q_2^2 + b_{111}^{(2)} q_1^3 + b_{112}^{(2)} q_1^2 q_2 + b_{122}^{(2)} q_1 q_2^2 + b_{222}^{(2)} q_2^3 = F^{(2)}. \end{aligned} \tag{D.1}$$

The coefficients of these equations can be found using two methods: analytical and numerical methods. The former method is quite an intensive process, as it requires solving lengthy equations, as was shown in B. Furthermore, to reduce complexity of the equations, the analytic method is limited to continuous or constant cross-section geometries. If one would try to build an analytic model that accounts for discontinuities in e.g. the cross-section of the structure, the model will quickly become complicated. The numerical models could make use of finite element methods (FEM) to determine the nonlinear stiffness of the structures. Muravyov and Rizzi presented a method, the STiffness Evaluation Procedure (STEP), to find the nonlinear coefficients of the modal equations of motion for any structure using FEM-software [22]. The following citation of Muravyov and Rizzi's article accurately portrays how this method works:

> "The equations of motion of a multiple degree-of-freedom, viscously damped geometrically non-

linear system can be written in the form:

$$\mathbf{M}\ddot{\mathbf{X}}(t) + \mathbf{C}\dot{\mathbf{X}}(t) + \mathbf{K}\mathbf{X}(t) + \Gamma(X(t)) = \mathbf{F}(t) \tag{D.2}$$

where **M**, **C**, **K** are the mass, proportional damping, and linear stiffness matrices, respectively, and **X** is the displacement response vector and **F** is the force excitation vector. For the problems of interest, the nonlinear stiffness force vector $\Gamma(\mathbf{X})$ represents a deviation from the linear stiffness force vector **KX** and is more than adequately represented by second and third order terms in $\mathbf{X}(t)$. When displacements are small, the second and third order terms become negligible and the total stiffness- related force vector is reduced to the regular linear term $\mathbf{K}\mathbf{X}(t)$. Solution to Eq. (1) via any method requires knowledge of the system matrices. In the context of a commercial finite element program, **M**, **C**, **K** are generally available. The nonlinear stiffness is related to Γ, which is typically not available within a commercial finite element program. Therefore, a means of numerically evaluating Γ to determine the nonlinear stiffness was developed. A set of coupled modal equations with reduced degrees- of-freedom is first obtained by applying the modal coordinate transformation

$$\mathbf{X} = \Phi\mathbf{q} \tag{D.3}$$

to Eq. (1), where Φ is the eigenvectors obtained from (1) without Γ, q is the vector of modal coordinates, and the time dependence is implied. Generally, a subset of L eigenvectors are included in the solution such that ($L \leq N$), and N is the number of physical degrees of freedom. In the SI system, Φ has units of [m]; **q** is non-dimensional

This coupled set is expressed as

$$\tilde{\mathbf{M}}\ddot{\mathbf{q}} + \tilde{\mathbf{C}}\dot{\mathbf{q}} + \tilde{\mathbf{K}}\mathbf{q} + \gamma(q_1, q_2, ..., q_L) = \tilde{\mathbf{F}} \tag{D.4}$$

where

$$\begin{aligned} \tilde{\mathbf{M}} &= \Phi^T\mathbf{M}\Phi = [\mathbf{I}] \\ \tilde{\mathbf{C}} &= \Phi^T\mathbf{C}\Phi = [2\zeta_r\omega_r] \\ \tilde{\mathbf{K}} &= \Phi^T\mathbf{K}\Phi = [2\zeta_r\omega_r] \\ \gamma &= \Phi^T\Gamma \\ \tilde{\mathbf{F}} &= \Phi^T\mathbf{F} \end{aligned} \tag{D.5}$$

$q_1, q_2, ..., q_L$ are the components of **q**, and ω_r are the undamped natural frequencies. In the SI system, entries of $\tilde{\mathbf{M}}$ have units of [Nms^2], entries of $\tilde{\mathbf{C}}$ have units of [Nms], and entries of $\tilde{\mathbf{K}}$, γ and $\tilde{\mathbf{F}}$ have units of [Nm]. By writing the nonlinear force vector in the form

$$\gamma_r(q_1, q_2, ..., q_L) = \sum_{j=1}^{L}\sum_{k=j}^{L} a_{jk}^r q_j q_k + \sum_{j=1}^{L}\sum_{k=j}^{L}\sum_{l=k}^{L} b_{jkl}^r q_j q_k q_l,\ r = 1, 2, ..., L \tag{D.6}$$

the problem of determining the nonlinear stiffness is reduced from one in which a large set of simultaneous nonlinear equations must be solved to one involving simple algebraic relations, as will be subsequently shown. This form is sufficient for characterizing the type of nonlinearity of interest in this paper and facilitates the subsequent solution of the equivalent linear system. Its evaluation entails solving for the coefficients a_{jk} and b_{jkl} using a new procedure developed for use with finite element programs having a nonlinear static solution capability. The procedure is based on the restoration of nodal applied forces by prescribing nodal displacements in both linear and nonlinear static solution settings. The total nodal force $\mathbf{F_T}$ may be written in physical coordinates as

$$\mathbf{F_T} = \mathbf{F_L} + \mathbf{F_{NL}} = \mathbf{K}\mathbf{X_c} + \Gamma(\mathbf{X_c}) \tag{D.7}$$

where $\mathbf{X_c}$ is a prescribed physical nodal displacement vector, and $\mathbf{F_L}$ and $\mathbf{F_{NL}}$ are the linear and nonlinear contributions to the total nodal force. Note that when displacements $\mathbf{X_c}$ are small, the nodal force vector is approximated by a regular linear term $\mathbf{F_L} = \mathbf{K}\mathbf{X_c}$, since nonlinear terms become negligible. $\mathbf{F_L}$ is first obtained by prescribing $\mathbf{X_c}$ in the linear static solution. $\mathbf{F_T}$ is then

obtained by prescribing $\mathbf{X_c}$ in the nonlinear static solution. Finally, the nonlinear contribution FNL is obtained by subtracting $\mathbf{F_L}$ from $\mathbf{F_T}$, or

$$\mathbf{F}_{NL} = \Gamma(\mathbf{X_c}) = \mathbf{F_T} - \mathbf{F_L} \tag{D.8}$$

To illustrate the technique, one can begin by prescribing the displacement fields

$$\begin{aligned} \mathbf{X_c} &= +\phi_1 q_1 \\ \mathbf{X_c} &= -\phi_1 q_1 \end{aligned} \tag{D.9}$$

The nonlinear nodal force contributions $\mathbf{F_{NL}}$ are determined using (7) after solving the linear and nonlinear static solutions. These may be written in modal coordinates as

$$\begin{aligned} \tilde{\mathbf{F}}_{NL_1} &= \Phi^T \mathbf{F}_{NL_1} = \Phi^T \gamma(+\phi_1 q_1) = [a^r_{11}] q_1 q_1 + [b^r_{111}] q_1 q_1 q_1 \\ \tilde{\mathbf{F}}_{NL_2} &= \Phi^T \mathbf{F}_{NL_2} = \Phi^T \gamma(-\phi_1 q_1) = [a^r_{11}] q_1 q_1 - [b^r_{111}] q_1 q_1 q_1 \end{aligned} \tag{D.10}$$

where the sought stiffness coefficients $[a^r_{11}]$ and $[b^r_{111}]$ are vectors of length L. Note that the other nonlinear terms do not appear in (9) since $q_j = 0$ for $j \neq 1$. Since q_1 is a known scalar, the coefficients $[a^r_{11}]$ and $[b^r_{111}]$ for $r = 1,2,...,L$ can be determined from the resulting system (9) of $2 \times L$ linear equations. The remaining coefficients $[a^r_{jj}]$ and $[b^r_{jjj}]$ for $j = 2,3,...,L$ can be determined in an analogous manner. A similar technique can be employed to determine stiffness coefficients with two unequal lower indices, e.g. $[a^r_{12}]$, $[b^r_{112}]$ and $[b^r_{122}]$. Coefficients of this type appear only if the number of retained eigenvectors is greater than or equal to two ($L \geq 2$). Prescribing the displacement fields

$$\begin{aligned} \mathbf{X_c} &= +\phi_1 q_1 + \phi_2 q_2 \\ \mathbf{X_c} &= -\phi_1 q_1 - \phi_2 q_2 \\ \mathbf{X_c} &= +\phi_1 q_1 - \phi_2 q_2 \end{aligned} \tag{D.11}$$

results in the following equations

$$\begin{gathered} \tilde{\mathbf{F}}_{NL_1} = \Phi^T \Gamma(+\phi_1 q_1 + \phi_2 q_2) = \\ [a^r_{11}] q_1 q_1 + [b^r_{111}] q_1 q_1 q_1 + [a^r_{22}] q_2 q_2 + [b^r_{222}] q_2 q_2 q_2 + [a^r_{12}] q_1 q_2 + [b^r_{112}] q_1 q_1 q_2 + [b^r_{122}] q_1 q_2 q_2 \\ \tilde{\mathbf{F}}_{NL_2} = \Phi^T \Gamma(-\phi_1 q_1 - \phi_2 q_2) = \\ [a^r_{11}] q_1 q_1 - [b^r_{111}] q_1 q_1 q_1 + [a^r_{22}] q_2 q_2 - [b^r_{222}] q_2 q_2 q_2 + [a^r_{12}] q_1 q_2 - [b^r_{112}] q_1 q_1 q_2 - [b^r_{122}] q_1 q_2 q_2 \\ \tilde{\mathbf{F}}_{NL_3} = \Phi^T \Gamma(+\phi_1 q_1 - \phi_2 q_2) = \\ [a^r_{11}] q_1 q_1 + [b^r_{111}] q_1 q_1 q_1 + [a^r_{22}] q_2 q_2 - [b^r_{222}] q_2 q_2 q_2 - [a^r_{12}] q_1 q_2 - [b^r_{112}] q_1 q_1 q_2 + [b^r_{122}] q_1 q_2 q_2 \end{gathered} \tag{D.12}$$

Summing the first two of Eq. (11) results in

$$\tilde{\mathbf{F}}_{NL_1} + \tilde{\mathbf{F}}_{NL_2} = 2[a^r_{11}] q_1 q_1 + 2[a^r_{22}] q_2 q_2 + 2[a^r_{12}] q_1 q_2 \tag{D.13}$$

from which the coefficients $[a^r_{12}]$ may be determined, since $[a^r_{11}]$ and $[a^r_{22}]$ were previously found. Then, from the first and third of Eq. (11), the coefficients $[b^r_{112}]$ and$[b^r_{122}]$ may be determined from the $2 \times L$ system of equations. In this manner, all coefficients of the type $[b^r_{jjk}]$ and $[b^r_{kkj}]$ for $j,k = 1,2,...,L$ may be found. For cases when the number of retained eigenvectors if greater than or equal to three ($L \geq 3$), coefficients with three unequal lower indices, e.g. $[b^r_{123}]$, may be determined by prescribing the displacement field

$$\mathbf{X_c} = +\phi_1 q_1 + \phi_2 q_2 + \phi_3 q_3 \tag{D.14}$$

The resulting equation

$$\begin{gathered} \tilde{\mathbf{F}}_{NL} = \phi^T \Gamma(+\phi_1 q_1 + \phi_2 q_2 + \phi_3 q_3) = \\ [a^r_{11}] q_1 q_1 + [a^r_{22}] q_2 q_2 + [a^r_{33}] q_3 q_3 + [a^r_{12}] q_1 q_2 + [a^r_{13}] q_1 q_3 + [a^r_{23}] q_2 q_3 + [b^r_{111}] q_1 q_1 q_1 + \\ [b^r_{222}] q_2 q_2 q_2 + [b^r_{333}] q_3 q_3 q_3 + [b^r_{112}] q_1 q_1 q_2 + [b^r_{221}] q_2 q_2 q_1 + [b^r_{113}] q_1 q_1 q_3 + [b^r_{331}] q_3 q_3 q_1 + \\ [b^r_{223}] q_2 q_2 q_3 + [b^r_{332}] q_3 q_3 q_2 + [b^r_{123}] q_1 q_2 q_3 \end{gathered} \tag{D.15}$$

contains one column of unknown coefficients $[b^r_{123}]$. All coefficients of type $[b^r_{jkl}] (j \neq k \neq l)$ can be found in this manner."

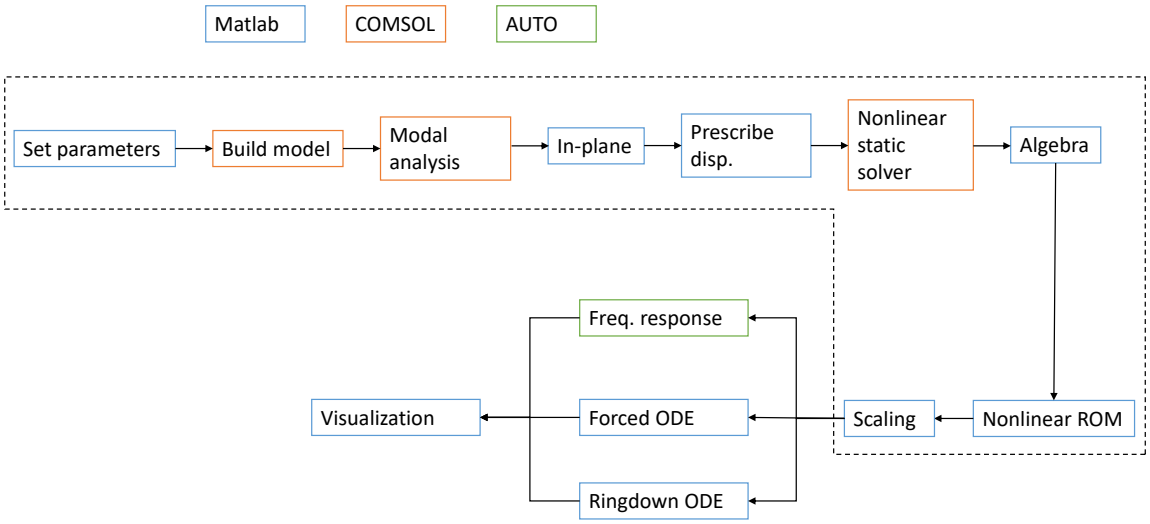

Figure D.1: Method for numerical analysis of the modal equations of motion. The dashed box is the STEP method. The subsequent steps are elaborated in the next section.

Eventually, the coefficients of the following mass-normalized nonlinear reduced order model (ROM) -of N modes- are found:

$$\ddot{q}_r + k_r^{(r)} q_r + \sum_{j=1}^{N} \sum_{k=j}^{N} a_{jk}^{(r)} q_j q_k + \sum_{j=1}^{N} \sum_{k=j}^{N} \sum_{l=k}^{L} b_{jkl}^{(r)} q_j q_k q_l = 0, \; r = 1,2,...,N \tag{D.16}$$

This method was implemented by Vincent Bos, a former DMN student, who built software which combines both Matlab and COMSOL Multiphysics. The software operates according to the flowchart in Fig. D.1.

The "in-plane" block indicates in what method the in-plane (longitudinal direction) modes are included in the model. Here, static condensation is used. This static condensation basically implies that the in-plane displacement direction is left free, such that the solver can search for an equilibrium position where the in-plane forces result in a small potential energy. This is quite an efficient procedure, as it only explicitly solves for the out-of-plane modes [5]. A more complicated procedure would be to explicitly include in-plane modes in the model, but this will significantly increase computation time.

This STEP method is employed on string models in COMSOL. These string models are built using COMSOL's truss physics, which account only for axial forces. The downsides of this method are as follows:

- The cross-sectional area of the model is assumed to be square or circular;
- Complicated displacement phenomena, such as bending or shear in the system are neglected. These will become more dominant with larger cross-sectional areas. Truss elements will have a constant stress distribution in the vertical and transverse directions;
- The resonator's boundary conditions are simply supported, where it would probably be more fit to model the system with clamped-clamped boundary conditions.

D.1.2. Vibration simulation schemes

Three simulation schemes are employed in this thesis: (1) frequency response simulations, (2) forced oscillation simulations and (3) free oscillation simulations (ringdown). Generally, each of these three methods solves the following equations of motion. Here, each method is based on a free parameter:

$$m^{(r)}\ddot{q}_r(t)+k^{(r)}q_r(t)+c^{(r)}\dot{q}_r(t)+\sum_{j=1}^{N}\sum_{k=1}^{N}a_{jk}^{(r)}q_j(t)q_k(t)+\sum_{j=1}^{N}\sum_{k=j}^{N}\sum_{l=k}^{N}b_{jkl}^{(r)}q_j(t)q_k(t)q_l(t)=F^{(r)}\sin(\omega_f t),\ r=1,2,...,N. \tag{D.17}$$

Where r denotes the mode number of the equation of motion: this ranges from 1 to the total amount of modes that are considered in the simulation: N. The variables $m^{(r)}$, $k^{(r)}$, $c^{(r)}$ and $F^{(r)}$ denote the modal mass, stiffness, damping and force coefficients. The nonlinear variables, $a_{jk}^{(r)}$ and $b_{jkl}^{(r)}$ denote the quadratic and cubic nonlinear modal coefficients of the equation. The $\sin(\omega_f t)$-term generates a harmonic excitation of the system, at forcing frequency ω_f. The degrees of freedom (the modal coordinates), are denoted by $q_r(t)$- and $q_j(t)$-, $q_k(t)$- and $q_l(t)$-terms. To generate shorter notations, the time dependency of these coordinates is not written down.

$$m^{(r)}\ddot{q}_r+k^{(r)}q_r+c^{(r)}\dot{q}_r+\sum_{j=1}^{N}\sum_{k=1}^{N}a_{jk}^{(r)}q_jq_k+\sum_{j=1}^{N}\sum_{k=j}^{N}\sum_{l=k}^{N}b_{jkl}^{(r)}q_jq_kq_l=F^{(r)}\sin(\omega_f t),\ r=1,2,...,N \tag{D.18}$$

Frequency response simulation

The frequency response of Eq. D.18 is simulated in AUTO, a powerful differential equation solver which generates periodic solutions which also allow for detection of bifurcations and continuation after such bifurcations.

This simulation consists of two sweeps: the force sweep and the frequency sweep. Initially, the force magnitude ($F^{(r)}$) is swept over a specified range of values (while the forcing frequency ω_f remains constant). Thereafter, the opposite is done: the force magnitude is kept constant while the forcing frequency is swept. The software subsequently calculates the modal responses for all N modes: $q^{(r)}$ for $r=1,2,...,N$. This generates amplitude versus frequency plots, which may be used to quantify the nonlinear behavior of resonators. These amplitude versus frequency plots depict the modal response to a certain (drive) frequency, which generate insight into both Duffing nonlinearity and modal coupling.

Forced oscillation simulations

The time evolution of forced oscillations may be monitored by solving Eq. D.18 for a constant force magnitude $F^{(r)}$. The results of this simulation are the modal amplitude and velocity over time. These simulations are conducted in Matlab, using the ODE45 solver, which may compute the solutions for non-stiff ODEs. The results from this method provide insight into the periodicity of the solution.

Free oscillation simulations

The time evolution of free oscillations (ringdown) may be monitored by solving Eq. D.18 for zero-force magnitudes, providing the time response of a system. The equation of motion that is solved here is hence as follows:

$$m^{(r)}\ddot{q}_r+k^{(r)}q_r+c^{(r)}\dot{q}_r+\sum_{j=1}^{N}\sum_{k=1}^{N}a_{jk}^{(r)}q_jq_k+\sum_{j=1}^{N}\sum_{k=j}^{N}\sum_{l=k}^{N}b_{jkl}^{(r)}q_jq_kq_l=0,\ r=1,2,...,N. \tag{D.19}$$

These simulations are also conducted using Matlab's ODE45 solver. This method is particularly relevant for studies on the decay of a system.

Simulation of forcing

The simulations of forced oscillations in this research are conducted for application of forces through base excitation. In experiments, this base excitation is generated by fixing (with tape) the chip (which contains the resonator) to a piezo-element. By applying a voltage to this piezo-element, a force is generated on the chip and is subsequently applied to the resonator. The force that is applied to the resonator through excitation of the chip is considered to be distributed homogeneously over the length of the resonator. The conversion from this distributed load to a modal force is shown in the following.

Consider a string of length L and a distributed force of $F_{\text{distr}}=\frac{F_{tot}}{L}$, as is depicted in Figure D.2.

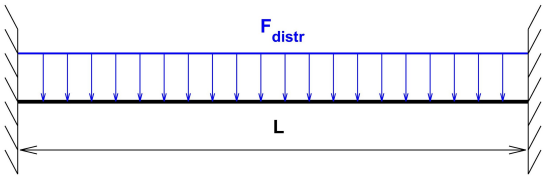

Figure D.2: Distributed force over a clamped-clamped string.

If the string is discretized over n elements, this will generate a distributed force vector $F_{d.n}$ of length n. Subsequently, to find the modal force (of mode r, $F^{(r)}$), one should multiply this distributed force vector of length n by the eigenvector (of length n) of the excited mode r:

$$F^{(r)} = \phi_{(r)}^T F_{d.n} \tag{D.20}$$

D.2. Equation scaling

D.2.1. Eigenvector scaling

Generally, there are two methods to express eigenvectors. The first method is to express the eigenvectors of mode n in terms of max-1 vectors (denoted by ϕ_{u_n}), the maximum magnitude ($\max(\phi_{u_n})$) of this vector is unity, making it particularly useful for analytical derivations (as was shown in Section B.1). The second method expresses the eigenvectors in terms of mass-normalized vectors ϕ_{m_n}, which generates a mass matrix for which the maximum is unity; this reduces the effort to solve the resulting equation.

To convert from one method to the other, it should be clear how each of the terms depend on any scaling parameters. This will will be shown in this section. The displacement is denoted by x and it is a function of the eigenvectors ϕ and the modal displacement q. This analysis is similar to that from Bos [5]. The displacements in terms of modal coordinates may be written as:

$$x = \phi_{u_n} q_{u_n} = \phi_{m_n} q_{m_n} \tag{D.21}$$

Where the relation between the two eigenvectors is as follows:

$$\phi_{m_n} = \alpha_n \phi_{u_n}. \tag{D.22}$$

The modal displacements (q_{u_n} and q_{m_n}) are thus related through this scaling parameter α as well:

$$q_{m_n} = \frac{q_{u_n}}{\alpha_n}. \tag{D.23}$$

The equation of motion (in matrix form) for the max-1 eigenvectors is written as:

$$\phi_{u_n}^T \mathbf{M} \phi_{u_n} \ddot{q}_{u_n} + \phi_{u_n}^T \mathbf{K} \phi_{u_n} q_{u_n} + \gamma_u(q_{u_j}, q_{u_k}, q_{u_l}) = \phi_{u_n}^T \mathbf{F} \tag{D.24}$$

Where the cubic nonlinear part of the equation -of which the nonlinear dependency on the eigenvectors is yet unknown- is written as $\gamma_u(q_{u_j}, q_{u_k}, q_{u_l})$. Substitution of equations D.22 and D.23 into Eq. D.24 gives the following equations:

$$\frac{1}{\alpha_n} \phi_{m_n}^T \mathbf{M} \phi_{m_n} \frac{1}{\alpha_n} \ddot{q}_{m_n} \alpha_n + \frac{1}{\alpha_n} \phi_{m_n}^T \mathbf{K} \phi_{m_n} \frac{1}{\alpha_n} q_{m_n} \alpha_n + \gamma_u(q_{m_j} \alpha_j, q_{m_k} \alpha_k, q_{m_l} \alpha_l) = \frac{1}{\alpha_n} \phi_{m_n}^T \mathbf{F} \tag{D.25}$$

$$\frac{1}{\alpha_n}\phi_{m_n}^T\mathbf{M}\phi_{m_n}\ddot{q}_{m_n}+\frac{1}{\alpha_n}\phi_{m_n}^T\mathbf{K}\phi_{m_n}q_{m_n}+\gamma_u(q_{m_j}\alpha_j,q_{m_k}\alpha_k,q_{m_l}\alpha_l)=\frac{1}{\alpha_n}\phi_{m_n}^T\mathbf{F} \tag{D.26}$$

$$\phi_{m_n}^T\mathbf{M}\phi_{m_n}\ddot{q}_{m_n}+\phi_{m_n}^T\mathbf{K}\phi_{m_n}q_{m_n}+\alpha_n\gamma_u(q_{m_j}\alpha_j,q_{m_k}\alpha_k,q_{m_l}\alpha_l)=\phi_{m_n}^T\mathbf{F} \tag{D.27}$$

Now, the γ_u-term essentially represents the following relation:

$$\gamma_u=b_{u_{jkl}}^{(i)}q_{u_j}q_{u_k}q_{u_l}. \tag{D.28}$$

The nonlinear term of the Eq. D.27 is thus:

$$\gamma_m=\alpha_n\gamma_u(q_{m_j}\alpha_j,q_{m_k}\alpha_k,q_{m_l}\alpha_l)=\alpha_n\alpha_j\alpha_k\alpha_l b_{u_{jkl}}^{(n)}q_{m_j}q_{m_k}q_{m_l}=b_{m_{jkl}}^{(n)}q_{m_j}q_{m_k}q_{m_l}. \tag{D.29}$$

Which shows that the nonlinear part has quartic depedency on the eigenvector scaling (α). However, to go from the mass matrix for max-1 eigenvectors ($\phi_{u_n}^T\mathbf{M}\phi_{u_n}$) to the mass matrix in terms of the mass-normalized eigenvectors ($\phi_{m_n}^T\mathbf{M}\phi_{m_n}$), this mass matrix has been multiplied by α_n^2 (assuming that $\alpha_n\approx\alpha_j\approx\alpha_k\approx\alpha_l$). Hence, the nonlinear part of the equation scales yet another time by α_n^2.

Eigenvector scaling for the w-displacement string model

For the w-displacement string model, with modal mass $\frac{mL}{2}$, (Section B.1.1) this (dimensionless) α_n-parameter should be chosen to be $\sqrt{\frac{1kg}{\frac{mL}{2}}}=\sqrt{\frac{2kg}{\rho AL}}$, where $m=\rho A$. The nonlinear part of Eq. A.10 (for $n=1$) may be approximated as:

$$\frac{1}{\alpha_n}\gamma_u(\frac{q_{m_n}}{\alpha_n})=\frac{1}{\alpha_n}\frac{3\pi^4n^4EA}{16L^3}\left(\frac{q_{m_n}}{\alpha_n}\right)^3=\gamma_m q_{m_n}^3=\frac{1}{\alpha_n^4}\frac{3\pi^4n^4EA}{16L^3}q_{m_n}^3=\frac{3\pi^4n^4EA}{4m^2L^5}q_{m_n}^3 \tag{D.30}$$

D.2.2. Space and time scaling

For computation efficiency, it convenient to scale the equations with respect to space and time. Consider the following (dimensional) equation of motion:

$$\ddot{q}_r+k^{(r)}q_r+c^{(r)}\dot{q}_r+\sum_{j=1}^{N}\sum_{k=1}^{N}a_{jk}^{(r)}q_jq_k+\sum_{j=1}^{N}\sum_{k=j}^{N}\sum_{l=k}^{N}b_{m_{jkl}}^{(r)}q_jq_kq_l=F^{(r)}\sin(\omega_f t),\ r=1,2,...,N \tag{D.31}$$

Now, if we choose an undamped single-degree-of-freedom model, where $r=1$ and $N=1$, we will arrive at the following modal equation of motion:

$$\ddot{q}_1+\omega_1^2q_1+a_{11}^{(1)}q_1^2+b_{111}^{(1)}q_1^3=F\sin(\omega_f t), \tag{D.32}$$

The equation is normalized using the following relations to normalize space and time respectively:

$$q_n=\tilde{q}_nh,\ t=\frac{\tau}{\omega_0} \tag{D.33}$$

This generates the following derivatives:

$$\begin{aligned}\frac{d}{dt}[q_n]&=\frac{d}{d\tau}\frac{dt}{d\tau}[q_n]=\omega_0\frac{d}{d\tau}[\tilde{q}_nh]=h\omega_0\frac{d}{d\tau}\tilde{q}_n=h\omega_0\dot{\tilde{q}}_n,\\ \frac{d^2}{dt^2}[q_n]&=\frac{d}{d\tau}\frac{dt}{d\tau}\left[\frac{d}{d\tau}\frac{dt}{d\tau}[q_n]\right]=\omega_0\frac{d}{d\tau}\left[\omega_0\frac{d}{d\tau}[\tilde{q}_nh]\right]=h\omega_0^2\frac{d^2}{d\tau^2}\tilde{q}_n=h\omega_0^2\ddot{\tilde{q}}_n\end{aligned} \tag{D.34}$$

Plugging these derivatives and the space scaling of Eq. D.33 into equation D.32 gives:

$$h\omega_0^2\ddot{\tilde{q}}_1+\omega_1^2h\tilde{q}_1+a_{11}^{(1)}h^2\tilde{q}_1^2+b_{111}^{(1)}h^3\tilde{q}_1^3=F\sin(\frac{\omega_f}{\omega_0}\tau) \tag{D.35}$$

Normalizing the inertia term:

$$\begin{aligned}\ddot{\tilde{q}}_1+\frac{\omega_1^2}{\omega_0^2}\tilde{q}_1+\frac{a_{11}^{(1)}h}{\omega_0^2}\tilde{q}_1^2+\frac{b_{111}^{(1)}h^2}{\omega_0^2}\tilde{q}_1^3&=\frac{F}{h\omega_0^2}\sin(\frac{\omega_f}{\omega_0}\tau)\\ \ddot{\tilde{q}}_1+\frac{\omega_1^2}{\omega_0^2}\tilde{q}_1+\tilde{a}_{11}^{(1)}\tilde{q}_1^2+\tilde{b}_{111}^{(1)}\tilde{q}_1^3&=\tilde{F}\sin(\frac{\omega_f}{\omega_0}\tau)\end{aligned} \tag{D.36}$$

The mass and linear stiffness terms appear to have no dependency on the variable h. It is thus possible to choose h to be any value, depending on what is most computationally efficient. Setting $\tilde{b}_{111}^{(1)} = 1$ would be most convenient, since this is a small nonlinearity. This requires the following relation for h:

$$h = \frac{\omega_0}{\sqrt{b_{111}^{(1)}}} \tag{D.37}$$

The coefficients will thus be:

$$\tilde{k}_1 = \frac{\omega_1^2}{\omega_0^2},\ \tilde{a}_{11}^{(1)} = \frac{a_{11}^{(1)}}{\omega_0\sqrt{b_{111}^{(1)}}},\ \tilde{b}_{111}^{(1)} = \frac{b_{111}^{(1)}\omega_0^2}{b_{111}^{(1)}\omega_0^2} = 1,\ \tilde{F} = \frac{F\sqrt{b_{111}^{(1)}}}{\omega_0^3} \tag{D.38}$$

D.3. Numerically reproducing experiments

Section B.3 showed experimental results of frequency characterization measurements on Si_3N_4 strings. Generally, to fit frequency response simulation results to experimental data, one should follow five steps. These steps allow the experimental response to be simulated properly. During these steps, the magnitudes of four variables are determined: Q, ω, F and E; the Q-factor, the resonance frequency, excitation force and the effective Young's modulus of the resonator, respectively. This section will show how the numerical results were fitted to the experimental results of a string with characteristics of Table B.10, according to the following five steps:

1. Convert the measurement data into the desired magnitudes;
2. Find the experimental Q-factor from ringdown and/or linear frequency response plots;
3. Find the linear resonance frequency to calculate the pre-stress of the string resonator. This pre-stress is used in numerical and/or analytical models;
4. Fit the baselines of the experimental data by varying the magnitude of the forcing;
5. Guess a Young's modulus and simulate the corresponding response. Plot the simulated amplitude versus frequency and amplitude squared versus frequency data for both the simulations and the experiments. Continue iterations to find accurate fits.

Step 1: Data conversion
The first step requires proper conversion of the data. The amplitudes of a single mode are measured using a Polytech vibrometer in combination with a lock-in amplifier and an attenuator, which attenuates noise below $-20dB$. The relation between the input and output voltages is:

$$\frac{V_{out}}{V_{in}}[dB] = 20\log\left(\frac{V_{out}}{V_{in}}\right) \rightarrow -20dB = 20\log\left(\frac{V_{out}}{V_{in}}\right) \rightarrow V_{out} = 10V_{in} \tag{D.39}$$

The outputted voltage (V_{out}) is expressed in a root-mean-square (RMS) voltage $V_{RMS} = V_{out} = 10V_{in}$. To determine the peak values (V_{peak}), one should convert this RMS voltage to the peak values, by imposing Eq. D.40 [1].

$$V_{peak} = V_{RMS}\sqrt{2} = 10\sqrt{2}V_{in} \tag{D.40}$$

Two options can be employed to convert this (peak) voltage into an amplitude in meters. The option that should be employed depends on the measurement scheme:

- If the modal velocities are detected, one should first convert the voltage V_{peak} into a velocity $\dot{x}(t)$, using a parameter C_{V2vel} $[\frac{m/s}{V}]$, before integrating with respect to time to find the amplitude $x(t)$. Assuming that the velocity signal is a Cosine function, the equations will become:

$$\dot{x}(t) = \dot{A}\cos(2\pi f t) = 10\sqrt{2}V_{in}C_{V2vel}\cos(2\pi f t) \tag{D.41}$$

$$x(t) = \frac{\dot{A}}{2\pi f}\sin(2\pi f t) = \frac{10\sqrt{2}V_{in}C_{V2vel}}{2\pi f}\sin(2\pi f t) \tag{D.42}$$

Where f is the measured frequency. The amplitude that is measured at this frequency is thus given by $x = \frac{10\sqrt{2}V_{in}C_{V2vel}}{2\pi f}$ [m].

- If the modal amplitudes are detected, one should first convert the voltage V_{peak} into an amplitude $x(t)$, using a parameter C_{V2amp} $[\frac{m}{V}]$:

$$x(t) = A\sin(2\pi f t) = 10\sqrt{2}V_{in}C_{V2amp}\sin(2\pi f t) \tag{D.43}$$

The amplitude that is measured at this frequency is thus given by $x = 10\sqrt{2}V_{in}C_{V2amp}$[m].

After this conversion, the experimental frequency response may be plotted. One measurement location will be shown here, but the same procedure works for any other frequency characterization measurement. Fig. D.3 depicts the experimental frequency response for 20 force levels, ranging from 0.001 to 0.5V.

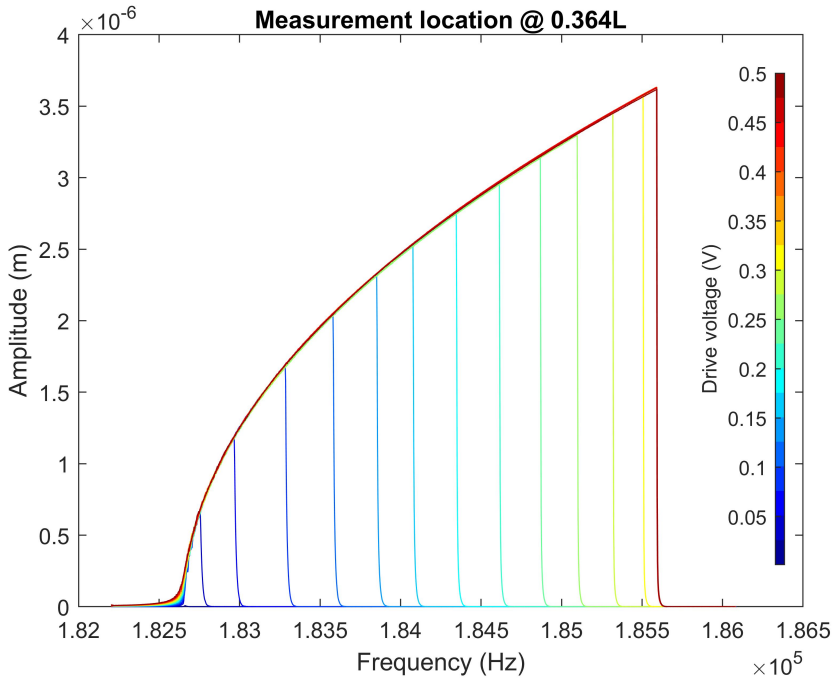

Figure D.3: Frequency response of a Si_3N_4 string of length 1110μm for drive levels ranging from 0.001 to 0.5V.

This response shows a hardening nonlinear effect. Before simulating the responses in the nonlinear regime, it is important to find proper fits for the linear response. This linear part determines the magnitude of the resonance frequency.

Step 2: Finding Q
The Q-factor of this response was already found in Section B.4 (Fig. B.6 depicts the ringdown). The Q-factor of this measurement was estimated to be approximately 2.00×10^5.

Step 3: Find the linear resonance frequency
The linear frequency in Fig. D.3 may be estimated to be around 182.65 kHz (where there is still some deep dark blue line visible). Fig. D.4 displays a zoom-in of the linear response (for a force level of 0.001V).

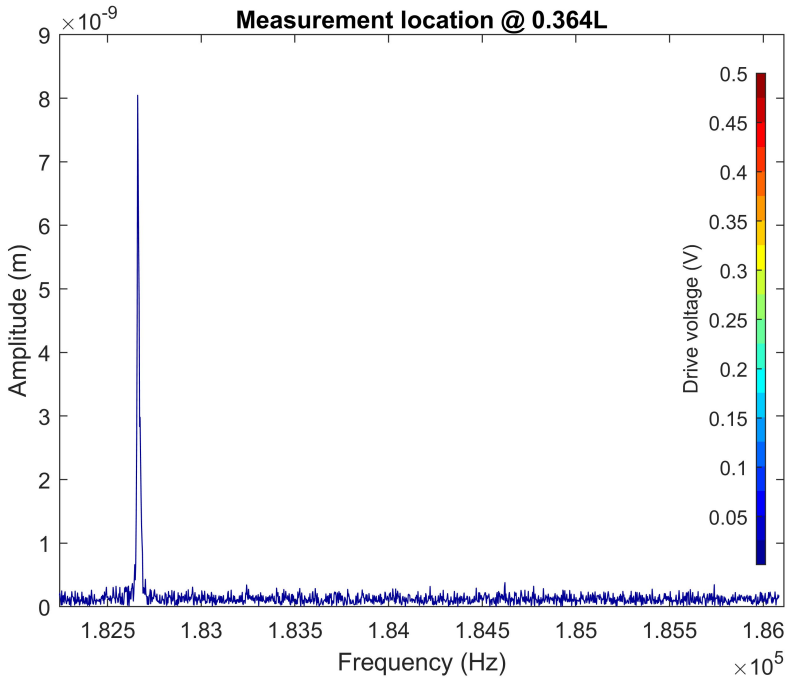

Figure D.4: Frequency response of a Si_3N_4 string at a drive level of 0.001V.

By using the equation (Eq. D.44) for the linear resonance frequency of the string, one may determine some parameters of the string, such that a numerical model may be formulated to replicate the string's dynamics.

$$\omega_1 = \frac{\pi}{L}\sqrt{\frac{\sigma_0}{\rho}} \tag{D.44}$$

This equation consists of three free parameters: the length L, the pre-stress of the string σ_0 and the material density ρ. Two of these variables are assumed to be known and constant: the length of the string and the material mass density. This leaves one unknown variable: the pre-stress σ_0. By choosing this pre-stress to be one of the fitting parameters, one may account for possible stress reduction in the material over time. Re-writing Eq. D.44 for the resonance frequency will deliver an expression for the pre-stress of the resonator:

$$\sigma_0 = 4\rho f^2 L^2. \tag{D.45}$$

For the considered resonator, one will find a pre-stress of approximately 509 MPa. This results in a linear plot that is shown in Fig D.5a, which shows good agreement for the linear response.

Step 4: Fitting the baselines

The following variable that needs to be determined is the excitation force. This variable is responsible for the amount of energy that is "pumped" into the system: increasing this force will increase the amplitude. Simulations with the correct excitation force will thus deliver correct simulation amplitudes. During this step, one should find a near perfect fit for the linear regime, though the fits in the nonlinear regime may still differ with the experimental response, as these will be improved in the next step. Fig. D.5 depicts the region that needs to be fit properly: the baselines of the experimental results should be simulated accurately, as is shown in Fig. D.5c.

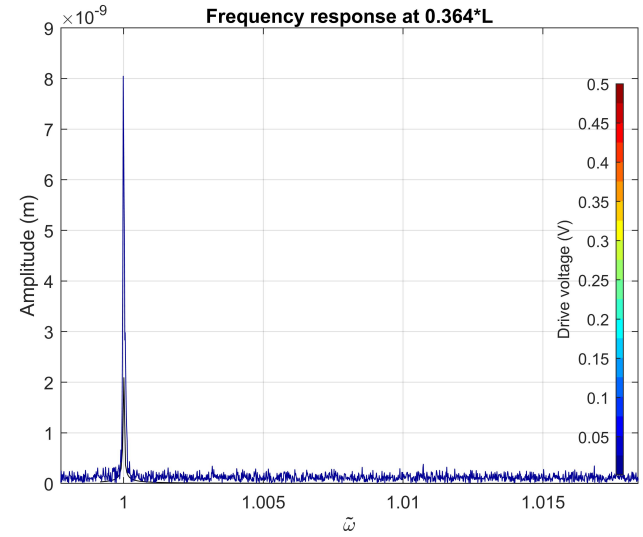

(a)

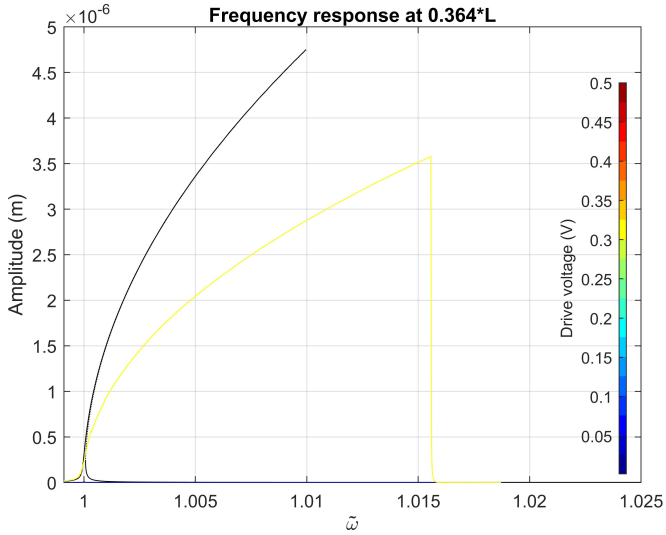

(b)

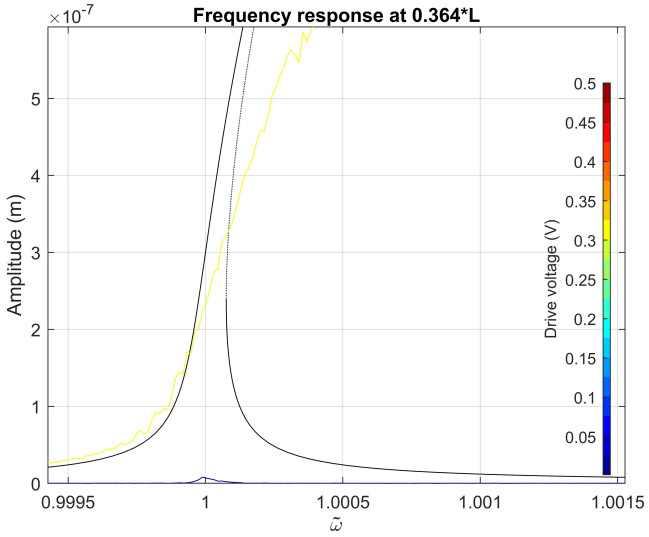

(c)

Figure D.5: Baseline fits for various drive forces. D.5a: Linear frequency response of a Si_3N_4 string for a drive level of 0.001V. Shown are the experimental (black line) and the simulated response (colored line). Note that the frequency axis is normalized with respect to the first mode's frequency. D.5b: Baseline fit in the nonlinear regime for an excitation level of 0.316V. Note that (to clarify this particular step) an incorrect magnitude of nonlinearity is used here. This may not be the case in the initial fit. D.5c Zoom-in of D.5b, showing the region of interest. Note the small magnitude of the linear response: the small peak at $\tilde{\omega} = 1$.

The accuracy of the force estimation can be verified by checking the relation between the fitted force level and the drive voltage. For piezo-elements, the produced force is known to scale linearly with the applied voltage, as shown in D.46 [32].

$$F \approx k\Delta l_0, \text{ where } \Delta l_0 \propto V \tag{D.46}$$

The force-voltage plot for the considered fits are depicted in Fig. D.6, which shows a required near-linear relation between the force values and the drive voltage.

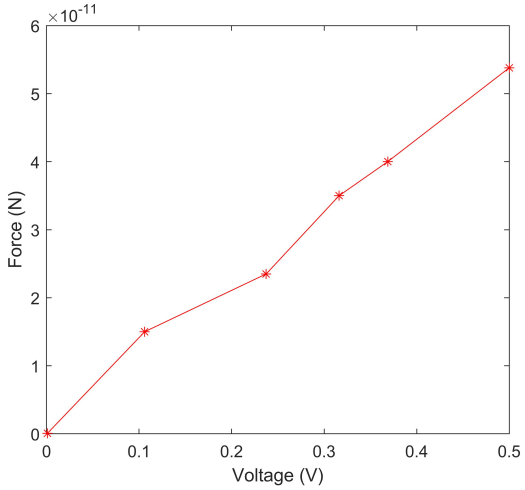

Figure D.6: Force versus voltage plot, showing a near-linear relation between the experimental drive voltage and the fitted force values.

Step 5: Guess the Young's modulus and iterate

Now that the resonance frequency, the linear damping factor and the force level are determined, the non-linear response may be simulated. To do so, one should revisit the single-mode equation of motion for the uw-displacement model from Eq. B.64 and set $n = 1$.

$$\begin{aligned} \frac{\rho AL}{2}\ddot{q}_{u_n} + \frac{\pi^2 n^2 T_0}{2L} q_{u_n} + \frac{3\pi^4 n^4 EA}{8L^3} q_{u_n}^3 &= 0 \\ \ddot{q}_{u_1} + \frac{\pi^2 \sigma_0}{L^2 \rho} q_{u_1} + \frac{2}{\rho AL}\frac{\pi^4 E}{4L^4 \rho} q_{u_1}^3 &= F_u^{(n)} \sin(\omega_n t) \end{aligned} \tag{D.47}$$

Here, the part of the equation that is linear in q_n is equal to the square of Eq. D.44. The last term of the equation is nonlinear in q_{u_n} and it is dependent on the Young's modulus E, the length L and mass density ρ. The length and mass density of the string are known, which leaves one free variable for fitting: the Young's modulus. Using this as the fitting parameter allows for compensation for changes in the Young's modulus over time (creep-like phenomena). To start the simulations, one could set a first guess for the magnitude of this parameter: 250GPa, the default Young's modulus of Silicon-Nitride. Fig. D.7 depicts two plots: an amplitude vs. frequency plot and an amplitude squared vs. frequency plot. The latter plot indicates how "good" the estimation of the nonlinear strength is. The frequency shift in a Duffing oscillator with nonlinearity b is dependent on the square of the amplitude (here, denoted by q), as is indicated by Eq. D.48 [19]. This equation shows that the shift of the frequency scales with the square of the modal amplitude q.

$$\omega_{\text{shift}} = \omega_0 + \frac{b}{m\omega_0} q^2 \tag{D.48}$$

Plotting the amplitude squared versus the frequency thus shows how good the estimation of the nonlinear parameter is.

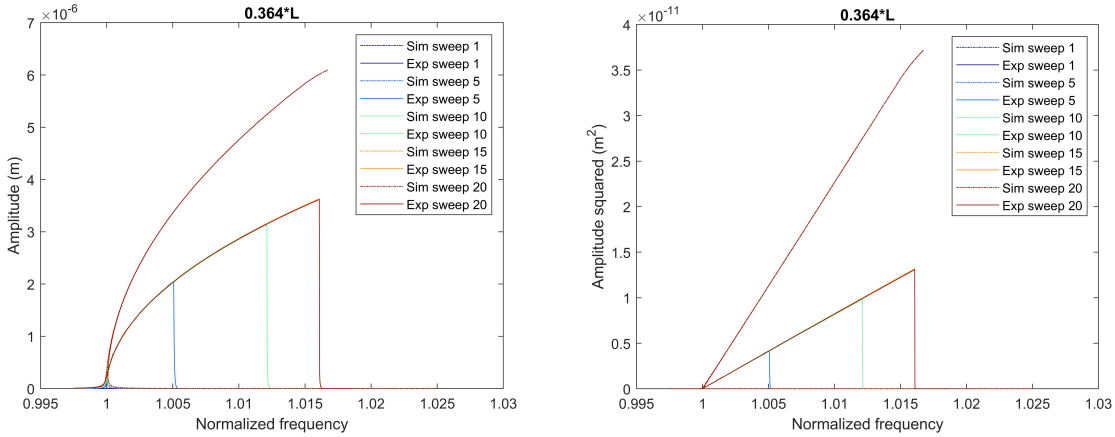

(a) Amplitude versus frequency.

(b) Amplitude squared versus frequency.

Figure D.7: Experimental (solid lines) and simulated (dashed lines) frequency response of a Si_3N_4 string for five drive levels, ranging between 0.001V and 0.5V. The estimated Young's modulus in the numerical model is 250GPa. Note that the frequency axis is normalized with respect to the first mode's frequency.

These plots indicate that the nonlinearity in the experiments is larger than that in the simulations, since the frequency shift in the experimental response is larger than the frequency shift in the simulated response. To find accurate fits, the Young's modulus should hence be increased. For this resonator, a Young's modulus of 675GPa shows a proper slope fit, as is shown in Fig. D.8.

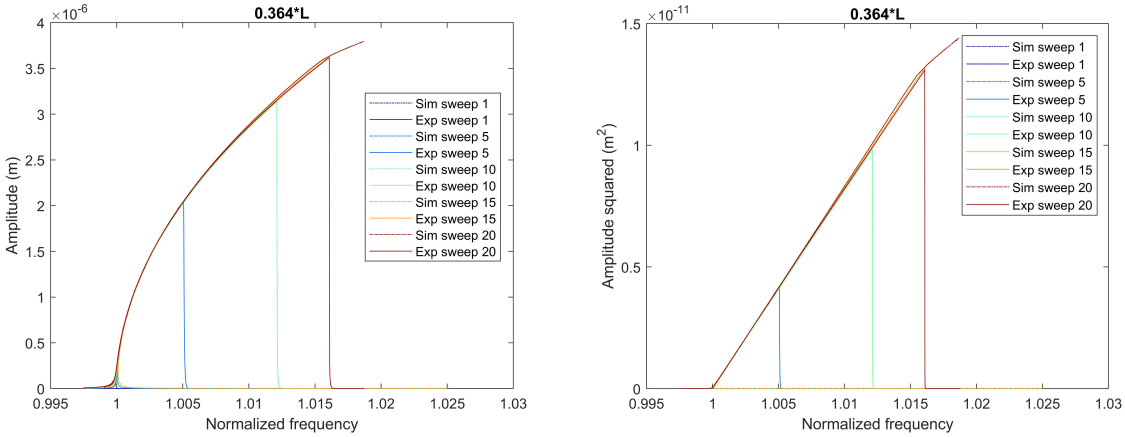

(a) Amplitude versus frequency.

(b) Amplitude squared versus frequency.

Figure D.8: Experimental (solid lines) and simulated (dashed lines) frequency response of a Si_3N_4 string for five drive levels, ranging between 0.001V and 0.5V. The estimated Young's modulus in the numerical model is 675GPa. Note that the frequency axis is normalized with respect to the first mode's frequency.

The overshooting of the numerical simulations is due to the continuation by AUTO from a bifurcation point, yielding an unstable solution which still increases both amplitude and frequency. Since this unstable solution cannot be traced in physical experiments: the amplitude jumps down after the bifurcation point, which is the origin of the vertical lines in the experimental plots.

Possible additional steps

This system showed no nonlinear damping, as could be seen from the ringdown plot in Fig. B.6 in Section B.3. In this figure, the decay was approximated very well by assuming that the decay is linear. Should this linear approximation be invalid, it would have been necessary to add another step in the fitting process: the inclusion of a nonlinear damping coefficient. This additional step could decrease the maximum amplitude in the frequency response. In addition, if frequency locking is observed, one could shift the resonance frequencies

of the higher modes slightly, such that the modal interaction at the bifurcation point is most significant. This technique is elaborated further in Section B.4.

Conclusion
These simulations show that the estimated effective Young's modulus of 675GPa is significantly higher than the Young's modulus of Silicon-Nitride (this is estimated to be 250GPa). The general string's dynamics could hence be predicted using this method, though quantitative conclusions should not be drawn from it. Additional experiments should be conducted, with multiple specimens (strings of different dimensions), to characterize the validity of this simulation method.

E

Modal coefficients

This section contains the single-mode and nonlinear coefficients of several models. All modal variables are computed for a string with characteristics similar to those from Table C.4, unless noted otherwise.

E.1. Modal coupling coefficients of the analytical models

E.1.1. w-displacement model

Table E.1: Single mode coefficients for the first 6 modes of an analytical string model that includes only **vertical** displacements (w-displacement model). The variables are computed for a string with characteristics similar to those from Table C.4.

Eq.	**(1)**	**(2)**	**(3)**	**(4)**	**(5)**	**(6)**
k_n [s^{-2}]	1.32×10^{12}	5.27×10^{12}	1.19×10^{13}	2.11×10^{13}	3.29×10^{13}	4.74×10^{13}
ω_n [rads^{-1}]	1.15×10^{6}	2.30×10^{6}	3.44×10^{6}	4.59×10^{6}	5.74×10^{6}	6.89×10^{6}
$b^{(n)}_{nnn}$ [m^{-2}s^{-2}]	3.07×10^{33}	4.91×10^{34}	2.49×10^{35}	7.84×10^{35}	1.92×10^{36}	4.00×10^{36}
$\frac{b^{(n)}_{nnn}}{k_n}$ [m]	2.33×10^{21}	9.32×10^{21}	2.09×10^{22}	3.72×10^{22}	5.84×10^{22}	8.44×10^{22}
$\tilde{k}_n$	1.00	4.00	9.00	16.00	25.00	36.00
$\tilde{\omega}_n$	1.00	2.00	3.00	4.00	5.00	6.00
$\tilde{b}^{(n)}_{nnn}$	1.00	16.00	81.00	256.00	625.00	1296.00

Table E.2: Modal coupling coefficients for the first 6 modes of an analytical string model that includes only the **vertical** displacements (w-displacement model). Note that the coefficients are scaled with respect to $\tilde{b}^{(1)}_{111}$.

Eq.	**(1)**	**(2)**	**(3)**	**(4)**	**(5)**	**(6)**
$\tilde{b}_{111}$	1	0	1	0	0	0
$\tilde{b}_{112}$	0	8	0	8	0	0
$\tilde{b}_{113}$	3	0	18	0	15	0
$\tilde{b}_{114}$	0	8	0	32	0	24
$\tilde{b}_{115}$	0	0	15	0	50	0
$\tilde{b}_{116}$	0	0	0	24	0	72
$\tilde{b}_{122}$	8	0	12	0	20	0
$\tilde{b}_{123}$	0	24	0	48	0	72
$\tilde{b}_{124}$	16	0	48	0	80	0
$\tilde{b}_{125}$	0	40	0	80	0	120
$\tilde{b}_{126}$	0	0	72	0	120	0
$\tilde{b}_{133}$	18	0	0	0	45	0
$\tilde{b}_{134}$	0	48	0	0	0	144
$\tilde{b}_{135}$	30	0	90	0	0	0
$\tilde{b}_{136}$	0	72	0	144	0	0
$\tilde{b}_{144}$	32	0	0	0	0	0
$\tilde{b}_{145}$	0	80	0	0	0	0
$\tilde{b}_{146}$	48	0	144	0	0	0
$\tilde{b}_{155}$	50	0	0	0	0	0
$\tilde{b}_{156}$	0	120	0	0	0	0
$\tilde{b}_{166}$	72	0	0	0	0	0
$\tilde{b}_{222}$	0	16	0	0	0	16
$\tilde{b}_{223}$	12	0	72	0	0	0
$\tilde{b}_{224}$	0	0	0	128	0	0
$\tilde{b}_{225}$	20	0	0	0	200	0
$\tilde{b}_{226}$	0	48	0	0	0	288
$\tilde{b}_{233}$	0	72	0	72	0	0
$\tilde{b}_{234}$	48	0	144	0	240	0
$\tilde{b}_{235}$	0	0	0	240	0	360
$\tilde{b}_{236}$	72	0	0	0	360	0
$\tilde{b}_{244}$	0	128	0	0	0	192
$\tilde{b}_{245}$	80	0	240	0	0	0
$\tilde{b}_{246}$	0	0	0	384	0	0
$\tilde{b}_{255}$	0	200	0	0	0	0
$\tilde{b}_{256}$	120	0	360	0	0	0
$\tilde{b}_{266}$	0	288	0	0	0	0
$\tilde{b}_{333}$	0	0	81	0	0	0
$\tilde{b}_{334}$	0	72	0	288	0	0
$\tilde{b}_{335}$	45	0	0	0	450	0
$\tilde{b}_{336}$	0	0	0	0	0	648
$\tilde{b}_{344}$	0	0	288	0	240	0
$\tilde{b}_{345}$	0	240	0	480	0	720
$\tilde{b}_{346}$	144	0	0	0	720	0
$\tilde{b}_{355}$	0	0	450	0	0	0
$\tilde{b}_{356}$	0	360	0	720	0	0
$\tilde{b}_{366}$	0	0	648	0	0	0
$\tilde{b}_{444}$	0	0	0	256	0	0
$\tilde{b}_{445}$	0	0	240	0	800	0
$\tilde{b}_{446}$	0	192	0	0	0	1152
$\tilde{b}_{455}$	0	0	0	800	0	600
$\tilde{b}_{456}$	0	0	720	0	1200	0
$\tilde{b}_{466}$	0	0	0	1152	0	0
$\tilde{b}_{555}$	0	0	0	0	625	0
$\tilde{b}_{556}$	0	0	0	600	0	1800
$\tilde{b}_{566}$	0	0	0	0	1800	0
$\tilde{b}_{666}$	0	0	0	0	0	1296

E.1.2. uw-displacement model

Table E.3: Single mode coefficients for the first 6 modes of an analytical string model that includes only the **longitudinal** and **vertical** displacements (uw-displacement model). The variables are computed for a string with characteristics similar to those from Table C.4.

Eq.	**(1)**	**(2)**	**(3)**	**(4)**	**(5)**	**(6)**
k_n [s^{-2}]	1.32×10^{12}	5.27×10^{12}	1.19×10^{13}	2.11×10^{13}	3.29×10^{13}	4.74×10^{13}
ω_n [rads^{-1}]	1.15×10^{6}	2.30×10^{6}	3.44×10^{6}	4.59×10^{6}	5.74×10^{6}	6.89×10^{6}
$b^{(n)}_{nnn}$ [m^{-2}s^{-2}]	2.04×10^{33}	3.27×10^{34}	1.66×10^{35}	5.23×10^{35}	1.28×10^{36}	2.65×10^{36}
$\frac{b^{(n)}_{nnn}}{k_n}$ [m]	1.55×10^{21}	6.20×10^{21}	1.39×10^{22}	2.48×10^{22}	3.89×10^{22}	5.59×10^{22}
$\tilde{k}_n$	1.00	4.00	9.00	16.00	25.00	36.00
$\tilde{\omega}_n$	1.00	2.00	3.00	4.00	5.00	6.00
$\tilde{b}^{(n)}_{nnn}$	1.00	16.00	81.00	256.00	625.00	1296.00

Table E.4: Modal coupling coefficients for the first 6 modes of an analytical string model that includes only the **longitudinal** and **vertical** displacements (uw-displacement model). Note that the coefficients are scaled with respect to $\tilde{b}^{(1)}_{111}$.

Eq.	**(1)**	**(2)**	**(3)**	**(4)**	**(5)**	**(6)**
$\tilde{b}_{111}$	1	0	0	0	0	0
$\tilde{b}_{112}$	0	4	0	0	0	0
$\tilde{b}_{113}$	0	0	9	0	0	0
$\tilde{b}_{114}$	0	0	0	16	0	0
$\tilde{b}_{115}$	0	0	0	0	25	0
$\tilde{b}_{116}$	0	0	0	0	0	36
$\tilde{b}_{122}$	4	0	0	0	0	0
$\tilde{b}_{123}$	0	0	0	0	0	0
$\tilde{b}_{124}$	0	0	0	0	0	0
$\tilde{b}_{125}$	0	0	0	0	0	0
$\tilde{b}_{126}$	0	0	0	0	0	0
$\tilde{b}_{133}$	9	0	0	0	0	0
$\tilde{b}_{134}$	0	0	0	0	0	0
$\tilde{b}_{135}$	0	0	0	0	0	0
$\tilde{b}_{136}$	0	0	0	0	0	0
$\tilde{b}_{144}$	16	0	0	0	0	0
$\tilde{b}_{145}$	0	0	0	0	0	0
$\tilde{b}_{146}$	0	0	0	0	0	0
$\tilde{b}_{155}$	25	0	0	0	0	0
$\tilde{b}_{156}$	0	0	0	0	0	0
$\tilde{b}_{166}$	36	0	0	0	0	0
$\tilde{b}_{222}$	0	16	0	0	0	0
$\tilde{b}_{223}$	0	0	36	0	0	0
$\tilde{b}_{224}$	0	0	0	64	0	0
$\tilde{b}_{225}$	0	0	0	0	100	0
$\tilde{b}_{226}$	0	0	0	0	0	144
$\tilde{b}_{233}$	0	36	0	0	0	0
$\tilde{b}_{234}$	0	0	0	0	0	0
$\tilde{b}_{235}$	0	0	0	0	0	0
$\tilde{b}_{236}$	0	0	0	0	0	0
$\tilde{b}_{244}$	0	64	0	0	0	0
$\tilde{b}_{245}$	0	0	0	0	0	0
$\tilde{b}_{246}$	0	0	0	0	0	0
$\tilde{b}_{255}$	0	100	0	0	0	0
$\tilde{b}_{256}$	0	0	0	0	0	0
$\tilde{b}_{266}$	0	144	0	0	0	0
$\tilde{b}_{333}$	0	0	81	0	0	0
$\tilde{b}_{334}$	0	0	0	144	0	0
$\tilde{b}_{335}$	0	0	0	0	225	0
$\tilde{b}_{336}$	0	0	0	0	0	324
$\tilde{b}_{344}$	0	0	144	0	0	0
$\tilde{b}_{345}$	0	0	0	0	0	0
$\tilde{b}_{346}$	0	0	0	0	0	0
$\tilde{b}_{355}$	0	0	225	0	0	0
$\tilde{b}_{356}$	0	0	0	0	0	0
$\tilde{b}_{366}$	0	0	324	0	0	0
$\tilde{b}_{444}$	0	0	0	256	0	0
$\tilde{b}_{445}$	0	0	0	0	400	0
$\tilde{b}_{446}$	0	0	0	0	0	576
$\tilde{b}_{455}$	0	0	0	400	0	0
$\tilde{b}_{456}$	0	0	0	0	0	0
$\tilde{b}_{466}$	0	0	0	576	0	0
$\tilde{b}_{555}$	0	0	0	0	625	0
$\tilde{b}_{556}$	0	0	0	0	0	900
$\tilde{b}_{566}$	0	0	0	0	900	0
$\tilde{b}_{666}$	0	0	0	0	0	1296

E.1.3. uvw-displacement model

Table E.5: Single mode coefficients for the first 6 modes of an analytical string model that includes only the **longitudinal**, **transverse** and **vertical** displacements (uvw-displacement model). The variables are computed for a string with characteristics similar to those from Table C.4.

Eq.	**(1)**	**(2)**	**(3)**	**(4)**	**(5)**	**(6)**
k_n [s^{-2}]	1.32×10^{12}	1.32×10^{12}	5.27×10^{12}	5.27×10^{12}	1.19×10^{13}	1.19×10^{13}
ω_n [rads^{-1}]	1.15×10^{6}	1.15×10^{6}	2.30×10^{6}	2.30×10^{6}	3.44×10^{6}	3.44×10^{6}
$b^{(n)}_{nnn}$ [m^{-2}s^{-2}]	2.04×10^{33}	2.04×10^{33}	3.27×10^{34}	3.27×10^{34}	1.66×10^{35}	1.66×10^{35}
$\frac{b^{(n)}_{nnn}}{k_n}$ [m]	1.55×10^{21}	1.55×10^{21}	6.20×10^{21}	6.20×10^{21}	1.39×10^{22}	1.39×10^{22}
$\tilde{k}_n$	1.00	1.00	4.00	4.00	9.00	9.00
$\tilde{\omega}_n$	1.00	1.00	2.00	2.00	3.00	3.00
$\tilde{b}^{(n)}_{nnn}$	1.00	1.00	16.00	16.00	81.00	81.00

Table E.6: Modal coupling coefficients for the first 6 modes of an analytical string model that includes **longitudinal**, **transverse** and **vertical** displacements (uvw-displacement model). Note that the coefficients are scaled with respect to $\tilde{b}^{(1)}_{111}$. The uneven modes represent vertical modes, the even modes represent the transverse modes.

Eq.	**(1)**	**(2)**	**(3)**	**(4)**	**(5)**	**(6)**
$\tilde{b}_{111}$	1	0	0	0	0	0
$\tilde{b}_{112}$	0	1	0	0	0	0
$\tilde{b}_{113}$	0	0	4	0	0	0
$\tilde{b}_{114}$	0	0	0	4	0	0
$\tilde{b}_{115}$	0	0	0	0	9	0
$\tilde{b}_{116}$	0	0	0	0	0	9
$\tilde{b}_{122}$	1	0	0	0	0	0
$\tilde{b}_{123}$	0	0	0	0	0	0
$\tilde{b}_{124}$	0	0	0	0	0	0
$\tilde{b}_{125}$	0	0	0	0	0	0
$\tilde{b}_{126}$	0	0	0	0	0	0
$\tilde{b}_{133}$	4	0	0	0	0	0
$\tilde{b}_{134}$	0	0	0	0	0	0
$\tilde{b}_{135}$	0	0	0	0	0	0
$\tilde{b}_{136}$	0	0	0	0	0	0
$\tilde{b}_{144}$	4	0	0	0	0	0
$\tilde{b}_{145}$	0	0	0	0	0	0
$\tilde{b}_{146}$	0	0	0	0	0	0
$\tilde{b}_{155}$	9	0	0	0	0	0
$\tilde{b}_{156}$	0	0	0	0	0	0
$\tilde{b}_{166}$	9	0	0	0	0	0
$\tilde{b}_{222}$	0	1	0	0	0	0
$\tilde{b}_{223}$	0	0	4	0	0	0
$\tilde{b}_{224}$	0	0	0	4	0	0
$\tilde{b}_{225}$	0	0	0	0	9	0
$\tilde{b}_{226}$	0	0	0	0	0	9
$\tilde{b}_{233}$	0	4	0	0	0	0
$\tilde{b}_{234}$	0	0	0	0	0	0
$\tilde{b}_{235}$	0	0	0	0	0	0
$\tilde{b}_{236}$	0	0	0	0	0	0
$\tilde{b}_{244}$	0	4	0	0	0	0
$\tilde{b}_{245}$	0	0	0	0	0	0
$\tilde{b}_{246}$	0	0	0	0	0	0
$\tilde{b}_{255}$	0	9	0	0	0	0
$\tilde{b}_{256}$	0	0	0	0	0	0
$\tilde{b}_{266}$	0	9	0	0	0	0
$\tilde{b}_{333}$	0	0	16	0	0	0
$\tilde{b}_{334}$	0	0	0	16	0	0
$\tilde{b}_{335}$	0	0	0	0	36	0
$\tilde{b}_{336}$	0	0	0	0	0	36
$\tilde{b}_{344}$	0	0	16	0	0	0
$\tilde{b}_{345}$	0	0	0	0	0	0
$\tilde{b}_{346}$	0	0	0	0	0	0
$\tilde{b}_{355}$	0	0	36	0	0	0
$\tilde{b}_{356}$	0	0	0	0	0	0
$\tilde{b}_{366}$	0	0	36	0	0	0
$\tilde{b}_{444}$	0	0	0	16	0	0
$\tilde{b}_{445}$	0	0	0	0	36	0
$\tilde{b}_{446}$	0	0	0	0	0	36
$\tilde{b}_{455}$	0	0	0	36	0	0
$\tilde{b}_{456}$	0	0	0	0	0	0
$\tilde{b}_{466}$	0	0	0	36	0	0
$\tilde{b}_{555}$	0	0	0	0	81	0
$\tilde{b}_{556}$	0	0	0	0	0	81
$\tilde{b}_{566}$	0	0	0	0	81	0
$\tilde{b}_{666}$	0	0	0	0	0	81

E.2. Modal coupling coefficients from STEP

E.2.1. uw-displacement model

Table E.7: Single mode coefficients for the first 6 modes of a STEP model that includes only the **longitudinal** and **vertical** displacements (uw-displacement model). The variables are computed for a string with characteristics similar to those from Table C.4.

Eq.	**(1)**	**(2)**	**(3)**	**(4)**	**(5)**	**(6)**
k_n [s^{-2}]	1.32×10^{12}	5.27×10^{12}	1.19×10^{13}	2.11×10^{13}	3.30×10^{13}	4.76×10^{13}
ω_n [s^{-2}]	1.15×10^{6}	2.30×10^{6}	3.44×10^{6}	4.59×10^{6}	5.74×10^{6}	6.90×10^{6}
$b^{(n)}_{nnn}$ [m^{-2}s^{-2}]	2.05×10^{33}	3.28×10^{34}	1.66×10^{35}	5.25×10^{35}	1.28×10^{36}	2.67×10^{36}
$\frac{b^{(n)}_{nnn}}{k_n}$ [m]	1.55×10^{21}	6.22×10^{21}	1.39×10^{22}	2.49×10^{22}	3.88×10^{22}	5.61×10^{22}
$\tilde{k}_n$	1.00	4.00	9.01	16.02	25.05	36.10
$\tilde{\omega}_n$	1.00	2.00	3.00	4.00	5.00	6.01
$\tilde{b}^{(n)}_{nnn}$	1.00	16.01	81.12	256.70	627.59	1303.91

Table E.8: Modal coupling coefficients for the first 6 modes of a STEP model that includes only the **longitudinal** and **vertical** displacements (uw-displacement model). Note that the coefficients are scaled with respect to $\tilde{b}^{(1)}_{111}$.

Eq.	**(1)**	**(2)**	**(3)**	**(4)**	**(5)**	**(6)**
$\tilde{b}_{111}$	1.00	0.00	0.00	−0.00	−0.01	−0.00
$\tilde{b}_{112}$	0.00	4.01	−0.00	0.03	−0.00	0.00
$\tilde{b}_{113}$	0.01	−0.00	9.04	−0.00	0.05	−0.00
$\tilde{b}_{114}$	−0.00	0.03	−0.00	16.08	−0.00	−0.08
$\tilde{b}_{115}$	−0.04	−0.00	0.05	−0.00	25.14	−0.01
$\tilde{b}_{116}$	−0.00	0.00	−0.00	−0.08	−0.01	36.25
$\tilde{b}_{122}$	4.01	0.00	0.04	0.00	0.06	0.00
$\tilde{b}_{123}$	−0.00	0.08	−0.00	0.16	−0.00	−0.25
$\tilde{b}_{124}$	0.05	0.00	0.16	0.00	0.27	0.00
$\tilde{b}_{125}$	−0.00	0.13	−0.00	0.27	−0.00	−0.42
$\tilde{b}_{126}$	0.00	0.00	−0.25	0.00	−0.42	0.00
$\tilde{b}_{133}$	9.04	−0.00	0.00	0.00	0.15	0.00
$\tilde{b}_{134}$	−0.00	0.16	0.00	−0.00	−0.00	−0.51
$\tilde{b}_{135}$	0.10	−0.00	0.30	−0.00	0.00	−0.01
$\tilde{b}_{136}$	−0.00	−0.25	0.00	−0.51	−0.01	−0.00
$\tilde{b}_{144}$	16.08	0.00	−0.00	−0.00	−0.00	0.00
$\tilde{b}_{145}$	−0.01	0.27	−0.00	−0.01	0.01	0.01
$\tilde{b}_{146}$	−0.16	0.00	−0.51	0.00	0.01	−0.00
$\tilde{b}_{155}$	25.14	−0.00	0.00	0.00	−0.00	0.01
$\tilde{b}_{156}$	−0.01	−0.42	−0.01	0.01	0.01	−0.02
$\tilde{b}_{166}$	36.25	0.00	−0.00	−0.00	−0.01	−0.00
$\tilde{b}_{222}$	0.00	16.01	−0.00	0.00	0.00	−0.05
$\tilde{b}_{223}$	0.04	−0.00	36.16	−0.01	0.01	−0.01
$\tilde{b}_{224}$	0.00	0.00	−0.01	64.33	−0.01	0.01
$\tilde{b}_{225}$	0.06	0.00	0.01	−0.01	100.61	−0.02
$\tilde{b}_{226}$	0.00	−0.16	−0.01	0.01	−0.02	145.04
$\tilde{b}_{233}$	−0.00	36.16	0.00	0.24	−0.01	0.01
$\tilde{b}_{234}$	0.16	−0.01	0.48	−0.02	0.85	−0.00
$\tilde{b}_{235}$	−0.00	0.01	−0.01	0.85	−0.01	−1.31
$\tilde{b}_{236}$	−0.25	−0.02	0.02	−0.00	−1.31	−0.02
$\tilde{b}_{244}$	0.00	64.33	−0.01	0.00	−0.01	−0.67
$\tilde{b}_{245}$	0.27	−0.02	0.85	−0.02	0.02	0.04
$\tilde{b}_{246}$	0.00	0.02	−0.00	−1.33	0.04	−0.04
$\tilde{b}_{255}$	−0.00	100.61	−0.01	0.01	−0.00	0.02
$\tilde{b}_{256}$	−0.42	−0.04	−1.31	0.04	0.04	−0.05
$\tilde{b}_{266}$	0.00	145.04	−0.01	−0.02	−0.02	−0.01
$\tilde{b}_{333}$	0.00	0.00	81.12	0.00	0.00	−0.00
$\tilde{b}_{334}$	0.00	0.24	0.00	144.81	−0.04	0.04
$\tilde{b}_{335}$	0.15	−0.01	0.01	−0.04	226.48	−0.06
$\tilde{b}_{336}$	0.00	0.01	−0.00	0.04	−0.06	326.51
$\tilde{b}_{344}$	−0.00	−0.01	144.81	−0.00	0.87	−0.04
$\tilde{b}_{345}$	−0.00	0.85	−0.07	1.73	−0.11	−2.66
$\tilde{b}_{346}$	−0.51	−0.00	0.07	−0.07	−2.66	−0.07
$\tilde{b}_{355}$	0.00	−0.01	226.48	−0.06	0.00	−0.06
$\tilde{b}_{356}$	−0.01	−1.31	−0.11	−2.66	−0.11	0.11
$\tilde{b}_{366}$	−0.00	−0.01	326.51	−0.04	0.06	0.00
$\tilde{b}_{444}$	−0.00	0.00	−0.00	256.70	0.00	−0.00
$\tilde{b}_{445}$	−0.00	−0.01	0.87	0.00	402.93	−0.05
$\tilde{b}_{446}$	0.00	−0.67	−0.04	−0.00	−0.05	580.90
$\tilde{b}_{455}$	0.00	0.01	−0.06	402.93	0.00	−2.16
$\tilde{b}_{456}$	0.01	0.04	−2.66	−0.10	−4.31	0.02
$\tilde{b}_{466}$	−0.00	−0.02	−0.04	580.90	0.01	−0.00
$\tilde{b}_{555}$	−0.00	−0.00	0.00	0.00	627.59	−0.00
$\tilde{b}_{556}$	0.01	0.02	−0.06	−2.16	−0.00	908.50
$\tilde{b}_{566}$	−0.01	−0.02	0.06	0.01	908.50	0.00
$\tilde{b}_{666}$	−0.00	−0.00	0.00	−0.00	0.00	1303.91

E.2.2. uvw-displacement model

Table E.9: Single mode coefficients for the first 6 modes of a STEP model that includes only the **longitudinal**, **transverse** and **vertical** displacements (uvw-displacement model). The variables are computed for a string with characteristics similar to those from Table C.4.

Eq.	**(1)**	**(2)**	**(3)**	**(4)**	**(5)**	**(6)**
k_n [s^{-2}]	1.32×10^{12}	1.32×10^{12}	5.27×10^{12}	5.27×10^{12}	1.19×10^{13}	1.19×10^{13}
ω_n [s^{-2}]	1.15×10^{6}	1.15×10^{6}	2.30×10^{6}	2.30×10^{6}	3.44×10^{6}	3.44×10^{6}
$b^{(n)}_{nnn}$ [m^{-2}s^{-2}]	2.02×10^{33}	2.02×10^{33}	3.32×10^{34}	3.32×10^{34}	1.66×10^{35}	1.66×10^{35}
$\frac{b^{(n)}_{nnn}}{k_n}$ [m]	1.53×10^{21}	1.53×10^{21}	6.30×10^{21}	6.30×10^{22}	1.39×10^{22}	1.39×10^{22}
$\tilde{k}_n$	1.00	1.00	4.00	4.00	9.01	9.01
$\tilde{\omega}_n$	1.00	1.00	2.00	2.00	3.00	3.00
$\tilde{b}^{(n)}_{nnn}$	1.00	1.00	16.00	16.44	81.97	81.97

Table E.10: Modal coefficients for the first 6 modes of a STEP model that **longitudinal**, **transverse** and **vertical** displacements (uvw-displacement model). Note that the coefficients are scaled with respect to $\tilde{b}^{(1)}_{111}$. The uneven modes represent vertical modes, the even modes represent the transverse modes.

Eq.	**(1)**	**(2)**	**(3)**	**(4)**	**(5)**	**(6)**
$\tilde{b}_{111}$	1.00	−0.00	0.00	0.00	−0.03	−0.00
$\tilde{b}_{112}$	−0.00	1.01	−0.00	0.00	0.00	−0.00
$\tilde{b}_{113}$	0.00	−0.00	4.06	0.01	−0.00	−0.00
$\tilde{b}_{114}$	0.00	0.00	0.01	4.05	−0.00	−0.00
$\tilde{b}_{115}$	−0.10	0.00	−0.00	−0.00	9.11	0.02
$\tilde{b}_{116}$	−0.01	−0.00	−0.00	−0.00	0.02	9.13
$\tilde{b}_{122}$	1.01	0.00	−0.00	0.00	0.00	0.00
$\tilde{b}_{123}$	−0.00	−0.00	−0.02	0.01	0.00	0.00
$\tilde{b}_{124}$	0.00	0.00	0.01	0.02	−0.00	0.00
$\tilde{b}_{125}$	0.01	0.00	0.00	−0.00	0.03	0.02
$\tilde{b}_{126}$	−0.00	0.01	0.00	0.00	0.02	−0.03
$\tilde{b}_{133}$	4.06	−0.01	−0.00	0.00	0.01	0.03
$\tilde{b}_{134}$	0.02	0.01	0.00	0.00	0.02	0.01
$\tilde{b}_{135}$	−0.00	0.00	0.01	0.02	−0.00	−0.00
$\tilde{b}_{136}$	−0.00	0.00	0.06	0.01	−0.00	−0.00
$\tilde{b}_{144}$	4.05	0.01	0.00	−0.00	0.02	0.01
$\tilde{b}_{145}$	−0.00	−0.00	0.02	0.04	−0.00	−0.00
$\tilde{b}_{146}$	−0.00	0.00	0.01	0.02	−0.00	−0.00
$\tilde{b}_{155}$	9.11	0.02	−0.00	−0.00	0.01	−0.00
$\tilde{b}_{156}$	0.03	0.02	−0.00	−0.00	−0.00	−0.00
$\tilde{b}_{166}$	9.13	−0.02	−0.00	−0.00	−0.00	−0.01
$\tilde{b}_{222}$	0.00	1.00	−0.00	0.00	−0.00	0.03
$\tilde{b}_{223}$	−0.00	−0.00	4.05	−0.01	−0.00	−0.00
$\tilde{b}_{224}$	0.00	0.00	−0.01	4.06	−0.00	−0.00
$\tilde{b}_{225}$	0.00	−0.01	−0.00	−0.00	9.13	−0.02
$\tilde{b}_{226}$	0.00	0.10	−0.00	−0.00	−0.02	9.11
$\tilde{b}_{233}$	−0.01	4.05	0.00	−0.00	0.01	−0.02
$\tilde{b}_{234}$	0.01	−0.02	−0.00	−0.00	−0.01	0.02
$\tilde{b}_{235}$	0.00	−0.00	0.02	−0.01	−0.00	0.00
$\tilde{b}_{236}$	0.00	−0.00	−0.04	0.02	0.00	0.00
$\tilde{b}_{244}$	0.01	4.06	−0.00	−0.00	0.03	−0.01
$\tilde{b}_{245}$	−0.00	−0.00	−0.01	0.06	−0.00	−0.00
$\tilde{b}_{246}$	0.00	−0.00	0.02	−0.01	−0.00	0.00
$\tilde{b}_{255}$	0.02	9.13	−0.00	−0.00	−0.01	0.00
$\tilde{b}_{256}$	0.02	−0.03	0.00	−0.00	0.00	−0.00
$\tilde{b}_{266}$	−0.02	9.11	0.00	0.00	−0.00	−0.01
$\tilde{b}_{333}$	−0.00	0.00	16.00	0.05	−0.00	0.00
$\tilde{b}_{334}$	0.00	−0.00	0.14	16.20	−0.00	−0.00
$\tilde{b}_{335}$	0.01	0.01	−0.00	−0.00	36.42	−0.00
$\tilde{b}_{336}$	0.03	−0.02	0.00	−0.00	−0.00	36.57
$\tilde{b}_{344}$	0.00	−0.00	16.20	−0.14	−0.00	−0.00
$\tilde{b}_{345}$	0.02	−0.01	−0.00	−0.00	−0.01	0.15
$\tilde{b}_{346}$	0.01	0.02	−0.00	−0.00	0.15	0.01
$\tilde{b}_{355}$	−0.00	−0.00	36.42	−0.00	−0.00	−0.00
$\tilde{b}_{356}$	−0.00	0.00	−0.01	0.15	−0.00	−0.00
$\tilde{b}_{366}$	−0.00	0.00	36.57	0.00	−0.00	−0.00
$\tilde{b}_{444}$	−0.00	−0.00	−0.05	16.44	0.00	0.00
$\tilde{b}_{445}$	0.02	0.03	−0.00	0.00	36.57	0.00
$\tilde{b}_{446}$	0.01	−0.01	−0.00	0.00	0.00	36.42
$\tilde{b}_{455}$	−0.00	−0.00	−0.00	36.57	−0.00	−0.00
$\tilde{b}_{456}$	−0.00	−0.00	0.15	0.01	−0.00	−0.00
$\tilde{b}_{466}$	−0.00	0.00	0.00	36.42	−0.00	−0.00
$\tilde{b}_{555}$	0.00	−0.00	−0.00	−0.00	81.97	0.05
$\tilde{b}_{556}$	−0.00	0.00	−0.00	−0.00	0.15	82.06
$\tilde{b}_{566}$	−0.00	−0.00	−0.00	−0.00	82.06	−0.15
$\tilde{b}_{666}$	−0.00	−0.00	−0.00	−0.00	−0.05	81.97

E.3. Modal coupling coefficients of new designs

E.3.1. Discretized string design with constant cross-sections

Table E.11: Single mode coefficients for the first 6 modes of a discretized string of 100 elements. The coefficients were found using STEP. The variables are computed for a string with characteristics similar to those from Table C.4.

Eq.	**(1)**	**(2)**	**(3)**	**(4)**	**(5)**	**(6)**
k_n [s^{-2}]	1.32×10^{12}	5.26×10^{12}	1.18×10^{13}	2.10×10^{13}	3.29×10^{13}	4.74×10^{13}
ω_n [rad s^{-1}]	1.15×10^{6}	2.29×10^{6}	3.44×10^{6}	4.59×10^{6}	5.73×10^{6}	6.88×10^{6}
$b^{(n)}_{nnn}$ [m^{-2}s^{-2}]	2.05×10^{33}	3.27×10^{34}	1.66×10^{35}	5.24×10^{35}	1.28×10^{36}	2.65×10^{36}
$\frac{b^{(n)}_{nnn}}{k_n}$ [m]	1.55×10^{21}	6.22×10^{21}	1.41×10^{22}	2.50×10^{22}	3.89×10^{22}	5.93×10^{22}
$\tilde{k}_n$	1.00	4.00	9.00	16.00	25.00	36.00
$\tilde{\omega}_n$	1.00	2.00	3.00	4.00	5.00	6.00
$\tilde{b}^{(n)}_{nnn}$	1.00	16.00	80.98	255.96	624.94	1295.99

Table E.12: Modal coupling coefficients for the first 6 modes of a discretized string of 100 elements. The coefficients were found using STEP. Note that the coefficients are scaled with respect to $\tilde{b}^{(1)}_{111}$.

Eq.	**(1)**	**(2)**	**(3)**	**(4)**	**(5)**	**(6)**
$\tilde{b}_{111}$	1.00	0.00	0.00	0.00	−0.01	0.01
$\tilde{b}_{112}$	0.00	4.01	−0.00	0.03	−0.00	−0.00
$\tilde{b}_{113}$	0.00	−0.00	9.03	0.00	0.05	0.00
$\tilde{b}_{114}$	0.01	0.03	0.00	16.05	0.00	0.09
$\tilde{b}_{115}$	−0.02	−0.00	0.05	0.00	25.09	0.01
$\tilde{b}_{116}$	0.03	−0.00	0.00	0.09	0.01	36.14
$\tilde{b}_{122}$	4.01	−0.00	0.04	−0.00	0.07	−0.00
$\tilde{b}_{123}$	−0.00	0.08	−0.00	0.16	−0.00	0.24
$\tilde{b}_{124}$	0.05	−0.00	0.16	−0.00	0.27	−0.00
$\tilde{b}_{125}$	−0.00	0.13	−0.00	0.27	−0.01	0.42
$\tilde{b}_{126}$	−0.00	−0.00	0.24	−0.00	0.42	−0.00
$\tilde{b}_{133}$	9.03	−0.00	0.00	−0.00	0.15	−0.00
$\tilde{b}_{134}$	0.00	0.16	−0.00	0.00	0.00	0.51
$\tilde{b}_{135}$	0.10	−0.00	0.30	0.00	0.01	0.01
$\tilde{b}_{136}$	0.00	0.24	−0.01	0.51	0.01	0.00
$\tilde{b}_{144}$	16.05	−0.00	0.00	−0.00	−0.00	−0.01
$\tilde{b}_{145}$	0.00	0.27	0.00	−0.00	−0.01	−0.01
$\tilde{b}_{146}$	0.17	−0.00	0.51	−0.01	−0.01	−0.02
$\tilde{b}_{155}$	25.09	−0.00	0.01	−0.01	0.01	−0.01
$\tilde{b}_{156}$	0.01	0.42	0.01	−0.01	−0.02	−0.00
$\tilde{b}_{166}$	36.14	−0.00	0.00	−0.01	−0.00	−0.01
$\tilde{b}_{222}$	−0.00	16.00	0.00	−0.01	0.01	0.03
$\tilde{b}_{223}$	0.04	0.01	36.12	0.00	0.01	0.01
$\tilde{b}_{224}$	−0.00	−0.02	0.00	64.21	0.01	0.01
$\tilde{b}_{225}$	0.07	0.04	0.01	0.01	100.36	0.02
$\tilde{b}_{226}$	−0.00	0.10	0.01	0.01	0.02	144.55
$\tilde{b}_{233}$	−0.00	36.12	−0.00	0.24	−0.01	−0.01
$\tilde{b}_{234}$	0.16	0.00	0.47	−0.00	0.83	0.02
$\tilde{b}_{235}$	−0.00	0.01	−0.02	0.83	−0.02	1.30
$\tilde{b}_{236}$	0.24	0.01	−0.01	0.02	1.30	−0.03
$\tilde{b}_{244}$	−0.00	64.21	−0.00	0.01	−0.01	0.67
$\tilde{b}_{245}$	0.27	0.02	0.83	−0.03	−0.01	0.01
$\tilde{b}_{246}$	−0.00	0.02	0.02	1.33	0.01	0.05
$\tilde{b}_{255}$	−0.00	100.36	−0.01	−0.01	−0.01	−0.02
$\tilde{b}_{256}$	0.42	0.04	1.30	0.01	−0.03	−0.06
$\tilde{b}_{266}$	−0.00	144.55	−0.02	0.03	−0.03	0.03
$\tilde{b}_{333}$	0.00	−0.00	80.98	0.01	−0.01	0.03
$\tilde{b}_{334}$	−0.00	0.24	0.02	144.50	0.03	0.04
$\tilde{b}_{335}$	0.15	−0.01	−0.04	0.03	225.82	0.05
$\tilde{b}_{336}$	−0.00	−0.01	0.08	0.04	0.05	325.27
$\tilde{b}_{344}$	0.00	−0.00	144.50	0.00	0.87	0.03
$\tilde{b}_{345}$	0.00	0.83	0.06	1.74	0.10	2.74
$\tilde{b}_{346}$	0.51	0.02	0.08	0.06	2.74	0.05
$\tilde{b}_{355}$	0.01	−0.01	225.82	0.05	0.01	0.05
$\tilde{b}_{356}$	0.01	1.30	0.10	2.74	0.10	0.13
$\tilde{b}_{366}$	0.00	−0.02	325.27	0.02	0.07	−0.02
$\tilde{b}_{444}$	−0.00	0.00	0.00	255.96	0.01	−0.03
$\tilde{b}_{445}$	−0.00	−0.01	0.87	0.04	401.52	0.14
$\tilde{b}_{446}$	−0.01	0.67	0.03	−0.08	0.14	578.34
$\tilde{b}_{455}$	−0.01	−0.01	0.05	401.52	0.00	2.35
$\tilde{b}_{456}$	−0.01	0.01	2.74	0.28	4.70	0.39
$\tilde{b}_{466}$	−0.01	0.03	0.02	578.34	0.20	0.02
$\tilde{b}_{555}$	0.00	−0.00	0.00	0.00	624.94	0.02
$\tilde{b}_{556}$	−0.01	−0.02	0.05	2.35	0.06	903.84
$\tilde{b}_{566}$	−0.00	−0.03	0.07	0.20	903.84	−0.01
$\tilde{b}_{666}$	−0.00	0.01	−0.01	0.01	−0.00	1295.99

E.3.2. Discretized string design with increased width at the edges and at 0.25L and 0.75L

Table E.13: Single mode coefficients for the first 6 modes of a discretized string of 100 elements with increased width near the clamping points and at 0.25L and 0.75L (similar to C.5b). $w_{\text{spring}} = 4\mu$m and $w_{\text{mass}} = 3w_{\text{spring}} = 12\mu$m. The coefficients were found using STEP. The variables are computed for a string with characteristics similar to those from Table C.4.

Eq.	**(1)**	**(2)**	**(3)**	**(4)**	**(5)**	**(6)**
k_n [s^{-2}]	2.55×10^{12}	7.34×10^{12}	2.24×10^{13}	4.44×10^{13}	6.23×10^{13}	9.37×10^{13}
ω_n [s^{-2}]	1.60×10^{6}	2.71×10^{6}	4.73×10^{6}	6.66×10^{6}	7.89×10^{6}	9.68×10^{6}
$b^{(n)}_{nnn}$ [ms^{-2}]	1.17×10^{33}	9.66×10^{33}	9.01×10^{34}	3.56×10^{35}	6.99×10^{35}	1.58×10^{36}
$\frac{b^{(n)}_{nnn}}{k_n}$ [m]	4.59×10^{21}	1.32×10^{21}	4.02×10^{21}	8.01×10^{21}	1.12×10^{22}	1.69×10^{22}
$\tilde{k}_n$	1.00	2.88	8.78	17.41	24.43	36.72
$\tilde{\omega}_n$	1.00	1.70	2.96	4.17	4.94	6.06
$\tilde{b}^{(n)}_{nnn}$	1.00	8.26	76.97	304.08	597.79	1348.82

Table E.14: Nonlinear modal coefficients for the first 6 modes of a discretized string of 100 elements with increased width near the clamping points and at 0.25L and 0.75L (similar to C.5b). The coefficients were found using STEP. $w_{\text{spring}} = 4\mu$m and $w_{\text{mass}} = 3w_{\text{spring}} = 12\mu$m. Note that the coefficients are scaled with respect to $\tilde{b}^{(1)}_{111}$.

Eq.	**(1)**	**(2)**	**(3)**	**(4)**	**(5)**	**(6)**
$\tilde{b}_{111}$	1.00	0.00	−0.00	−0.01	−0.01	−0.03
$\tilde{b}_{112}$	0.00	2.90	0.00	−0.05	0.00	−0.01
$\tilde{b}_{113}$	−0.00	0.00	8.80	0.00	−0.13	−0.00
$\tilde{b}_{114}$	−0.03	−0.05	0.00	17.54	0.00	0.23
$\tilde{b}_{115}$	−0.04	0.00	−0.13	0.00	24.63	−0.01
$\tilde{b}_{116}$	−0.10	−0.01	−0.00	0.23	−0.01	37.01
$\tilde{b}_{122}$	2.90	0.00	−0.05	0.00	0.08	−0.00
$\tilde{b}_{123}$	0.00	−0.09	−0.00	0.21	−0.00	0.34
$\tilde{b}_{124}$	−0.10	0.00	0.21	−0.00	−0.52	0.00
$\tilde{b}_{125}$	0.00	0.15	−0.00	−0.52	−0.00	−0.84
$\tilde{b}_{126}$	−0.02	−0.00	0.34	0.00	−0.84	−0.00
$\tilde{b}_{133}$	8.80	−0.00	0.13	0.00	0.10	−0.00
$\tilde{b}_{134}$	0.00	0.21	0.01	0.42	−0.00	−0.80
$\tilde{b}_{135}$	−0.26	−0.00	0.20	−0.00	0.34	−0.00
$\tilde{b}_{136}$	−0.00	0.34	−0.00	−0.80	−0.00	−0.24
$\tilde{b}_{144}$	17.54	−0.00	0.21	0.00	−0.50	−0.00
$\tilde{b}_{145}$	0.01	−0.52	−0.00	−1.00	−0.01	0.27
$\tilde{b}_{146}$	0.46	0.00	−0.80	−0.00	0.27	0.01
$\tilde{b}_{155}$	24.63	−0.00	0.17	−0.00	−0.63	−0.01
$\tilde{b}_{156}$	−0.01	−0.84	−0.00	0.27	−0.01	0.86
$\tilde{b}_{166}$	37.01	−0.00	−0.12	0.00	0.43	0.01
$\tilde{b}_{222}$	0.00	8.26	−0.00	−0.01	0.02	−0.00
$\tilde{b}_{223}$	−0.05	−0.01	25.34	0.00	−0.02	−0.00
$\tilde{b}_{224}$	0.00	−0.02	0.00	50.25	0.01	0.16
$\tilde{b}_{225}$	0.08	0.06	−0.02	0.01	70.59	−0.02
$\tilde{b}_{226}$	−0.00	−0.00	−0.00	0.16	−0.02	106.41
$\tilde{b}_{233}$	−0.00	25.34	−0.01	−0.27	0.00	0.25
$\tilde{b}_{234}$	0.21	0.00	−0.54	0.00	0.88	0.01
$\tilde{b}_{235}$	−0.00	−0.05	0.01	0.88	0.01	1.81
$\tilde{b}_{236}$	0.34	−0.01	0.51	0.01	1.81	0.02
$\tilde{b}_{244}$	−0.00	50.25	0.00	−0.21	0.01	−0.89
$\tilde{b}_{245}$	−0.52	0.02	0.88	0.01	−0.27	0.01
$\tilde{b}_{246}$	0.00	0.31	0.01	−1.78	0.01	−1.32
$\tilde{b}_{255}$	−0.00	70.59	0.00	−0.14	−0.01	−0.37
$\tilde{b}_{256}$	−0.84	−0.03	1.81	0.01	−0.75	0.06
$\tilde{b}_{266}$	−0.00	106.41	0.01	−0.66	0.03	−1.52
$\tilde{b}_{333}$	0.04	−0.00	76.97	0.03	−0.02	0.12
$\tilde{b}_{334}$	0.00	−0.27	0.10	154.02	0.03	−0.37
$\tilde{b}_{335}$	0.10	0.00	−0.05	0.03	216.06	−0.05
$\tilde{b}_{336}$	−0.00	0.25	0.37	−0.37	−0.05	324.65
$\tilde{b}_{344}$	0.21	0.00	154.02	0.02	−3.30	−0.03
$\tilde{b}_{345}$	−0.00	0.88	0.05	−6.60	−0.09	−4.71
$\tilde{b}_{346}$	−0.80	0.01	−0.74	−0.07	−4.71	0.05
$\tilde{b}_{355}$	0.17	0.00	216.06	−0.05	−3.44	0.00
$\tilde{b}_{356}$	−0.00	1.81	−0.09	−4.71	0.01	−3.80
$\tilde{b}_{366}$	−0.12	0.01	324.65	0.03	−1.90	0.01
$\tilde{b}_{444}$	0.00	−0.07	0.01	304.08	−0.05	0.70
$\tilde{b}_{445}$	−0.50	0.01	−3.30	−0.14	432.09	−0.04
$\tilde{b}_{446}$	−0.00	−0.89	−0.03	2.09	−0.04	645.41
$\tilde{b}_{455}$	−0.00	−0.14	−0.05	432.09	−0.07	6.86
$\tilde{b}_{456}$	0.27	0.01	−4.71	−0.08	13.71	0.02
$\tilde{b}_{466}$	0.00	−0.66	0.03	645.41	0.01	5.78
$\tilde{b}_{555}$	−0.21	−0.00	−1.15	−0.02	597.79	−0.11
$\tilde{b}_{556}$	−0.01	−0.37	0.00	6.86	−0.33	905.87
$\tilde{b}_{566}$	0.43	0.03	−1.90	0.01	905.87	−0.18
$\tilde{b}_{666}$	0.00	−0.51	0.00	1.93	−0.06	1348.82

E.3.3. Discretized string design with decreased width at 0.25L and 0.75L

Table E.15: Single mode coefficients for the first 6 modes of a discretized string of 100 elements with decreased width near the clamping points and at 0.25L and 0.75L (similar to C.5c). $w_{\text{spring}} = 4\mu\text{m}$ and $w_{\text{mass}} = \frac{1}{3} = \frac{4}{3}\mu\text{m}$. The coefficients were found using STEP. The variables are computed for a string with characteristics similar to those from Table C.4.

Eq.	**(1)**	**(2)**	**(3)**	**(4)**	**(5)**	**(6)**
k_n [s^{-2}]	1.57×10^{12}	8.03×10^{12}	1.66×10^{13}	2.40×10^{13}	3.89×10^{13}	6.55×10^{13}
ω_n [s^{-2}]	1.25×10^{6}	2.83×10^{6}	4.08×10^{6}	4.90×10^{6}	6.23×10^{6}	8.10×10^{6}
$b^{(n)}_{nnn}$ [ms^{-2}]	1.83×10^{33}	4.80×10^{34}	2.05×10^{35}	4.26×10^{35}	1.12×10^{36}	3.19×10^{36}
$\frac{b^{(n)}_{nnn}}{k_n}$ [m]	1.17×10^{21}	5.98×10^{21}	1.23×10^{22}	1.78×10^{22}	2.88×10^{22}	4.87×10^{22}
$\tilde{k}_n$	1.00	5.11	10.58	15.26	24.73	41.70
$\tilde{\omega}_n$	1.00	2.26	3.25	3.91	4.97	6.46
$\tilde{b}^{(n)}_{nnn}$	1.00	26.17	111.95	232.44	611.07	1740.80

Table E.16: Nonlinear modal coefficients for the first 6 modes of a discretized string of 100 elements with increased width near the clamping points and at 0.25L and 0.75L (similar to C.5b). The coefficients were found using STEP. $w_{\text{spring}} = 4\mu\text{m}$ and $w_{\text{mass}} = \frac{1}{3} = \frac{4}{3}\mu\text{m}$. Note that the coefficients are scaled with respect to $\tilde{b}^{(1)}_{111}$.

Eq.	**(1)**	**(2)**	**(3)**	**(4)**	**(5)**	**(6)**
$\tilde{b}_{111}$	1.00	0.00	0.00	0.01	0.01	−0.02
$\tilde{b}_{112}$	0.00	5.12	0.00	0.05	0.00	0.01
$\tilde{b}_{113}$	0.01	0.00	10.63	0.00	0.07	0.00
$\tilde{b}_{114}$	0.03	0.05	0.00	15.33	0.00	−0.08
$\tilde{b}_{115}$	0.04	0.00	0.07	0.00	24.76	0.01
$\tilde{b}_{116}$	−0.06	0.01	0.00	−0.08	0.01	41.76
$\tilde{b}_{122}$	5.12	−0.00	0.11	0.00	0.17	0.00
$\tilde{b}_{123}$	0.00	0.22	0.00	0.46	0.01	−0.46
$\tilde{b}_{124}$	0.10	0.00	0.46	0.00	0.41	0.00
$\tilde{b}_{125}$	0.00	0.34	0.01	0.41	0.01	−0.26
$\tilde{b}_{126}$	0.02	0.00	−0.46	0.00	−0.26	−0.00
$\tilde{b}_{133}$	10.63	0.00	0.31	0.00	0.42	0.00
$\tilde{b}_{134}$	0.00	0.46	0.01	0.53	0.01	−0.74
$\tilde{b}_{135}$	0.13	0.01	0.83	0.01	−0.06	0.01
$\tilde{b}_{136}$	0.01	−0.46	0.01	−0.74	0.01	−0.36
$\tilde{b}_{144}$	15.33	0.00	0.26	−0.00	0.22	0.00
$\tilde{b}_{145}$	0.00	0.41	0.01	0.45	0.01	0.06
$\tilde{b}_{146}$	−0.15	0.00	−0.74	0.01	0.06	−0.00
$\tilde{b}_{155}$	24.76	0.00	−0.03	0.01	0.85	0.03
$\tilde{b}_{156}$	0.01	−0.26	0.01	0.06	0.06	1.63
$\tilde{b}_{166}$	41.76	−0.00	−0.18	−0.00	0.82	0.00
$\tilde{b}_{222}$	−0.00	26.17	0.01	−0.01	0.03	−0.15
$\tilde{b}_{223}$	0.11	0.04	54.42	0.01	−0.11	0.02
$\tilde{b}_{224}$	0.00	−0.03	0.01	78.46	0.01	0.30
$\tilde{b}_{225}$	0.17	0.08	−0.11	0.01	127.19	0.04
$\tilde{b}_{226}$	0.00	−0.45	0.02	0.30	0.04	214.59
$\tilde{b}_{233}$	0.00	54.42	0.01	0.85	0.01	−0.18
$\tilde{b}_{234}$	0.46	0.02	1.69	0.03	1.88	0.01
$\tilde{b}_{235}$	0.01	−0.22	0.02	1.88	−0.00	−2.60
$\tilde{b}_{236}$	−0.46	0.03	−0.37	0.01	−2.60	0.00
$\tilde{b}_{244}$	0.00	78.46	0.01	0.64	0.01	−1.45
$\tilde{b}_{245}$	0.41	0.02	1.88	0.03	−0.39	−0.04
$\tilde{b}_{246}$	0.00	0.59	0.01	−2.90	−0.04	−1.39
$\tilde{b}_{255}$	0.00	127.19	−0.00	−0.20	−0.00	0.77
$\tilde{b}_{256}$	−0.26	0.08	−2.60	−0.04	1.54	0.11
$\tilde{b}_{266}$	−0.00	214.59	0.00	−0.70	0.06	−0.78
$\tilde{b}_{333}$	0.10	0.00	111.95	0.03	−0.02	−0.08
$\tilde{b}_{334}$	0.00	0.85	0.10	162.64	0.04	−0.67
$\tilde{b}_{335}$	0.42	0.01	−0.07	0.04	262.98	0.06
$\tilde{b}_{336}$	0.00	−0.18	−0.25	−0.67	0.06	443.41
$\tilde{b}_{344}$	0.26	0.01	162.64	0.04	1.52	0.04
$\tilde{b}_{345}$	0.01	1.88	0.08	3.04	0.07	−4.15
$\tilde{b}_{346}$	−0.74	0.01	−1.33	0.08	−4.15	0.04
$\tilde{b}_{355}$	−0.03	−0.00	262.98	0.03	−2.83	−0.01
$\tilde{b}_{356}$	0.01	−2.60	0.11	−4.15	−0.02	−6.78
$\tilde{b}_{366}$	−0.18	0.00	443.41	0.02	−3.39	0.02
$\tilde{b}_{444}$	−0.00	0.21	0.01	232.44	0.04	0.04
$\tilde{b}_{445}$	0.22	0.01	1.52	0.12	378.24	0.07
$\tilde{b}_{446}$	0.00	−1.45	0.04	0.13	0.07	638.22
$\tilde{b}_{455}$	0.01	−0.20	0.03	378.24	0.03	−1.08
$\tilde{b}_{456}$	0.06	−0.04	−4.15	0.15	−2.17	0.16
$\tilde{b}_{466}$	−0.00	−0.70	0.02	638.22	0.08	6.38
$\tilde{b}_{555}$	0.28	−0.00	−0.94	0.01	611.07	−0.04
$\tilde{b}_{556}$	0.03	0.77	−0.01	−1.08	−0.12	1036.92
$\tilde{b}_{566}$	0.82	0.06	−3.39	0.08	1036.92	0.01
$\tilde{b}_{666}$	0.00	−0.26	0.01	2.13	0.00	1740.80

E.3.4. Discretized zipper-like string designs for $w_{\text{mass}} = 4\,w_{\text{spring}}$

Table E.17: Linear modal coefficients for the first 6 modes of a discretized string of 100 elements from Figure C.8. The coefficients were found using STEP. $w_{\text{spring}} = 4\mu$m and $w_{\text{mass}} = 16\mu$m. The variables are computed for a string with characteristics similar to those from Table C.4.

Eq.	**(1)**	**(2)**	**(3)**	**(4)**	**(5)**	**(6)**
k_n [s^{-2}]	6.57×10^{11}	2.63×10^{12}	5.90×10^{12}	1.05×10^{13}	1.63×10^{13}	2.33×10^{13}
ω_n [rad s^{-1}]	8.11×10^{5}	1.62×10^{6}	2.43×10^{6}	3.23×10^{6}	4.03×10^{6}	4.83×10^{6}
$b^{(n)}_{nnn}$ [m^{-2}s^{-2}]	6.72×10^{32}	1.07×10^{34}	5.41×10^{34}	1.70×10^{35}	4.12×10^{35}	8.46×10^{35}
$\frac{b^{(n)}_{nnn}}{k_n}$ [m]	1.02×10^{21}	4.07×10^{21}	9.17×10^{21}	1.62×10^{21}	2.53×10^{22}	3.63×10^{22}
$\tilde{k}_n$	1.00	4.00	8.97	15.90	24.75	35.46
$\tilde{\omega}_n$	1.00	2.00	3.00	3.99	4.98	5.96
$\tilde{b}^{(n)}_{nnn}$	1.00	15.96	80.48	252.90	612.68	1257.60

Table E.18: Nonlinear modal coefficients for the first 6 modes of a discretized string of 100 elements from Figure C.8. The coefficients were found using STEP. $w_{\text{spring}} = 4\mu$m and $w_{\text{mass}} = 16\mu$m. Note that the coefficients are scaled with respect to $\tilde{b}^{(1)}_{111}$.

Eq.	**(1)**	**(2)**	**(3)**	**(4)**	**(5)**	**(6)**
$\tilde{b}_{111}$	1.00	0.00	0.00	0.00	−0.01	0.01
$\tilde{b}_{112}$	0.00	4.00	0.00	0.02	−0.00	−0.00
$\tilde{b}_{113}$	0.00	0.00	8.99	−0.00	0.04	−0.00
$\tilde{b}_{114}$	0.01	0.02	−0.00	15.95	0.00	0.07
$\tilde{b}_{115}$	−0.02	−0.00	0.04	0.00	24.82	0.01
$\tilde{b}_{116}$	0.02	−0.00	−0.00	0.07	0.01	35.57
$\tilde{b}_{122}$	4.00	−0.00	0.03	−0.00	0.05	−0.00
$\tilde{b}_{123}$	0.00	0.06	0.00	0.12	0.00	0.19
$\tilde{b}_{124}$	0.04	−0.00	0.12	−0.00	0.21	−0.00
$\tilde{b}_{125}$	−0.00	0.10	0.00	0.21	−0.01	0.33
$\tilde{b}_{126}$	−0.00	−0.00	0.19	−0.00	0.33	−0.00
$\tilde{b}_{133}$	8.99	0.00	−0.00	−0.00	0.11	−0.00
$\tilde{b}_{134}$	−0.00	0.12	−0.00	0.00	−0.01	0.40
$\tilde{b}_{135}$	0.07	0.00	0.23	−0.01	−0.01	−0.01
$\tilde{b}_{136}$	−0.01	0.19	−0.01	0.40	−0.01	0.01
$\tilde{b}_{144}$	15.95	−0.00	0.00	−0.01	−0.00	−0.01
$\tilde{b}_{145}$	0.01	0.21	−0.01	−0.01	−0.01	0.00
$\tilde{b}_{146}$	0.13	−0.00	0.40	−0.01	0.00	−0.02
$\tilde{b}_{155}$	24.82	−0.00	−0.00	−0.01	−0.01	−0.01
$\tilde{b}_{156}$	0.01	0.33	−0.01	0.00	−0.02	−0.01
$\tilde{b}_{166}$	35.57	−0.00	0.01	−0.01	−0.00	−0.01
$\tilde{b}_{222}$	−0.00	15.96	0.00	−0.00	0.01	0.03
$\tilde{b}_{223}$	0.03	0.00	35.94	−0.00	−0.01	−0.01
$\tilde{b}_{224}$	−0.00	−0.01	−0.00	63.71	0.01	0.01
$\tilde{b}_{225}$	0.05	0.02	−0.01	0.01	99.18	0.02
$\tilde{b}_{226}$	−0.00	0.08	−0.01	0.01	0.02	142.13
$\tilde{b}_{233}$	0.00	35.94	−0.00	0.18	−0.01	−0.01
$\tilde{b}_{234}$	0.12	−0.01	0.36	−0.01	0.64	−0.02
$\tilde{b}_{235}$	0.00	−0.01	−0.02	0.64	0.00	1.03
$\tilde{b}_{236}$	0.19	−0.02	−0.02	−0.02	1.03	0.01
$\tilde{b}_{244}$	−0.00	63.71	−0.00	−0.01	−0.02	0.51
$\tilde{b}_{245}$	0.21	0.02	0.64	−0.03	−0.02	0.01
$\tilde{b}_{246}$	−0.00	0.02	−0.02	1.02	0.01	0.05
$\tilde{b}_{255}$	−0.00	99.18	0.00	−0.01	−0.01	−0.02
$\tilde{b}_{256}$	0.33	0.04	1.03	0.01	−0.04	−0.07
$\tilde{b}_{266}$	−0.00	142.13	0.00	0.02	−0.03	−0.01
$\tilde{b}_{333}$	−0.00	−0.00	80.48	0.00	−0.02	0.02
$\tilde{b}_{334}$	−0.00	0.18	0.01	143.09	0.01	0.03
$\tilde{b}_{335}$	0.11	−0.01	−0.05	0.01	222.75	0.05
$\tilde{b}_{336}$	−0.00	−0.01	0.05	0.03	0.05	319.20
$\tilde{b}_{344}$	0.00	−0.00	143.09	−0.00	0.63	−0.04
$\tilde{b}_{345}$	−0.01	0.64	0.02	1.25	−0.01	2.13
$\tilde{b}_{346}$	0.40	−0.02	0.07	−0.08	2.13	−0.10
$\tilde{b}_{355}$	−0.00	0.00	222.75	−0.00	−0.02	−0.06
$\tilde{b}_{356}$	−0.01	1.03	0.11	2.13	−0.13	−0.09
$\tilde{b}_{366}$	0.01	0.00	319.20	−0.05	−0.05	−0.02
$\tilde{b}_{444}$	−0.00	−0.00	−0.00	252.90	0.01	−0.03
$\tilde{b}_{445}$	−0.00	−0.02	0.63	0.02	394.92	0.14
$\tilde{b}_{446}$	−0.01	0.51	−0.04	−0.08	0.14	565.93
$\tilde{b}_{455}$	−0.01	−0.01	−0.00	394.92	−0.01	1.86
$\tilde{b}_{456}$	0.00	0.01	2.13	0.28	3.72	0.39
$\tilde{b}_{466}$	−0.01	0.02	−0.05	565.93	0.19	−0.05
$\tilde{b}_{555}$	−0.00	−0.00	−0.01	−0.00	612.68	0.01
$\tilde{b}_{556}$	−0.01	−0.02	−0.06	1.86	0.03	881.02
$\tilde{b}_{566}$	−0.00	−0.03	−0.05	0.19	881.02	−0.02
$\tilde{b}_{666}$	−0.00	−0.00	−0.01	−0.02	−0.01	1257.60

E.3.5. Discretized zipper-like string designs for $w_{\text{mass}} = 10\,w_{\text{spring}}$

Table E.19: Linear modal coefficients for the first 6 modes of a discretized string of 100 elements from Figure C.8. $w_{\text{spring}} = 4\mu$m and $w_{\text{mass}} = 40\mu$m. The coefficients were found using STEP. The variables are computed for a string with characteristics similar to those from Table C.4.

Eq.	**(1)**	**(2)**	**(3)**	**(4)**	**(5)**	**(6)**
k_n [s^{-2}]	3.29×10^{11}	1.31×10^{12}	2.94×10^{12}	5.19×10^{12}	8.04×10^{12}	1.15×10^{13}
ω_n [rad s^{-1}]	5.73×10^{5}	1.14×10^{6}	1.71×10^{6}	2.28×10^{6}	2.84×10^{6}	3.39×10^{6}
$b^{(n)}_{nnn}$ [m^{-2}s^{-2}]	1.79×10^{32}	2.85×10^{33}	1.43×10^{34}	4.47×10^{34}	1.07×10^{35}	2.18×10^{35}
$\frac{b^{(n)}_{nnn}}{k_n}$ [m]	5.44×10^{20}	2.18×10^{21}	4.86×10^{21}	8.61×10^{21}	1.33×10^{22}	1.90×10^{22}
$\tilde{k}_n$	1.00	3.99	8.94	15.80	24.48	34.88
$\tilde{\omega}_n$	1.00	2.00	2.99	3.97	4.95	5.91
$\tilde{b}^{(n)}_{nnn}$	1.00	15.92	79.92	249.52	599.29	1216.77

Table E.20: Nonlinear modal coefficients for the first 6 modes of a discretized string of 100 elements from Figure C.8. The coefficients were found using STEP. $w_{\text{spring}} = 4\mu$m and $w_{\text{mass}} = 40\mu$m. Note that the coefficients are scaled with respect to $\tilde{b}^{(1)}_{111}$.

Eq.	**(1)**	**(2)**	**(3)**	**(4)**	**(5)**	**(6)**
$\tilde{b}_{111}$	1.00	0.00	0.00	0.00	−0.01	0.01
$\tilde{b}_{112}$	0.00	4.00	0.00	0.02	−0.00	−0.00
$\tilde{b}_{113}$	0.01	0.00	8.96	0.00	0.03	−0.00
$\tilde{b}_{114}$	0.01	0.02	0.00	15.84	−0.00	0.05
$\tilde{b}_{115}$	−0.03	−0.00	0.03	−0.00	24.55	0.01
$\tilde{b}_{116}$	0.02	−0.00	−0.00	0.05	0.01	34.99
$\tilde{b}_{122}$	4.00	−0.00	0.03	0.00	0.05	−0.00
$\tilde{b}_{123}$	0.00	0.06	0.00	0.12	0.00	0.18
$\tilde{b}_{124}$	0.04	0.00	0.12	−0.00	0.20	−0.00
$\tilde{b}_{125}$	−0.00	0.09	0.00	0.20	−0.01	0.31
$\tilde{b}_{126}$	−0.00	−0.00	0.18	−0.00	0.31	−0.00
$\tilde{b}_{133}$	8.96	0.00	−0.00	0.00	0.11	−0.00
$\tilde{b}_{134}$	0.00	0.12	0.00	0.00	0.01	0.37
$\tilde{b}_{135}$	0.07	0.00	0.21	0.01	−0.01	−0.01
$\tilde{b}_{136}$	−0.01	0.18	−0.01	0.37	−0.01	0.01
$\tilde{b}_{144}$	15.84	−0.00	0.00	−0.01	−0.00	−0.00
$\tilde{b}_{145}$	−0.01	0.20	0.01	−0.01	0.00	0.01
$\tilde{b}_{146}$	0.11	−0.00	0.37	−0.01	0.01	−0.01
$\tilde{b}_{155}$	24.55	−0.00	−0.00	0.00	−0.01	−0.01
$\tilde{b}_{156}$	0.01	0.31	−0.01	0.01	−0.02	−0.01
$\tilde{b}_{166}$	34.99	−0.00	0.01	−0.00	−0.00	−0.01
$\tilde{b}_{222}$	−0.00	15.92	0.00	−0.01	0.01	0.02
$\tilde{b}_{223}$	0.03	0.00	35.76	0.00	−0.01	−0.01
$\tilde{b}_{224}$	0.00	−0.02	0.00	63.20	−0.01	−0.01
$\tilde{b}_{225}$	0.05	0.02	−0.01	−0.01	97.96	0.02
$\tilde{b}_{226}$	−0.00	0.07	−0.01	−0.01	0.02	139.61
$\tilde{b}_{233}$	0.00	35.76	−0.00	0.18	−0.01	−0.01
$\tilde{b}_{234}$	0.12	0.01	0.35	0.01	0.61	−0.00
$\tilde{b}_{235}$	0.00	−0.02	−0.02	0.61	0.00	0.96
$\tilde{b}_{236}$	0.18	−0.02	−0.02	−0.00	0.96	0.01
$\tilde{b}_{244}$	−0.00	63.20	0.01	−0.01	−0.02	0.48
$\tilde{b}_{245}$	0.20	−0.03	0.61	−0.03	0.03	−0.04
$\tilde{b}_{246}$	−0.00	−0.03	−0.00	0.95	−0.04	−0.01
$\tilde{b}_{255}$	−0.00	97.96	0.00	0.01	−0.01	−0.02
$\tilde{b}_{256}$	0.31	0.05	0.96	−0.04	−0.04	−0.07
$\tilde{b}_{266}$	−0.00	139.61	0.00	−0.01	−0.04	−0.02
$\tilde{b}_{333}$	−0.00	−0.00	79.92	0.00	−0.01	0.01
$\tilde{b}_{334}$	0.00	0.18	0.01	141.61	−0.02	−0.04
$\tilde{b}_{335}$	0.11	−0.01	−0.04	−0.02	219.51	0.06
$\tilde{b}_{336}$	−0.00	−0.01	0.04	−0.04	0.06	312.84
$\tilde{b}_{344}$	0.00	0.01	141.61	−0.01	0.58	−0.04
$\tilde{b}_{345}$	0.01	0.61	−0.04	1.16	−0.02	1.91
$\tilde{b}_{346}$	0.37	−0.00	−0.08	−0.09	1.91	0.06
$\tilde{b}_{355}$	−0.00	0.00	219.51	−0.01	−0.03	−0.07
$\tilde{b}_{356}$	−0.01	0.96	0.11	1.91	−0.13	−0.08
$\tilde{b}_{366}$	0.01	0.00	312.84	0.03	−0.04	−0.02
$\tilde{b}_{444}$	−0.00	−0.00	−0.00	249.52	0.00	−0.02
$\tilde{b}_{445}$	−0.00	−0.02	0.58	0.01	387.93	0.05
$\tilde{b}_{446}$	−0.00	0.48	−0.04	−0.05	0.05	552.88
$\tilde{b}_{455}$	0.00	0.01	−0.01	387.93	−0.01	1.53
$\tilde{b}_{456}$	0.01	−0.04	1.91	0.10	3.07	−0.04
$\tilde{b}_{466}$	−0.00	−0.01	0.03	552.88	−0.02	−0.05
$\tilde{b}_{555}$	−0.00	−0.00	−0.01	−0.00	599.29	0.01
$\tilde{b}_{556}$	−0.01	−0.02	−0.07	1.53	0.02	857.00
$\tilde{b}_{566}$	−0.00	−0.04	−0.04	−0.02	857.00	−0.02
$\tilde{b}_{666}$	−0.00	−0.01	−0.01	−0.02	−0.01	1216.77

E.3.6. Discretized asymmetrical string design

Table E.21: Linear stiffness and Duffing coefficients for the first 6 modes of an asymmetrical discretized string of 100 elements from Figure C.9. The coefficients were found using STEP. $w_{\text{spring}} = 4\mu$m and $w_{\text{mass}} = 40\mu$m. The variables are computed for a string with characteristics similar to those from Table C.4.

Eq.	**(1)**	**(2)**	**(3)**	**(4)**	**(5)**	**(6)**
k_n [s^{-2}]	2.86×10^{11}	1.88×10^{12}	3.77×10^{12}	6.80×10^{12}	1.23×10^{13}	1.60×10^{13}
ω_n [rad s^{-1}]	5.35×10^{5}	1.37×10^{6}	1.94×10^{6}	2.61×10^{6}	3.51×10^{6}	4.00×10^{6}
$b^{(n)}_{nnn}$ [m^{-2}s^{-2}]	1.33×10^{32}	5.75×10^{33}	2.30×10^{34}	7.52×10^{34}	2.47×10^{35}	4.15×10^{35}
$\frac{b^{(n)}_{nnn}}{k_n}$ [m]	4.65×10^{20}	3.06×10^{21}	6.10×10^{21}	1.11×10^{22}	2.01×10^{22}	2.59×10^{22}
$\tilde{k}_n$	1.00	6.58	13.18	23.76	43.11	55.93
$\tilde{\omega}_n$	1.00	2.56	3.63	4.87	6.57	7.48
$\tilde{b}^{(n)}_{nnn}$	1.00	43.32	173.50	566.05	1860.76	3127.26

Table E.22: Nonlinear modal coefficients for the first 6 modes of an asymmetrical discretized string of 100 elements from Figure C.9. The coefficients were found using STEP. $w_{\text{spring}} = 4\mu$m and $w_{\text{mass}} = 40\mu$m. Note that the coefficients are scaled with respect to $\tilde{b}^{(1)}_{111}$.

Eq.	**(1)**	**(2)**	**(3)**	**(4)**	**(5)**	**(6)**
$\tilde{b}_{111}$	1.00	−0.00	0.00	0.00	−0.00	0.00
$\tilde{b}_{112}$	−0.01	6.59	−0.02	0.03	−0.01	−0.00
$\tilde{b}_{113}$	0.00	−0.02	13.19	−0.05	0.03	0.01
$\tilde{b}_{114}$	0.00	0.03	−0.05	23.84	−0.11	−0.07
$\tilde{b}_{115}$	−0.01	−0.01	0.03	−0.11	43.20	0.13
$\tilde{b}_{116}$	0.00	−0.00	0.01	−0.07	0.13	55.99
$\tilde{b}_{122}$	6.59	0.02	−0.00	−0.03	0.12	0.07
$\tilde{b}_{123}$	−0.05	−0.00	0.09	0.04	−0.09	−0.29
$\tilde{b}_{124}$	0.07	−0.05	0.04	0.18	0.09	0.19
$\tilde{b}_{125}$	−0.02	0.23	−0.09	0.09	0.33	−0.03
$\tilde{b}_{126}$	−0.00	0.13	−0.29	0.19	−0.03	0.45
$\tilde{b}_{133}$	13.19	0.04	−0.08	0.10	0.12	−0.09
$\tilde{b}_{134}$	−0.09	0.04	0.20	−0.42	0.25	−0.26
$\tilde{b}_{135}$	0.06	−0.09	0.24	0.25	−0.60	−0.49
$\tilde{b}_{136}$	0.01	−0.29	−0.18	−0.26	−0.49	−0.61
$\tilde{b}_{144}$	23.84	0.09	−0.21	0.51	−0.36	−0.27
$\tilde{b}_{145}$	−0.21	0.09	0.25	−0.72	1.23	0.95
$\tilde{b}_{146}$	−0.14	0.19	−0.26	−0.54	0.95	1.09
$\tilde{b}_{155}$	43.20	0.17	−0.30	0.61	−0.40	−0.36
$\tilde{b}_{156}$	0.26	−0.03	−0.49	0.95	−0.71	−0.75
$\tilde{b}_{166}$	55.99	0.23	−0.30	0.55	−0.37	−0.55
$\tilde{b}_{222}$	0.01	43.32	−0.08	−0.14	0.10	−0.04
$\tilde{b}_{223}$	−0.00	−0.24	86.81	−0.22	−0.43	−0.43
$\tilde{b}_{224}$	−0.03	−0.42	−0.22	157.38	−0.08	0.87
$\tilde{b}_{225}$	0.12	0.30	−0.43	−0.08	284.92	1.25
$\tilde{b}_{226}$	0.07	−0.12	−0.43	0.87	1.25	369.01
$\tilde{b}_{233}$	0.04	86.81	−0.05	0.23	0.22	0.21
$\tilde{b}_{234}$	0.04	−0.44	0.47	−0.75	1.34	−0.10
$\tilde{b}_{235}$	−0.09	−0.87	0.44	1.34	−0.74	−2.08
$\tilde{b}_{236}$	−0.29	−0.86	0.43	−0.10	−2.08	−0.39
$\tilde{b}_{244}$	0.09	157.38	−0.37	−1.39	−0.61	−1.66
$\tilde{b}_{245}$	0.09	−0.17	1.34	−1.22	−2.50	−1.23
$\tilde{b}_{246}$	0.19	1.74	−0.10	−3.31	−1.23	−2.68
$\tilde{b}_{255}$	0.17	284.92	−0.37	−1.25	1.12	0.73
$\tilde{b}_{256}$	−0.03	2.51	−2.08	−1.23	1.47	1.45
$\tilde{b}_{266}$	0.23	369.01	−0.19	−1.34	0.72	0.50
$\tilde{b}_{333}$	−0.03	−0.02	173.50	−0.11	−0.19	−0.05
$\tilde{b}_{334}$	0.10	0.23	−0.34	313.81	−0.02	0.39
$\tilde{b}_{335}$	0.12	0.22	−0.58	−0.02	569.43	0.21
$\tilde{b}_{336}$	−0.09	0.21	−0.16	0.39	0.21	738.53
$\tilde{b}_{344}$	−0.21	−0.37	313.81	−2.30	0.35	−0.46
$\tilde{b}_{345}$	0.25	1.34	−0.03	0.69	−3.34	−4.89
$\tilde{b}_{346}$	−0.26	−0.10	0.77	−0.92	−4.89	−2.14
$\tilde{b}_{355}$	−0.30	−0.37	569.43	−1.67	−2.80	−1.76
$\tilde{b}_{356}$	−0.49	−2.08	0.42	−4.89	−3.52	−3.42
$\tilde{b}_{366}$	−0.30	−0.19	738.53	−1.07	−1.71	−1.93
$\tilde{b}_{444}$	0.17	−0.46	−0.77	566.05	−0.68	0.92
$\tilde{b}_{445}$	−0.36	−0.61	0.35	−2.03	1030.41	5.49
$\tilde{b}_{446}$	−0.27	−1.66	−0.46	2.77	5.49	1335.16
$\tilde{b}_{455}$	0.61	−1.25	−1.67	1030.41	−2.08	−2.10
$\tilde{b}_{456}$	0.95	−1.23	−4.89	10.98	−4.19	0.30
$\tilde{b}_{466}$	0.55	−1.34	−1.07	1335.16	0.15	3.28
$\tilde{b}_{555}$	−0.13	0.37	−0.93	−0.69	1860.76	4.25
$\tilde{b}_{556}$	−0.36	0.73	−1.76	−2.10	12.75	2423.08
$\tilde{b}_{566}$	−0.37	0.72	−1.71	0.15	2423.08	10.73
$\tilde{b}_{666}$	−0.18	0.17	−0.64	1.09	3.58	3127.26

F

Code

F.1. Matlab codes

F.1.1. FPUT simulation

```
% FPUT code - can run default FPUT problem or run the simulation for string parameters
clear all; clc

% Load string variables
S_A_structure_par_string_Minxing

% Load FPU vars
N = 16;
k = 1; m = 1;
m_vec = m*ones(1,N);
% mass matrix
M = diag(m_vec);
% lin stiff matrix
kd = 2*k*ones(N,1); % diag matrix vector
kd_UL = -k*ones(N-1,1); % upper/lower matrix vector
KD = diag(kd); % diagonal matrix
KD_U = diag(kd_UL,1); KD_L = diag(kd_UL,-1); % upper and lower
K = KD + KD_U + KD_L; % total matrix

% modal analysis
[V, D] = eig(K,M);
alpha = max(max(V)); % Scaling of eigenvectors with modal mass (alpha = sqrt(2/m_tot))
modmassmat = V'*M*V; % should be unity
modstiffmat = V'*K*V; % modstiffmat = D-matrix

k_modal = diag(modstiffmat); % take diagonal since stiffmatrix is diagonal
ind_eig = [1 2 3 4 5 6];

% Select string parameters
stringvals = 1 % string parameters or not?
perf_freq = 0;

if stringvals == 0
    beta = 8;
    omega = sqrt(k_modal);
elseif stringvals == 1
    % For string
    m_string = rho*As*Length;
    alpha = sqrt(2/(rho*As*Length)); % Eigvector scale parameter
    for n_i = 1:length(ind_eig)
    k_modal(n_i) = (ind_eig(n_i)^2*sig0*pi^2)/((Length^2)*rho);
    b_simpleSTEP(n_i) = (3/8)*((ind_eig(n_i)^4*Emod*pi^4)/((Length^4)*rho))*alpha^2; ...
        % this one matches with STEP
    end
```

```
    beta = b_simpleSTEP(1)/(0.000102323); % beta for string parameters
end

Q = [1e5];
zeta  = 1./(2*Q);
c_modal    = 2.0.*zeta.*sqrt(k_modal/k_modal(1)); % ND already

n_solve = 6;
k_modal = k_modal(1:n_solve);
if perf_freq == 0
k_modal = k_modal(1).*diag(modstiffmat(:,1:n_solve))/modstiffmat(1,1);
end

% If f5 is integer
% k_modal(5) = k_modal(5)*1.07 % scales f5/f1 to 5.00

c_modal = 1*c_modal(1:n_solve);
a = zeros(21,6);
min_stringb = 1e-25; % onset of destroyed FPU is at 1e-3
if stringvals == 0
    b_FPU = b_matrix(beta);
elseif stringvals == 1
    [b_FPU, b_string] = b_matrix_string_simple(b_simpleSTEP(1), min_stringb);
end

%{
% Uncomment this to find the needed coupling terms
b_nonzero = ones(56,6)
% 1st EoM: terms with modes 1, 3 and 5
b_nonzero(3,1) = 0;
b_nonzero(12,1) = 0; b_nonzero(14,1) = 0;
b_nonzero(19,1) = 0; b_nonzero(39,1) = 0;

% 3rd EoM: terms with modes 1, 3 and 5
b_nonzero(1,3) = 0;
b_nonzero(3,3) = 0; b_nonzero(3,5) = 0;
b_nonzero(14,3) = 0; b_nonzero(44,3) = 0;

% 5th EoM: terms with modes 1, 3 and 5
b_nonzero(3,5) = 0; b_nonzero(5,5) = 0;
b_nonzero(12,5) = 0; b_nonzero(39,5) = 0;
b_FPU = b_nonzero.*b_FPU

% COMPARE TO STRING VALUES
% if stringvals == 1
%     simple = 1;
%         if simple == 0
%         [b_compS, b_string, b_larger, b_string_l] = b_matrix_string(b_FPU, ...
    min_stringb); % u and w-disp model
%         elseif simple == 1
%         [b_compS, b_string] = b_matrix_string_simple(b_FPU, min_stringb); % w-only ...
    model
%         end
%     b_FPU = b_compS; % This sets either the simple or the full model --> dep of simple
%     b_FPU_norm = b_FPU./b_FPU(1,1); % This normalizes the b-matrix
% end
%}

% Time and space normalization
T = sqrt(1/k_modal(1)); % Time scaling parameter = 1/omega_0
k_ND = k_modal.*T^2;
h = sqrt(k_modal(1))/sqrt(b_FPU(1,1));
a_ND = a*h/k_modal(1);
b_ND_FPU = b_FPU.*h^2.*T^2;
b_ND = b_ND_FPU;

% This is the total space scaling: also with max eigenvector
u_scale = h*alpha;

ND = 1; % Sets the ND or Dimensional equation of motion
clear t_span q_free E
```

```
options = odeset('Reltol',1e-14,'Abstol',1e-12,'OutputSel',[1,2,n_solve]);
w0 = zeros(1,2*n_solve);
if ND == 1
dt = 0.01;
tspan = 0:dt:300;
if stringvals == 1
    w0(1) = 11.82e-6;
%     w0(1) = 0.8*11.82e-6;
%     w0(3) = 0.15*11.82e-6;
%     w0(5) = 0.05*11.82e-6;
%     w0(7) = w0(1)*sqrt(k_modal(1));
%     w0(9) = w0(3)*sqrt(k_modal(3));
%     w0(11) = w0(5)*sqrt(k_modal(5));
elseif stringvals == 0
    w0(1) = 1;
end
    q0 = w0./u_scale; % scales it to the nondimensional space using the eigenvect and ...
        space scaling
    q0(7:end) = q0(7:end).*T;
    [t_free,q_free] = ...
        ode45(@(t,q)freeODE_6D(t,q,k_ND,c_modal,a_ND,b_ND),tspan,q0,options);
    q_free = q_free.*h; % scales the amplitude and vel back to mass-norm space: for ...
        energy comp
    q_free(:,7:end) = q_free(:,7:end)./T; % scales the vel back to original time
    q_free_PA = q_free.*alpha; % scales the amplitude and vel back to original space: ...
        incl alpha
elseif ND == 0
    q0 = w0/alpha;
%     q0(1) = 5 % for m = 0.1
    dt = 0.1;
    tspan = 0:dt:2000;
    [t_free,q_free] = ...
        ode45(@(t,q)freeODE_6D(t,q,k_modal,c_modal,a,b_FPU),tspan,q0,options);
end

tspan = tspan.*T;
% Find peak values of signal to find max points for energy criterion
[t_maxq1, q_maxq1, i_rec, rec1_time, rec1_perc, E.E1peak, E.E1potpeak, E.E1kinpeak, ...
    E.E1NLpeak] = fT_PeakFinder(q_free,tspan,1,k_modal,b_FPU);
[t_maxq2, q_maxq2, ¬, ¬, ¬, E.E2peak, E.E2potpeak, E.E2kinpeak, E.E2NLpeak] = ...
    fT_PeakFinder(q_free,tspan,2,k_modal,b_FPU);
[t_maxq3, q_maxq3, ¬, ¬, ¬, E.E3peak, E.E3potpeak, E.E3kinpeak, E.E3NLpeak] = ...
    fT_PeakFinder(q_free,tspan,3,k_modal,b_FPU);
[t_maxq4, q_maxq4, ¬, ¬, ¬, E.E4peak, E.E4potpeak, E.E4kinpeak, E.E4NLpeak] = ...
    fT_PeakFinder(q_free,tspan,4,k_modal,b_FPU);
[t_maxq5, q_maxq5, ¬, ¬, ¬, E.E5peak, E.E5potpeak, E.E5kinpeak, E.E5NLpeak] = ...
    fT_PeakFinder(q_free,tspan,5,k_modal,b_FPU);
[t_maxq6, q_maxq6, ¬, ¬, ¬, E.E6peak, E.E6potpeak, E.E6kinpeak, E.E6NLpeak] = ...
    fT_PeakFinder(q_free,tspan,6,k_modal,b_FPU);

% total single-mode energy at these peaks
E.E1totpeak = E.E1peak + E.E1NLpeak(:,1); E.E2totpeak = E.E2peak + E.E2NLpeak(:,1); ...
    E.E3totpeak = E.E3peak + E.E3NLpeak(:,1);
E.E4totpeak = E.E4peak + E.E4NLpeak(:,1); E.E5totpeak = E.E5peak + E.E5NLpeak(:,1); ...
    E.E6totpeak = E.E6peak + E.E6NLpeak(:,1);
E.E0 = 0.5*k_modal(1)*q_free(1,1)^2 + 0.5*1*q_free(1,1+n_solve)^2;

[max_Erectot,i_rectot] = max(E.E1totpeak(2:end,1)); i_rectot = 1 + i_rectot;
perc_recTot = max_Erectot/E.E1totpeak(1)

% Compute energies
for i = 1:length(tspan)
E.E1(i) = 0.5*k_modal(1)*q_free(i,1)^2 + 0.5*1*q_free(i,1+n_solve)^2;
E.E2(i) = 0.5*k_modal(2)*q_free(i,2)^2 + 0.5*1*q_free(i,2+n_solve)^2;
E.E3(i) = 0.5*k_modal(3)*q_free(i,3)^2 + 0.5*1*q_free(i,3+n_solve)^2;
E.E4(i) = 0.5*k_modal(4)*q_free(i,4)^2 + 0.5*1*q_free(i,4+n_solve)^2;
E.E5(i) = 0.5*k_modal(5)*q_free(i,5)^2 + 0.5*1*q_free(i,5+n_solve)^2;
E.E6(i) = 0.5*k_modal(6)*q_free(i,6)^2 + 0.5*1*q_free(i,6+n_solve)^2;
E.E1pot(i) = 0.5*k_modal(1)*q_free(i,1)^2;
E.E2pot(i) = 0.5*k_modal(2)*q_free(i,2)^2;
E.E3pot(i) = 0.5*k_modal(3)*q_free(i,3)^2;
```

```
E.E4pot(i) = 0.5*k_modal(4)*q_free(i,4)^2;
E.E5pot(i) = 0.5*k_modal(5)*q_free(i,5)^2;
E.E6pot(i) = 0.5*k_modal(6)*q_free(i,6)^2;
E.E1kin(i) = 0.5*1*q_free(i,1+n_solve)^2;
E.E2kin(i) = 0.5*1*q_free(i,2+n_solve)^2;
E.E3kin(i) = 0.5*1*q_free(i,3+n_solve)^2;
E.E4kin(i) = 0.5*1*q_free(i,4+n_solve)^2;
E.E5kin(i) = 0.5*1*q_free(i,5+n_solve)^2;
E.E6kin(i) = 0.5*1*q_free(i,6+n_solve)^2;
E.diffE3E1(i) = E.E3(i)-E.E1(i);
E.diffE5E1(i) = E.E5(i)-E.E1(i);
[E.NL1(i), E.NL2(i), E.NL3(i), E.NL4(i), E.NL5(i), E.NL6(i), E.coup(i), ...
    E.coupuneven(i)] = fT_ModalEnergy(b_FPU,q_free,i);
end

[E.maxdomE3E1, E.imaxdomE3E1] = max(E.diffE3E1);
[E.maxdomE5E1, E.imaxdomE5E1] = max(E.diffE5E1);
EdomE3E1 = E.maxdomE3E1/E.E0
EdomE5E1 = E.maxdomE5E1/E.E0

%b-coefficients
count_b = 1;
for i = 1:6
    for j = i:6
        for k = j:6
        b_name(count_b,:) = [i, j, k];
        count_b = count_b+1;
        end
    end
end


% Criteria
% (1) linear frequency ratio
k_ND;

% (2) structure-specific Linear vs Nonlinear strength
mn = 1; % modenumber
b_111 = b_FPU(1,1); % this is the reference NL variable
k_b111 = k_modal(mn)/b_111;

% (3) Damping
Q;

% (4) Initial force ratio
b = b_FPU;
q1 = q0(1); q2 = q0(2); q3 = q0(3); q4 = q0(4); q5 = q0(5); q6 = q0(6);
q1_or = q0(1)*u_scale; q2_or = q0(2)*u_scale; q3_or = q0(3)*u_scale; q4_or = ...
    q0(4)*u_scale; q5_or = q0(5)*u_scale; q6_or = q0(6)*u_scale;

F_lin_or = k_modal(1).*q1_or;
F_lin = k_ND(1).*q1;
for mn = 1
F_NL = ...
    a_ND(1,mn)*q1^2+a_ND(2,mn)*q1*q2+a_ND(3,mn)*q1*q3+a_ND(4,mn)*q1*q4+a_ND(5,mn)*q1*q5+
a_ND(6,mn)*q1*q6...
    +a_ND(7,mn)*q2*q2+a_ND(8,mn)*q2*q3+a_ND(9,mn)*q2*q4+a_ND(10,mn)*q2*q5+a_ND(11,mn)*q2*q6...
    +a_ND(12,mn)*q3*q3+a_ND(13,mn)*q3*q4+a_ND(14,mn)*q3*q5+a_ND(15,mn)*q3*q6...
    +a_ND(16,mn)*q4*q4+a_ND(17,mn)*q4*q5+a_ND(18,mn)*q4*q6...
    +a_ND(19,mn)*q5*q5+a_ND(20,mn)*q5*q6...
    +a_ND(21,mn)*q6*q6...
    +b_ND(1,mn)*q1^3+b_ND(1,2)*q1^2*q2+b_ND(3,mn)*q1^2*q3+b_ND(4,mn)*q1^2*q4
    +b_ND(5,mn)*q1^2*q5+b_ND(6,mn)*q1^2*q6...
    +b_ND(7,mn)*q1*q2^2+b_ND(8,mn)*q1*q2*q3+b_ND(9,mn)*q1*q2*q4+b_ND(10,mn)*q1*q2*q5+
    b_ND(11,mn)*q1*q2*q6...
    +b_ND(12,mn)*q1*q3*q3+b_ND(13,mn)*q1*q3*q4+b_ND(14,mn)*q1*q3*q5+b_ND(15,mn)*q1*q3*q6...
    +b_ND(16,mn)*q1*q4*q4+b_ND(17,mn)*q1*q4*q5+b_ND(18,mn)*q1*q4*q6...
    +b_ND(19,mn)*q1*q5*q5+b_ND(20,mn)*q1*q5*q6...
    +b_ND(21,mn)*q1*q6*q6...
    +b_ND(22,mn)*q2*q2^2+b_ND(23,mn)*q2*q2*q3+b_ND(24,mn)*q2*q2*q4+b_ND(25,mn)*q2*q2*q5
    +b_ND(26,mn)*q1*q2*q6...
```

```
    +b_ND(27,mn)*q2*q3*q3+b_ND(28,mn)*q2*q3*q4+b_ND(29,mn)*q2*q3*q5+b_ND(30,mn)*q2*q3*q6...
    +b_ND(31,mn)*q2*q4*q4+b_ND(32,mn)*q2*q4*q5+b_ND(33,mn)*q2*q4*q6...
    +b_ND(34,mn)*q2*q5*q5+b_ND(35,mn)*q2*q5*q6...
    +b_ND(36,mn)*q2*q6*q6...
    +b_ND(37,mn)*q3*q3*q3+b_ND(38,mn)*q3*q3*q4+b_ND(39,mn)*q3*q3*q5+b_ND(40,mn)*q3*q3*q6...
    +b_ND(41,mn)*q3*q4*q4+b_ND(42,mn)*q3*q4*q5+b_ND(33,mn)*q3*q4*q6...
    +b_ND(44,mn)*q3*q5*q5+b_ND(45,mn)*q3*q5*q6...
    +b_ND(46,mn)*q3*q6*q6...
    +b_ND(47,mn)*q4*q4*q4+b_ND(48,mn)*q4*q4*q5+b_ND(49,mn)*q4*q4*q6...
    +b_ND(50,mn)*q4*q5*q5+b_ND(51,mn)*q4*q5*q6...
    +b_ND(52,mn)*q4*q6*q6...
    +b_ND(53,mn)*q5*q5*q5+b_ND(54,mn)*q5*q5*q6...
    +b_ND(55,mn)*q5*q6*q6...
    +b_ND(56,mn)*q6*q6*q6;
end
F_ratio = F_NL/F_lin;


% Visualize it
figure(1); clf
plot(t_maxq1,E.E1peak(:,1),t_maxq2,E.E2peak,t_maxq3(1:3:end),E.E3peak(1:3:end),t_maxq4,
E.E4peak,t_maxq5(1:5:end),E.E5peak(1:5:end),t_maxq6,E.E6peak); hold on % smooth
legend('Mode 1','Mode 2','Mode 3','Mode 4','Mode 5','Mode 6','1st rec.')
xlabel('Time (s)','FontSize',12); ylabel('Energy (a.u.)','FontSize',12)
xlim([0 tspan(end)])

figure(2); clf
subplot(5,1,1)
plot(tspan,E.E1,tspan,E.E2,tspan,E.E3,tspan,E.E4,tspan,E.E5,tspan,E.E6); hold on
plot(t_maxq1(i_rec),E.E1peak(i_rec),'k*');
legend('Mode 1','Mode 2','Mode 3','Mode 4','Mode 5','Mode 6','1st rec.')
xlabel('^{Time (s)}','FontSize',10); ylabel('Energy (a.u.)')
xlim([0 tspan(end)])
title('Total linear energy')

subplot(5,1,2)
E.E1tot = E.E1+E.NL1; E.E2tot = E.E2+E.NL2; E.E3tot = E.E3+E.NL3;
E.E4tot = E.E4+E.NL4; E.E5tot = E.E5+E.NL5; E.E6tot = E.E6+E.NL6;
E1diff = (E.E1tot - E.E1)/E.E1; max_E1diff = max(E1diff)
plot(tspan,E.E1tot,tspan,E.E2tot,tspan,E.E3tot,tspan,E.E4tot,tspan,E.E5tot,tspan,E.E6tot); ...
    hold on
legend('Mode 1','Mode 2','Mode 3','Mode 4','Mode 5','Mode 6','1st rec.')
title('Single-mode (linear + nonlinear) energy')
xlabel('^{Time (s)}','FontSize',10); ylabel('Energy (a.u.)')

subplot(5,1,3)
plot(tspan,E.coup);
title('Coupling energy','FontSize', 9)
xlabel('^{Time (s)}','FontSize',10); ylabel('Energy (a.u.)')
xlim([0 tspan(end)])

subplot(5,1,4)
plot(tspan,q_free_PA(:,1),tspan,q_free_PA(:,2),tspan,q_free_PA(:,3),tspan,q_free_PA(:,4),
tspan,q_free_PA(:,5),tspan,q_free_PA(:,6)); hold on
legend('Mode 1','Mode 2','Mode 3','Mode 4','Mode 5','Mode 6','Mode 1','Mode 2','Mode ...
    3','Mode 4','Mode 5','Mode 6')
xlabel('^{Time (s)}','FontSize',10); ylabel('Amplitude (m)','FontSize',8)
xlim([0 tspan(end)])
title('Modal amplitudes','FontSize',8)

subplot(5,1,5)
plot(tspan,q_free_PA(:,1+n_solve),tspan,q_free_PA(:,2+n_solve),tspan,q_free_PA(:,3+n_solve)
,tspan,q_free_PA(:,4+n_solve),tspan,q_free_PA(:,5+n_solve),tspan,q_free_PA(:,6+n_solve));
hold on
legend('Mode 1','Mode 2','Mode 3','Mode 4','Mode 5','Mode 6','Mode 1','Mode 2','Mode ...
    3','Mode 4','Mode 5','Mode 6')
xlabel('^{Time (s)}','FontSize',10); ylabel('Velocity (m/s)','FontSize',8)
xlim([0 tspan(end)])
title('Modal velocities','FontSize',8)

annotation('textbox', [0.08, 0.95, 0, 0], 'string', '\bf (a)','FontSize', 9)
```

```
annotation('textbox', [0.08, 0.775, 0, 0], 'string', '\bf (b)','FontSize', 9)
annotation('textbox', [0.08, 0.6, 0, 0], 'string', '\bf (c)','FontSize', 9)
annotation('textbox', [0.08, 0.43, 0, 0], 'string', '\bf (d)','FontSize', 9)
annotation('textbox', [0.08, 0.26, 0, 0], 'string', '\bf (e)','FontSize', 9)
```

F.1.2. STEP and AUTO simulations

```
% Used to determine modal coefficients from STEP and run them in AUTO
% HEAD - RUNS ALL SCRIPTS
% Vincent Bos - adapted by Tim Jansen


clear all
close all
clc

matlabfolder    = pwd;
add_folders                                                 % define location of AUTO ...
    files
cd(autofolder); delete 'fort.*';        cd(matlabfolder);   % remove old AUTO files

% SETTINGS
ind_eig     = [1 2 3 4 5 6];                % select eigenmodes

n_eig_solve = max(ind_eig);         % number of eigenmodes searched for in eigenvalue ...
    solver
n_eig       = length(ind_eig);      % number of modes in the ROM

% Option 1: continuous structure
loc = 0.364;
S_A_structure_par_string_Minxing
[a_coefname,b_coefname,a_coef_un,b_coef_un,Km_value_un, MD] = ...
    fsnaar_model_out_of_plane_Minxing(n_eig_solve,ind_eig,MP_snaar);    % string
hardcode = 1;
if hardcode == 0
fprintf('ATTENTION! NOT hardcoded!')
elseif hardcode == 1
fprintf('ATTENTION! Hardcoded!')
end

if hardcode == 1
Km_value_un(2:end) = Km_value_un(1)*(1.00533^2)*[ind_eig(2:end).^2]
end

% Matching, scaling and generation of dimless variables
[a_coef_un,b_coef_un] = fmatchcoef(a_coef_un,b_coef_un,a_coefname,b_coefname); ...
             % correct coefficients

[a_coef,b_coef,Km_value,scale_h,scale_T] = ...
    fscalecoef(a_coef_un,b_coef_un,Km_value_un); %scale_h = (1/sqrt(20))*scale_h;
[a, b, k_modal, m_modal] = ...
    fT_odevars(a_coefname,a_coef,n_eig,b_coefname,b_coef,Km_value, MD);

for n_i = 1:length(ind_eig)
b_analytical(n_i) = (ind_eig(n_i)^4*Emod*pi^4)/(4*(Length^4)*rho);
b_analySTEP(n_i) = ((ind_eig(n_i)^4*Emod*pi^4)/(4*(Length^4)*rho))*MD.alpha(1)^2;
k_analytical(n_i) = (ind_eig(n_i)^2*sig0*pi^2)/((Length^2)*rho);
end

%% AUTO
% AUTO preparation

% cd(autofolder); delete 'fort.*';        cd(matlabfolder);   % remove old AUTO files
clear leg leg1 leg_exp leg_sim_point f_res
clear Mf7 Mf7_point

figure(100)
clf
figure(400)
```

```
clf
Q = [2e5, 2e5]; % for characterization: 1.45e5
zeta  = 1./(2*Q);                % set damping
 %FAST SETTING: omega_start = 0.9002, omega_end = 4, NMX = 10k

omega_start = 0.9991; % start freq sweep low values can give errors 6 modes = 0.97
omega_end   = 1.025; % end   freq sweep
omega_1     = 1;       % keep this fixed
slaop = 0; savefigs = 0;

Volt = linspace(1e-3,0.5,20);
sweep = [13]; sweeps = [1 5 10 13 14 15 16 17 18 19 20];
for jj = 1:length(sweep)
    figure(400); clf; figure(100); clf;
Fsweepvalues = [0.275e-13, 65e-13, 100e-13, 135e-13, 150e-13, 160e-13, 170e-13, ...
    180e-13, 190e-13, 200e-13, 215e-13]; % For mode 1 only:  % without any exp scaling

Fvalues = Fsweepvalues(find(sweeps==sweep(jj)));
Fmode_exc = ones(1,length(ind_eig)); Fmode_exc(1) = 1;
F_exc = zeros(length(ind_eig),1); F_exc(ind_eig==Fmode_exc) = 1;

for i = 1:length(Fvalues)
    cd(autofolder); delete 'fort.*';        cd(matlabfolder);   % remove old AUTO files
    clear Mf7 Mf7_point leg legpoint
    sweepno = sweeps(sweeps==sweep(jj));

    Fvalue = Fvalues(i);

    Cm_value    = 2.0.*zeta(i).*sqrt(Km_value);  Mm_value = diag(MD.mat.Mm); ...
                            % add damping

    i_u         = 1:2:n_eig*2; i_v = i_u + 1;  n_dim_U = n_eig*2 + 2; % indices of U ...
        with the amplitude and velocity
    CO          = ...
        fvar2struc(a_coef,b_coef,a_coefname,b_coefname,Km_value,Mm_value,n_eig,i_u); ...
        CO.Cm_value = Cm_value;       % write coeff to structure
    fstruc2var(MD)                              % load model parameters

    [map1,I]    = fcoord2mod_correct(coord1,MD,Length); % MAPS FORCE TO MODAL
    % determine mapping according to excitation point
    F_sweep     = F_exc .* map1 .* Fvalue .* scale_T^2 ./ scale_h; % modal force vector

    u_scale_axvec = scale_h*MD.alpha; %scales dimens to ND and modal to physical
    % MD.alpha is the max eig vect scaling


    u_scale_ax0   = diag(reshape(repmat(u_scale_axvec,2,1),[],1));  % scaling matrix ...
        for state space dof

    % ******************** FREQUENCY RESPONSE AUTO ********************** %%

    error = ...
        fwrite_equation(a_coef,b_coef,a_coefname,b_coefname,Km_value,Cm_value,omega_start,
    n_eig,mostfolder,F_sweep);    % write equations
    system(command); system(command);            % compile equations

    S_A_auto_base_1mode % this controls the two sweeps and places them into the Mf7 ...
        matrix    % run AUTO frequency sweep

    % READ FORT 8 INITIAL CURVE
    n_labels    = Mf7(end,4);                                       % pre-allocate ...
        for reading fort8
    [Dat_f8]    = freadfort8(n_labels,NTST,autofolder);             % read fort 8
    Xp          = fFRFpoint_fast(Dat_f8,scale_h,MD,I);              % map data ...
        (scaled to real displ) to point (point sensor) ORIGINAL
    Mf7_point   = fpointMf7(Xp,Mf7,[],[]);                          % rewrite data in ...
        Mf7 matrix for easy plotting

   if slaop == 1
        L = (Length - 2*5e-6)*1e6;
```

```
116         filenamedatsave_point = ...
                sprintf('Mf7_pointL%d_E%d_loc%.3f_sweep%d_F%.0fn_%.0f.mat',L,Emod/1e9,loc,
117         sweep(jj),round(Fvalue/1e-13),ind_eig(end));
118         save(filenamedatsave_point,'Mf7_point'); fprintf('Data sweep %d is ...
                saved!\n',sweep(jj));
119         filenamedatsave = ...
                sprintf('Mf7_L%d_E%d_loc%.3f_sweep%d_F%.0fn_%.0f.mat',L,Emod/1e9,loc,
120         sweep(jj),round(Fvalue/1e-13),ind_eig(end));
121         save(filenamedatsave,'Mf7'); fprintf('Data sweep %d is saved!\n',sweep(jj));
122     elseif slaop == 0
123         fprintf('ATTENTION! Data sweep %d is NOT saved!\n',sweep(i)')
124    end
125
126    S_A_plot_physical_base                                          % plot physical domain
127
128 %      3. DEFINE LEGENDS
129     legpoint.length(i) = length(p1);
130     legpoint.lengthsum(i) = sum(legpoint.length(1:i));
131     if i == 1
132         figure(400)
133         title(sprintf('Frequency response physical point at %.3f*L', ...
                coord1(1)/Length)); hold on
134      end
135
136 end
137
138 % PLOT THE EXPERIMENTAL DATA IN POINT PLOT
139 sweepno_exp = [1:1:20]; % Define experimental sweep data
140
141 [fwd, bwd, f_abs_exp, vel_exp, amp_exp, f_res_exp, freq_creep_exp, leg.exp] = ...
        fT_plot_expdata(loc,sweepno_exp, efreq, ind_eig, colorv,Fvalues);
142 leg.all(1:length(legpoint.sim)) = legpoint.sim;
143 leg.all(length(legpoint.sim)+1:length(legpoint.sim)+length(leg.exp)) = leg.exp;
144
145 legend(leg.all,'Location','northwest')
146 title('')
147 fig100 = figure(100);
148 xlim([omega_start omega_end])
149
150 if savefigs == 1
151     filename_100 = ...
            sprintf('Full_L%d_E%d_loc%.3f_sweep%d_F%.0fn_%.0f.fig',L,Emod/1e9,loc,sweep(jj)
152     ,round(Fvalue/1e-13),ind_eig(end));
153     filename_400 = ...
            sprintf('Point_L%d_E%d_loc%.3f_sweep%d_F%.0fn_%.0f.fig',L,Emod/1e9,loc,sweep(jj)
154     ,round(Fvalue/1e-13),ind_eig(end));
155     saveas(fig400,filename_400); saveas(fig100,filename_100)
156 end
157 end
```

F.2. Mathematica codes

F.2.1. Modal conversion FPUT problem

```
1  In[1]:= a = 0
2  T1 = 0.5*m*y1'[t]^2; T2 = 0.5*m*y2'[t]^2; T3 = 0.5*m*y3'[t]^2; T4 =
3   0.5*m*y4'[t]^2;
4  T5 = 0.5*m*y5'[t]^2; T6 = 0.5*m*y6'[t]^2; T7 = 0.5*m*y7'[t]^2; T8 =
5   0.5*m*y8'[t]^2;
6  T9 = 0.5*m*y9'[t]^2; T10 = 0.5*m*y10'[t]^2; T11 =
7   0.5*m*y11'[t]^2; T12 = 0.5*m*y12'[t]^2;
8  T13 = 0.5*m*y13'[t]^2; T14 = 0.5*m*y14'[t]^2; T15 =
9   0.5*m*y15'[t]^2; T16 = 0.5*m*y16'[t]^2;
10 T = T1 + T2 + T3 + T4 + T5 + T6 + T7 + T8 + T9 + T10 + T11 + T12 +
11   T13 + T14 + T15 + T16  (* Total kinetic energy *)
12 V1 = 0.5*k*y1[t]^2 + (1/3)*a*y1[t]^3 + 0.25*b*y1[t]^4;
13 V2 = 0.5*k*(y2[t] - y1[t])^2 + (1/3)*a*(y2[t] - y1[t])^3 +
14    0.25*b*(y2[t] - y1[t])^4;
15 V3 = 0.5*k*(y3[t] - y2[t])^2 + (1/3)*a*(y3[t] - y2[t])^3 +
```

```
    0.25*b*(y3[t] - y2[t])^4;
V4 = 0.5*k*(y4[t] - y3[t])^2 + (1/3)*a*(y4[t] - y3[t])^3 +
    0.25*b*(y4[t] - y3[t])^4;
V5 = 0.5*k*(y5[t] - y4[t])^2 + (1/3)*a*(y5[t] - y4[t])^3 +
    0.25*b*(y5[t] - y4[t])^4;
V6 = 0.5*k*(y6[t] - y5[t])^2 + (1/3)*a*(y6[t] - y5[t])^3 +
    0.25*b*(y6[t] - y5[t])^4;
V7 = 0.5*k*(y7[t] - y6[t])^2 + (1/3)*a*(y7[t] - y6[t])^3 +
    0.25*b*(y7[t] - y6[t])^4;
V8 = 0.5*k*(y8[t] - y7[t])^2 + (1/3)*a*(y8[t] - y7[t])^3 +
    0.25*b*(y8[t] - y7[t])^4;
V9 = 0.5*k*(y9[t] - y8[t])^2 + (1/3)*a*(y9[t] - y8[t])^3 +
    0.25*b*(y9[t] - y8[t])^4;
 {
 {V10 = 0.5*k*(y10[t] - y9[t])^2 + (1/3)*a*(y10[t] - y9[t])^3 +
      0.25*b*(y10[t] - y9[t])^4;},
 {V11 = 0.5*k*(y11[t] - y10[t])^2 + (1/3)*a*(y11[t] - y10[t])^3 +
      0.25*b*(y11[t] - y10[t])^4;},
 {V12 = 0.5*k*(y12[t] - y11[t])^2 + (1/3)*a*(y12[t] - y11[t])^3 +
      0.25*b*(y12[t] - y11[t])^4;
  V13 = 0.5*k*(y13[t] - y12[t])^2 + (1/3)*a*(y13[t] - y12[t])^3 +
      0.25*b*(y13[t] - y12[t])^4;
  V14 = 0.5*k*(y14[t] - y13[t])^2 + (1/3)*a*(y14[t] - y13[t])^3 +
      0.25*b*(y14[t] - y13[t])^4;}
}
V15 = 0.5*k*(y15[t] - y14[t])^2 + (1/3)*a*(y15[t] - y14[t])^3 +
    0.25*b*(y15[t] - y14[t])^4;
V16 = 0.5*k*(y16[t] - y15[t])^2 + (1/3)*a*(y16[t] - y15[t])^3 +
    0.25*b*(y16[t] - y15[t])^4;
V17 = 0.5*k*y16[t]^2 + (1/3)*a*y16[t]^3 + 0.25*b*y16[t]^4;
V = V1 + V2 + V3 + V4 + V5 + V6 + V7 + V8 + V9 + V10 + V11 + V12 +
  V13 + V14 + V15 + V16 + V17(* Total potential energy *)

(*Check Equations of Motion*)
In[21]:= EoMx1 = D[D[T, y1'[t]], t] + D[V, y1[t]]
EoMx2 = D[D[T, y2'[t]], t] + D[V, y2[t]]
EoMx3 = D[D[T, y3'[t]], t] + D[V, y3[t]]
EoMx4 = D[D[T, y4'[t]], t] + D[V, y4[t]]
EoMx5 = D[D[T, y5'[t]], t] + D[V, y5[t]]
EoMx6 = D[D[T, y6'[t]], t] + D[V, y6[t]]
EoMx7 = D[D[T, y7'[t]], t] + D[V, y7[t]]
EoMx8 = D[D[T, y8'[t]], t] + D[V, y8[t]]
EoMx9 = D[D[T, y9'[t]], t] + D[V, y9[t]]
EoMx10 = D[D[T, y10'[t]], t] + D[V, y10[t]]
EoMx11 = D[D[T, y11'[t]], t] + D[V, y11[t]]
EoMx12 = D[D[T, y12'[t]], t] + D[V, y12[t]]
EoMx13 = D[D[T, y13'[t]], t] + D[V, y13[t]]
EoMx14 = D[D[T, y14'[t]], t] + D[V, y14[t]]
EoMx15 = D[D[T, y15'[t]], t] + D[V, y15[t]]
EoMx16 = D[D[T, y16'[t]], t] + D[V, y16[t]]


In[57]:= (*Define mode shapes*) (*1*)
A1r1 = 0.18453671892660;
A1r2 = 0.36278926121756; A1r3 = 0.52868745033551; A1r4 = \
0.67658182242300; A1r5 = 0.80143601201832; A1r6 = 0.89899825944091; \
A1r7 = 0.96594619936780; A1r8 = 1.00000000000000; A1r9 = \
1.00000000000000; A1r10 = 0.96594619936780; A1r11 = 0.89899825944091; \
A1r12 = 0.80143601201832; A1r13 = 0.67658182242300; A1r14 = \
0.52868745033552; A1r15 = 0.36278926121756; A1r16 = 0.18453671892660;
(*2*)
A2r1 = 0.36278926121756; A2r2 = 0.67658182242300; A2r3 = \
0.89899825944091; A2r4 = 1.00000000000000; A2r5 = 0.96594619936780; \
A2r6 = 0.80143601201832; A2r7 = 0.52868745033552; A2r8 = \
0.18453671892660; A2r9 = -0.18453671892660; A2r10 = \
-0.52868745033551; A2r11 = -0.80143601201832; A2r12 = \
-0.96594619936780; A2r13 = -1.00000000000000; A2r14 = \
-0.89899825944091; A2r15 = -0.67658182242300; A2r16 = \
-0.36278926121756;
(*3*)
A3r1 = 0.52868745033551; A3r2 = 0.89899825944091; A3r3 = \
```

```
1.00000000000000; A3r4 = 0.80143601201832; A3r5 = 0.36278926121756; \
A3r6 = -0.18453671892660; A3r7 = -0.67658182242300; A3r8 = \
-0.96594619936780; A3r9 = -0.96594619936780; A3r10 = \
-0.67658182242300; A3r11 = -0.18453671892660; A3r12 = \
0.36278926121756; A3r13 = 0.80143601201832; A3r14 = 1.00000000000000; \
A3r15 = 0.89899825944091; A3r16 = 0.52868745033552;
(*4*)
A4r1 = 0.67658182242300; A4r2 = 1.00000000000000; A4r3 = \
0.80143601201832; A4r4 = 0.18453671892660; A4r5 = -0.52868745033551; \
A4r6 = -0.96594619936780; A4r7 = -0.89899825944091; A4r8 = \
-0.36278926121756; A4r9 = 0.36278926121756; A4r10 = 0.89899825944091; \
A4r11 = 0.96594619936780; A4r12 = 0.52868745033552; A4r13 = \
-0.18453671892660; A4r14 = -0.80143601201832; A4r15 = \
-1.00000000000000; A4r16 = -0.67658182242300;
(*5*)
A5r1 = 0.82969011373806; A5r2 = 1.00000000000000; A5r3 = \
0.37557915902045; A5r4 = -0.54732598014417; A5r5 = -1.03525434507065; \
A5r6 = -0.70043427145923; A5r7 = 0.19104244009385; A5r8 = \
0.93069185429715; A5r9 = 0.93069185429715; A5r10 = 0.19104244009385; \
A5r11 = -0.70043427145923; A5r12 = -1.03525434507065; A5r13 = \
-0.54732598014417; A5r14 = 0.37557915902045; A5r15 = \
1.00000000000000; A5r16 = 0.82969011373806;
(*6*)
A6r1 = 0.89899825944091; A6r2 = 0.80143601201832; A6r3 = \
-0.18453671892660; A6r4 = -0.96594619936780; A6r5 = \
-0.67658182242300; A6r6 = 0.36278926121756; A6r7 = 1.00000000000000; \
A6r8 = 0.52868745033552; A6r9 = -0.52868745033551; A6r10 = \
-1.00000000000000; A6r11 = -0.36278926121756; A6r12 = \
0.67658182242300; A6r13 = 0.96594619936780; A6r14 = 0.18453671892660; \
A6r15 = -0.80143601201832; A6r16 = -0.89899825944091;
(*7*)
A7r1 = 0.96594619936780; A7r2 = 0.52868745033552; A7r3 = \
-0.67658182242300; A7r4 = -0.89899825944091; A7r5 = 0.18453671892660; \
A7r6 = 1.00000000000000; A7r7 = 0.36278926121756; A7r8 = \
-0.80143601201832; A7r9 = -0.80143601201832; A7r10 = \
0.36278926121756; A7r11 = 1.00000000000000; A7r12 = 0.18453671892660; \
A7r13 = -0.89899825944091; A7r14 = -0.67658182242300; A7r15 = \
0.52868745033551; A7r16 = 0.96594619936780;
(*8*)
A8r1 = 1.00000000000000; A8r2 = 0.18453671892660; A8r3 = \
-0.96594619936780; A8r4 = -0.36278926121756; A8r5 = 0.89899825944091; \
A8r6 = 0.52868745033552; A8r7 = -0.80143601201832; A8r8 = \
-0.67658182242300; A8r9 = 0.67658182242300; A8r10 = 0.80143601201832; \
A8r11 = -0.52868745033551; A8r12 = -0.89899825944091; A8r13 = \
0.36278926121756; A8r14 = 0.96594619936780; A8r15 = \
-0.18453671892660; A8r16 = -1.00000000000000;
(*9*)
A9r1 = 1.00000000000000; A9r2 = -0.18453671892660; A9r3 = \
-0.96594619936780; A9r4 = 0.36278926121756; A9r5 = 0.89899825944091; \
A9r6 = -0.52868745033551; A9r7 = -0.80143601201832; A9r8 = \
0.67658182242300; A9r9 = 0.67658182242300; A9r10 = -0.80143601201832; \
A9r11 = -0.52868745033552; A9r12 = 0.89899825944091; A9r13 = \
0.36278926121756; A9r14 = -0.96594619936780; A9r15 = \
-0.18453671892661; A9r16 = 1.00000000000000;
(*10*)
A10r1 = 0.96594619936780; A10r2 = -0.52868745033551; A10r3 = \
-0.67658182242300; A10r4 = 0.89899825944091; A10r5 = \
0.18453671892660; A10r6 = -1.00000000000000; A10r7 = \
0.36278926121756; A10r8 = 0.80143601201832; A10r9 = \
-0.80143601201832; A10r10 = -0.36278926121756; A10r11 = \
1.00000000000000; A10r12 = -0.18453671892660; A10r13 = \
-0.89899825944091; A10r14 = 0.67658182242300; A10r15 = \
0.52868745033552; A10r16 = -0.96594619936780;
(*11*)
A11r1 = 0.89899825944091; A11r2 = -0.80143601201832; A11r3 = \
-0.18453671892660; A11r4 = 0.96594619936780; A11r5 = \
-0.67658182242300; A11r6 = -0.36278926121756; A11r7 = \
1.00000000000000; A11r8 = -0.52868745033551; A11r9 = \
-0.52868745033552; A11r10 = 1.00000000000000; A11r11 = \
-0.36278926121756; A11r12 = -0.67658182242300; A11r13 = \
0.96594619936780; A11r14 = -0.18453671892660; A11r15 = \
```

```
-0.80143601201832; A11r16 = 0.89899825944090;
(*12*)
A12r1 = 0.80143601201832; A12r2 = -0.96594619936780; A12r3 = \
0.36278926121756; A12r4 = 0.52868745033552; A12r5 = \
-1.00000000000000; A12r6 = 0.67658182242300; A12r7 = \
0.18453671892660; A12r8 = -0.89899825944091; A12r9 = \
0.89899825944091; A12r10 = -0.18453671892660; A12r11 = \
-0.67658182242300; A12r12 = 1.00000000000000; A12r13 = \
-0.52868745033551; A12r14 = -0.36278926121756; A12r15 = \
0.96594619936780; A12r16 = -0.80143601201832;
(*13*)
A13r1 = 0.70043427145923; A13r2 = -1.03525434507065; A13r3 = \
0.82969011373806; A13r4 = -0.19104244009385; A13r5 = \
-0.54732598014416; A13r6 = 1.00000000000000; A13r7 = \
-0.93069185429715; A13r8 = 0.37557915902045; A13r9 = \
0.37557915902045; A13r10 = -0.93069185429715; A13r11 = \
1.00000000000000; A13r12 = -0.54732598014417; A13r13 = \
-0.19104244009385; A13r14 = 0.82969011373806; A13r15 = \
-1.03525434507065; A13r16 = 0.70043427145923;
(*14*)
A14r1 = 0.52868745033552; A14r2 = -0.89899825944091; A14r3 = \
1.00000000000000; A14r4 = -0.80143601201832; A14r5 = \
0.36278926121756; A14r6 = 0.18453671892660; A14r7 = \
-0.67658182242300; A14r8 = 0.96594619936780; A14r9 = \
-0.96594619936780; A14r10 = 0.67658182242300; A14r11 = \
-0.18453671892660; A14r12 = -0.36278926121756; A14r13 = \
0.80143601201832; A14r14 = -1.00000000000000; A14r15 = \
0.89899825944091; A14r16 = -0.52868745033551;
(*15*)
A15r1 = 0.37557915902045; A15r2 = -0.70043427145923; A15r3 = \
0.93069185429715; A15r4 = -1.03525434507065; A15r5 = \
1.00000000000000; A15r6 = -0.82969011373806; A15r7 = \
0.54732598014416; A15r8 = -0.19104244009384; A15r9 = \
-0.19104244009385; A15r10 = 0.54732598014417; A15r11 = \
-0.82969011373806; A15r12 = 1.00000000000000; A15r13 = \
-1.03525434507065; A15r14 = 0.93069185429715; A15r15 = \
-0.70043427145923; A15r16 = 0.37557915902044;
(*16*)
A16r1 = 0.18453671892660; A16r2 = -0.36278926121756; A16r3 = \
0.52868745033552; A16r4 = -0.67658182242300; A16r5 = \
0.80143601201832; A16r6 = -0.89899825944091; A16r7 = \
0.96594619936780; A16r8 = -1.00000000000000; A16r9 = \
1.00000000000000; A16r10 = -0.96594619936780; A16r11 = \
0.89899825944090; A16r12 = -0.80143601201832; A16r13 = \
0.67658182242300; A16r14 = -0.52868745033551; A16r15 = \
0.36278926121756; A16r16 = -0.18453671892660;

Vmode1 = V;
Vmode1 = Chop[
  Expand[Vmode1 /. {y1[t] -> A1r1*q1, y2[t] -> A1r2*q1,
     y3[t] -> A1r3*q1, y4[t] -> A1r4*q1, y5[t] -> A1r5*q1,
     y6[t] -> A1r6*q1, y7[t] -> A1r7*q1, y8[t] -> A1r8*q1,
     y9[t] -> A1r9*q1, y10[t] -> A1r10*q1, y11[t] -> A1r11*q1,
     y12[t] -> A1r12*q1, y13[t] -> A1r13*q1, y14[t] -> A1r14*q1,
     y15[t] -> A1r15*q1, y16[t] -> A1r16*q1 }]]
EoMmod1 = D[Vmode1, q1]

In[77]:= Vmode2 = V;
Vmode2 = Chop[
   Expand[Vmode2 /. {y1[t] -> A2r1*q2, y2[t] -> A2r2*q2,
      y3[t] -> A2r3*q2, y4[t] -> A2r4*q2, y5[t] -> A2r5*q2,
      y6[t] -> A2r6*q2, y7[t] -> A2r7*q2, y8[t] -> A2r8*q2,
      y9[t] -> A2r9*q2, y10[t] -> A2r10*q2, y11[t] -> A2r11*q2,
      y12[t] -> A2r12*q2, y13[t] -> A2r13*q2, y14[t] -> A2r14*q2,
      y15[t] -> A2r15*q2, y16[t] -> A2r16*q2 }]];
EoMmod2 = D[Vmode2, q2]
Vmode3 = V;
Vmode3 = Chop[
   Expand[Vmode3 /. {y1[t] -> A3r1*q3, y2[t] -> A3r2*q3,
      y3[t] -> A3r3*q3, y4[t] -> A3r4*q3, y5[t] -> A3r5*q3,
      y6[t] -> A3r6*q3, y7[t] -> A3r7*q3, y8[t] -> A3r8*q3,
```

```
      y9[t] -> A3r9*q3, y10[t] -> A3r10*q3, y11[t] -> A3r11*q3,
      y12[t] -> A3r12*q3, y13[t] -> A3r13*q3, y14[t] -> A3r14*q3,
      y15[t] -> A3r15*q3, y16[t] -> A3r16*q3 }]];
EoMmod3 = D[Vmode3, q3]
Vmode4 = V;
Vmode4 = Chop[
   Expand[Vmode4 /. {y1[t] -> A4r1*q4, y2[t] -> A4r2*q4,
      y3[t] -> A4r3*q4, y4[t] -> A4r4*q4, y5[t] -> A4r5*q4,
      y6[t] -> A4r6*q4, y7[t] -> A4r7*q4, y8[t] -> A4r8*q4,
      y9[t] -> A4r9*q4, y10[t] -> A4r10*q4, y11[t] -> A4r11*q4,
      y12[t] -> A4r12*q4, y13[t] -> A4r13*q4, y14[t] -> A4r14*q4,
      y15[t] -> A4r15*q4, y16[t] -> A4r16*q4 }]];
EoMmod4 = D[Vmode4, q4]
Vmode5 = V;
Vmode5 = Chop[
   Expand[Vmode5 /. {y1[t] -> A5r1*q5, y2[t] -> A5r2*q5,
      y3[t] -> A5r3*q5, y4[t] -> A5r4*q5, y5[t] -> A5r5*q5,
      y6[t] -> A5r6*q5, y7[t] -> A5r7*q5, y8[t] -> A5r8*q5,
      y9[t] -> A5r9*q5, y10[t] -> A5r10*q5, y11[t] -> A5r11*q5,
      y12[t] -> A5r12*q5, y13[t] -> A5r13*q5, y14[t] -> A5r14*q5,
      y15[t] -> A5r15*q5, y16[t] -> A5r16*q5 }]];
EoMmod5 = D[Vmode5, q5]
Vmode6 = V;
Vmode6 = Chop[
   Expand[Vmode6 /. {y1[t] -> A6r1*q6, y2[t] -> A6r2*q6,
      y3[t] -> A6r3*q6, y4[t] -> A6r4*q6, y5[t] -> A6r5*q6,
      y6[t] -> A6r6*q6, y7[t] -> A6r7*q6, y8[t] -> A6r8*q6,
      y9[t] -> A6r9*q6, y10[t] -> A6r10*q6, y11[t] -> A6r11*q6,
      y12[t] -> A6r12*q6, y13[t] -> A6r13*q6, y14[t] -> A6r14*q6,
      y15[t] -> A6r15*q6, y16[t] -> A6r16*q6 }]];
EoMmod6 = D[Vmode6, q6]

In[92]:= Vmode12 = V;
Vmode12 =
 Expand[Vmode12 /. {y1[t] -> A1r1*q1 + A2r1*q2,
    y2[t] -> A1r2*q1 + A2r2*q2, y3[t] -> A1r3*q1 + A2r3*q2,
    y4[t] -> A1r4*q1 + A2r4*q2, y5[t] -> A1r5*q1 + A2r5*q2,
    y6[t] -> A1r6*q1 + A2r6*q2, y7[t] -> A1r7*q1 + A2r7*q2,
    y8[t] -> A1r8*q1 + A2r8*q2, y9[t] -> A1r9*q1 + A2r9*q2,
    y10[t] -> A1r10*q1 + A2r10*q2, y11[t] -> A1r11*q1 + A2r11*q2,
    y12[t] -> A1r12*q1 + A2r12*q2, y13[t] -> A1r13*q1 + A2r13*q2,
    y14[t] -> A1r14*q1 + A2r14*q2, y15[t] -> A1r15*q1 + A2r15*q2,
    y16[t] -> A1r16*q1 + A2r16*q2 }]
EoM1mod1a2 = Chop[D[Vmode12, q1] - EoMmod1]

In[129]:= Vmode13 = V; Vmode13 =
 Expand[Vmode13 /. {y1[t] -> A1r1*q1 + A3r1*q3,
    y2[t] -> A1r2*q1 + A3r2*q3, y3[t] -> A1r3*q1 + A3r3*q3,
    y4[t] -> A1r4*q1 + A3r4*q3, y5[t] -> A1r5*q1 + A3r5*q3,
    y6[t] -> A1r6*q1 + A3r6*q3, y7[t] -> A1r7*q1 + A3r7*q3,
    y8[t] -> A1r8*q1 + A3r8*q3, y9[t] -> A1r9*q1 + A3r9*q3,
    y10[t] -> A1r10*q1 + A3r10*q3, y11[t] -> A1r11*q1 + A3r11*q3,
    y12[t] -> A1r12*q1 + A3r12*q3, y13[t] -> A1r13*q1 + A3r13*q3,
    y14[t] -> A1r14*q1 + A3r14*q3, y15[t] -> A1r15*q1 + A3r15*q3,
    y16[t] -> A1r16*q1 + A3r16*q3 }]
EoM1mod1a3 = Chop[D[Vmode13, q1] - EoMmod1]


In[95]:= Vmode14 = V; Vmode14 =
 Expand[Vmode14 /. {y1[t] -> A1r1*q1 + A4r1*q4,
    y2[t] -> A1r2*q1 + A4r2*q4, y3[t] -> A1r3*q1 + A4r3*q4,
    y4[t] -> A1r4*q1 + A4r4*q4, y5[t] -> A1r5*q1 + A4r5*q4,
    y6[t] -> A1r6*q1 + A4r6*q4, y7[t] -> A1r7*q1 + A4r7*q4,
    y8[t] -> A1r8*q1 + A4r8*q4, y9[t] -> A1r9*q1 + A4r9*q4,
    y10[t] -> A1r10*q1 + A4r10*q4, y11[t] -> A1r11*q1 + A4r11*q4,
    y12[t] -> A1r12*q1 + A4r12*q4, y13[t] -> A1r13*q1 + A4r13*q4,
    y14[t] -> A1r14*q1 + A4r14*q4, y15[t] -> A1r15*q1 + A4r15*q4,
    y16[t] -> A1r16*q1 + A4r16*q4 }]
EoM1mod1a4 = Chop[D[Vmode14, q1] - EoMmod1]

In[97]:= Vmode15 = V; Vmode15 =
```

```
 Expand[Vmode15 /. {y1[t] -> A1r1*q1 + A5r1*q5,
    y2[t] -> A1r2*q1 + A5r2*q5, y3[t] -> A1r3*q1 + A5r3*q5,
    y4[t] -> A1r4*q1 + A5r4*q5, y5[t] -> A1r5*q1 + A5r5*q5,
    y6[t] -> A1r6*q1 + A5r6*q5, y7[t] -> A1r7*q1 + A5r7*q5,
    y8[t] -> A1r8*q1 + A5r8*q5, y9[t] -> A1r9*q1 + A5r9*q5,
    y10[t] -> A1r10*q1 + A5r10*q5, y11[t] -> A1r11*q1 + A5r11*q5,
    y12[t] -> A1r12*q1 + A5r12*q5, y13[t] -> A1r13*q1 + A5r13*q5,
    y14[t] -> A1r14*q1 + A5r14*q5, y15[t] -> A1r15*q1 + A5r15*q5,
    y16[t] -> A1r16*q1 + A5r16*q5 }]
EoM1mod1a5 = Chop[D[Vmode15, q1] - EoMmod1]

In[99]:= Vmode16 = V; Vmode16 =
 Expand[Vmode16 /. {y1[t] -> A1r1*q1 + A6r1*q6,
    y2[t] -> A1r2*q1 + A6r2*q6, y3[t] -> A1r3*q1 + A6r3*q6,
    y4[t] -> A1r4*q1 + A6r4*q6, y5[t] -> A1r5*q1 + A6r5*q6,
    y6[t] -> A1r6*q1 + A6r6*q6, y7[t] -> A1r7*q1 + A6r7*q6,
    y8[t] -> A1r8*q1 + A6r8*q6, y9[t] -> A1r9*q1 + A6r9*q6,
    y10[t] -> A1r10*q1 + A6r10*q6, y11[t] -> A1r11*q1 + A6r11*q6,
    y12[t] -> A1r12*q1 + A6r12*q6, y13[t] -> A1r13*q1 + A6r13*q6,
    y14[t] -> A1r14*q1 + A6r14*q6, y15[t] -> A1r15*q1 + A6r15*q6,
    y16[t] -> A1r16*q1 + A6r16*q6 }]
EoM1mod1a6 = Chop[D[Vmode16, q1] - EoMmod1]
```

F.2.2. Modal EoMs of strings

```
(*Displacements*)
ux = D[u[x], x]; vx = D[v[x], x]; wx = D[w[x], x];
ds = ((1 + ux)^2 + vx^2 +
     wx^2)^0.5; (*this is initial formulation of the stretched element*)
dsux = Normal[
   Series[ds, {ux, 0,
     1}]];(*this is initial formulation of the stretched element series ux*)
dsvx = Normal[Series[dsux, {vx, 0, 3}]];
dswx = Normal[Series[dsvx, {wx, 0, 3}]]
dsdx = Expand[dswx] /. ux*vx^2 -> 0 /. ux*wx^2 -> 0 /.
  vx^2*wx^2 -> 0 (*Taylor expansion of ds/dx*)

dxds = Expand[
       Normal[Series[
         Series[Series[1/dsdx, {ux, 0, 2}], {vx, 0, 2}], {wx, 0,
          2}]]] /. ux*vx^2 -> 0 /. ux*wx^2 -> 0 /. vx^2*wx^2 -> 0 /.
   ux^2 vx^2 -> 0 /. ux^2 wx^2 -> 0(*this is dx/ds*)

T = Simplify[(T0 + EA*(dsdx - 1))] ;(*Tension*)
(*Tension in each direction*)
Tx = T*(1 + ux)*dxds; Tx =
 Chop[Expand[Tx] ] /. {ux^2 -> 0, ux^3 -> 0, ux^4 -> 0, ux*vx^2 -> 0,
   ux*wx^2 -> 0, vx^4 -> 0, ux *vx^4 -> 0, vx^2 wx^2 -> 0, wx^4 -> 0,
   ux*wx^4 -> 0}(*x-dir strain is 1+ux*)
Ty = T*vx*dxds; Ty =
 Chop[Expand[Ty] /. {ux^2 -> 0, ux^3 -> 0, ux*wx^2*vx -> 0,
    wx^4*vx -> 0, ux*vx^3 -> 0, wx^2*vx^3 -> 0, vx^5 -> 0}]
Tz = T*wx*dxds; Tz =
 Chop[ Expand[Tz] /. {ux^2 -> 0, ux^3 -> 0, ux*vx^2*wx -> 0,
    vx^4*wx -> 0, ux*wx^3 -> 0, vx^2*wx^3 -> 0, wx^5 -> 0}]

(*EoM in each direction*)
EoMx = Simplify[m*D[D[u[t], t], t] - D[Tx, x]]; EoMx = EoMx
EoMy = Simplify[m*D[D[v[t], t], t] - D[Ty, x]]; EoMy =
 EoMy /. {-1.5*EA + 1.5*T0 -> -1.5*EA, -0.5*EA + 0.5*T0 -> -0.5*
     EA, -1.*EA + 1.*T0 -> -1.*
     EA} (*This latter assumes that EA>>T0*)
EoMz = Simplify[m*D[D[w[t], t], t] - D[Tz, x]]; EoMz =
 EoMz /. {-1.5*EA + 1.5*T0 -> -1.5*EA, -0.5*EA + 0.5*T0 -> -0.5*
     EA, -1.*EA + 1.*T0 -> -1.*
     EA}(*This latter assumes that EA>>T0*)
EoMx = Chop[EoMx /. {T0 -> 0, u``[t] -> 0}]; EoMx =
 Simplify[EoMx/(1.*EA)] (*Here we assume that EA>>T0 and utt = 0*)
d2udx2 = Simplify[EoMx + 1. u``[x]]
```

```
45
46 (*Calculate modal EoM*)
47 weight = Sin[3*Pi*x/L]; (*Galerkin's weight Function of mode 3*)
48 V[x] = Sin[1*Pi*x/L]*q1y[t] + Sin[2*Pi*x/L]*q2y[t] +
49    Sin[3*Pi*x/L]*q3y[t]; (*Transverse displ. of modes 1, 2 and 3*)
50 dVdx = D[V[x], x];
51 d2Vdx2 = D[D[V[x], x], x];
52 d2Vdt2 = D[D[V[x], t], t];
53 W[x] = Sin[1*Pi*x/L]*q1z[t] + Sin[2*Pi*x/L]*q2z[t] +
54    Sin[3*Pi*x/L]*q3z[t]; (*Vertical displ. of modes 1, 2 and 3*)
55 dWdx = D[W[x], x];
56 d2Wdx2 = D[D[W[x], x], x];
57 d2Wdt2 = D[D[W[x], t], t];
58 d2Udx2 = -0.5*D[dVdx^2 + dWdx^2, x];
59 dUdx = -0.5*(dVdx^2 + dWdx^2) + (1/(2*L)) Integrate[
60      dVdx^2 + dWdx^2, {x, 0, L}];
61 U = -0.5*Integrate[(dVdx^2 + dWdx^2), {x, 0,
62       x}] + (x/(2*L)) Integrate[dVdx^2 + dWdx^2, {x, 0, L}];
63 prefacV  = Integrate[weight*d2Vdt2, {x, 0, L}]/D[D[q1y[t], t], t]; (*Pre-factor = ...
       modal mass*)
64 EoMVtot =
65   d2Vdt2 - 1.5* (EA/m)* (dVdx^2)* d2Vdx2 - (T0/m)*d2Vdx2 - (EA/m) *
66     dUdx*d2Vdx2 -
67    0.5*(EA/m) *(dWdx^2)*d2Vdx2 - (EA/m) *dVdx*d2Udx2 - (EA/m)*dVdx*
68     dWdx*d2Wdx2; (*Total EoM- transverse*)
69 EoMmodalV = Chop[Expand[Integrate[weight*EoMVtot, {x, 0, L}]]];
70 EoMmodalV = Expand[EoMmodalV/prefacV] (*Modal result*)
71 prefacW = Integrate[weight*d2Wdt2, {x, 0, L}]/D[D[q1z[t], t], t]; (*Pre-factor = ...
       modal mass*)
72 EoMWtot =
73   d2Wdt2 - 1.5* (EA/m)* (dWdx^2)* d2Wdx2 - (T0/m)*d2Wdx2 - (EA/m) *
74     dUdx*d2Wdx2 -
75    0.5*(EA/m) *(dVdx^2)*d2Wdx2 - (EA/m) *dWdx*d2Udx2 - (EA/m)*dWdx*
76     dVdx*d2Vdx2;(*Total EoM- vertical*)
77 EoMmodalW = Chop[Expand[Integrate[weight*EoMWtot, {x, 0, L}]]];
78 EoMmodalW = Expand[EoMmodalW/prefacW]
```

Bibliography

[1] Principles of lock-in detection. URL https://www.zhinst.com/europe/en/resources/principles-of-lock-in-detection.

[2] G.V. Anand. Large-Amplitude Damped Free Vibration of a Stretched String. *The Journal of the Acoustical Society of America*, 45(5):1089–1096, 1969. ISSN 0001-4966. doi: 10.1121/1.1911578.

[3] A. Barnard, M. Zhang, G. Wiederhecker, M. Lipson, and P.L. McEuen. Real-time vibrations of a carbon nanotube. *Nature*, (7742):89–93. ISSN 14764687. doi: 10.1038/s41586-018-0861-0.

[4] G. P. Berman and F. M. Izrailev. The Fermi-Pasta-Ulam problem: Fifty years of progress. *Chaos*, 15(1), 2005. ISSN 10541500. doi: 10.1063/1.1855036.

[5] V. Bos. Nonlinear dynamics of graphene membranes. Master's thesis, Delft University of Technology, 1 2020.

[6] B. V. Chirikov, F. M. Izrailev, and V. A. Tayursky. Numerical experiments on the statistical behaviour of dynamical systems with a few degrees of freedom. *Computer Physics Communications*, 5(1):11–16, 1973. ISSN 00104655. doi: 10.1016/0010-4655(73)90003-9.

[7] T. Dauxois, M. Peyrard, and S. Ruffo. The Fermi-Pasta-Ulam 'numerical experiment': History and pedagogical perspectives. *European Journal of Physics*, 26(5):3–11, 2005. ISSN 01430807. doi: 10.1088/0143-0807/26/5/S01.

[8] D. Davidovikj, F. Alijani, S. J. Cartamil-Bueno, H. S.J. Van Der Zant, M. Amabili, and P. G. Steeneken. Nonlinear dynamic characterization of two-dimensional materials. *Nature Communications*, (1):1–7. ISSN 20411723. doi: 10.1038/s41467-017-01351-4.

[9] S. Dou, B.S. Strachan, S.W. Shaw, and J.S. Jensen. Structural optimization for nonlinear dynamic response. *Philosophical Transactions of the Royal Society A: Mathematical, Physical and Engineering Sciences*, 373(2051), 2015. ISSN 1364503X. doi: 10.1098/rsta.2014.0408.

[10] N. Engelsen, A. Ghadimi, S. Fedorov, T. Kippenberg, M. Bereyhi, R. Schilling, and D. Wilson. Elastic Strain Engineering for Ultralow Mechanical Dissipation. *International Conference on Optical MEMS and Nanophotonics*, 2018-July(May):1–6, 2018. ISSN 21605041. doi: 10.1109/OMN.2018.8454645.

[11] E. Fermi, P Pasta, S Ulam, and M Tsingou. Studies of the nonlinear problems. doi: 10.2172/4376203. URL https://www.osti.gov/biblio/4376203.

[12] J. Ford. The fermi-pasta-ulam problem: paradox turns discovery. *Physics Reports*, 213(5):271–310, 1992.

[13] A. H. Ghadimi, D. J. Wilson, and T. J. Kippenberg. Dissipation engineering of high-stress silicon nitride nanobeams. 2016.

[14] J. Güttinger, A. Noury, P. Weber, A. Eriksson, C. Lagoin, J. Moser, C. Eichler, A. Wallraff, A. Isacsson, and A. Bachtold. Energy-dependent path of dissipation in nanomechanical resonators. *Nature Nanotechnology*, 12(7):631–636, 2017. ISSN 17483395. doi: 10.1038/nnano.2017.86.

[15] G.A. Holzapfel. *Nonlinear Solid Mechanics: A Continuum Approach for Engineering*. Wiley, 2000. ISBN 9780471823193.

[16] Daniel J. Inman. *Engineering Vibrations*. Pearson, 2014.

[17] A. Keşkekler, O. Shoshani, M. Lee, H. van der Zant, P. Steeneken, and F. Alijani. Tuning nonlinear damping in graphene nanoresonators by parametric–direct internal resonance. *Nature Communications*, 12(1):1–7, 2021. ISSN 20411723. doi: 10.1038/s41467-021-21334-w.

[18] L. Li, P. Polunin, S. Dou, O. Shoshani, B. Strachan, J.. Jensen, S. Shaw, and K. Turner. Tailoring the nonlinear response of MEMS resonators using shape optimization. *Applied Physics Letters*, 110(8), 2017. ISSN 00036951. doi: 10.1063/1.4976749.

[19] R. Lifshitz and M. C. Cross. Nonlinear Dynamics of Nanomechanical and Micromechanical Resonators. *Reviews of Nonlinear Dynamics and Complexity*, pages 1–52, 2009. doi: 10.1002/9783527626359.ch1.

[20] L. Meirovitch. *Fundamentals of Vibrations*. Waveland Press, 2010. ISBN 9781577666912.

[21] D. Midtvedt, A. Croy, A. Isacsson, Z. Qi, and H. S. Park. Fermi-pasta-ulam physics with nanomechanical graphene resonators: Intrinsic relaxation and thermalization from flexural mode coupling. *Physical Review Letters*, 112(14):1–5, 2014. ISSN 10797114. doi: 10.1103/PhysRevLett.112.145503.

[22] A.A. Muravyov and S.A. Rizzi. Determination of nonlinear stiffness with application to random vibration of geometrically nonlinear structures. *Computers Structures*, 81(15):1513 – 1523, 2003. ISSN 0045-7949. doi: https://doi.org/10.1016/S0045-7949(03)00145-7.

[23] A. Mussot, C. Naveau, M. Conforti, A. Kudlinski, F. Copie, P. Szriftgiser, and S. Trillo. Fibre multi-wave mixing combs reveal the broken symmetry of Fermi-Pasta-Ulam recurrence. *Nature Photonics*, (5):303–308. ISSN 17494893. doi: 10.1038/s41566-018-0136-1.

[24] A.H. Nayfeh. Applied nonlinear dynamics: analytical, computational, and experimental methods. *Choice Reviews Online*, 32(11):32–6286–32–6286, 1995. ISSN 0009-4978. doi: 10.5860/choice.32-6286.

[25] A.H. Nayfeh. *Nonlinear Oscillations*, chapter 7, pages 444–543. John Wiley Sons, Ltd, 1995. ISBN 9783527617586. doi: https://doi.org/10.1002/9783527617586.ch7.

[26] H. Nelson, M.A. Porter, and Bhaskar Choubey. Variability in Fermi-Pasta-Ulam-Tsingou arrays can prevent recurrences. *Physical Review E*, 98(6):1–10, 2018. ISSN 24700053. doi: 10.1103/PhysRevE.98.062210.

[27] R.A. Norte, J.P. Moura, and S. Gröblacher. Mechanical Resonators for Quantum Optomechanics Experiments at Room Temperature. *Physical Review Letters*, 116(14):1–6, 2016. ISSN 10797114. doi: 10.1103/PhysRevLett.116.147202.

[28] S.D. Pace and D.K. Campbell. Behavior and breakdown of higher-order Fermi-Pasta-Ulam-Tsingou recurrences. *Chaos*, 29(2), 2019. ISSN 10541500. doi: 10.1063/1.5079659.

[29] S. Schmid and C. Hierold. Damping mechanisms of single-clamped and prestressed double-clamped resonant polymer microbeams. *Journal of Applied Physics*, 104(9), 2008. ISSN 00218979. doi: 10.1063/1.3008032.

[30] S. Schmid, K. D. Jensen, K. H. Nielsen, and A. Boisen. Damping mechanisms in high-Q micro and nanomechanical string resonators. *Physical Review B - Condensed Matter and Materials Physics*, 84(16):1–6, 2011. ISSN 10980121. doi: 10.1103/PhysRevB.84.165307.

[31] S. Schmid, L.G. Villanueva, and M.L. Roukes. *Fundamentals of nanomechanical resonators*. 2016. ISBN 9783319286914. doi: 10.1007/978-3-319-28691-4.

[32] R. Munnig Schmidt, G. Schitter, A. Rankers, and J. Van Eijk. *The Design of High Performance Mechatronics: High-Tech Functionality by Multidisciplinary System Integration*. IOS Press, NLD, 2nd edition, 2014. ISBN 161499367X.

[33] D.S. Sholl and B.I. Henry. Recurrence times in cubic and quartic Fermi-Pasta-Ulam chains: A shifted-frequency perturbation treatment. *Physical Review A*, 44(10):6364–6374, 1991. ISSN 10502947. doi: 10.1103/PhysRevA.44.6364.

[34] J. L. Tuck and M. T. Menzel. The superperiod of the nonlinear weighted string (FPU) problem. *Advances in Mathematics*, 9(3):399–407, 1972. ISSN 10902082. doi: 10.1016/0001-8708(72)90024-2.

[35] G. Van Simaeys and Ph Emplit. Experimental demonstration of the fermi-pasta-ulam recurrence in a modulationally unstable optical wave. *Physical Review Letters*, 87(3):33902–1–33902–4, 2001. ISSN 10797114. doi: 10.1103/PhysRevLett.87.033902.

[36] Scott S. Verbridge, Jeevak M. Parpia, Robert B. Reichenbach, Leon M. Bellan, and H. G. Craighead. High quality factor resonance at room temperature with nanostrings under high tensile stress. *Journal of Applied Physics*, 99(12), 2006. ISSN 00218979. doi: 10.1063/1.2204829.

[37] S.S. Verbridge, H.G. Craighead, and J.M. Parpia. A megahertz nanomechanical resonator with room temperature quality factor over a million. *Applied Physics Letters*, 92(1):8–11, 2008. ISSN 00036951. doi: 10.1063/1.2822406.

[38] D.M. Zhao, S.P. Li, Y. Zhang, and J.L. Liu. Nonlinear Vibration of an Elastic Soft String: Large Amplitude and Large Curvature. *Mathematical Problems in Engineering*, 2018, 2018. ISSN 15635147. doi: 10.1155/2018/7909876.